



Novel brain white matter disorders and their genetic causes

Sietske H.G. Kavelam

**Novel brain white matter disorders
and their genetic causes**

Sietske H.G. Kevelam

The research in this thesis was funded by the Dutch Organization for Scientific Research (ZonMw TOP 91211005). The funding agencies had no direct involvement with the contents of the study. Financial support for printing this thesis was kindly provided by Stichting Researchfonds Kindergeneeskunde, VU University Medical Center, Amsterdam, The Netherlands and by the Graduate School Neurosciences Amsterdam Rotterdam (ONWAR).

Author: Sietske H.G. Kevelam
Cover design and Lay-out: Ridderprint BV, the Netherlands
Printed by: Ridderprint BV, the Netherlands

ISBN: 978-94-6299-395-2

©2016, S.H.G. Kevelam.
All rights reserved. No part of this thesis may be reproduced or transmitted in any form or by any means, without permission of the author.

VRIJE UNIVERSITEIT

**Novel brain white matter disorders
and their genetic causes**

ACADEMISCH PROEFSCHRIFT

ter verkrijging van de graad Doctor aan
de Vrije Universiteit Amsterdam,
op gezag van de rector magnificus
prof.dr. V. Subramaniam,
in het openbaar te verdedigen
ten overstaan van de promotiecommissie
van de Faculteit der Geneeskunde
op vrijdag 14 oktober 2016 om 11.45 uur
in het auditorium van de universiteit,
De Boelelaan 1105

door

Sietske Hanneke Geertje Kevelam
geboren te Nijmegen

promotor: prof.dr. M.S. van der Knaap

copromotoren: dr. N.I. Wolf
dr. Q. Waisfisz

CONTENTS

Chapter 1	General introduction	9
Part I	Expansion of the phenotypic spectrum of a known disorder	29
Chapter 2	Altered <i>PLP1</i> splicing causes hypomyelination of early myelinating structures	31
Chapter 3	Exome sequencing reveals mutated <i>SLC19A3</i> in patients with an early-infantile, lethal encephalopathy	63
Chapter 3.2	Reply: Infantile Leigh-like syndrome caused by <i>SLC19A3</i> mutations is a treatable disease	93
Chapter 4	<i>LAMA2</i> mutations in adult-onset muscular dystrophy with leukoencephalopathy	97
Chapter 5	Absent thalami caused by a homozygous <i>EARS2</i> mutation: expanding disease spectrum of LTBL	103
Part II	Novel disease entity associated with a known gene	113
Chapter 6	Novel (ovario)leukodystrophy related to <i>AARS2</i> mutations	115
Chapter 7	Acute intermittent porphyria-related leukoencephalopathy	145
Chapter 8	Cathepsin A-related arteriopathy with strokes and leukoencephalopathy (CARASAL)	161

Part III	Novel disorder associated with a gene previously not linked to a human disorder or clear phenotype	195
Chapter 9	<i>NUBPL</i> mutations in patients with complex I deficiency and a distinct MRI pattern	197
Chapter 10	Recessive <i>ITPA</i> mutations cause an early-infantile encephalopathy	223
Part IV	Update on leukodystrophies	247
Chapter 11	Leukodystrophies: origin, evolution and two revolutions	249
Chapter 12	Summary, discussion and future perspectives	265
Chapter 13	Nederlandse samenvatting	291
	Dankwoord	301
	List of publications	305
	Curriculum vitae	309

Chapter 1

General introduction



LEUKODYSTROPHIES

Leukoencephalopathies can be defined as all conditions in which the white matter of the central nervous system (CNS) is predominantly or exclusively affected, assuming primary white matter involvement.¹ This is opposed to white matter abnormalities secondary to Wallerian degeneration in neuronal degeneration and to white matter abnormalities in the context of a disease non-selectively affecting gray and white matter. Causes of leukoencephalopathies are numerous and include acquired conditions, such as inflammatory, autoimmune, vascular, neurotoxic, or infectious disorders, and genetic conditions.² Genetic leukoencephalopathies are referred to as leukodystrophies. Leukodystrophies are most prevalent in children, and although each distinct leukodystrophy is rare to ultra-rare, our estimation is that the overall incidence is higher than generally appreciated. Bonkowsky *et al* reported a live birth incidence of 1:7,663 (i.e. 13 leukodystrophy patients per 100.000 live births).³

Leukodystrophies are clinically heterogeneous and can present with a wide variety of neurological signs and symptoms, ranging from a mild developmental delay or exclusively motor deficits to severe combined cognitive and motor impairment.² Although epilepsy is seen in almost half of the cases,³ it rarely dominates the clinical picture, whereas it is more frequent and characteristic for neuronal disorders. Onset can be as early as *in utero* affecting fetal brain development or later in infancy, childhood, adolescence, adulthood or even senescence.² Initially leukodystrophies were thought to be invariably progressive.⁴ In more recent years it has become clear that this is not true for all disorders, as illustrated by patients with leukoencephalopathy and thalamus and brainstem involvement and high lactate (LTBL), who typically have an early infantile presentation and impressive initial magnetic resonance imaging (MRI) abnormalities with subsequent clinical amelioration and dramatic improvement of MRI abnormalities over time.⁵ The morbidity as well as the mortality over life time is high. Bonkowsky *et al.*, reported a mortality of 34% with a median age at death of 8.2 years in a cohort of 122 children with a leukodystrophy in a 9 year period,³ and another study reported a mortality of 22% in a cohort of 78 children with a genetic white matter disorder in a 5 year period, which was strikingly higher than in patients with an acquired leukoencephalopathy, of whom none died.⁶

The road to reach a definitive diagnosis is often (very) long. It comprises numerous specialist visits, tests and sometimes invasive diagnostic procedures, which are a burden for patients and families and also very expensive. And even after this long diagnostic odyssey, a diagnosis cannot be established in many cases. In 2010 it was

found that despite the use of brain MRI and extensive biochemical and metabolic investigations, no diagnosis could be established in more than 50% of the patients with a leukodystrophy.³ Importantly, a genetic diagnosis can only be realized when the gene associated with that disease is known, whereas this information lacks for several defined leukodystrophies and for all the unclassified leukodystrophies.

MRI PATTERN RECOGNITION AND LEUKODYSTROPHIES

In the past two centuries different approaches and techniques have been used to identify and define 'new' leukoencephalopathies and subsequently diagnose them based on state-of-art techniques of that time. Neuropathology was the first technique available to study brain diseases. In the 19th century, neuropathological observations in post-mortem brain tissue led to the distinction between a disorder characterized by multiple white matter lesions ('multiple sclerosis') and a disorder characterized by diffuse abnormality of the white matter ('diffuse sclerosis').^{7,8} In the beginning of the 20th century Neubürger noted that the term 'diffuse sclerosis' was applied to very different disease entities.⁹ Further differentiation between these disease entities in the next decades was possible due to advances in the development of novel histochemical methods and biochemical assays of body fluids, later followed by metabolic studies on fibroblasts or muscle, specific enzyme function tests and electron microscopy.¹⁰ In the 1980s, the advent of the MRI had a major impact on the studies of leukoencephalopathies, because white matter abnormalities could be visualized in detail in vivo for the first time.¹¹ The subsequent development of MRI pattern recognition in the early 1990s¹² was a big step forward in the diagnostic workup of leukoencephalopathies and MRI became the most important tool in the diagnostic process of these disorders.^{12,13}

MRI creates high-resolution anatomic images and is highly sensitive in the detection of white matter abnormalities.¹⁴ Different pulse sequences can be used that each result in different contrast between tissues. The T_1 - and T_2 -weighted sequences are best known. Unmyelinated white matter has a very long T_1 and T_2 , resulting in a lower signal than gray matter structures on T_1 -weighted images and a higher signal on T_2 -weighted images.^{15,16} At birth, the brain is still largely unmyelinated and the increasing deposition of myelin in the first two years of life results in shortening of first the T_1 and then the T_2 , leading to a reversal of the gray-white matter contrast on T_1 - and T_2 -weighted images.^{15,16} Fully myelinated white matter structures have a higher signal on T_1 -weighted images than gray matter structures and a lower signal on T_2 -weighted images than gray matter structures.¹⁵⁻¹⁷ Lack of myelin deposition (if permanent called 'hypomyelination') leads to a mildly elevated

1

signal on T_2 -weighted images and a variable signal on T_1 -weighted images, depending on the amount of myelin deposited.^{18,19} Abnormalities of the white matter other than lack of myelin deposition result in a much lower T_1 signal and a much higher T_2 signal than gray matter structures, allowing distinction between hypomyelination and other pathologies *in vivo*.¹⁸ Importantly, cerebrospinal fluid (CSF) has a high signal on T_2 -weighted images and a low signal on T_1 -weighted images, precluding differentiation between abnormal and cystic white matter. Images based on additional pulse sequences, such as fluid-attenuated inversion recovery (FLAIR) and proton density (PD) images, facilitate visualization of cystic lesions or rarefaction of tissue, because fluid has a low signal. Diffusion-weighting provides measures for the degree of freedom of movement of water molecules in brain tissue. Abnormalities on diffusion-weighted images (DWI) have to be confirmed by the apparent diffusion coefficient (ADC) values to avoid false positive results due to 'T₂-shine through'.²⁰ Restricted diffusion is seen in conditions with compression of extracellular spaces, for example due to (1) cytotoxic edema, as may occur in mitochondrial defects, (2) myelin micro-vacuolization, which may be present in neonates with maple syrup urine disease or in patients with a mitochondrial disorder, (3) high cell density as seen in the relatively spared white matter in vanishing white matter (VWM) (MIM 603896), or (4) storage of substances in lysosomal storage disorders.²¹ Increased diffusion can be observed in disorders with increased water spaces, such as megalencephalic leukoencephalopathy with subcortical cysts (MLC, MIM 604004) as the result of enlarged extracellular spaces and myelin macro-vacuolization.²² In some leukodystrophies, such as X-linked adrenoleukodystrophy (MIM 3001001) and Alexander disease (MIM 203450), the blood-brain barrier is grossly compromised, which can be shown by the use of contrast enhanced MR images.

MRI pattern recognition is based on the observation that individuals with the same leukoencephalopathy usually present with the same, distinct pattern of MRI abnormalities, while patients with other leukoencephalopathies have different MRI patterns.^{12,13,18} In MRI pattern recognition, major MRI discriminators are the nature of the white matter abnormalities (hypomyelination versus other pathologies), the aspect of the white matter abnormalities (e.g. confluent versus multifocal and symmetrical versus asymmetrical), the predominant location of the abnormalities (e.g. supra- or infratentorial, frontal or parietal, periventricular or subcortical) and special MRI features (e.g. cystic degeneration and/or rarefaction, contrast enhancement, diffusion restriction and microbleeds).¹⁸

The starting point of the road to reach a definitive molecular diagnosis begins with the identification and classification of patients. MRI pattern recognition has not only proven to be highly successful for the recognition of known leukoencephalopathies, but also for

the identification and classification of novel disorders among the unclassified cases.^{12,13} In our studies we use MRI pattern recognition as a primary tool in the search for novel disorders among the unclassified leukoencephalopathies. We identify and classify the patients from an MRI database present in the Center for Childhood White Matter Disorders at the VU Medical Center in Amsterdam including over 3000 MRIs of patients with an unclassified leukoencephalopathy from all over the world.

GENETICS AND LEUKODYSTROPHIES

In the last two decades several novel leukodystrophies have been defined using MRI pattern recognition analysis often combined with clinical and sometimes with laboratory data (e.g. VWM, MLC, hypomyelination and congenital cataract (HCC, MIM 603532), Leukoencephalopathy with brainstem and spinal cord involvement and lactate elevation (LBSL) and hypomyelination, hypodontia and hypogonadotropic hypogonadism (4H syndrome, MIM 607694).²³⁻²⁸ The validity of this approach has been shown by the identification of the associated genes (in 2001 and 2002 *EIF2B1-5* mutations in patients with VWM^{29,30} and mutations in *MLC1* in patients with MLC,³¹ in 2007 mutations in the gene *FAM126A* in patients with HCC syndrome,³² in 2007 *DARS2* mutations in patients with LBSL,³³ and in 2011 mutations in the genes *POLR3A* and *POLR3B* in patients with 4H syndrome^{34,35}). The identification of the molecular cause of these disorders was accomplished after time-consuming, laborious and costly efforts that included linkage by positional cloning to pinpoint the chromosomal location of the candidate gene and subsequent narrowing the candidate region, followed by reconstructing which genes were located in the candidate region and sequential analysis of candidate genes in the region by Sanger sequencing.³⁰⁻³⁵ This approach required the presence of multiple, preferably large and/or consanguineous families to identify a small enough candidate region with a significant logarithm of odds (LOD) score. Although this approach was indeed successful for the disorders mentioned above, for substantial numbers of patients with an unclassified or defined, but molecularly undetermined leukodystrophy this technique was not applicable. The rarity of these disorders and the presence of only a few mostly small families hampered the success of this approach and made it impossible to successfully apply the traditional gene-discovery approaches. In addition, *de novo* germ line mutations could not be identified using this technique. The introduction of Next-Generation-Sequencing (NGS) technologies could overcome these problems and created opportunities to perform unbiased gene search approaches to identify the mutated gene in patients with extremely rare Mendelian disorders, including most leukodystrophies.

NEXT-GENERATION SEQUENCING TECHNIQUES

A whole new genetic explorative era has emerged since the release of the first draft of the human genome sequence in 2001 and the first NGS platform release in the market in 2005.³⁶ NGS is often referred to as massive parallel sequencing, which means that millions or even billions of small fragments of DNA are sequenced simultaneously, creating a massive pool of data.³⁷ Whole-exome sequencing (WES) refers to massive parallel sequencing of the protein-coding part of the genome comprising 1% (30 Mb) of total human genome.^{37,38} Three main steps form the key elements of WES.³⁹ The first step is exome enrichment (exome capture kits are offered by different companies), which is accomplished by using oligonucleotide probes to hybridize fragment of interests. The second step is high through-put parallel sequencing which can be executed using different available platforms (e.g. Illumina HiSeqTM, Life TechnologiesTM, SOLiD4TM, and Roche 454 GS FLX). In our studies we work with Illumina HiSeq2000 for sequencing, which uses clonal bridge amplification and sequencing by synthesis approach.⁴⁰ This platform creates 600 Gb of 100 bp paired-end reads in a ten-day run.⁴¹ The third step is bioinformatics processing of the reads including quality assessment, mapping and alignment to the human reference genome and variant calling and annotation.³⁹

The initial proof of concept of the utility of WES in disease gene discovery came in 2009 with the demonstration that the causative gene for a known Mendelian disorder, Freeman-Sheldon syndrome (MIM 193700), could be identified directly by WES.³⁸ In 2010, the first discovery of the genetic cause for a rare Mendelian disorder of unknown cause, Miller syndrome (MIM 274200), was established.⁴² At the time of the start of my PhD project in September 2011, an increasing number of 30 novel genes and eight new clinical phenotypes linked to a known gene using WES were published within a time period of roughly two years.⁴³ In addition, during the first month of my PhD project, the first mutations in a novel gene associated with a leukodystrophy were identified with WES (*CSF1R* mutations in patients with 'Hereditary Diffuse Leukoencephalopathy with Spheroids', MIM 221820),⁴⁴ and soon thereafter our research group identified *EARS2* mutations in patients with LTBL using WES.⁴⁵ The exponential increase of the identification of novel genes associated with a broad variety of rare Mendelian disorders illustrates the high potential of this technique for gene finding in this field.⁴³

Successful WES depends firstly on the variant being detected in the captured portion of the genome and secondly on our ability to identify the variant of interest. Thorough prioritization of variants is therefore crucial to the gene finding process. After sequencing and bioinformatics processing, approximately 20.000 to 25.000 variants can be identified

in each individual exome.^{38,43,46} The challenge is to pinpoint the variant of interest within this large pool of insignificant variants. Filtering strategies to identify mutations usually rely on certain assumptions. For most Mendelian disorders prioritization assumes that the mutation has a potentially large effect and is therefore unique or extremely rare (i.e. only present in patients), located within the protein coding part of the genome and is predicted to have a direct effect on the function of the protein (e.g. non-synonymous single nucleotide variants (SNVs), insertions/deletions (indels) or splice-site mutations). The initial filtering approach commonly used is the exclusion of common variants (e.g. SNVs present in public databases such as dbSNP, 1000Genomes, and the NHBI Exome Variant Server genome database), which can reduce the number of potential candidate variants substantially by 90-95%.⁴⁶ After that, a total of 150-500 rare non-synonymous SNVs, indels or splice-site mutations will remain for further prioritizing.⁴⁶ Leukodystrophies can present with any inheritance pattern, and information on inheritance can further reduce the number of candidate variants substantially (Figure 1).

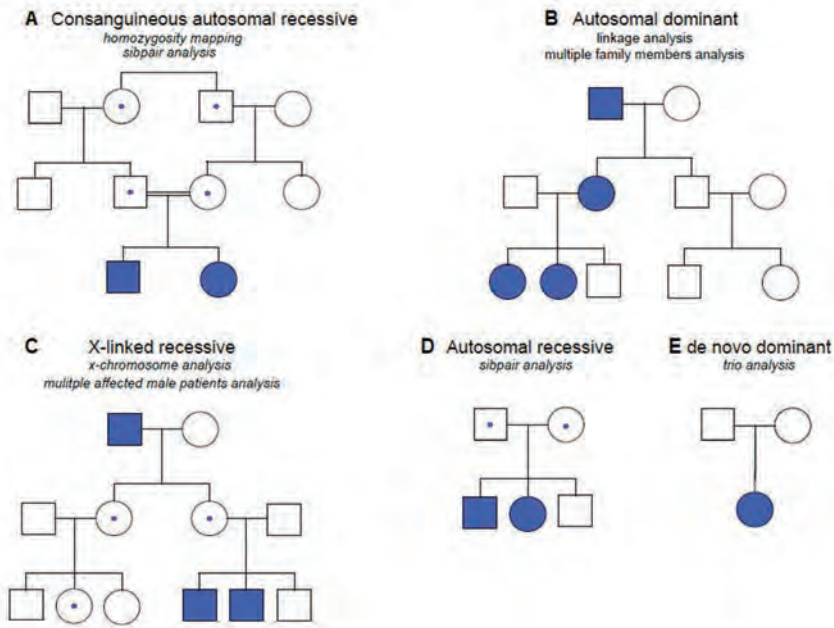


Figure 1. Different inheritance patterns with different approaches for WES analysis.

Circles represent females; squares males. Blue solid symbols indicate affected individuals; symbols with a dot indicate unaffected carriers. In the situation of a consanguineous autosomal recessive inheritance (A), homozygosity mapping in combination with WES of sib-pairs can be helpful. With an autosomal dominant inheritance pattern (B) in a large family additional linkage analysis with WES of multiple family members is an effective approach. When an X-linked recessive disorder is suspected (C), focusing first on the X-chromosome and sequencing multiple affected male patients is useful. When a recessive disorder is suspected but no consanguinity (D) is present sib-pair analysis (with or without parents) can be performed best. In case of a strong suspicion of a *de novo* disorder, trio analysis (E) is the appropriate first approach.

1

Different approaches can be applied to achieve the most efficient reduction of candidate variants for a certain supposed inheritance pattern. *De novo* mutations can be identified using a trio-based approach. WES is performed in both unaffected parents and the affected child, and the data are subsequently filtered for *de novo* variants. Theoretically this would be extremely efficient because the average exome only contains 0-3 true *de novo* mutations.⁴⁶ In the case of an autosomal recessively inherited disorder with reported consanguinity additional genetic techniques like a single nucleotide polymorphism (SNP) microarray can reduce the number of candidate variants by selection of an overlapping homozygous region between affected patients. In large families with an autosomal dominant disorder conventional genetic linkage analyses preceding WES could be helpful by narrowing down the candidate search area.⁴⁷ Although the combination of these filtering strategies will ultimately reduce the number of candidate variants significantly, comparison of identified variants among unrelated patients with (presumably) the same disorder is often required to pinpoint the candidate gene, especially in disorders caused by a novel gene. Importantly, effective intra-group comparison depends on precise phenotyping of the patients and the absence of genetic heterogeneity.

It is important to realize that every filtering step used can discard the pathogenic variant. For example, the inheritance pattern is often not definitively known and although causal variants are expected to be novel or extremely rare, this is not always the case, as illustrated by the high carrier frequency (1:95 in the Finnish population) of the *DARS2* splice mutation in intron 2.^{48,49} Furthermore, in addition to SNVs, patients can carry copy number variations (CNVs), inversions and deletions, which can be missed by WES due to limitations of this technique.^{50,51} Also, insufficient exome coverage, which is most often caused by the presence of extreme GC rich regions hampering good exome capture and sequencing, may result in negative results. Furthermore, it is estimated that 85% of the disease-causing mutations are located in functional and coding regions of the genome,^{52,53} the remaining part (non-coding causal mutations) is refractory to WES analysis and requires whole-genome sequencing (WGS).

For the studies described in this thesis we use WES as the main approach to identify the molecular cause of novel leukodystrophies. We consider intra-group comparison an effective additional filtering approach because this strategy will not only reduce the number of candidate variants substantially, it will also provide prove of the causality of the identified variant, when (different) variants in the same gene are found in multiple unrelated patients with the same phenotype. By using MRI pattern recognition for the classification of patients we aim at creating phenotypically homogeneous groups

of patients that represent a reliable discovery cohort for the application WES. We will especially focus on leukodystrophies with a (suspected) mitochondrial etiology or hypomyelination.

MITOCHONDRIAL DISORDERS

Mitochondrial disorders constitute a large proportion of the patients presenting with an unknown leukodystrophy.¹⁸ Mitochondrial disorders affect approximately 1 in 5.000 births.⁵⁴ They result from defective energy generation via oxidative phosphorylation (OXPHOS), which involves four electron-transferring respiratory chain complexes (complexes I-IV, CI-CIV), ATP synthase (complex V, CV) and two electron carriers coenzyme Q and cytochrome C, together comprising around 85 subunits.⁵⁵ Additionally, numerous assembly factors are necessary to form functional complexes. In 1951, Leigh reported the first patient with a mitochondrial disorder and from about this time onwards numerous other cases were reported.⁵⁶ Although initially deep gray matter involvement was the most frequently reported finding, white matter abnormalities are increasingly recognized as a common finding in mitochondrial disorders.⁵⁷ Numerous cells within the brain are extremely vulnerable for mitochondrial dysfunction. Axons in the white matter have a high energy demand, required to maintain the ionic gradient and structural integrity necessary to support neurotransmission.⁵⁸ Proper mitochondrial function is also vital for oligodendrocyte differentiation, viability and formation of myelin.⁵⁹⁻⁶¹ Energy produced in astrocytes supports neuronal function, and several mitochondrial enzymes within astrocytes, e.g. creatine kinase, malate-aspartase, glutamate dehydrogenase and pyruvate carboxylase are required to provide high-energy substrates to neurons.⁵⁷

Mitochondrial disorders can be caused by defects in the mitochondrial DNA (mtDNA) or nuclear DNA (nDNA). mtDNA consists of a double-stranded circular genome of 16,569 base pairs, which is present in 2-10 copies per mitochondrion.⁶² It was the first DNA of the human genome that was fully sequenced and it can easily be analyzed because it only contains 37 genes. These genes encode 13 subunits of the OXPHOS enzyme complex, plus 22 tRNAs and two rRNAs.⁶³ mtDNA is maternally inherited. In the 1990s most research concerning mitochondrial disorders was focused on mtDNA and leukodystrophies ascribed to mitochondrial syndromes were therefore associated with mutations or rearrangements in the mtDNA (e.g. mitochondrial encephalopathy, lactic acidosis and stroke-like episodes (MELAS, MIM 540000),^{64,65} Leber hereditary optic neuropathy (LHON, MIM 535000)^{66,67} and Kearns-Sayre syndrome (MIM 530000).^{68,69} In

1

1995, the first mutations in a nuclear gene (flavoprotein) involving a subunit of complex II were found in two sisters with Leigh syndrome and in 1999 recessive mutations in the gene thymidine phosphorylase were shown to be responsible for mitochondrial neurogastrointestinal encephalopathy (MNGIE, MIM 603041).^{70,71} The following years more and more mutations in nuclear genes were discovered, and it became evident that most mitochondrial disorders are caused by nuclear gene defects.⁷²

Of the five respiratory chain complexes present in OXPHOS, the most frequent deficiency in children is that of complex I (CI), NADH: ubiquinone oxidoreductase (EC1.6.5.3).⁷³ This complex comprises seven core subunits encoded by mitochondrial DNA, 38 nuclear encoded core subunits and many (still unknown) nuclear encoded assembly factors.⁷⁴ Besides defects of subunits and assembly factors of the respiratory chain complexes, it is increasingly shown that mitochondrial disorders can be the result of nuclear gene defects encoding mitochondrial tRNA synthetases and modification proteins, mitochondrial ribosomal proteins, proteins mediating mitochondrial mRNA translation (e.g. initiation, elongation and termination), proteins involved in mitochondrial dynamics and mitochondria quality control, defects of mtDNA maintenance, mitochondrial metabolite transporters and the import, modification and insertion of cofactors like heme, the iron-sulphur clusters and metals.^{57,75,76}

Clinically, mitochondrial disorders present with an extreme phenotypic variability; there is no obvious correlation between the type of respiratory chain defect and the clinical presentation.⁷⁷ Laboratory assessment of mitochondrial function in cultured fibroblasts or tissue (most often muscle biopsy) can reveal an isolated respiratory chain complex deficiency, a combined complex deficiency or even nonspecific or negative results.^{78,79} Elevated lactate in plasma and/or CSF is suggestive for a mitochondrial disorder, but a normal lactate does not exclude it.⁷⁷ MRI findings suggestive of a mitochondrial disorder are involvement of both white and gray matter structures, cystic lesions in the abnormal white matter, restricted diffusion, contrast enhancement, and elevated lactate on magnetic resonance spectroscopy (MRS) of the brain.^{20,80} Several mitochondrial leukodystrophies are associated with a distinct MRI pattern. For example, in MNGIE, patients' MRI shows a diffuse high T₂-signal intensity of the cerebral and cerebellar white matter with sparing of the U-fibers and corpus callosum. The thalami and basal nuclei may display patchy signal abnormalities.⁸¹ Recessive mutations in *DARS2*, encoding mitochondrial aspartyl-tRNA synthase, are associated with a characteristic MRI pattern involving cerebral white matter abnormalities with signal changes in specific brainstem and spinal cord tracts and elevated lactate.³³ Specific features seen on the MRI can also provide hints for the underlying diagnosis, like stroke-like lesions in MELAS⁶⁵ and calcium

deposits in the globus pallidus and caudate nucleus in Kearns-Sayre syndrome.^{69,82} However, not all mitochondrial defects present with such a characteristic MRI pattern or clues. This is illustrated by Leigh syndrome (MIM 256000), which is a distinct phenotype defined by developmental regression and MRI signal abnormalities in the basal ganglia, thalamus and brainstem that can be caused by mutations in more than 25 genes located both in mtDNA and nDNA.⁸³

In 2010 it was estimated that 114 genes were known to be associated with a mitochondrial disorder.⁸⁴ This is in striking contrast with the 1500 nuclear-encoded proteins that could be involved in mitochondrial functioning and if mutated could lead to disease.⁸⁵ In line with this, the majority of patients with a suspected mitochondrial leukodystrophy have no identifiable genetic etiology.⁸⁶ In addition to the wide phenotypic variation, genetic heterogeneity, and often poor genotype-phenotype correlation, a large proportion of the 'mitochondrial genes' has as yet not been associated with a disease, hampering the diagnosis in numerous patients. Until now, linkage analysis and homozygosity mapping were the main genetic techniques used in the discovery of novel mitochondrial disease genes, which have major limitations when used in small groups of patients, as discussed above.

WES would provide an unbiased approach to identify the genetic defect in rare, suspected mitochondrial leukoencephalopathies, as genes can be sequenced irrespective of their predicted role in disease pathology, or even without any evidence of mitochondrial localization. Phenotypic classification of patients groups with a suspected mitochondrial disorder is challenging due to the wide clinical and biochemical heterogeneity. We consider classification based on MRI pattern the most successful and valid approach for the identification of novel distinct mitochondrial disorders. An additional advantage of using this approach is that by identification of the causal gene defects, definition of disease entities is confirmed, which will make the diagnostic process in patients with a mitochondrial disorder more efficient and successful in the future.

HYPOMYELINATING DISORDERS

Patients with hypomyelination represent the largest single category among the patients with a leukoencephalopathy with unknown origin.¹³ At the end of the 19th century the first hypomyelinating disorder was described, Pelizaeus-Merzbacher disease (PMD, MIM 312080), which was characterized by the widespread lack of myelin staining in the white matter.^{87,88} On MRI, hypomyelination has a characteristic appearance. Hypomyelinated

1

white matter structures have a mild hyperintensity as compared to gray matter structures on T₂-weighted images and, dependent on the amount of myelin deposited, a hyper-, iso, or hypointense signal relative to gray matter structures on T₁-weighted images.¹⁸ The diagnosis hypomyelination can be made when there is a stable lack of myelin on two successive MRI scans that were performed at least six months apart with the second MRI after one year of age.¹⁸ At first sight hypomyelinating disorders have a rather similar appearance, both on MRI and clinically, making a definitive diagnosis in this group a challenge.^{18,19} Steenweg *et al.*, showed in 2010 that using MRI-pattern recognition in patients with hypomyelination it is possible to form clusters of patients based on MRI features and that these clusters correspond to specific hypomyelinating disorders.¹⁹ For example, 4H syndrome presents with a specific pattern of hypomyelination characterized by T₂ hypointensity of the optic radiation, pyramidal tracts at the level of the posterior limb of the internal capsule and the anterolateral part of the thalamus.^{19,23,89} Fucosidosis (MIM 230000), a lysosomal storage disorder caused by deficiency of α-L-fucosidase⁹⁰, is characterized by T₂ hypointensity of the globus pallidus¹⁹ and patients with HCC syndrome³² have hypomyelination in combination with focal lesions of more prominent T₂ hyperintensity and T₁ hypointensity in the periventricular and deep cerebral white matter and a more normal appearance of the subcortical white matter on T₁ weighted images.¹⁹ This MRI-based approach also proved to be successful in defining novel hypomyelinating disorders among the group of hypomyelinating disorders of unknown origin.¹⁹ One newly defined disorder was 'Hypomyelination of Early Myelinating Structures' (HEMS) which was identified in four male patients, suggesting an X-linked inheritance.⁹¹ During normal brain development tracts become myelinated at the time they become functional, resulting in a fixed spatiotemporal sequence of myelination.¹⁷ In patients with HEMS early myelinating structures (e.g. brainstem, hilus of the dentate nucleus, posterior limb of the internal capsule, optic tracts, and tracts to the pericentral cortex) are poorly myelinated, in contrast to structures that normally myelinate in later developmental stages.^{17,91} A genetic diagnosis could not be made in these patients using conventional genetic techniques (i.e. Sanger sequencing), although a gene involved in the early regulation of myelination was suspected.⁹¹

In September 2011, at the time I started my PhD project, 15 distinct inherited hypomyelinating disorders were defined, but the molecular cause was only known in nine of these disorders.⁹² The most common hypomyelinating disorder, PMD, is caused by mutations in the proteolipid protein-1 gene (*PLP1*), encoding proteolipid protein (PLP) and DM20.⁹³ PLP and DM20 are major myelin components in the central nervous system, constituting approximately 50% and 30% of the total protein, respectively.⁹⁴ Conformational changes of the PLP/DM20 protein result in oligodendrocyte loss

due to endoplasmic reticulum stress-induced apoptosis, while excessive PLP (gene duplications) may accumulate in the late endosomes and lead to oligodendrocyte arrested maturation, dysfunction and loss of the protein.⁹⁵ Null mutations result in a lack of synthesis of the protein, leading to formation of compact myelin lacking PLP.⁹⁵ Considering the role of this protein within myelin, it is no surprise that a defect in this protein disturbs myelination. It is, however, important to realize that the process of myelination is complex and depends on numerous processes, involving oligodendrocyte progenitor proliferation, migration and differentiation, and normal function and interaction of oligodendrocytes, neurons and astrocytes.^{96,97} This whole process is regulated by several signaling pathways, transcription and growth factors, epigenetic factors, DNA methylation and non-coding RNAs.^{96,97} This extensive list of potential candidate genes and proteins involved makes gene finding for both classified and unclassified hypomyelination disorders extremely difficult. Moreover, genes involved in DNA repair mechanisms; *ERCC6* and *ERCC8* in Cockayne syndrome (MIM 216400), and *ERCC2*, *ERCC3*, *GTF2H5*, and *MPLKIP* in patients with trichothiodystrophy with hypersensitivity to sunlight (MIM 601675 and MIM 616395) are also associated with hypomyelination, making it even more complex. In September 2011, the molecular cause of 4H syndrome,^{23,89} one of the most prevalent hypomyelinating disorders, was identified.⁹⁸ Patients had recessive mutations in *POLR3A* or *POLR3B*, encoding the largest and second largest subunits of RNA Polymerase III (Pol III), RPC1 and RPC2, respectively, extending the list of potential genetic possibilities.^{34,35}

We expected the unbiased gene search approach of WES to be of great benefit for patients with hypomyelination of unknown origin. As shown by Steenweg *et al.*, disease classification based on MRI patterns is also a reliable method in patients with hypomyelination.¹⁹ One of the groups with a novel hypomyelination pattern and without molecular cause (HEMS) identified by Steenweg *et al.* would be an excellent cohort for the application of WES.

CONTENT OF THIS THESIS

The elucidation of the molecular bases of unclassified leukodystrophies is extremely important for patients and families because this means a DNA-confirmed diagnosis, information, prognosis and options for family planning (e.g. carrier testing, prenatal or preimplantation genetic diagnosis). Gene discovery is also the essential starting point for better insight into the white matter components and their role in disease mechanisms. Subsequently, new treatment options can be explored depending on the defect identified.

The aim of this thesis is to classify novel leukodystrophies among the unclassified ones by MRI pattern recognition analysis and to identify their underlying genetic defect by using WES.

The thesis is divided into four parts. The first three parts are classified according to the genes identified.

- I Expansion of the phenotypic spectrum of a known disorder**
- II Novel disease entity associated with a known gene**
- III Novel disorder associated with a gene previously not linked to a human disorder or clear phenotype**
- IV Update on leukodystrophies**

REFERENCES

1. van der Knaap MS and Valk J. Myelin and White Matter. In: *Magnetic Resonance of Myelination and Myelin Disorders*. Heidelberg: Springer; 2005.p. 1-19.
2. van der Knaap MS and Valk J. *Magnetic Resonance of Myelination and Myelin Disorders*. Heidelberg: Springer; 2005.
3. Bonkowsky JL, Nelson C, Kingston JL, Filloux FM, Mundorff MB, Srivastava R. The burden of inherited leukodystrophies in children. *Neurology* 2010;75:718-725.
4. Lyon G, Fattal-Valevski A, Kolodny EH. Leukodystrophies: clinical and genetic aspects. *Top Magn Reson Imaging* 2006;17:219-242.
5. Steenweg ME, Vanderver A, Ceulemans B, et al. Novel infantile-onset leukoencephalopathy with high lactate level and slow improvement. *Arch Neurol* 2012;69:718-722.
6. Vanderver A, Prust M, Tonduti D, et al. Case definition and classification of leukodystrophies and leukoencephalopathies. *Mol Genet Metab* 2015;114:494-500.
7. Carswell R. *Pathological anatomy. Illustrations of the elementary forms of disease*. London: Longman, Orme, Brown, Green & Longman; 1838.
8. Heubner O. Über diffuse Hirnsclerose. *Charité Ann* 1897;22:298-310.
9. Neuburger K. Zur histopathologie der multiplen sklerose im kindesalter. *Z Neurol* 1922;76:384-414.
10. van der Knaap MS and Valk J. Classification of myelin disorders. In: *Magnetic Resonance of Myelination and Myelin Disorders*. Heidelberg: Springer; 2005.p. 20-24.
11. Young IR, Hall AS, Pallis CA, Legg NJ, Bydder GM, Steiner RE. Nuclear magnetic resonance imaging of the brain in multiple sclerosis. *Lancet* 1981;2:1063-1066.
12. van der Knaap MS, Valk J, de Neeling N, Nauta JJ. Pattern recognition in magnetic resonance imaging of white matter disorders in children and young adults. *Neuroradiology* 1991;33:478-493.
13. van der Knaap MS, Breiter SN, Naidu S, Hart AA, Valk J. Defining and categorizing leukoencephalopathies of unknown origin: MR imaging approach. *Radiology* 1999;213:121-133.
14. Miller DH, Robb SA, Ormerod IE, et al. Magnetic resonance imaging of inflammatory and demyelinating white-matter diseases of childhood. *Dev Med Child Neurol* 1990;32:97-107.
15. Barkovich AJ, Kjos BO, Jackson DE, Jr., Norman D. Normal maturation of the neonatal and infant brain: MR imaging at 1.5 T. *Radiology* 1988;166:173-180.
16. Barkovich AJ. Concepts of myelin and myelination in neuroradiology. *AJNR Am J Neuroradiol* 2000;21:1099-1109.
17. van der Knaap MS and Valk J. Myelination and Retarded Myelination. In: *Magnetic Resonance of Myelination and Myelin Disorders*. Heidelberg: Springer; 2005.p. 37-65.
18. Schiffmann R and van der Knaap MS. Invited article: an MRI-based approach to the diagnosis of white matter disorders. *Neurology* 2009;72:750-759.
19. Steenweg ME, Vanderver A, Blaser S, et al. Magnetic resonance imaging pattern recognition in hypomyelinating disorders. *Brain* 2010;133:2971-2982.
20. van der Knaap MS and Valk J. Diffusion-Weighted Imaging. In: *Magnetic Resonance of Myelination and Myelin Disorders*. Heidelberg: Springer; 2005.p. 834-853.
21. van der Knaap MS and Valk J. Maple Syrup Urine Disease. In: *Magnetic Resonance of Myelination and Myelin Disorders*. Heidelberg: Springer; 2005.p. 311-320.
22. van der Knaap MS and Valk J. Megalencephalic Leukoencephalopathy with Subcortical Cysts. In: *Magnetic Resonance of Myelination and Myelin Disorders*. Heidelberg: Springer; 2005.p. 442-450.
23. Wolf NI, Harting I, Boltshauser E, et al. Leukoencephalopathy with ataxia, hypodontia, and hypomyelination. *Neurology* 2005;64:1461-1464.
24. van der Knaap MS, Barth PG, Stroink H, et al. Leukoencephalopathy with swelling and a discrepantly mild clinical course in eight children. *Ann Neurol* 1995;37:324-334.
25. van der Knaap MS, van der Voorn P, Barkhof F, et al. A new leukoencephalopathy with brainstem and spinal cord involvement and high lactate. *Ann Neurol* 2003;53:252-258.
26. van der Knaap MS, Naidu S, Pouwels PJ, et al. New syndrome characterized by hypomyelination with atrophy of the basal ganglia and cerebellum. *AJNR Am J Neuroradiol* 2002;23:1466-1474.
27. van der Knaap MS, Barth PG, Gabreels FJ, et al. A new leukoencephalopathy with vanishing white matter. *Neurology* 1997;48:845-855.
28. Schiffmann R, Moller JR, Trapp BD, et al. Childhood ataxia with diffuse central nervous system hypomyelination. *Ann Neurol* 1994;35:331-340.

29. Leegwater PA, Konst AA, Kuyt B, et al. The gene for leukoencephalopathy with vanishing white matter is located on chromosome 3q27. *Am J Hum Genet* 1999;65:728-734.
30. Leegwater PA, Vermeulen G, Konst AA, et al. Subunits of the translation initiation factor eIF2B are mutant in leukoencephalopathy with vanishing white matter. *Nat Genet* 2001;29:383-388.
31. Leegwater PA, Yuan BQ, van der Steen J, et al. Mutations of MLC1 (KIAA0027), encoding a putative membrane protein, cause megalencephalic leukoencephalopathy with subcortical cysts. *Am J Hum Genet* 2001;68:831-838.
32. Zara F, Biancheri R, Bruno C, et al. Deficiency of hyccin, a newly identified membrane protein, causes hypomyelination and congenital cataract. *Nat Genet* 2006;38:1111-1113.
33. Scheper GC, van der Kloot T, van Andel RJ, et al. Mitochondrial aspartyl-tRNA synthetase deficiency causes leukoencephalopathy with brain stem and spinal cord involvement and lactate elevation. *Nat Genet* 2007;39:534-539.
34. Tetreault M, Choquet K, Orcesi S, et al. Recessive mutations in POLR3B, encoding the second largest subunit of Pol III, cause a rare hypomyelinating leukodystrophy. *Am J Hum Genet* 2011;89:652-655.
35. Bernard G, Chouery E, Putorti ML, et al. Mutations of POLR3A encoding a catalytic subunit of RNA polymerase Pol III cause a recessive hypomyelinating leukodystrophy. *Am J Hum Genet* 2011;89:415-423.
36. Margulies M, Egholm M, Altman WE, et al. Genome sequencing in microfabricated high-density picolitre reactors. *Nature* 2005;437:376-380.
37. Shendure J and Ji H. Next-generation DNA sequencing. *Nat Biotechnol* 2008;26:1135-1145.
38. Ng SB, Turner EH, Robertson PD, et al. Targeted capture and massively parallel sequencing of 12 human exomes. *Nature* 2009;461:272-276.
39. Weiss MM, Van der Zwaag B, Jongbloed JD, et al. Best practice guidelines for the use of next-generation sequencing applications in genome diagnostics: a national collaborative study of Dutch genome diagnostic laboratories. *Hum Mutat* 2013;34:1313-1321.
40. Buermans HP and den Dunnen JT. Next generation sequencing technology: Advances and applications. *Biochim Biophys Acta* 2014;1842:1932-1941.
41. Glenn TC. Field guide to next-generation DNA sequencers. *Mol Ecol Resour* 2011;11:759-769.
42. Ng SB, Buckingham KJ, Lee C, et al. Exome sequencing identifies the cause of a mendelian disorder. *Nat Genet* 2010;42:30-35.
43. Boycott KM, Vanstone MR, Bulman DE, MacKenzie AE. Rare-disease genetics in the era of next-generation sequencing: discovery to translation. *Nat Rev Genet* 2013;14:681-691.
44. Rademakers R, Baker M, Nicholson AM, et al. Mutations in the colony stimulating factor 1 receptor (CSF1R) gene cause hereditary diffuse leukoencephalopathy with spheroids. *Nat Genet* 2011;44:200-205.
45. Steenweg ME, Ghezzi D, Haack T, et al. Leukoencephalopathy with thalamus and brainstem involvement and high lactate 'LTBL' caused by EARS2 mutations. *Brain* 2012;135:1387-1394.
46. Gilissen C, Hoischen A, Brunner HG, Veltman JA. Disease gene identification strategies for exome sequencing. *Eur J Hum Genet* 2012;20:490-497.
47. Wang JL, Yang X, Xia K, et al. TGM6 identified as a novel causative gene of spinocerebellar ataxias using exome sequencing. *Brain* 2010;133:3510-3518.
48. van Berge L, Hamilton EM, Linnankivi T, et al. Leukoencephalopathy with brainstem and spinal cord involvement and lactate elevation: clinical and genetic characterization and target for therapy. *Brain* 2014;137:1019-1029.
49. Isohanni P, Linnankivi T, Buzkova J, et al. DARS2 mutations in mitochondrial leukoencephalopathy and multiple sclerosis. *J Med Genet* 2010;47:66-70.
50. Norton N, Li D, Rieder MJ, et al. Genome-wide studies of copy number variation and exome sequencing identify rare variants in BAG3 as a cause of dilated cardiomyopathy. *Am J Hum Genet* 2011;88:273-282.
51. Ng SB, Bigham AW, Buckingham KJ, et al. Exome sequencing identifies MLL2 mutations as a cause of Kabuki syndrome. *Nat Genet* 2010;42:790-793.
52. Botstein D and Risch N. Discovering genotypes underlying human phenotypes: past successes for mendelian disease, future approaches for complex disease. *Nat Genet* 2003;33 Suppl:228-237.
53. Majewski J, Schwartzentruber J, Lalonde E, Montpetit A, Jabado N. What can exome sequencing do for you? *J Med Genet* 2011;48:580-589.

54. Skladal D, Halliday J, Thorburn DR. Minimum birth prevalence of mitochondrial respiratory chain disorders in children. *Brain* 2003;126:1905-1912.
55. Smeitink J, van den Heuvel L, DiMauro S. The genetics and pathology of oxidative phosphorylation. *Nat Rev Genet* 2001;2:342-352.
56. Leigh D. Subacute necrotizing encephalomyelopathy in an infant. *J Neurol Neurosurg Psychiatry* 1951;14:216-221.
57. Morato L, Bertini E, Verrigni D, et al. Mitochondrial dysfunction in central nervous system white matter disorders. *Glia* 2014;62:1878-1894.
58. Court FA and Coleman MP. Mitochondria as a central sensor for axonal degenerative stimuli. *Trends Neurosci* 2012;35:364-372.
59. Schoenfeld R, Wong A, Silva J, et al. Oligodendroglial differentiation induces mitochondrial genes and inhibition of mitochondrial function represses oligodendroglial differentiation. *Mitochondrion* 2010;10:143-150.
60. Silva JM, Wong A, Carelli V, Cortopassi GA. Inhibition of mitochondrial function induces an integrated stress response in oligodendroglia. *Neurobiol Dis* 2009;34:357-365.
61. Ziabreva I, Campbell G, Rist J, et al. Injury and differentiation following inhibition of mitochondrial respiratory chain complex IV in rat oligodendrocytes. *Glia* 2010;58:1827-1837.
62. Clayton DA and Vinograd J. Circular dimer and catenate forms of mitochondrial DNA in human leukaemic leucocytes. *Nature* 1967;216:652-657.
63. Anderson S, Bankier AT, Barrell BG, et al. Sequence and organization of the human mitochondrial genome. *Nature* 1981;290:457-465.
64. Goto Y, Nonaka I, Horai S. A mutation in the tRNA(Leu)(UUR) gene associated with the MELAS subgroup of mitochondrial encephalomyopathies. *Nature* 1990;348:651-653.
65. Barkovich AJ, Good WV, Koch TK, Berg BO. Mitochondrial disorders: analysis of their clinical and imaging characteristics. *AJNR Am J Neuroradiol* 1993;14:1119-1137.
66. Wallace DC, Singh G, Lott MT, et al. Mitochondrial DNA mutation associated with Leber's hereditary optic neuropathy. *Science* 1988;242:1427-1430.
67. van der Knaap MS and Valk J. Leber Hereditary Optic Neuropathy. In: *Magnetic Resonance of Myelination and Myelin Disorders*. Heidelberg: Springer; 2015.p. 212-220.
68. Zeviani M, Moraes CT, DiMauro S, et al. Deletions of mitochondrial DNA in Kearns-Sayre syndrome. *Neurology* 1988;38:1339-1346.
69. Kamata Y, Mashima Y, Yokoyama M, Tanaka K, Goto Y, Oguchi Y. Patient with Kearns-Sayre syndrome exhibiting abnormal magnetic resonance image of the brain. *J Neuroophthalmol* 1998;18:284-288.
70. Bourgeron T, Rustin P, Chretien D, et al. Mutation of a nuclear succinate dehydrogenase gene results in mitochondrial respiratory chain deficiency. *Nat Genet* 1995;11:144-149.
71. Nishino I, Spinazzola A, Hirano M. Thymidine phosphorylase gene mutations in MNGIE, a human mitochondrial disorder. *Science* 1999;283:689-692.
72. Shoubridge EA. Nuclear genetic defects of oxidative phosphorylation. *Hum Mol Genet* 2001;10:2277-2284.
73. Loeffen JL, Smeitink JA, Trijbels JM, et al. Isolated complex I deficiency in children: clinical, biochemical and genetic aspects. *Hum Mutat* 2000;15:123-134.
74. Carroll J, Fearnley IM, Skehel JM, Shannon RJ, Hirst J, Walker JE. Bovine complex I is a complex of 45 different subunits. *J Biol Chem* 2006;281:32724-32727.
75. Taylor RW, Pyle A, Griffin H, et al. Use of whole-exome sequencing to determine the genetic basis of multiple mitochondrial respiratory chain complex deficiencies. *JAMA* 2014;312:68-77.
76. Palmieri F. Diseases caused by defects of mitochondrial carriers: a review. *Biochim Biophys Acta* 2008;1777:564-578.
77. Delonlay P, Rotig A, Sarnat HB. Respiratory chain deficiencies. *Handb Clin Neurol* 2013;113:1651-66.:1651-1666.
78. Rodenburg RJ. Biochemical diagnosis of mitochondrial disorders. *J Inher Metab Dis* 2011;34:283-292.
79. Rodenburg RJ, Schoonderwoerd GC, Tiranti V, et al. A multi-center comparison of diagnostic methods for the biochemical evaluation of suspected mitochondrial disorders. *Mitochondrion* 2013;13:36-43.
80. Lerman-Sagie T, Leshinsky-Silver E, Watemberg N, Luckman Y, Lev D. White matter involvement in mitochondrial diseases. *Mol Genet Metab* 2005;84:127-136.

81. van der Knaap MS and Valk J. Mitochondrial Neurogastrointestinal Encephalopathy. In: Magnetic Resonance of Myelination and Myelin Disorders. Heidelberg: Springer; 2005.p. 221-223.
82. van der Knaap MS and Valk J. Kearns-Sayre syndrome. In: Magnetic Resonance of Myelination and Myelin Disorders. Heidelberg: Springer; 2005.p. 215-220.
83. Thorburn DR and Rahman S. Mitochondrial DNA-Associated Leigh Syndrome and NARP. University of Washinton 2014;1993-2015.
84. Tucker EJ, Compton AG, Thorburn DR. Recent advances in the genetics of mitochondrial encephalopathies. *Curr Neurol Neurosci Rep* 2010;10:277-285.
85. Lopez MF, Kristal BS, Chernokalskaya E, et al. High-throughput profiling of the mitochondrial proteome using affinity fractionation and automation. *Electrophoresis* 2000;21:3427-3440.
86. McCormick E, Place E, Falk MJ. Molecular genetic testing for mitochondrial disease: from one generation to the next. *Neurotherapeutics* 2013;10:251-261.
87. Pelizaeus F. Über eine eigenartige familiäre Entwicklungshemmung vornehmlich auf motorischem Gebiet. *Archiv für psychiatrie und Nervenkrankheiten* 1899;31:100-104.
88. Merzbacher L. Eine eigenartige familiar-hereditäre Erkrankungsform (aplasia axialis extra corticalis congenita). *Zeitschrift für die gesamte Neurologie und Psychiatrie* 1910;1-38.
89. Wolf NI, Harting I, Innes AM, et al. Ataxia, delayed dentition and hypomyelination: a novel leukoencephalopathy. *Neuropediatrics* 2007;38:64-70.
90. van Hoof F and Hers HG. Mucopolysaccharidosis by absence of alpha-fucosidase. *Lancet* 1968;1:1198.
91. Steenweg ME, Wolf NI, Schieving JH, et al. Novel hypomyelinating leukoencephalopathy affecting early myelinating structures. *Arch Neurol* 2012;69:125-128.
92. Pouwels PJ, Vanderver A, Bernard G, et al. Hypomyelinating leukodystrophies: Translational research progress and prospects. *Ann Neurol* 2014;76:5-19.
93. Gencic S, Abuelo D, Ambler M, Hudson LD. Pelizaeus-Merzbacher disease: an X-linked neurologic disorder of myelin metabolism with a novel mutation in the gene encoding proteolipid protein. *Am J Hum Genet* 1989;45:435-442.
94. Eng LF, Chao FC, Gerstl B, Pratt D, Tavaststjerna MG. The maturation of human white matter myelin. Fractionation of the myelin membrane proteins. *Biochemistry* 1968;7:4455-4465.
95. Inoue K. PLP1-related inherited dysmyelinating disorders: Pelizaeus-Merzbacher disease and spastic paraplegia type 2. *Neurogenetics* 2005;6:1-16.
96. Emery B. Regulation of oligodendrocyte differentiation and myelination. *Science* 2010;330:779-782.
97. Mitew S, Hay CM, Peckham H, Xiao J, Koenning M, Emery B. Mechanisms regulating the development of oligodendrocytes and central nervous system myelin. *Neuroscience* 2014;276:29-47:29-47.
98. Cayami FK, La Piana R, van Spaendonk RM, et al. POLR3A and POLR3B Mutations in Unclassified Hypomyelination. *Neuropediatrics* 2015;46:221-228.



Expansion of the phenotypic spectrum of a known disorder

Chapter 2

Altered *PLP1* splicing causes hypomyelination of early myelinating structures

Sietske H. Kevelam,* Jennifer R. Taube,* Rosalina M.L. van Spaendonk, Enrico Bertini, Karen Sperle, Mark Tarnopolsky, Davide Tonduti, Enza Maria Valente, Lorena Travaglini, Erik A. Siermans, Geneviève Bernard, Coriene E. Catsman-Berrevoets, Clara D.M. van Karnebeek, John R. Østergaard, Richard L. Friederich, Mahmoud Fawzi Elsaid, Jolanda H. Schieving, Maja Tarailo-Graovac, Simona Orcesi, Marjan E. Steenweg, Carola G.M. van Berkel, Quinten Waisfisz, Truus E.M. Abbink, Marjo S. van der Knaap, Grace M. Hobson,** and Nicole I. Wolf **

* These authors share first authorship.

** These authors share senior authorship.

ABSTRACT

Objective

The objective of this study was to investigate the genetic etiology of the X-linked disorder “Hypomyelination of Early Myelinating Structures” (HEMS).

Methods

We included 16 patients from 10 families diagnosed with HEMS by brain MRI criteria. Exome sequencing was used to search for causal mutations. In silico analysis of effects of the mutations on splicing and RNA folding was performed. In vitro gene splicing was examined in RNA from patients’ fibroblasts and an immortalized immature oligodendrocyte cell line after transfection with mutant minigene splicing constructs.

Results

All patients had unusual hemizygous mutations of *PLP1* located in exon 3B (one deletion, one missense and two silent), which is spliced out in isoform *DM20*, or in intron 3 (five mutations). The deletion led to truncation of *PLP1*, but not *DM20*. Four mutations were predicted to affect *PLP1/DM20* alternative splicing by creating exonic splicing silencer motifs or new splice donor sites or by affecting the local RNA structure of the *PLP1* splice donor site. Four deep intronic mutations were predicted to destabilize a long-distance interaction structure in the secondary *PLP1* RNA fragment involved in regulating *PLP1/DM20* alternative splicing. Splicing studies in fibroblasts and transfected cells confirmed a decreased *PLP1/DM20* ratio.

Interpretation

Brain structures that normally myelinate early are poorly myelinated in HEMS, while they are the best myelinated structures in Pelizaeus–Merzbacher disease, also caused by *PLP1* alterations. Our data extend the phenotypic spectrum of *PLP1*-related disorders indicating that normal *PLP1/DM20* alternative splicing is essential for early myelination and support the need to include intron 3 in diagnostic sequencing.

INTRODUCTION

Among the childhood leukodystrophies, hypomyelinating disorders constitute a large, highly heterogeneous group of patients, many of whom remain without a genetically confirmed diagnosis.¹⁻⁴ Using magnetic resonance imaging (MRI) pattern recognition analysis, we previously identified a novel hypomyelinating disorder in four male patients in which hypomyelination is specifically pronounced in early myelinating structures.¹ As this distribution of hypomyelination is different from other hypomyelinating disorders, in which these early myelinating structures as a rule contain more myelin than the later myelinating structures,^{4,5} we proposed a new disease called “Hypomyelination of Early Myelinating Structures” (HEMS).¹ Family history suggested X-linked inheritance, supported by the report of two brothers with the same clinical picture and MRI pattern.^{1,6} The clinical phenotype of HEMS patients resembled that of other well-known hypomyelinating disorders, with onset of symptoms in late infancy, including ataxia and increasing spasticity, and relatively preserved cognition.^{1,4,7-9} We hypothesized that HEMS could be caused by mutations of an X-chromosomal gene involved in the regulation of early myelination.^{1,6} Diagnostic Sanger sequencing for known causes of hypomyelination, including Pelizaeus–Merzbacher disease (PMD), caused by X-linked *PLP1* mutations, and Pelizaeus–Merzbacher-like disease (PMLD), caused by *GJC2* mutations, had been unrevealing.¹

The combination of MRI pattern recognition analysis, which is used for the categorization of homogeneous groups of patients with an unclassified white matter disorder and exome sequencing has been shown to be successful in identifying novel disease genes and new phenotypes associated with known disease genes.¹⁰⁻¹² In this study, we used the same approach and ascertained mutations in a specific region of *PLP1* that had initially not been identified. *PLP1* is located on the X-chromosome, contains seven exons and encodes both proteolipid protein 1 (PLP1) and its smaller isoform DM20 that is derived by the use of an alternative splice donor site within exon 3.¹³ In all HEMS patients, the *PLP1* mutations are located either in the PLP1-specific region encoded by exon 3B that is spliced out in DM20 or in intron 3. Using *in silico* splicing prediction programs, *in silico* analysis of predicted secondary RNA structures, and *in vitro* analysis of gene splicing in RNA prepared from patients’ fibroblasts and transfection studies, we show that these mutations play a role in alternative splicing of *PLP1*.

PATIENTS AND METHODS

MRI studies and clinical examination

We included 16 male patients from 10 unrelated families (Table 1). Thirteen of the 16 patients were included based on their specific MRI pattern compatible with HEMS.¹ Seven of these 13 patients were identified from our MRI-database of over 3000 cases with an unclassified leukoencephalopathy using MRI pattern recognition analysis,³ and six patients were previously identified and described (patients 8, 9, 11, and 12,¹ and patients 4 and 10⁶). S. H. K. and N. I. W. evaluated the MRIs according to a published protocol.³ Three affected male siblings (patients 5, 15, and 16) were included without MR images. Clinical and laboratory investigations were retrospectively reviewed. Diagnostic Sanger sequencing of *PLP1* in patients 1, 2, 3, 8, 9, 11, 12, and 14 had previously been performed in diverse laboratories and reported unrevealing.

Informed consent

We received approval of the ethical standards committee for our gene identification research on patients with unclassified leukoencephalopathies at the VU University Medical Center in Amsterdam. All guardians of the patients participating in this study gave written informed consent. Approval was also obtained from the Institutional Review Board at Nemours/Alfred I. duPont Hospital for Children and the BC Children's Hospital, University of British Columbia, Canada, and informed consent was obtained as appropriate on the patients studied at these institutions.

Whole-exome sequencing

Whole-exome sequencing (WES) on DNA from patients 5 and 11 (brothers), their mother, and patient 9, was performed using SeqCap EZ Human Library v3.0 kit (Nimblegen, Madison, WI, US) on a HiSeq2000 (Illumina, San Diego, CA). Coverage of at least 20× was reached for >96% of the targeted regions. Average sequencing depth ranged between 58 and 71. Data analysis was performed as described previously.¹⁴ For three families, WES had been initiated in three other institutes, and available WES data were used for identification of mutations after recognition of the gene.

Targeted sequencing of the X-chromosome exome

X-chromosome exome sequencing on DNA from patients 4 and 10 (brothers), 5 and 11 (brothers), 8 (including parents), 9 and 12 (including parents), was performed using SureSelectXT X-chromosome kit (Agilent, Santa Clara, CA, US) on a HiSeq2000 (Illumina, San Diego, CA). For all samples, coverage of at least 30× was reached for >80% of the targeted regions. Average sequencing depth ranged between 335 and 645.

Data analysis was performed as described previously.¹⁵

Validation and detection of *PLP1* variants

Validation and segregation of the identified *PLP1* variants in patients 1, 4, 5, and 7–12 by exome sequencing analysis was performed using standard Sanger sequencing. Primers were designed (Primer 3 V.0.4.0)^{16,17} using reference sequence: *PLP1*, NM_000533.3. In patient 6, all 7 exons and intron–exon boundaries of *PLP1* were sequenced; in the remaining patients, only exon 3 and intron 3 of *PLP1* were sequenced using suitable primers (available upon request).

In silico analysis of effects of the identified variants

Pathogenicity of missense variants was predicted using SIFT,¹⁸ PolyPhen-2¹⁹ and Mutation Taster.²⁰ Conservation of nucleotides was analyzed using Phastcons scores, obtained via Alamut version 2.4.

In silico splicing analysis

The predicted effects of identified variants in *PLP1* on splicing were analyzed using different programs (details see in Data S1). A deviation of $\geq 10\%$ from the normal score was considered as a change likely to affect splicing if present in at least three splice site prediction tools²¹ (indicated by “yes” in Table 1). A deviation of $\geq 10\%$ from the normal score in less than 3 splice site predictions tools was considered an inconclusive result. Changes of $< 10\%$ were regarded as not significant and not reported. Predicted changes of number of exonic splice enhancer and silencer motifs were determined using default threshold values.

In silico analysis of secondary *PLP1* RNA folding

The mfold program accessed via their web server with standard parameters was used to analyze *PLP1* normal and mutant RNA sequences for changes in the secondary pre-mRNA structure and stability (<http://mfold.rna.albany.edu/?q=mfold/RNA-Folding-Form>).²² Using mfold, the four intronic mutations c.453+159G>A, c.453+164G>A, c.454–312C>G, and c.454–314T>G were analyzed using mutant RNA sequences including two regions within intron 3 of *PLP1*: 20 bases from c.453+150 to +169 and 20 bases from c.454–326 to –307, separated by 15 random bases (N_{15}), as previously described by us.²³ The four mutations c.404T>G, c.436C>T, c.441A>T, and c.453+7A>G were analyzed using mutant *PLP1* RNA sequences comprising exon 3 (c.192–c.453) and 40 flanking intronic nucleotides. As a measurement for the splice donor site accessibility by the spliceosome, conformational changes of the *PLP1* splice donor site in exon 3B and the *DM20* splice donor site in exon 3A, were visually examined and quantified by

counting the nucleotides of the consensus *PLP1* splice donor site (c.451 to c.453+6: AAGGUGAUC) that were predicted to form base pairs.

***PLP1/DM20* alternative splicing studies**

Minigene splicing construct transfection assay

The effects of three *PLP1* mutations c.436C>T, c.441A>T, and c.453+7G>A on *PLP1/DM20* alternative splicing were individually investigated in a minigene splicing reporter construct transfection assay using Oli-neu cells, an immortalized cell line representing immature oligodendrocytes, as previously described, with modified reverse transcription (RT) (details in Data S1).^{23,24}

Skin fibroblast cultures

PLP1/DM20 alternative splicing was investigated in skin fibroblasts from patient 6 harboring the c.453+7A>G intronic mutation. In addition, skin fibroblasts were available from a patient described in 1991 with the c.441A>T silent mutation,²⁵ the same as identified in patient 8 from our HEMS cohort. RT-PCR analysis of RNA prepared from cultured skin fibroblasts was performed as previously described with modified RT reaction (details in Data S1).²³

RESULTS

MRI findings

Detailed MRI findings of all patients in our cohort except three affected siblings are provided in Table S1 and Figures 1 and 2. These patients had the characteristic MRI features corresponding to the previously described disorder “HEMS”.¹ On initial MRIs, patients had mild T₂ hyperintensity of the medulla oblongata, the pons, especially at the border with the medulla oblongata, and the hilus of the dentate nucleus, with variable T₂ hyperintensity of the peridentate white matter, indicating hypomyelination of these regions (Figure 1, A and B and Figure 2, I and J). Mild T₂ hyperintensity of the optic radiation, periventricular white matter and parietal white matter was observed in all patients (Figure 1, C and Figure 2, K), with extensions into the subcortical white matter under the pericentral cortex in eight patients (Figure 1, D and Figure 2, L). Patients 1 and 6 had more extensive subcortical white matter hypomyelination. All patients had alternating T₂ hyperintense–hypointense–hyperintense stripes in the posterior limb of the internal capsule (Figure 1, C and Figure 2, K). The thalamus had a mildly elevated T₂ signal, except for its ventrolateral part, which was darker, a configuration that is normally seen in neonates (Figure 1, C and

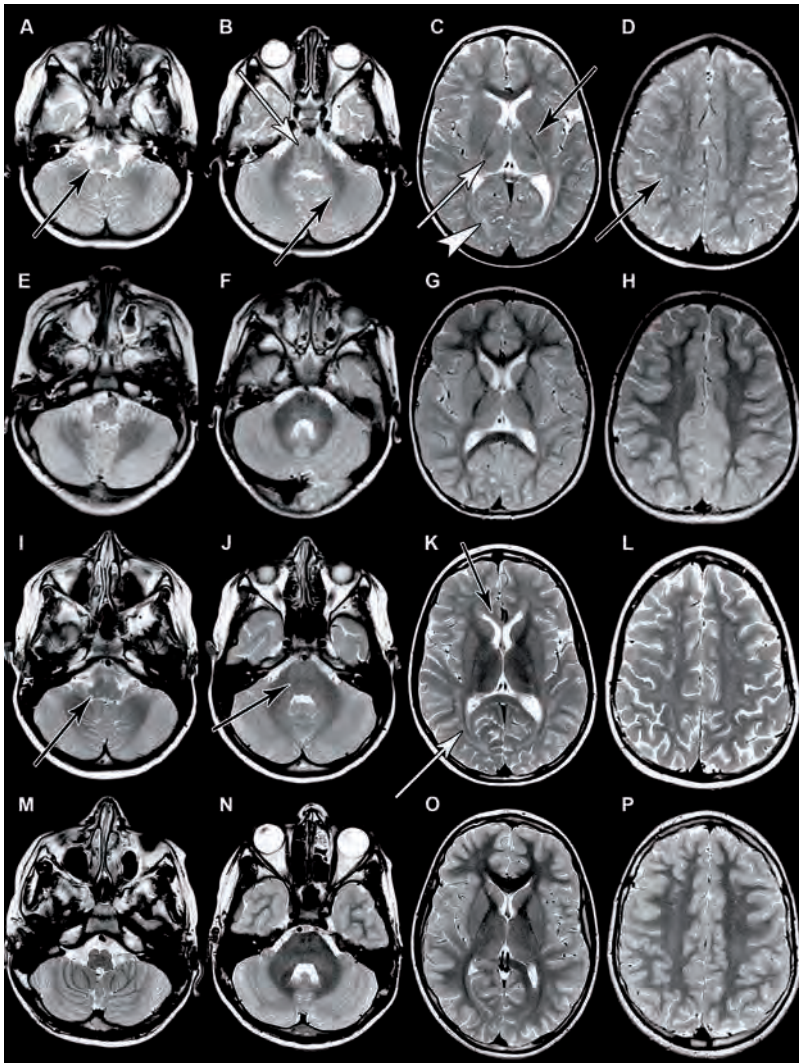


Figure 1. MRI of HEMS patients.

Initial MRIs of patient 9 (A–D, age 3 years), and of an age-matched control (E–H, 2.5 years) and follow-up MRIs of patient 9 (I–L, age 12.4 years), and of an age-matched control (M–P, 12 years). All images are axial T_2 -weighted. MRIs of patient 9 show mild T_2 hyperintensity of the medulla oblongata (A, arrow), the pons (B, white arrow) and the hilus of the dentate nucleus (B, black arrow). The thalamus is mildly T_2 hyperintense, except for its ventrolateral part, which is dark (C, white arrow). The posterior limb of the internal capsule shows alternating hyperintense–hypointense–hyperintense stripes (C, black arrow). There is mild T_2 hyperintensity of the optic radiation (C, white arrowhead) and the periventricular white matter that extends into the central subcortical white matter (D, black arrow). At later stages, the T_2 signal in the medulla and pons improves (I and J), but the T_2 hyperintensity of the optic radiation (K, white arrow), the corpus callosum (K, black arrow) and the periventricular white matter and subcortical white matter increases. Control images (E–H and M–P) show the normal myelination pattern with respect to age.

Figure 2, K). On follow-up, the T_2 signal abnormalities of the medulla oblongata and pons improved in four of the eight patients in whom repeat images were available, indicating progressing myelination (Figure 1, I and J). The periventricular and deep white matter and/or corpus callosum showed more extensive T_2 hyperintensity than before in seven of the eight patients, indicating myelin loss (Figure 1, K and L).

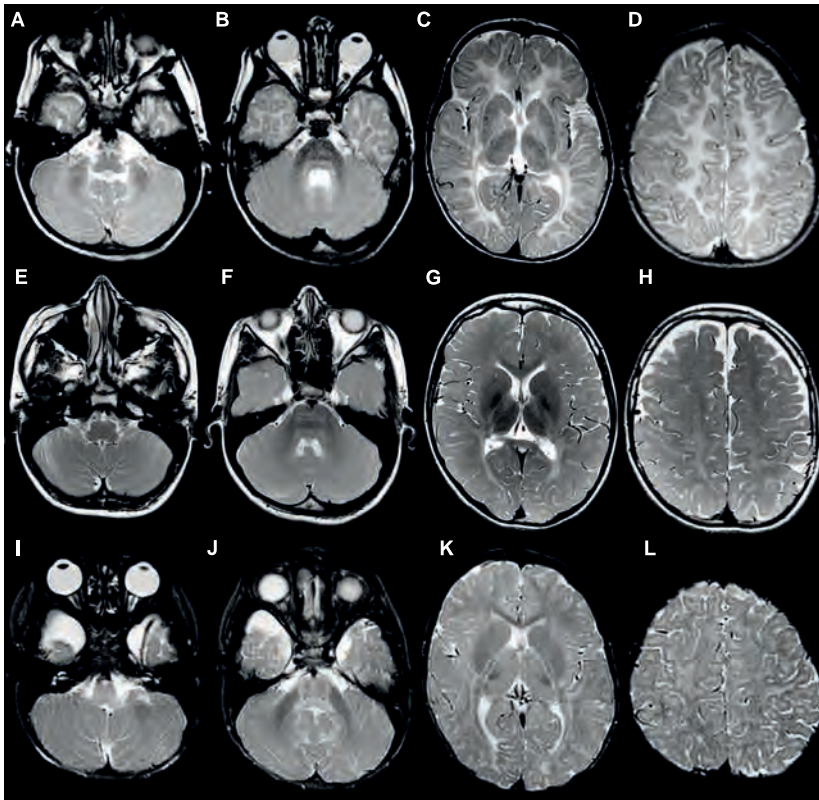


Figure 2. MRI of *PLP1*-related disorders.

MRI of a patient with: classic Pelizaeus–Merzbacher disease (PMD) harboring a *PLP1* duplication (A–D, age 23 months), Spastic Paraplegia type 2 (SPG2) with a frameshift mutation (c.263-delC, p.(Ala88Valfs*26)) (E–H, age 11.4 years) and patient 11 with hypomyelination of early myelinating structures (HEMS) harboring an intronic mutation (c.453+159G>A) (I–L, age 20 months). All MR images are axial T_2 -weighted. Note that in the patients with PMD (A and B) and SPG2 (E and F), the medulla oblongata and the pons show a normal dark T_2 signal, in contrast to the patient with HEMS (I and J), in whom these structures are mildly T_2 hyperintense. The alternating hyperintense–hypointense–hyperintense stripes in the posterior limb of the internal capsule seen commonly in HEMS patients (K) are not present in the patient with PMD (C) or SPG2 (G). All the three illustrated patients have T_2 hyperintensity of the periventricular white matter, deep white matter and subcortical white matter, which is diffuse and extensive in the patient with PMD (C and D), restricted in the patient with SPG2 (G and H), and intermediate in the patient with HEMS (K and L).

After identification of mutations in the gene *PLP1* (see below), two clinically asymptomatic female carriers (c.454–312C>G, age 40 years, and c.453+159G>A, age 53 years) underwent brain MRI, which demonstrated mild global atrophy of the cerebral hemispheres and diffuse mild T₂ hyperintensity of the supratentorial white matter (data not shown).

Clinical profiles and laboratory results

Detailed clinical characteristics are provided in Table S2. Twelve of the 16 patients presented with nystagmus in the first or second year of life. The other four patients presented first with cerebellar dysfunction or developmental delay. All patients continued to gain motor skills, but mostly delayed. All developed progressive spasticity of the legs and signs of cerebellar dysfunction. At last clinical follow-up, five patients (age range 3–12 years) could still walk without support, although they had an evident spastic-ataxic gait. Five patients used braces or a walker for ambulation, and five needed a wheelchair. One was still too young to judge his ability to walk. Cognitive capabilities were normal or mildly impaired. All female carriers were clinically normal. Nerve conduction studies performed in eight patients revealed normal motor and sensory conduction velocities in all except patient 1 who had delayed conduction velocities in his legs.

Genetic analysis

We first performed WES in two brothers and their mother and an unrelated patient. Under the hypothesis of an X-linked recessive inheritance model, we selected all rare hemizygous variants (variants with a minor allele frequency of ≤1% in known public control databases; 1000 Genomes, dbSNP137 and National Heart, Lung, and Blood Institute Exome Sequencing Project (<http://evs.gs.washington.edu/EVS/>), and absence from our in-house control samples), located on the X-chromosome. With this approach we were unable to identify a candidate gene. We subsequently performed targeted sequencing of the X-chromosome exome including four additional HEMS patients and parents. The same filtering strategy was used, and genes were selected if variants were present in at least two unrelated patients. This led us to the identification of one candidate gene: *PLP1* (MIM 300401), encoding PLP1 (shown in Figure 3, A). Two exonic variants were identified: a c.404T>G missense variant, predicting p.(Leu135Trp) and a c.441A>T silent variant. Manual analysis of the intron data revealed three variants located deep in intron 3. Coverage of two of these variants, c.454–312C>G and c.454–314T>G, was very poor for both the WES and the X-chromosome exome approach (<5 reads), while the c.453+159G>A variant was sufficiently covered with the X-chromosome exome (63–97 reads) (data not shown). In the nine remaining HEMS patients *PLP1* variants were identified either by Sanger sequencing or by WES data retrieved from other institutes.

In total, nine different *PLP1* variants were identified in 16 patients (10 families) (Table 1, Figure 3, B). All variants were located in exon 3B or intron 3 (Figure 3, A and B). The mutations were maternally inherited in five families and de novo in three families. In two families, the mother was not available for testing. However, multiple affected family members indicated obligate carriership.

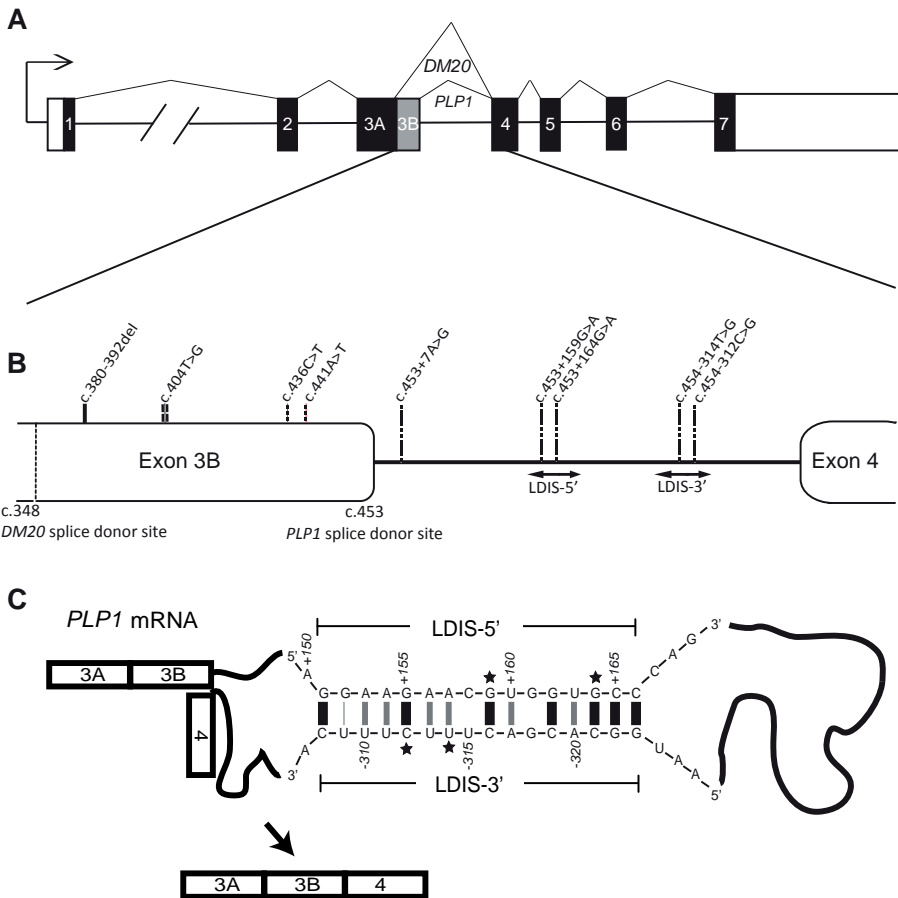


Figure 3. Overview of *PLP1* mutations and predicted secondary *PLP1* RNA structure.

This overview illustrates *PLP1* gene structure with its seven exons (black boxes) and the two alternative transcripts, *PLP1* or *DM20*, resulting from a splice donor site within exon 3 (A). Close-up of exon 3B and intron 3 is depicted in (B). All nine mutations found in our hypomyelination of early myelinating structures (HEMS) cohort are shown. The frameshift mutation is indicated with a black solid line, the two silent mutations with a dashed line and the single missense mutation with two striped lines. Intronic mutations are indicated with an interrupted line. The secondary *PLP1* RNA structure is displayed in (C), illustrating the formation of the predicted long-distance interaction (LDI) structure between LDIS-5' and LDIS-3' within intron 3. Mutated positions in our HEMS cohort are indicated with stars. Adapted from Taube et al.²³ with permission of Oxford University press.

Table 1. *PLP1* mutations, in silico predictions and *PLP1/DM20* ratio

Patients	c. DNA	Protein	Mother carrier	Nuc. conservation ¹	SIFT/Polyphe/Phen2/Mutation Taster	Missense prediction	In-silico predictions				In vitro studies	
							Predicted new splice sites ²	Predicted change of strength natural <i>PLP1</i> splice donor site ²	Splicing effects	Mfold analysis	Predicted conformational change <i>PLP1</i> splice donor site exon 3B	<i>PLP1/DM20</i> ratio of normal
1	c.380_392del	p.(Arg127Lys) ¹⁶	yes	1	n.a.	n.d.	n.d.	n.d.	n.d.	n.d.	n.d.	n.d.
4 ^{6,7} ,10 ^{6,7}	c.404T>G	p.(Leu135Trp)	yes	1	D/B/B	no	no	+2 ESS	n.d.	yes	n.d.	n.d.
13 ⁷ ,14 ⁷	c.436C>T	p.=	yes	1	n.a.	yes ⁸	no	+2 ESS	n.d.	no	0.18	n.d.
8 ^a	c.441A>T	p.=	no	1	n.a.	inconclusive ¹⁰	no	+1 ESS	n.d.	yes	0.14	0.01
6	c.453+7A>G	p.?	n.d.	1	n.a.	inconclusive ¹¹	Inconclusive ¹²	+1 ESE (sc35)	n.d.	yes	0.05	0.06
2 ¹³ ,3 ¹³ ,5 ⁷ ,11 ^{9,7} ,15 ¹³ ,16 ¹³	c.453+159G>A	p.?	2,3,7,15,16 n.d.;5&11 yes	1	n.a.	no	no	no	+5.1	n.d.	n.d.	n.d.
7	c.453+164G>A	p.?	no	1	n.a.	inconclusive ¹⁴	no	change strength ESE (sc35)	+5.9	n.d.	n.d.	n.d.
9 ⁹	c.454-312C>G	p.?	yes	1	n.a.	no	no	+3 ESS, +1 ESE (sc35)	+4.1	n.d.	n.d.	n.d.
12 ⁹	c.454-314T>G	p.?	no	1	n.a.	no	no	no	+1.6	n.d.	0.12 ¹⁵	n.d.

For a detailed description of methods and programs used see Data S11. c.DNA, complementary DNA; nuc., nucleotide; n.a., not applicable; n.d., not done; B, benign; D, damaging; LDIS-5; long-distance interaction site 5; LDIS-3; long-distance interaction site 3; SC35, serine/arginine-rich splicing factor 2.
¹Assessed using Phastcons scores (0 = no conservation, 1 = high conservation).
²Predicted new splice donor or acceptor sites. Yes = significant change, inconclusive = inconclusive change.
³Predicted change in number exonic splicing enhancers (ESE) motifs identified by ESE Finder 3.0.
⁴Predicted change in number exonic splicing silencer (ESS) motifs identified by FAS-ESS web server using the FAS-hex2 set.
⁵Difference of ΔG = minimal Gibbs energy, free energy, kcal/mole of the intra-intronic RNA structure fragment between the normal and mutant. Normal ΔG = -17.6 kcal/mole.
⁶Patients previously published by Tonduti et al.⁶
⁷Sibling pairs are as follows: 4 and 10; 5 and 11, and 13 and 14.
⁸Predicted strength of new splice donor site at c.434 of 87 by Human splice site finder (HSF) (normal range 0-100), 0.8 by NNSplice (normal range 0-1), 76.3 by Splice Site Finder (normal range 0-100), 0.8 confidence by Netgene2 (normal confidence range 0-1) and 3.4 by MaxEnt (normal range 0-12)
⁹Patients previously published by Steenweg et al.¹
¹⁰Predicted strength of new splice donor site at c.439 of 79, by HSF (normal range 0-100).
¹¹Predicted increase in potential acceptor splice site at c.453+15 strength of 45.7% (2.6-3.8) by MaxEnt (normal range 0-16)
¹²Predicted decrease of 21% (0.7-0.5) by NNSplice (normal range 0-1).
¹³Patients belong to the same family
¹⁴Predicted strength new splice donor site at c.453+161 of 2.3 by MaxEnt (normal range 0-12).
¹⁵Previously investigated and reported by us.²³

In silico analyses of effects of the identified *PLP1* variants

The c.380_392del variant was predicted to result in a frameshift p.(Arg127Lysfs*16) truncating *PLP1*, but not *DM20*. For the other eight identified *PLP1* variants, we performed several in silico bioinformatics prediction analyses to investigate pathogenicity. An overview of the results is depicted in Table 1.

In silico splicing analysis

Of the eight variants, only the silent c.436C>T change was predicted to have an effect on splice sites by creating a new splice donor site in exon 3B at position c.434. Analysis of splice regulatory elements showed that for all three exonic variants and the c.454–312C>G variant 1–3 new exonic splicing silencer motifs were predicted.

In silico analysis of secondary *PLP1* RNA folding

Using mfold, we previously found that two regions within intron 3 of *PLP1* form an intramolecular base-pairing interaction in the predicted secondary *PLP1* RNA structure and play an important role in the control of *PLP1/DM20* alternative splicing.²³ In our HEMS cohort, we found four variants in either of these two regions (Figure 3, B and C). The 5' region (c.453+151 to c.453+166) is referred to as the long-distance interaction (LDI) site 5' (LDIS-5') and the 3' region (c.454–323 to c.454–308) as the LDIS-3' (Figure 3, C). Mutations created in LDIS-5' and LDIS-3' sequences that were predicted to destabilize this secondary *PLP1* RNA structure (initial Gibbs free energy [ΔG] value less than -16.4 kcal/mole) decreased the ratio of alternatively spliced products *PLP1* to *DM20* in a minigene reporter system, while mutations of the central nonpairing bases, c.453+158 and c.454–315, and mutations that were predicted to maintain the secondary structure did not.²³ We investigated the effect of the four variants identified in our families, two in LDIS-5' (c.453+159G>A and c.453+164G>A) and two in LDIS-3' (c.454–312C>G and c.454–314T>G), on the LDI structure and found that in all cases the stability of the mutant LDI structures was predicted to be reduced ([ΔG] values of less than -16.4 kcal/mole) compared with the normal fragment ([ΔG of -17.6 kcal/mole]) (Figure S1).

Analysis of the predicted secondary *PLP1* RNA structures for the remaining four variants c.404T>G, c.436C>T, c.441A>T, and c.453+7A>G showed that all except the c.436C>T variant increased the stability of the local RNA structure of the *PLP1* splice donor site, while leaving the structure of the *DM20* splice donor site unchanged (Table S3). These predictions suggest that the *PLP1* splice donor site is more engaged in intramolecular base pairing in the mutated RNA fragments than in the normal RNA fragments.

***PLP1/DM20* alternative splicing studies in a minigene splicing construct assay**

In a reporter construct transfection assay,^{23,24} we investigated the effects of the c.436C>T, the c.441A>T, and the c.453+7A>G mutation on *PLP1/DM20* alternative splicing. These mutations resulted in a significant reduction in the *PLP1/DM20* ratio to 0.18 (c.436C>T), 0.14 (c.441A>T), and 0.05 (c.453+7A>G) of normal (Figure 4, A). We could not detect the potentially aberrantly spliced product from the new splice donor site predicted for the c.436C>T mutation. The effect of the c.454–314T>G mutation was previously reported by us and resulted in a *PLP1/DM20* ratio of 0.15 of normal.²³

***PLP1/DM20* alternative splicing studies in fibroblasts**

In patient fibroblasts, we investigated the effect of the c.441A>T and the c.453+7A>G mutation on the *PLP1/DM20* ratio and found it reduced to 0.01 and 0.06 of normal (Figure 4, B). We consider this to be a rough estimate of the reduction in *PLP1/DM20* ratio because there is very little *PLP1* compared with *DM20* in skin fibroblasts and we noted that the amount of total *PLP1* (*PLP1* + *DM20*) decreases with passage number.

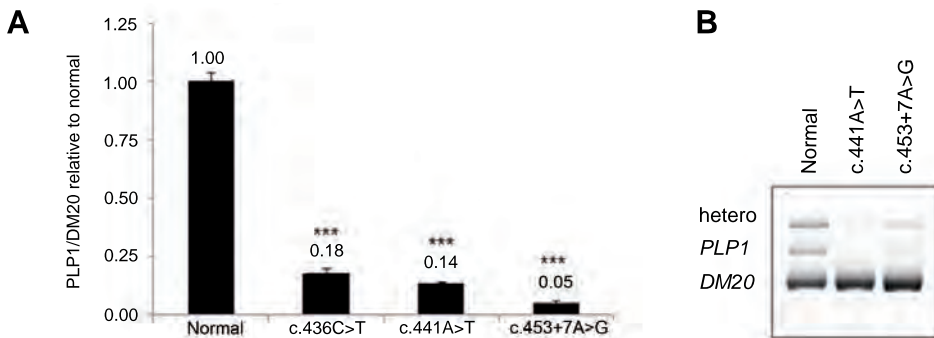


Figure 4. Dysregulation of *PLP1* splicing by patients' mutations.

Quantitation of *PLP1/DM20* mRNA produced in an immature immortalized oligodendrocyte cell line from the transfected splicing minigene reporter construct indicated a significant decrease in the *PLP1/DM20* ratio with patients' mutations compared with normal construct (A). The graph shows the ratio of *PLP1* product to the *DM20* product from each patient construct normalized to the normal construct (mean of replicates \pm SD). All constructs were tested in triplicate. All three patient constructs had a ratio significantly different from the normal construct, as measured by Student's t-test: ***, $P < 0.001$. Analysis of skin fibroblast RNA by RT-PCR indicated a decrease in *PLP1/DM20* ratio with patients' mutations (B). The primers that amplify from exon 2 to exon 5 *PLP1* readily detect *PLP1* and *DM20* signal in the same reaction as different sized bands. A heteroduplex of *PLP1* and *DM20* is also visible (*PLP1* and *DM20* heteroduplex formation has been described previously).²⁴ Quantitation performed by dividing *PLP1* + $\frac{1}{2}$ heteroduplex band by *DM20* and normalizing, indicated *PLP1/DM20* ratio in patient fibroblasts was 0.01 of normal for c.441A>T and 0.06 of normal for c.453+7A>G. The *PLP1* band was 105 bases larger than the *DM20* band.

DISCUSSION

Using exome sequencing, we identified the genetic defect causing HEMS.¹ All patients had hemizygous mutations in the *PLP1* gene, which encodes both PLP1 and its smaller isoform DM20 that is derived by the use of an alternative splice donor site within exon 3.¹³ Together the proteins constitute more than half of the total protein mass of myelin in the central nervous system (CNS).²⁶ The *DM20* transcript is preferentially expressed in the developing CNS before initiation of myelination, whereas the *PLP1* transcript dominates during myelination and adulthood, suggesting tightly regulated *PLP1/DM20* alternative splicing.

PLP1 mutations are known to be associated with a broad continuum of neurological phenotypes ranging from congenital PMD with severe hypomyelination to pure X-linked spastic paraplegia type 2 (SPG2) with even normal brain imaging in some cases.^{5,7-9} Different genetic alterations have been identified to cause these different phenotypes, with duplication of the entire *PLP1* gene as the most common change usually leading to the classic form of PMD.²⁷ More severe forms are associated with missense mutations in highly conserved regions or, in rare cases, with triplications and higher copy number of *PLP1*, while patients with null mutations or missense mutations in less conserved regions present with milder signs.^{28,29} Previously, we had defined HEMS based on the distinctive abnormalities seen on brain MRI. With the identification of *PLP1* mutations in this group, HEMS should be added as a recognizable new MRI phenotype within the broad spectrum of *PLP1*-related disorders.

Clinically, most patients with HEMS have a relatively mild functional disability and can be classified as complicated SPG2. All patients, except for patient 1 harboring the truncating *PLP1* mutation (p.(Arg127Lysfs*16)) have normal nerve conduction studies or sensory function on physical examination. This is in agreement with the hypothesis that only patients lacking PLP1 due to a functional null mutation or a truncating mutation in the PLP1-specific region have a peripheral neuropathy.^{28,30-32} In five families, the mutation was inherited from the mother. All female carriers were clinically asymptomatic, but the two females who underwent MR imaging showed abnormalities consisting of mild atrophy of the cerebral hemispheres and a diffuse T₂ hyperintensity of the white matter. This phenomenon has also been observed in carriers of mutations associated with a mild PMD phenotype,^{32,33} and can be explained by random X-inactivation due to the mild effects of these mutations.^{8,9}

Remarkably, in our HEMS cohort, the identified *PLP1* mutations were restricted to the *PLP1* specific region encoded by exon 3B that is spliced out in *DM20*, and to intron 3 (Figure 3, A and B). Only one family carried an obvious pathogenic *PLP1* mutation (p.(Arg127Lysfs*16)). The other nine families had presumed “subtle” *PLP1* mutations: these mutations were located in the noncoding region outside the splice donor and acceptor sites of exon 3B in six families; a silent mutation was identified in two families, and a missense mutation for which pathogenicity predictions were contradictory was identified in one family. This is in contrast to the commonly reported mutations in exon 3B that are mainly missense, truncating or located at the splice donor site sequence of exon 3B.^{28,30-32,34-47}

We provide evidence that the mutations ascertained in our HEMS cohort alter *PLP1/DM20* alternative splicing and must therefore be interpreted as pathogenic. Splicing is a complex mechanism not only controlled by the canonical splice donor and acceptor sites and branch sites but also by exonic or intronic enhancers and silencers and by regulation through the secondary RNA structure.^{23,24,42,45,48-51} We first performed in silico prediction analysis on the effects of the variants concerning these regulatory factors. Splice site predictions for the c.436C>T mutation showed a new *PLP1* splice donor site at c.434. For all three exonic substitutions (including c.436C>T) and for the intronic c.454–312C>G mutation, the creation of putative new exonic silencer motifs was predicted. This mechanism had previously been found associated with loss of the *PLP1* isoform for a *PLP1* c.436C>G missense mutation.⁵² Analysis of predicted secondary *PLP1* RNA structures containing the c.404T>G, c.441A>T and 453+7A>G mutations revealed potential conformational changes of the *PLP1* splice donor site that could result in a less accessible splice site for the spliceosome. This change may shift the balance between the usage of *DM20* and the *PLP1* exon 3 splice donor sites in disadvantage of the latter. Interestingly, the four noncoding mutations restricted to two specific regions deep within intron 3 of *PLP1* (LDIS-5' and LDIS-3') were predicted to reduce the stability of the secondary LDI *PLP1* RNA structure, which has been found associated with a decreased *PLP1* to *DM20* ratio.²³ Overall, these results indicate that the identified variants have an impact on *PLP1/DM20* alternative splicing. For the three tested variants (c.453+7A>G, c.436C>T, c.441A>T), we could confirm these predictions in vitro by detecting a decreased *PLP1/DM20* ratio in fibroblasts or in our minigene reporter transfection assay. Several additional algorithms applied for prediction of the impact of the single missense variant (c.404T>G) on protein structure and function showed contradictory results.

2

Although mutations in *PLP1* are also associated with PMD or SPG2, the MRI pattern of HEMS contrasts with the MRI findings in these disorders (see Figure 2).^{1,4,5} Normally, tracts become myelinated at the time they become functional, resulting in a fixed spatiotemporal sequence of myelination.⁵³ In patients with HEMS, the brain structures that normally myelinate early (e.g., brainstem, hilus of the dentate nucleus, posterior limb of the internal capsule, optic tracts and tracts to the pericentral cortex) are poorly myelinated in contrast to structures that normally myelinate at a later developmental stage, which show better myelination.^{1,53} In patients with PMD and SPG2, however, the early myelinated structures are relatively better myelinated than other brain structures (Figure 2, A–H). This indicates that *PLP1/DM20* alternative splicing and maintenance of a certain *PLP1* to *DM20* ratio are important for early myelination.

Noteworthy, three mutations identified in our HEMS cohort have been reported before (c.436C>T,³⁴ c.441A>T,²⁵ and c.453+7A>G⁴⁶). The patient with the c.436C>T had mild functional disability.³⁴ For the patients with the c.441A>T and c.453+7A>G mutation only the clinical diagnosis “PMD” was provided.^{25,46} We recently also identified three PMD families with mutations in the LDIS-3’ region (including c.454–314T>G), with a mild clinical phenotype, comparable to HEMS patients.²³ No MRI data were available for these patients, so we were not able to evaluate whether these patients have an MRI phenotype compatible with HEMS.

Our HEMS cohort presents a challenge for *PLP1* Sanger sequencing in a diagnostic setting. For most mutations, pathogenicity was difficult to prove. For example, the two silent mutations, c.436C>T and c.441A>T, had already been identified in the past in our patients, but were thought to be benign. Moreover, the noncoding regions LDIS-5’ and LDIS-3’ in intron 3 are currently not included in *PLP1* diagnostic sequencing. Our data support the proposal that sequencing of intron 3 of *PLP1* should be included in standard diagnostic procedures because of the importance of this region for controlling *PLP1/DM20* alternative splicing.²³ Furthermore, this study illustrates that caution is warranted in case of negative exome sequencing results, as coverage is often not optimal for intronic regions. Thanks to the number of patients with identical clinical and MRI presentation, we were able to identify the genetic basis of HEMS. The identification of more patients with mutations in this or other regions of *PLP1* altering *PLP1/DM20* alternative splicing will further elucidate the specificity of the HEMS MRI phenotype within the PMD spectrum. Future research will show whether these mutations that affect *PLP1/DM20* alternative splicing could be potential targets for treatment aimed at correction of the *PLP1* to *DM20* ratio.

REFERENCES

1. Steenweg ME, Wolf NI, Schieving JH, et al. Novel hypomyelinating leukoencephalopathy affecting early myelinating structures. *Arch Neurol* 2012;69:125-128.
2. Steenweg ME, Vanderver A, Blaser S, et al. Magnetic resonance imaging pattern recognition in hypomyelinating disorders. *Brain* 2010;133:2971-2982.
3. van der Knaap MS, Breiter SN, Naidu S, Hart AA, Valk J. Defining and categorizing leukoencephalopathies of unknown origin: MR imaging approach. *Radiology* 1999;213:121-133.
4. Pouwels PJ, Vanderver A, Bernard G, et al. Hypomyelinating leukodystrophies: Translational research progress and prospects. *Ann Neurol* 2014;76:5-19.
5. van der Knaap MS and Valk J. Pelizaeus-Merzbacher Disease and X-linked Spastic Paraplegia Type 2. In: *Magnetic Resonance Imaging of Myelination and Myelin Disorders*. Heidelberg: Springer; 2005. p. 272-280.
6. Tonducci D, Pichiecchio A, Wolf NI, et al. Novel hypomyelinating leukoencephalopathy affecting early myelinating structures: clinical course in two brothers. *Neuropediatrics* 2013;44:213-217.
7. Woodward KJ. The molecular and cellular defects underlying Pelizaeus-Merzbacher disease. *Expert Rev Mol Med* 2008;10:e14.
8. Inoue K. PLP1-related inherited dysmyelinating disorders: Pelizaeus-Merzbacher disease and spastic paraplegia type 2. *Neurogenetics* 2005;6:1-16.
9. Hudson LD. Pelizaeus-Merzbacher disease and spastic paraplegia type 2: two faces of myelin loss from mutations in the same gene. *J Child Neurol* 2003;18:616-624.
10. Kevelam SH, Bugiani M, Salomons GS, et al. Exome sequencing reveals mutated SLC19A3 in patients with an early-infantile, lethal encephalopathy. *Brain* 2013;136:1534-1543.
11. Dallabona C, Diodato D, Kevelam SH, et al. Novel (ovario) leukodystrophy related to AARS2 mutations. *Neurology* 2014;82:2063-2071.
12. Taft RJ, Vanderver A, Leventer RJ, et al. Mutations in DARS cause hypomyelination with brain stem and spinal cord involvement and leg spasticity. *Am J Hum Genet* 2013;92:774-780.
13. Nave KA, Lai C, Bloom FE, Milner RJ. Splice site selection in the proteolipid protein (PLP) gene transcript and primary structure of the DM-20 protein of central nervous system myelin. *Proc Natl Acad Sci U S A* 1987;84:5665-5669.
14. Wolf NI, Salomons GS, Rodenburg RJ, et al. Mutations in RARS cause hypomyelination. *Ann Neurol* 2014;76:134-139.
15. Ameziane N, Sie D, Dentro S, et al. Diagnosis of fanconi anemia: mutation analysis by next-generation sequencing. *Anemia* 2012;2012:132856.
16. Untergasser A, Cutcutache I, Koressaar T, et al. Primer3--new capabilities and interfaces. *Nucleic Acids Res* 2012;40:e115
17. Koressaar T and Remm M. Enhancements and modifications of primer design program Primer3. *Bioinformatics* 2007;23:1289-1291.
18. Ng PC and Henikoff S. Predicting deleterious amino acid substitutions. *Genome Res* 2001;11:863-874.
19. Adzhubei I, Jordan DM, Sunyaev SR. Predicting functional effect of human missense mutations using PolyPhen-2. *Curr Protoc Hum Genet* 2013;Chapter 7:Unit7.20.
20. Schwarz JM, Cooper DN, Schuelke M, Seelow D. MutationTaster2: mutation prediction for the deep-sequencing age. *Nat Methods* 2014;11:361-362.
21. Wallis Y, Payne S, McAnult C, et al. Practice Guidelines for the Evaluation of Pathogenicity and the Reporting of Sequence Variants in Clinical Molecular Genetics. *ACGS/VKGL* 2013.
22. Zuker M. Mfold web server for nucleic acid folding and hybridization prediction. *Nucleic Acids Res* 2003;31:3406-3415.
23. Taube JR, Sperle K, Banser L, et al. PMD patient mutations reveal a long-distance intronic interaction that regulates PLP1/DM20 alternative splicing. *Hum Mol Genet* 2014;23:5464-5478.
24. Hobson GM, Huang Z, Sperle K, Stabley DL, Marks HG, Cambi F. A PLP splicing abnormality is associated with an unusual presentation of PMD. *Ann Neurol* 2002;52:477-488.
25. Pratt VM, Dlouhy SR, Hodes ME. Possible cryptic splice site found in the PLP gene in a patient with Pelizaeus-Merzbacher disease. *Am J Hum Genet* 1991;49 (suppl):393-451.
26. Eng LF, Chao FC, Gerstl B, Pratt D, Tavaststjerna MG. The maturation of human white matter myelin. Fractionation of the myelin membrane proteins. *Biochemistry* 1968;7:4455-4465.

27. Sistermans EA, de Coe RF, De Wijs IJ, Van Oost BA. Duplication of the proteolipid protein gene is the major cause of Pelizaeus-Merzbacher disease. *Neurology* 1998;50:1749-1754.
28. Cailloux F, Gauthier-Barichard F, Mimault C, et al. Genotype-phenotype correlation in inherited brain myelination defects due to proteolipid protein gene mutations. Clinical European Network on Brain Demyelinating Disease. *Eur J Hum Genet* 2000;8:837-845.
29. Wolf NI, Sistermans EA, Cundall M, et al. Three or more copies of the proteolipid protein gene *PLP1* cause severe Pelizaeus-Merzbacher disease. *Brain* 2005;128:743-751.
30. Shy ME, Hobson G, Jain M, et al. Schwann cell expression of *PLP1* but not *DM20* is necessary to prevent neuropathy. *Ann Neurol* 2003;53:354-365.
31. Osaka H, Kawanishi C, Inoue K, et al. Novel nonsense proteolipid protein gene mutation as a cause of X-linked spastic paraplegia in twin males. *Biochem Biophys Res Commun* 1995;215:835-841.
32. Hodes ME, Blank CA, Pratt VM, Morales J, Napier J, Dlouhy SR. Nonsense mutation in exon 3 of the proteolipid protein gene (*PLP*) in a family with an unusual form of Pelizaeus-Merzbacher disease. *Am J Med Genet* 1997;69:121-125.
33. Nance MA, Boyadjev S, Pratt VM, Taylor S, Hodes ME, Dlouhy SR. Adult-onset neurodegenerative disorder due to proteolipid protein gene mutation in the mother of a man with Pelizaeus-Merzbacher disease. *Neurology* 1996;47:1333-1335.
34. Laukka JJ, Stanley JA, Garbern JY, et al. Neuroradiologic correlates of clinical disability and progression in the X-linked leukodystrophy Pelizaeus-Merzbacher disease. *J Neurol Sci* 2013;335:75-81.
35. Saugier-Verber P, Munnich A, Bonneau D, et al. X-linked spastic paraplegia and Pelizaeus-Merzbacher disease are allelic disorders at the proteolipid protein locus. *Nat Genet* 1994;6:257-262.
36. Sivakumar K, Sambuughin N, Selenge B, et al. Novel exon 3B proteolipid protein gene mutation causing late-onset spastic paraplegia type 2 with variable penetrance in female family members. *Ann Neurol* 1999;45:680-683.
37. Gorman MP, Golomb MR, Walsh LE, et al. Steroid-responsive neurologic relapses in a child with a proteolipid protein-1 mutation. *Neurology* 2007;68:1305-1307.
38. Grossi S, Regis S, Biancheri R, et al. Molecular genetic analysis of the *PLP1* gene in 38 families with *PLP1*-related disorders: identification and functional characterization of 11 novel *PLP1* mutations. *Orphanet J Rare Dis* 2011;6:40-46.
39. Osaka H, Koizume S, Aoyama H, et al. Mild phenotype in Pelizaeus-Merzbacher disease caused by a *PLP1*-specific mutation. *Brain Dev* 2010;32:703-707.
40. Pratt VM, Trofatter JA, Larsen MB, Hodes ME, Dlouhy SR. New variant in exon 3 of the proteolipid protein (*PLP*) gene in a family with Pelizaeus-Merzbacher disease. *Am J Med Genet* 1992;43:642-646.
41. Pretorius E, Naude H, Ribbens C, Bosman C. Pelizaeus-Merzbacher Disease: A Developmental Disorder Affecting Myelin Formation in the Nervous System. *J dev Phys disabil* 2005;17:173-183.
42. Hobson GM, Huang Z, Sperle K, et al. Splice-site contribution in alternative splicing of *PLP1* and *DM20*: molecular studies in oligodendrocytes. *Hum Mutat* 2006;27:69-77.
43. Pratt VM, Naidu S, Dlouhy SR, Marks HG, Hodes ME. A novel mutation in exon 3 of the proteolipid protein gene in Pelizaeus-Merzbacher disease. *Neurology* 1995;45:394-395.
44. Lassuthova P, Zaliova M, Inoue K, et al. Three New *PLP1* Splicing Mutations Demonstrate Pathogenic and Phenotypic Diversity of Pelizaeus-Merzbacher Disease. *J Child Neurol* 2013;29:924-931.
45. Hobson GM, Davis AP, Stowell NC, et al. Mutations in noncoding regions of the proteolipid protein gene in Pelizaeus-Merzbacher disease. *Neurology* 2000;55:1089-1096.
46. Hubner CA, Orth U, Senning A, et al. Seventeen novel *PLP1* mutations in patients with Pelizaeus-Merzbacher disease. *Hum Mutat* 2005;25:321-322.
47. Bridge PJ and Wilkens PJ. The role of proteolipid protein gene in Pelizaeus-Merzbacher disease. *Am J Hum Genet* 1992;52 (suppl).
48. Bonnet-Dupeyron MN, Combes P, Santander P, Cailloux F, Boespflug-Tanguy O, Vaurs-Barriere C. *PLP1* splicing abnormalities identified in Pelizaeus-Merzbacher disease and *SPG2* fibroblasts are associated with different types of mutations. *Hum Mutat* 2008;29:1028-1036.
49. Wang E, Huang Z, Hobson GM, et al. *PLP1* alternative splicing in differentiating oligodendrocytes: characterization of an exonic splicing enhancer. *J Cell Biochem* 2006;97:999-1016.
50. Wang E, Dimova N, Cambi F. *PLP/DM20* ratio is regulated by *hnRNPH* and *F* and a novel G-rich enhancer in oligodendrocytes. *Nucleic Acids Res* 2007;35:4164-4178.

51. Warf MB and Berglund JA. Role of RNA structure in regulating pre-mRNA splicing. *Trends Biochem Sci* 2010;35:169-178.
52. Regis S, Corsolini F, Grossi S, Tappino B, Cooper DN, Filocamo M. Restoration of the normal splicing pattern of the *PLP1* gene by means of an antisense oligonucleotide directed against an exonic mutation. *PLoS One* 2013;8:e73633-
53. van der Knaap MS and Valk J. Myelination and Retarded Myelination. In: *Magnetic Resonance of Myelination and Myelin Disorders*. Heidelberg: Springer; 2005. p. 37-65.

SUPPORTING INFORMATION

Data S1. Supplementary methods

Figure S1. Intramolecular base-pairing interaction in the predicted secondary *PLP1* structures

Table S1. MRI characteristics

Table S2. Clinical characteristics

Table S3. Quantitation of predicted intramolecular basepairs at the *PLP1* splice donor site in normal and mutant *PLP1* mRNA

DATA S1. SUPPLEMENTARY METHODS

In silico splicing analysis

The predicted effects of identified variants on splice sites were analyzed using 5 prediction tools: NNSplice (http://www.fruitfly.org/seq_tools/splice.html),¹ Netgene2 (<http://www.cbs.dtu.dk/services/NetGene2/>),² the Human Splicing Finder (<http://www.umd.be/HSF/>),³ MaxEnt (http://genes.mit.edu/burgelab/maxent/Xmaxentscan_scoreseq.html),⁴ SpliceSiteFinder-like, an algorithm based on Alex Dong Li's Splice Site Finder (no longer available), and scores obtained via Alamut, version 2.4. Analysis of exonic splicing regulatory elements was performed using ESEfinder 3.0 (<http://rulai.cshl.edu/cgi-bin/tools/ESE3/esefinder.cgi?process=home>)⁵ and the FAS-ESS web server (FAS-Hex2 set) (<http://genes.mit.edu/fas-ess/>)⁶ was used for analysis of exonic splicing silencer (ESS) motifs using default settings for significance.

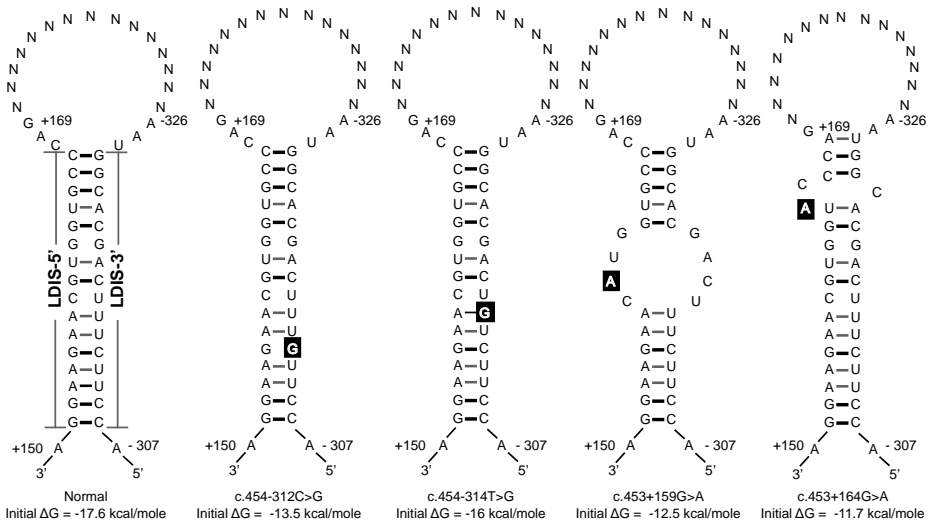
PLP1/DM20 alternative splicing studies

Minigene splicing construct transfection assay

The effects of 3 *PLP1* mutations c.436C>T, c.441A>T and c.453+7G>A on *PLP1/DM20* alternative splicing were individually investigated in a minigene splicing reporter construct transfection assay using Oli-neu cells, an immortalized cell line representing immature oligodendrocytes, as previously described, with modified reverse transcription (RT).⁷ RT was performed prior to PCR by first denaturing 1 µg of RNA in a 10 µl volume at 65 °C for 5 min and then adding 1x RT buffer (Applied Biosystems, Foster City, CA), 4 mM each dNTP (Applied Biosystems), 1 µM Oligo (dT) 15 primer (Promega, Fitchburg, WI), 10 units recombinant RNasin (Promega) and 50 units MultiScribe Reverse Transcriptase (Applied Biosystems) in a final volume of 20 µl and incubating at 25 °C for 5 min, 37 °C for 120 min, 85 °C for 5 min and kept at 4 °C.

Skin fibroblast cultures

PLP1/DM20 alternative splicing was investigated in skin fibroblasts from patient 6 harboring the c.453+7A>G intronic mutation. In addition, skin fibroblasts were available from a patient described in 1991 with the c.441A>T silent mutation,⁸ the same as identified in patient 8 from our cohort. RT-PCR analysis of RNA prepared from cultured skin fibroblasts was performed as previously described with modified RT reaction as above.⁷ The PCR reactions in a 20 μ l volume were performed using GAPDH primers with 0.8 μ l cDNA from the RT reaction and 25 cycles or *PLP1* primers with 2 μ l cDNA from the RT reaction and 35 cycles. Images were made on the Typhoon Trio (GE Healthcare, Littlechalfont, UK) and analyzed using ImageQuant TL (GE Healthcare).



Supplementary figure 1. Intra-molecular base pairing interaction in the predicted secondary *PLP1* structures.

Fragments were analyzed using normal and mutant RNA sequences including 2 regions within intron 3 of *PLP1*: 20 bases from c.453+150 to +169 and 20 bases from c.454-326 to -307, separated by 15 random bases (N15), as we previously described.⁷ Horizontal lines indicate strength of hydrogen bonding: black and thick, triple hydrogen bond between guanine and cytosine; dark gray and intermediate thickness, double hydrogen bond between adenine and uracil; light gray and thin, single hydrogen bond between guanine and uracil. The predicted structures formed by long distance interaction site (LDIS)-5' and LDIS-3' for normal and mutant RNA sequences are shown with their ΔG values. Mutations are indicated in white within a black box.

Supplementary table 1. MRI characteristics

Patient number	1	2 ^d	3 ^d	4 ^{b,c}	5 ^c	6	7	8 ^a
Age at first MRI (y)	1	1.1	1.4	4.1	not evaluated	2	1.11	6.4
Increased T₂ signal of:								
Optic radiation	+	+	+	+		+	+	+
Periventricular WM	+	+	+	+		+	+	+
Pericentral subcortical WM	+	-	+	+		+	-	+
Corpus callosum	-	-	-	-		-	-	+
Internal capsule, anterior limb	-	-	-	-		+	-	-
Internal capsule, posterior limb	+, tram track	+, tram track	+, tram track	+, tram track		+, tram track	+, tram track	+, tram track to diffuse
External capsule	+	-	-	-		+	-	-
Hilus of the dentate nucleus	+	+	+, also peridentate WM	+		+	n.e.	+, also peridentate WM
Cerebellar white matter	-	-	-	-		-	-	-
Middle cerebellar peduncles	-	-	-	-		-	-	-
Cerebral cortex	-	-	-	-		-	-	-
Basal nuclei	-	-	-	-		-	-	-
Thalamus	+, except lat. part	+, except lat. part	+, except lat. part	+/-		+, except lat. part	+, except lat. part	+, except lat. part
Dentate nucleus	+	+	+	+		+	n.e.	+
Cerebellar cortex	-	-	-	-		-	-	-
Midbrain	-	-	-	-		-	-	-
Pons	+, esp. border with medulla	+, esp. border with medulla	+, esp. border with medulla	+, esp. border with medulla		+, esp. border with medulla	+, esp. border with medulla	+, esp. border with medulla
Medulla	+	+	+	+		+	+	+

Supplementary table 1. MRI characteristics continued

Patient number	9 ^a	10 ^{b,c}	11 ^{a,c}	12 ^b	13 ^c	14 ^c	15 ^d	16 ^d
Age at first MRI (y)	3	1.5	1.9	1.5	6.2	5.6	not evaluated	not evaluated
Increased T₂ signal of:								
Optic radiation	+	+	+	+	+	+		
Periventricular WM	+	+	+	+	+	+		
Pericentral subcortical WM	+	-	+	+	+	+		
Corpus callosum	-	-	-	-	-	+		
Internal capsule, anterior limb	-	-	-	+	-	-		
Internal capsule, posterior limb	+	tram track	tram track	tram track	tram track	tram track		tram track to diffuse
External capsule	-	-	-	-	-	-		
Hilus of the dentate nucleus	+, also peridentate WM	+, also peridentate WM	+, also peridentate WM	+	+	+		
Cerebellar white matter	-	-	-	-	-	-		
Middle cerebellar peduncles	-	-	-	-	-	-		
Cerebral cortex	-	-	-	-	-	-		
Basal nuclei	-	-	-	-	-	-		
Thalamus	+, except lat. part	+, except lat. part	+, except lat. part	+, except lat. part	+, except lat. part	+, except lat. part		+, except lat. part
Dentate nucleus	+	+	+	+	+	+		
Cerebellar cortex	-	-	-	-	-	-		
Midbrain	-	-	-	-	-	-		
Pons	+, esp. border with medulla	+, esp. border with medulla	+, esp. border with medulla	+, esp. border with medulla	+, esp. border with medulla	+, esp. border with medulla		+, esp. border with medulla
Medulla	+	+	+	+	+	+		+

Supplementary table 1. MRI characteristics continued

Patient number	4 ^{b,c}	6	8 ^a	9 ^a	10 ^{b,c}	12 ^a	13 ^c	14 ^c
Age at most recent MRI (y)	6.7	6	7.4	12	11.8	5.2	9.1	11.6
Increased T ₂ signal of:								
Optic radiation	+	+	+	+	+	+	+	+
Periventricular WM	+	+	+	+	+	+	+	+
Pericentral subcortical WM	+	+	+	+	+	-	+	+
Corpus callosum	+/-	+	+	+	+	-	+	+
Internal capsule, anterior limb	-	-	-	-	-	-	-	-
Internal capsule, posterior limb	+, diffuse	+, diffuse	+, diffuse	+/-	+, diffuse	+, tram track	+, diffuse	+, diffuse
External capsule	-	-	-	-	-	-	-	-
Hilus of the dentate nucleus	+	+	+, also peridentate WM	+	+	+	+	+
Cerebellar white matter	-	-	-	-	-	-	-	-
Middle cerebellar peduncles	-	-	-	-	-	-	-	-
Cerebral cortex	-	-	-	-	-	-	-	-
Basal nuclei	-	-	-	-	-	-	-	-
Thalamus	+, except lat. part	+, except lat. part	+, except lat. part	-	+, except lat. part	+, except lat. part	+, except lat. part mild	+, except lat. part
Dentate nucleus	+	+	+	+	+	+	+	+
Cerebellar cortex	-	-	-	-	-	-	-	-
Midbrain	-	-	-	-	-	-	-	-
Pons	+, esp. border with medulla	+, esp. border with medulla	+, esp. border with medulla	+, esp. border with medulla +/-	+, esp. border with medulla	+, esp. border with medulla	+, esp. border with medulla +/-, improved	+, esp. border with medulla +/-, improved
Medulla	+	+	+	medulla better myelinated, periventricular and deep WM worse	brainstem improved, corpus callosum, periventricular and deep WM worse	subcortical improved, periventricular worse	brainstem improved, periventricular worse	brainstem improved, periventricular / deep WM worse
Follow-up	unchanged	loss of normal myelin signal in corpus callosum	deep WM and corpus callosum worse					

^aPublished by Steenweg *et al.*, 2012⁹

^bPublished by Tonduci *et al.*, 2013¹⁰

^cSibling pairs: 4 and 10, 5 and 11, and 13 and 14.

^dBelong to the same family

Abbreviations: y = year; tram track = T₂ hyperintense-hypointense-hyperintense; + = increased T₂ signal; - = no signal abnormalities; n.e. = not evaluable; WM = white matter; abn = abnormalities; lat. = lateral; esp. = especially

Supplementary table 2. Clinical characteristics

Patient number	1	2 ^d	3 ^d	4 ^{b,c}	5 ^c	6	7	8 ^a
Gender	male	Male	male	male	male	male	male	male
Year of birth	2011	2011	2010	2008	2003	2003	2003	2002
Siblings (affected (F or M) / unaffected (F or M))	0/1M	0/1F	0/1F	1M/0	1M/0	0/1M	0/1M	0/1
Past History								
Pregnancy and delivery	normal	normal	normal	normal	normal	normal	normal	caesarian section (no progress)
Initial development	mildly delayed	normal	normal	normal	normal	normal	delayed language development	mildly delayed
Presentation								
Age at onset (months)	4.5	3	12	6	20	unknown	birth	6
Signs at presentation	nystagmus	nystagmus	nystagmus	nystagmus	nystagmus	nystagmus	nystagmus	nystagmus
Course over time								
Further signs	truncal & limb ataxia, head titubation, progressive spasticity legs	ataxic gait & truncal ataxia, spasticity of the legs	ataxic gait, spasticity of the legs	dysarthria, dysmetria, trunk titubation, spasticity of the legs	ataxia, progressive spasticity of the legs	trunk ataxia, intention tremor, progressive spasticity of the legs	ataxia, dysarthria, progressive spasticity of the legs, distal contractures	ataxic gait, hand tremor
Improvement of nystagmus	yes	yes	no	yes	yes	yes	yes	yes
Episodes of regression	yes	no	no	no	no	no	no	no
Continuing developmental progress	yes, but globally delayed	yes, but motor milestones delayed	yes, but motor milestones delayed	yes, but globally delayed	yes, but motor milestones delayed	yes, but motor milestones delayed	yes, but globally delayed	yes, but motor milestones delayed
Unsupported walking (months)	never	24	18	never	never	never	never	26
Present cognitive level	mildly impaired	normal	normal	mildly impaired	normal	mildly impaired	normal	normal
Present motor level	crawling; no walking	unsupported walking	unsupported walking	wheelchair	supported walking	wheelchair and supported walking	wheelchair bound	unsupported walking
Symptoms in the mother								
	no	no	no	no	no	deceased	no	no

Supplementary table 2. Clinical characteristics continued

Patient number	9 ^a	10 ^{b,c}	11 ^{a,c}	12 ^a	13 ^c	14 ^c	15 ^d	16 ^d
Gender	male	male	male	male	male	male	male	male
Year of birth	2002	2001	2001	2000	1997	1995	1983	1979
Siblings (affected (F or M)/unaffected (F or M))	0/1F	1m/0	1M/0	0/1F	1M/1F	1M/1F	0/1F	0/0
Past History								
Pregnancy and delivery	gestational hypertension	normal	normal	normal	normal	elective caesarian section	normal	normal
Initial development	normal	normal	normal	normal	normal	normal	delayed	normal
Presentation								
Age at onset (months)	11	6	19	20	60	24	12	12
Signs at presentation	nystagmus	nystagmus	nystagmus	nystagmus, delay in walking	ataxic gait, intension tremor, spasticity/legs	gross and fine motor delay, balance problems	motor and speech delay	gross and fine motor delay
Course over time								
Further signs	ataxic gait & dysmetria, spasticity of the legs	dysarthria, dysmetria, titubation, increases tone	ataxic gait and ataxic reach & grasp, trunk titubation	ataxic gait & dysmetria, increased muscle tone legs	nystagmus, progressive spasticity of legs	nystagmus, trunk ataxia, progressive spasticity of legs	spastic ataxic gait, stuttering	mild ataxia; severe spasticity of the legs
Improvement of nystagmus	no (12 y)	yes	no (13 y)	yes	no	no	never present	never present (34 y)
Episodes of regression	no	no	loss of independent ambulation at 12 y	no	no	no	no	no
Continuing developmental progress	yes, but motor milestones delayed	yes, but globally delayed	yes, but motor milestones delayed	yes, but motor milestones delayed	yes, but motor milestones delayed	yes, but globally delayed	yes, but globally delayed	yes, but motor milestones delayed
Unsupported walking (months)	36	never	12	20	14	12	yes	no
Cognitive outcome	mildly impaired	mildly impaired	normal	normal	impaired	moderately impaired	mildly impaired	normal
Motor outcome	unsupported at home, otherwise with support	wheelchair	supported walking	unsupported walking	unsupported, with braces	wheel chair and walking with braces	unsupported walking	supported walking
Symptoms in the mother								
	no	no	no	no	no	no	no	no

Supplementary table 2. Clinical characteristics, physical examination

Latest examination	1	2 ^d	3 ^d	4 ^{b,c}	5 ^c	6	7	8 ^a
Age at latest examination (years)	2.5	2	3	6	9	6.8 months	9	6
Head circumference	normal	normal	normal	normal	normal	normal	normal	normal
Language	delayed	delayed	normal	normal	normal	normal	delayed	normal
Eyes, vision	myopia	normal	normal	astigmatism	normal	normal	myopia	normal
Eye movements	nystagmus	nystagmus	nystagmus	nystagmus	nystagmus	nystagmus	abn. pursuits & saccades	nystagmus
Head titubation	yes	no	no	no	no	yes	no	yes
Speech	dysarthric	normal	normal	dysarthric	dysarthric	normal	dysarthric	normal
Arms								
Tone	increased	mildly increased	mildly increased	mildly increased	normal	increased	increased	decreased
Reflexes	Increased	normal	normal	normal	increased	increased	increased	normal
Spasticity	no	no	no	mild	no	no	yes	no
Ataxia	yes	yes	yes	yes	yes	yes	yes	no
Extrapyramidal signs	no	no	no	no	no	no	no	no
Sensory function	not evidently affected	not evidently affected	not evidently affected	normal	normal	not evidently affected	normal	normal
Legs								
Tone	increased	increased	increased	increased	increased	increased	increased	decreased
Reflexes	increased, ankle clonus	increased, ankle clonus	increased, ankle clonus	increased, ankle clonus	increased, ankle clonus	increased, ankle clonus	increased	brisk
Babinski signs	yes	yes	yes	yes	yes	yes	yes	yes
Spasticity	yes	yes	yes	yes, prominent	yes, prominent	yes	yes, prominent	yes
Ataxia	yes	yes	yes	yes	yes	yes	yes	no
Extrapyramidal signs	no	no	no	no	no	no	no	no
Sensory function	not evidently affected	not evidently affected	not evidently affected	normal	normal	not evidently affected	normal	normal
Gait	n.a.	spastic & ataxic	spastic & ataxic	not achieved	spastic & ataxic	spastic & ataxic	n.a.	mildly ataxic
Nerve conduction studies	delayed in legs	normal	normal	not done	not done	not done	normal	normal

Supplementary table 2. Clinical characteristics, physical examination continued

Latest examination	9 ^a	10 ^{b,c}	11 ^{a,c}	12 ^a	13 ^c	14 ^c	15 ^d	16 ^d
Age at latest examination (years)	12	13	12	14	15	16.5	31	35
Head circumference	normal	normal	normal	normal	normal	normal	normal	normal
Language	normal	mildly impaired	normal	normal	normal	delayed	normal	normal
Eyes, vision	partly corrected with glasses	astigmatic	normal with glasses	normal	normal with glasses	normal with glasses	astigmatism /myopia	astigmatism
Eye movements	nystagmus	nystagmus	nystagmus	nystagmus	nystagmus	nystagmus	no	no
Head titubation	no	no	no	yes	no	no	no	no
Hearing	normal	normal	normal	normal	normal	normal	normal	normal
Speech	dysarthric	dysarthric	normal	dysarthric	spastic dysarthric	spastic dysarthric	normal	normal
Arms								
Tone	mildly increased	mildly increased	normal	increased	increased	increased	normal	increased
Muscle strength	normal	normal	normal	low-normal	normal	normal	normal	low normal
Reflexes	normal	normal	brisk	normal	brisk	brisk	increased	brisk
Spasticity	no	mild	no	no	yes	yes	no	increased
Ataxia	yes	yes	yes	yes	yes	yes	yes	yes
Extrapyramidal signs	no	no	no	no	no	no	no	no
Sensory function	normal	normal	normal	normal	normal	normal	normal	normal
Legs								
Tone	increased	increased	moderately increased	increased	increased	increased	no	increased
Muscle strength	decreased	decrease	normal	decreased	mild decreased	decreased (R>L)	normal	low normal
Reflexes	increased, ankle clonus	increased, ankle clonus	brisk	brisk	increased, ankle clonus	increased, ankle clonus	normal	brisk
Babinski signs	yes	yes	no	yes	yes	yes	no	yes
Spasticity	yes	yes, prominent	yes	yes	yes, prominent	yes, prominent	yes	yes
Ataxia	yes	yes	yes	yes	yes	yes	yes	yes
Extrapyramidal signs	no	no	no	no	no	no	no	no
Sensory function	normal	normal	normal	normal	normal	normal	normal	normal
Gait	spastic & ataxic	not achieved	ataxic	spastic & ataxic	spastic & ataxic	spastic (scissoring)	ataxic	spastic (scissoring)
Nerve conduction studies	not done	not done	not done	not done	normal	not done	normal	normal

^aPublished by Steenweg *et al.*, 2012. ^bPublished by Tonduti *et al.*, 2013. ¹⁰Sibling pairs: 4 and 10, 5 and 11, and 13 and 14. ^dBelong to the same family

Abbreviations: F = female; M = male; y = year; n.a. = not applicable; R = right; L = left; abn = abnormal

Supplementary table 3. Quantification of predicted intramolecular basepairs at the *PLP1* splice donor site in normal and mutant *PLP1* mRNA.

	Normal						c.453+7A>G						c.441A>T						c.404T>G						c.436C>T					
	GC	AU	GU	Tot.	GC	AU	GU	Tot.	GC	AU	GU	Tot.	GC	AU	GU	Tot.	GC	AU	GU	Tot.	GC	AU	GU	Tot.	GC	AU	GU	Tot.		
<i>PLP1</i> structures ^a																														
#1	1	1	2	4	3	2	0	5	1	2	2	5	2	2	2	3	7	1	1	1	2	2	2	3	7	1	1	2	4	
#2	1	1	2	4	3	2	0	5	1	2	2	5	2	2	2	3	7	1	1	1	2	2	2	3	7	1	1	2	4	
#3	1	1	2	4	3	2	0	5	2	2	3	7	2	2	2	3	7	0	3	3	2	2	2	3	6	0	3	3	6	
#4	2	2	3	7	3	2	0	5	2	2	3	7	2	2	2	3	7	1	2	2	2	2	2	3	6	1	2	3	6	
#5	3	3	1	7	1	1	2	4	2	2	3	7	1	1	1	2	4	2	2	2	2	2	2	3	7	2	2	3	7	
#6	3	2	0	5	3	2	0	5	2	2	3	7	3	3	0	6	2	2	2	2	2	2	2	3	7	2	2	3	7	
#7	2	2	3	7	3	3	0	6	2	2	3	7	3	2	0	5	2	2	2	2	2	2	2	3	7	2	2	3	7	
#8	2	3	3	7	3	2	0	5	3	2	2	7	2	2	1	4	2	1	1	1	2	2	1	4	2	1	1	4	4	
#9	2	2	3	7	1	2	3	6	2	2	3	7	2	2	2	3	7	2	2	2	2	2	2	3	7	2	2	3	7	
#10	2	2	3	7	1	1	2	4	1	1	2	4	2	2	2	3	7	1	1	1	2	2	2	3	7	1	1	1	3	
#11	2	1	1	4	3	2	0	5	2	2	0	4	2	2	2	3	7	1	1	1	2	2	2	3	7	1	1	2	4	
#12	3	2	0	5					2	2	3	7	2	2	2	3	7	1	1	1	2	2	2	3	7	1	1	2	4	
#13	2	0	0	2					3	3	1	5	0	0	0	2	2	2	0	0	2	2	2	3	7	2	0	0	2	
#14	1	2	2	5					1	2	2	5	1	1	1	2	4	1	1	1	2	2	2	3	7	1	1	2	4	
#15	1	1	2	4					3	2	2	7	1	2	2	4	1	2	2	2	2	2	2	3	7	1	1	2	4	
#16	1	1	2	4					1	2	2	5	2	2	2	4	1	2	2	2	2	2	2	3	7	2	2	2	4	
#17	1	1	2	4					1	2	2	5	2	2	2	3	7	1	2	2	2	2	2	3	7	2	2	2	4	

^aPredicted structures are ranked according to ΔG ; #1 is predicted as most stable with the lowest ΔG . We discriminated GC, AU and GU basepairs in the predicted RNA foldings. A significant change was defined as more total base pairs in all top 3 ranked predictions for the mutant *PLP1* fragment compared to the top 3 predictions of the normal fragment. Abbreviations: Tot., total

SUPPLEMENTARY REFERENCES

1. Reese MG, Eeckman FH, Kulp D, et al. Improved splice site detection in Genie. *J Comput Biol* 1997;4:311-323.
2. Hebsgaard SM, Korning PG, Tolstrup N, et al. Splice site prediction in *Arabidopsis thaliana* pre-mRNA by combining local and global sequence information. *Nucleic Acids Res* 1996;24:3439-3452.
3. Desmet FO, Hamroun D, Lalande M, et al. Human Splicing Finder: an online bioinformatics tool to predict splicing signals. *Nucleic Acids Res* 2009;37:e67.
4. Yeo G and Burge CB. Maximum entropy modeling of short sequence motifs with applications to RNA splicing signals. *J Comput Biol* 2004;11:377-394.
5. Cartegni L, Wang J, Zhu Z, et al. ESEfinder: A web resource to identify exonic splicing enhancers. *Nucleic Acids Res* 2003;31:3568-3571.
6. Wang Z, Rolish ME, Yeo G, et al. Systematic identification and analysis of exonic splicing silencers. *Cell* 2004;119:831-845.
7. Taube JR, Sperle K, Banser L, et al. PMD patient mutations reveal a long-distance intronic interaction that regulates *PLP1/DM20* alternative splicing. *Hum Mol Genet* 2014;23:5464-5478.
8. Pratt VM, Dlouhy SR, Hodes ME. Possible cryptic splice site found in the *PL* gene in a patient with Pelizaeus-Merzbacher disease. *Am J Hum Genet* 1991;49 (suppl):393-451.
9. Steenweg ME, Wolf NI, Schieving JH, et al. Novel hypomyelinating leukoencephalopathy affecting early myelinating structures. *Arch Neurol* 2012;69:125-128.
10. Tonduti D, Pichiecchio A, Wolf NI, et al. Novel hypomyelinating leukoencephalopathy affecting early myelinating structures: clinical course in two brothers. *Neuropediatrics* 2013;44:213-217.

Chapter 3

Exome sequencing reveals mutated *SLC19A3* in patients with an early-infantile, lethal encephalopathy

Sietske H. Kevelam, Marianna Bugiani, Gajja S. Salomons, Annette Feigenbaum,
Susan Blaser, Chitra Prasad, Johannes Häberle, Ivo Barić, Ingrid M. C. Bakker,
Nienke L. Postma, Warsha A. Kanhai, Nicole I. Wolf, Truus E. M. Abbink,
Quinten Waisfisz, Peter Heutink, and Marjo S. van der Knaap

Brain. 2013 May;136(Pt 5):1534-1543.

ABSTRACT

To accomplish a diagnosis in patients with a rare unclassified disorder is difficult. In this study, we used magnetic resonance imaging pattern recognition analysis to identify patients with the same novel heritable disorder. Whole-exome sequencing was performed to discover the mutated gene. We identified seven patients sharing a previously undescribed magnetic resonance imaging pattern, characterized by initial swelling with T₂ hyperintensity of the basal nuclei, thalami, cerebral white matter and cortex, pons and midbrain, followed by rarefaction or cystic degeneration of the white matter and, eventually, by progressive cerebral, cerebellar and brainstem atrophy. All patients developed a severe encephalopathy with rapid deterioration of neurological functions a few weeks after birth, followed by respiratory failure and death. Lactate was elevated in body fluids and on magnetic resonance spectroscopy in most patients. Whole-exome sequencing in a single patient revealed two predicted pathogenic, heterozygous missense mutations in the *SLC19A3* gene, encoding the second thiamine transporter. Additional predicted pathogenic mutations and deletions were detected by Sanger sequencing in all six other patients. Pathology of brain tissue of two patients demonstrated severe cerebral atrophy and microscopic brain lesions similar to Leigh's syndrome. Although the localization of *SLC19A3* expression in brain was similar in the two investigated patients compared to age-matched control subjects, the intensity of the immunoreactivity was increased. Previously published patients with *SLC19A3* mutations have a milder clinical phenotype, no laboratory evidence of mitochondrial dysfunction and more limited lesions on magnetic resonance imaging. In some, cerebral atrophy has been reported. The identification of this new, severe, lethal phenotype characterized by subtotal brain degeneration broadens the phenotypic spectrum of *SLC19A3* mutations. Recognition of the associated magnetic resonance imaging pattern allows a fast diagnosis in affected infants.

INTRODUCTION

Early-infantile onset encephalopathies have a major impact on families. They come with an urgent need for a proper diagnosis in view of immediate therapeutic decisions. Additionally, the diagnosis is important for genetic counselling and family planning. MRI pattern recognition has been proven to be highly successful in facilitating a rapid correct classification and diagnosis.¹ Several novel childhood encephalopathies have been defined by their distinct pattern of MRI abnormalities and in most cases the aetiology has been identified, confirming the validity of this approach.²⁻⁷ Most of these disorders have a genetic aetiology with a Mendelian inheritance pattern. Different genetic techniques, including genome-wide linkage studies and homozygosity mapping, have been used to identify the associated genes.²⁻⁵ Although successful for common Mendelian disorders and large or consanguineous families, these conventional techniques fail to elucidate the related gene in extremely rare Mendelian disorders, unrelated cases from different families, and sporadic cases owing to *de novo* mutations. The recent introduction of whole-exome sequencing has created the opportunity to identify the mutated gene in these cases leading to rapid new gene discoveries.⁶⁻⁸ In the present study we used MRI pattern recognition for the classification of a group of seven patients with a lethal encephalopathy of unknown origin and performed whole-exome sequencing as a first-tier genetic technique to identify the related gene.

PATIENTS AND METHODS

Seven patients from five unrelated families, sharing a previously undescribed distinct MRI pattern, were identified from our MRI database of more than 3000 cases with an unclassified leukoencephalopathy. Patients were included if they met the following MRI criteria: (i) bilateral signal abnormalities of the nucleus caudatus, putamen, globus pallidus and thalamus; (ii) extensive signal abnormalities of the subcortical and central cerebral white matter and the cerebral cortex; (iii) diffuse signal abnormalities of the cerebellar white matter with or without involvement of the cortex; (iv) extensive signal abnormalities in the pons and midbrain; and (v) in the case of follow-up MRIs, atrophy of affected structures.

Detailed clinical information, laboratory investigations and autopsy results were retrospectively collected and reviewed. A molecular diagnosis was not achieved in any of the patients. Blood and/or fibroblasts of all patients were collected. Approval of the ethical standards committee was received for whole-exome sequencing in patients with unclassified leukoencephalopathies, with written informed consent of the parents.

Magnetic resonance imaging pattern recognition

A total number of 15 MRIs were available for the study. MRIs were evaluated according to a previously published protocol by consensus of two investigators (S.H.K. and M.S.v.d.K.).⁹ Studies typically included sagittal T₁-weighted spin-echo images and axial T₁-weighted, T₂-weighted and proton density spin-echo images. FLAIR images were available in six patients. Signal changes were defined as abnormally high signals on T₂-weighted images. White matter rarefaction was defined as T₂-hyperintense white matter areas with low signal on FLAIR or proton density, but not as low as the signal CSF. Cystic degeneration was defined as T₂-hyperintense white matter areas with a low signal on FLAIR or proton density, as low as the signal of CSF. Cerebral atrophy was scored as mild, moderate or severe, based on the presence of cerebral or cerebellar sulcal prominence, enlargement of the ventricles and subjective assessment of brainstem size. Apparent diffusion coefficient maps were used to assess restricted diffusion to avoid the T₂-shinethrough effects. Because magnetic resonance spectroscopy studies were obtained with different techniques on machines from different vendors, we only looked at the presence of lactate, represented by a doublet centred at 1.33 parts per million. The MRIs of four disease stages (acute, post-acute, intermediate and end-stage) were grouped together.

Whole-exome sequencing

Whole-exome sequencing was performed in Patient 2. Genomic DNA was extracted by standard methods. Exonic targets were enriched with SeqCap EZ Human Exome Library v2.0 kit (Nimblegen). Sequencing was performed with 100 bp paired-end reads on a Hiseq2000 (Illumina). Read alignment to the human genome assembly hg19 was performed with Burrows-Wheeler Aligner tool (v0.5.9) (<http://bio-bwa.sourceforge.net>).¹⁰ Single-nucleotide variants and small insertions and deletions were called with Varscan v2.2.5 (<http://varscan.sourceforge.net>)¹¹ and annotated with Annovar (<http://www.openbioinformatics.org/annovar>).¹² Novelty of variants was determined using public single nucleotide polymorphism databases, including dbSNP132 (<http://www.ncbi.nlm.nih.gov/projects/SNP>) and the 1000 Genomes project (release November 2010), and our in-house control exomes (yielding 17 exomes of patients with different disease phenotypes). PolyPhen-2 was used for pathogenicity prediction of variants (<http://genetics.bwh.harvard.edu/pph2/>).¹³

Mutation analysis

All coding exons and the adjacent splice sites of the *SLC19A3* gene of the index patients were amplified by PCR (NG_016359.1). For one case the full length open reading frame was amplified by reverse-transcription PCR (NM_025243.3). The DNA of parents was only

investigated for the amplicons containing the familial mutations. All *SLC19A3* amplicons were analysed by direct DNA sequence analysis. The amplicons were analysed by capillary electrophoresis using an ABI3130xl genetic analyser (Applied Biosystems) and assessed using Mutation Surveyor® (Softgenetics). Primer sequences are available on request.

Pathology

Brain tissue from Patients 3 and 4 was collected at autopsy at The Hospital for Sick Children, Toronto, Ontario, Canada. Macroscopic and microscopic characteristics and the expression patterns of *SLC19A3* and *SLC19A2* were studied. To investigate the normal expression of *SLC19A3* and *SLC19A2*, post-mortem brain tissue samples were obtained from four unrelated age-matched control subjects without significant confounding neuropathological findings at autopsy and from one 2-year-old child with Leigh's syndrome. Leigh's syndrome was diagnosed based on the clinical course, the typical MRI pattern and pathology findings of Leigh's syndrome at autopsy. No molecular diagnosis was achieved. Formalin-fixed, paraffin-embedded tissue was sectioned at 6 µm and stained for haematoxylin and eosin or Kluver-periodic acid Schiff according to standard methods. Additionally, tissue sections were incubated with antibodies against the following epitopes: *SLC19A3* (Sigma, 1:500) and *SLC19A2* (Sigma, 1:100), glial fibrillary acidic protein (GFAP, marker of astrocytes; Millipore, 1:1000), proteolipid protein (PLP, myelin marker; AbDSerotec, 1:3000), neuronal nuclear antigen (NeuN, marker of neurons; Sigma, 1:500), platelet endothelial cell adhesion molecule 1 (PECAM1/CD31, vascular endothelial cell marker; Dako, 1:50), and collagen IV (basement membrane marker; Dako, 1:50). Negative controls by omitting the primary antibody were included in each experiment to verify the specificity of the immunohistochemical labelling. Briefly, sections were deparaffinized and rehydrated. Endogenous peroxidase activity was quenched by incubating the slides in 0.3% hydrogen peroxide in methanol. Slides were rinsed with distilled water and transferred to citric acid (pH 6). Heat-induced antigen retrieval was performed using microwave irradiation for 15 min on low setting. Tissue sections were then cooled to room temperature, rinsed and incubated overnight with primary antibodies. Slides were rinsed and the antibody visualized with diaminobenzidine tetrachloride. Between incubation steps, sections were thoroughly washed. After a short rinse in tap water, sections were counterstained with haematoxylin, washed, dehydrated and mounted with polyvinyl alcohol medium with Dabco® (Sigma). Double and triple fluorescence immunohistochemical stainings were performed on cryosections of snap-frozen brain tissue from the same control subjects. Tissue sections were fixed in 2% paraformaldehyde, subsequently permeabilized with 0.1% saponin, blocked in 5% normal goat serum and incubated with primary antibodies overnight at

4°C. After staining with secondary antibodies (Alexa Fluor® 488-, 568-, and 647-tagged; Molecular Probes, 1:400), sections were counterstained with DAPI (nuclear stain; Molecular Probes, 10 ng/ml) and photographed using a Leica DM6000B microscope (Leica Microsystems).

RESULTS

Magnetic resonance imaging findings

Detailed MRI findings are outlined in Supplementary Table 1. Most patients had more than one brain MRI; only Patients 1 and 2 had a single MRI. Four follow-up MRIs were available in Patient 5, illustrating all four disease stages (Supplementary Figure 1). The acute phase (MRI of two patients, Supplementary Table 1; Figure 1, A–C, Patient 1) was characterized by severe swelling and diffuse T_2 -hyperintensity of the cerebral and cerebellar white matter and cortex. Typically, the depths of the sulci of the cerebral and cerebellar cortex were affected, with a high T_2 -signal, while the gyral crowns had a more normal, low T_2 -signal. Severe swelling and T_2 -hyperintensity of central grey nuclei, including the thalamus, putamen, globus pallidus, caudate nucleus and dentate nucleus were present in both patients. The brainstem displayed extensive signal abnormalities with relative sparing of the medulla oblongata. Rarefaction of the deep cerebral white matter was seen in Patient 1. Diffusion imaging of Patient 5 showed restricted diffusion in multiple areas of the cerebral cortex and white matter, corpus callosum, basal nuclei, thalamus, brainstem, and cerebellar white matter.

The post-acute phase (MRI of three patients, Supplementary Table 1; Figure 2, A–F, Patient 6) was characterized by partial resolution of cerebral white matter swelling with rarefaction and/or cystic degeneration of predominantly the subcortical white matter, the basal nuclei and thalamus. The pulvinar was relatively spared in Patients 6 and 7. Diffusion imaging was performed in Patient 6 and revealed extensive areas of restricted diffusion in cerebral white and grey matter structures (Figure 2, D and E). The widespread signal abnormalities of midbrain and pons persisted in all patients and new signal abnormalities of the medulla oblongata developed in Patient 5.

The intermediate phase (MRI of six patients, Supplementary Table 1; Figure 3, A–C; Patient 3) consisted of a variable degree of atrophy of the brainstem, thalami, basal nuclei, cerebral white matter and corpus callosum, accompanied by extensive thinning of the cerebral cortex. Rarefaction of cerebral and/or cerebellar white matter was present in three of the six patients.

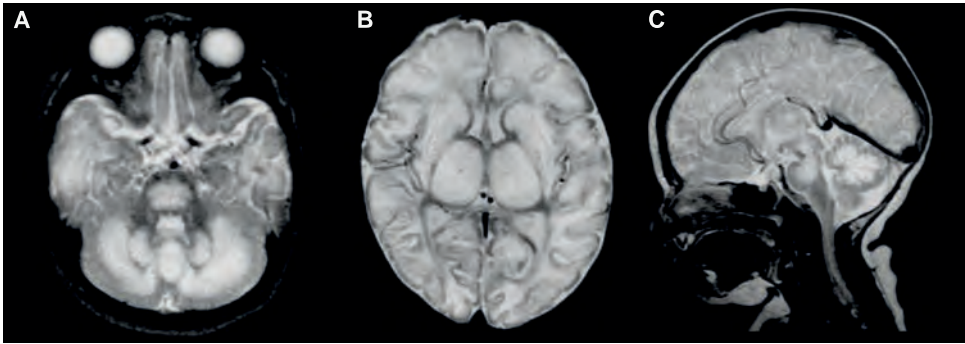


Figure 1. Axial (A and B) and sagittal (C) T₂-weighted images in Patient 1 at 3 months of age, illustrating the acute phase. Note the extensive swelling and T₂-hyperintensity of the cerebral and cerebellar white matter, basal nuclei and thalami (B). The depths of the gyri of the cerebral and cerebellar cortex are more affected than the gyral crowns (B and C).

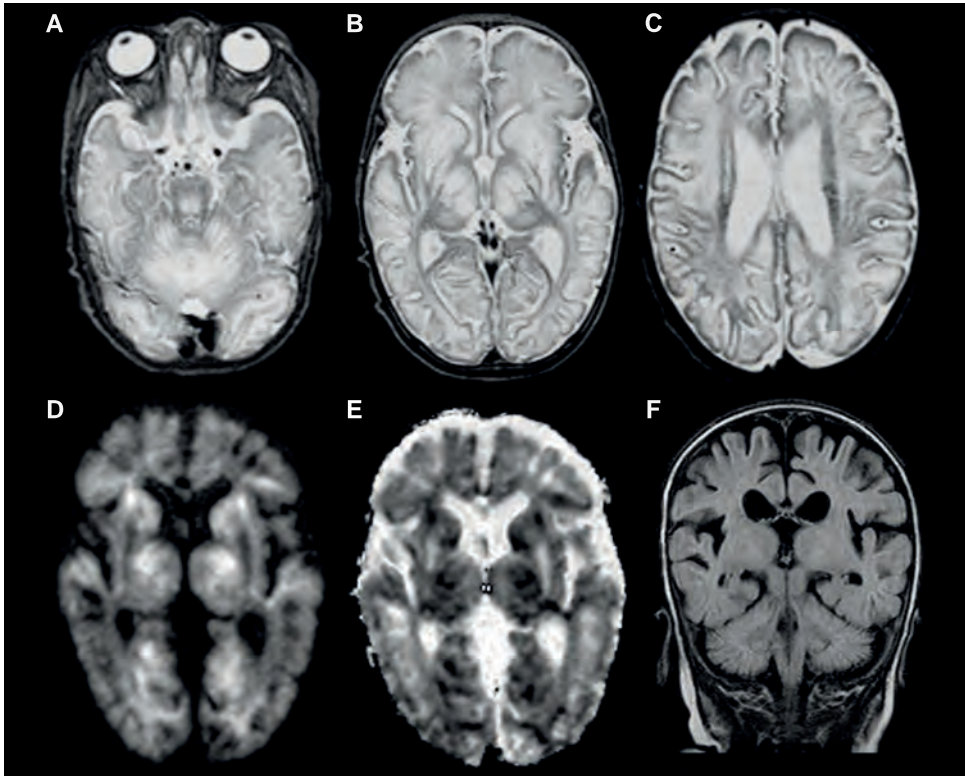


Figure 2. Axial T₂-weighted images (A–C), diffusion-weighted images (D and E), and a coronal FLAIR image (F) in Patient 6 at 2.9 months of age, illustrating the post-acute phase. Moderate swelling of the cerebral white matter, basal nuclei and thalami is observed (B and C). Note the relative sparing of the pulvinar (B). There is restricted diffusion in the thalami, caudate nucleus and different parts of the cerebral white matter (D and E). Multiple areas of rarefied white matter are present (F).

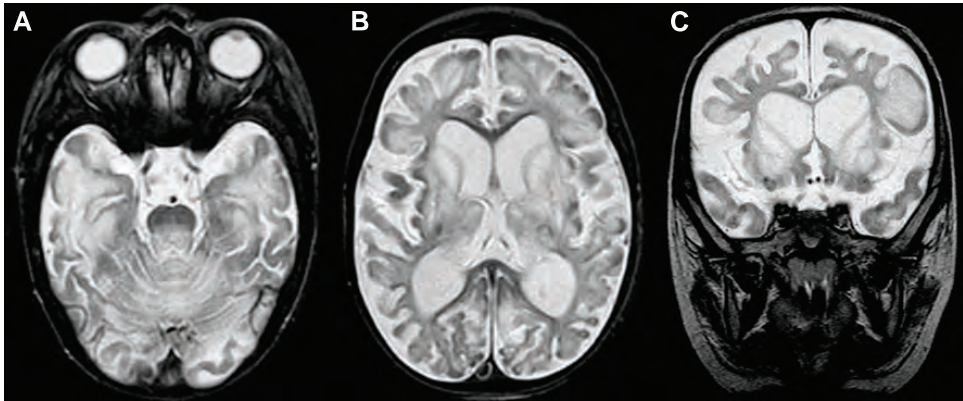


Figure 3. Axial (A and B) and coronal (C) T_2 -weighted images in Patient 3 at 2.3 months of age, illustrating the intermediate phase. Note the atrophy of the cerebral white matter and thinning of the cortex (B and C). Cystic lesions of the basal nuclei, thalami and subcortical white matter are present (B and C). The T_2 -hyperintensity of the pons is restricted to the central-dorsal area (A).

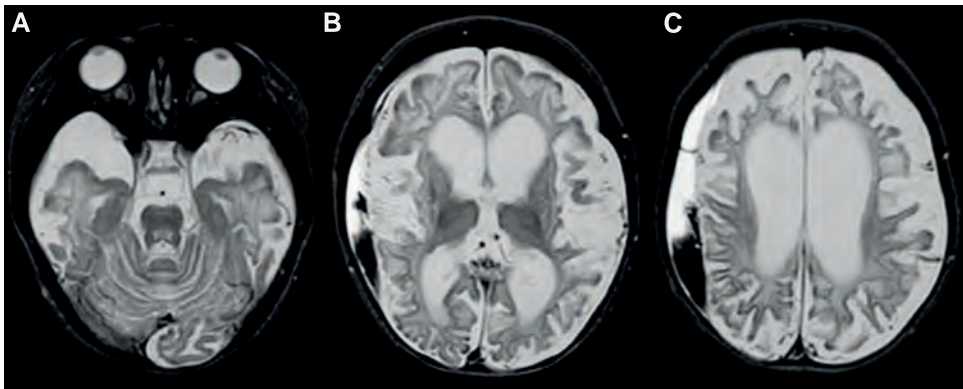


Figure 4. Axial T_2 -weighted images in Patient 4 at 9.5 months of age, illustrating the end phase. Note the advanced atrophy of the cerebral white matter, basal nuclei, thalami and cortex (A–C). The signal abnormalities of the pons have almost completely disappeared (A).

Cyst-like structures were present throughout the cerebral white matter, the thalami, basal nuclei, and cerebellar white matter in two patients. Although the widespread T_2 -hyperintensity of the brainstem decreased, focal T_2 -signal abnormalities localized in the central-dorsal area of the tegmentum of pons and midbrain persisted. Previously detected areas of restricted diffusion resolved. A subdural haematoma developed in three patients, most likely due to advancing cerebral atrophy.

The end stage (MRI of five patients, Supplementary Table 1; Figure 4, A–C, Patient 4) was characterized by severe atrophy of the cerebral white matter and cortex, corpus callosum, thalami and basal nuclei. Cerebellar atrophy was noted in three patients.

Atrophy of the pons and midbrain with persisting T₂-hyperintensity of the central-dorsal area of the tegmentum of pons and midbrain was present in four patients.

Elevated lactate in affected white and grey matter was found by magnetic resonance spectroscopy in five patients during one or more disease stages (Supplementary Table 1). Contrast was given to Patients 6 and 7 during the post-acute phase, and to Patient 5 during the intermediate phase. No enhancement was observed. It is important to note that the four disease stages followed each other rapidly and that the brain abnormalities evolved in the course of a few weeks to months.

Clinical findings

Detailed clinical characteristics and findings at last examination are described in Supplementary Table 2. Patients 2 and 4, as well as Patients 5 and 7 are siblings. Consanguinity was present in two families. Pregnancy and delivery were uneventful for all patients. Early psychomotor development was delayed in the siblings Patients 5 and 7. The initial signs were noted between 8 weeks and 5.5 months of age (mean 2.7 months) and included irritability, seizures or suspected seizures, sometimes infantile spasms, loss of contact, somnolence and lowering of consciousness, extensor spasms, feeding difficulties and failure of achieving developmental milestones. A preceding event was evident in six patients, including (viral) infection or vaccination shortly before onset. Within a few weeks after the first signs, all patients showed rapid and severe regression of neurological functions with progressive spasticity, deterioration of contact, feeding difficulties, and eventually respiratory failure. Six patients died before the age of 2 years (range 4–20 months); Patient 6 died at the age of 4 years and 8 months. Neurological examination predominantly showed pyramidal signs of arms and legs; no extrapyramidal signs were present. Ophthalmological investigation revealed optic nerve atrophy in most patients. None of the seven patients had involvement of other organs or dysmorphic features. Patients 1 and 3 received a 'mitochondrial' cocktail, including vitamin B6, co-enzyme Q, riboflavin, nicotinamide, and biotin, but no thiamine. No beneficial effect of the supplements was observed.

Laboratory findings

Laboratory findings are summarized in Supplementary Table 3. Plasma lactate levels were elevated in five patients at initial presentation (range 3.3–4.6 mmol/l, normal values 1.2–2.2 mmol/l) and showed a subsequent gradual decline during follow-up. Amino acid levels in blood revealed a slightly elevated alanine in three patients with increased ornithine and glycine in one patient. Plasma thiamine levels were not measured. Urinary organic acids were normal in all patients. A slightly reduced activity of one or more

respiratory chain enzyme complexes in muscle was found in three patients. However, normal enzyme activities were measured in skin fibroblasts. Ragged red fibers or structural mitochondrial abnormalities were not observed. Mutation analysis of whole mitochondrial DNA in blood or targeted mutation analysis of mitochondrial DNA in muscle or blood revealed no mutations in the tested patients.

Whole-exome analysis

Whole-exome sequencing was performed in DNA of Patient 2. To prioritize candidate disease genes, we filtered the raw data based on the assumptions that the causal variant was not present in control exomes, was compliant with an autosomal recessive inheritance and altered the amino acid sequence, as summarized in Supplementary Table 4. This approach selected three genes with variants fulfilling these criteria: *SLC19A3* (MIM*606152), *SLC34A1* (MIM*182309) and *OBSL1* (MIM*610991). Based on conservation status, predicted pathogenicity using Polyphen-2¹³ and a literature search for disease phenotypes linked to these genes, we selected *SLC19A3* as the best candidate gene. The two heterozygous *SLC19A3* variants detected in Patient 2, a c.541T>C transition predicting the replacement of serine at protein position 181 by proline p.Ser181Pro and a c.1154T>G transversion predicting a p.Leu385Arg replacement, were confirmed by Sanger sequencing. DNA from the parents was not available to confirm compound heterozygosity.

SLC19A3 mutation analysis

Sanger sequencing of *SLC19A3* identified missense and nonsense mutations and deletions in all seven patients (Table 1). Except for Patients 5 and 7, no DNA from parents was available so carrier status in the parents could not be confirmed. All identified mutations were not present in 13 000 control chromosomes of subjects included in the NHLBI GO Exome Sequencing Project database and were predicted to be probably pathogenic by Polyphen-2¹³ (Table 1). Patient 1 harboured the p.Gly23Val mutation on one allele, which was previously found in homozygous state in two patients from a Yemeni family with biotin-responsive basal ganglia disease.¹⁴

Brain pathology

Macroscopic examination of the brain of Patients 3 and 4 showed severe atrophy of the cerebral cortex, deep grey matter structures and subcortical and central white matter. Microscopic examination confirmed the involvement of both grey and white matter with multiple, bilateral and often symmetric infarct-like lesions in the cerebrum, brainstem (Figure 5, G) and cerebellum. All lesions were characterized by rarefaction and vacuolar degeneration to cavitory necrosis of the neuropil and surrounding white

Table 1. *SLC19A3* mutations in present patients

Patient	Country of origin	c.DNA	Deduced effect ^a	Type of mutation	State	Exon
1	Canadian	c.68G>T ^b	p.Gly23Val ^b	missense	heterozygous	2
		r.1173_1314del	p.Gln393*	exon deletion	heterozygous	5
2 and 4 (sibs)	European	c.541T>C	p.Ser181Pro	missense	heterozygous	3
		c.1154T>G	p.Leu385Arg	missense	heterozygous	4
3	European	c.507C>G	p.Tyr169*	nonsense	heterozygous	3
		c.527C>A	p.Ser176Tyr	missense	heterozygous	3
5 and 7 (sibs)	Lebanese	c.895_925del	p.Val299fs*	frameshift	homozygous ^c	3
6	Moroccan	c.1332C>G	p.Ser444Arg	missense	homozygous	6

The missense mutations described in this table are presumed to be pathogenic, because all mutations have been analysed with Polyphen-2 and had prediction scores of ≥ 0.92 , the amino acids involved are all moderately to highly conserved, and none of the mutations were detected in ≥ 13000 control alleles. However, to confirm pathogenicity overexpression studies need to be performed. All other type of mutations detected in this study should be considered pathogenic based on their truncating nature.

^a Nomenclature rules of den Dunnen JT and Antonarakis SE.¹⁵

^b Known mutation.¹⁴

^c Both parents are carrier of the mutation, confirming homozygosity for the mutation in their affected children

matter, accompanied by prominent, dilated capillaries and reactive astrogliosis (Figure 5, A–D). In the cerebral and cerebellar cortex these lesions affected preferentially the depth of the sulci and extended to the pial surface (Figure 5, E and F). Here subtotal loss of neurons was associated with infiltration of lipid-laden macrophages and mineralization of the residual neurons (Figure 5, B).

The lesions in the basal nuclei (Figure 5, D), brainstem and cerebellum had the same histopathological features. Notably, well-preserved neurons in the context of necrotizing areas were found in the midbrain and pontine tegmentum (Figure 5, H). Although relatively spared, the deep white matter also showed myelin pallor, microcystic changes, dilated perivascular spaces, and marked isomorphic reactive astrogliosis (data not shown).

In the non-neurological controls, *SLC19A2* and *SLC19A3* were expressed in the blood vessels throughout the brain (Figure 6, A and B). Double labelling showed co-localization of *SLC19A3* with collagen IV at the basement membrane and in the surrounding pericytes (Supplementary Figure 2, A). By contrast, *SLC19A2* immunoreactivity was found only at the luminal side of the blood vessels, where it co-localized with the endothelial marker CD31 (Supplementary Figure 2, D). In the control cerebral cortex, *SLC19A3* expression was also found in meningeal cells and in some NeuN-positive small neurons in the deeper cortical layers (Supplementary Figure 2, F) and immediately subcortical cerebral white matter (Figure 6, A). Scattered *SLC19A3*-positive neurons were also seen in the brainstem and cerebellar nuclei. No *SLC19A3* expression was seen in astrocytes (Figure 6, A; Supplementary Figure 2, E and F). No other *SLC19A2*-positive cell types beside

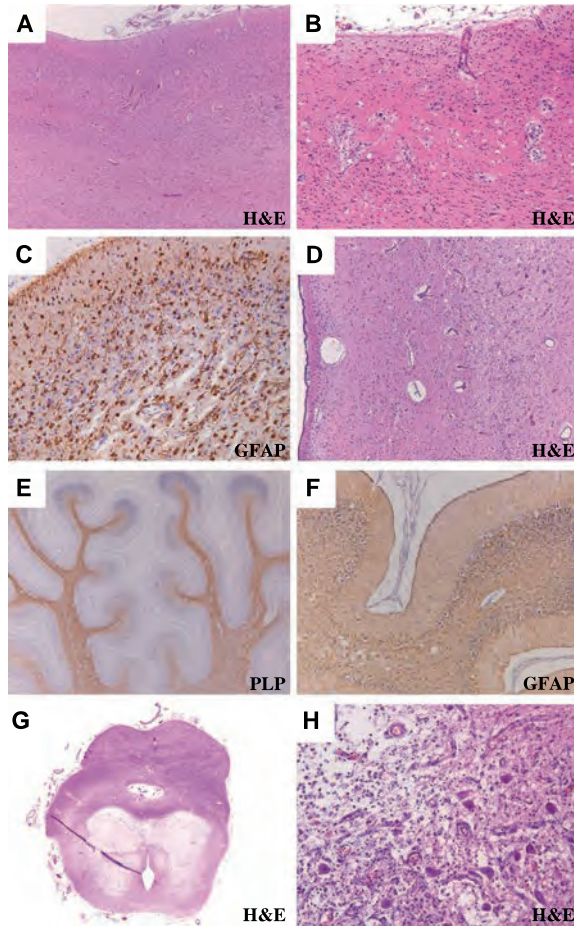


Figure 5. Haematoxylin and eosin (H&E) stain of the cerebral cortex shows an infarct-like lesion extending to the pial surface and to the subcortical white matter (A, Patient 4). Note the relatively spared cortex on the left side of the picture. At higher magnification lesions display rarefaction and loosening of the neuropil with subtotal loss of neurons, lipophages and chronic fibrillary astrogliosis (B, Patient 4). Immunolabelling for glial fibrillary acidic protein (GFAP) shows marked reactive proliferation of astroglial cells (C, Patient 4). Haematoxylin and eosin stain of the basal nuclei shows rarefaction of the neuropil with vascular prominence in the putamen (D, Patient 4). Immunostain for the proteolipid protein (PLP) shows white matter rarefaction with loss of stainable myelin deeper in the folia. Note also the moderate cortical atrophy and the relative sparing of the cortex at the crowns of the gyri, with still visible external and internal granular layers (E, Patient 3). Immunolabelling for glial fibrillary acidic protein from the same patient shows reactive proliferation of the white matter astrocytes and of the Bergmann glia. Note also the total loss of neurons in the depth of the gyri, including the Purkinje cells (F, Patient 3). Whole mount of haematoxylin and eosin-stained cross section through the pontomesencephalic junction shows bilaterally symmetric necrotizing lesions in the tectum and tegmentum with relative sparing of the peri-aqueductal areas. Note the presence of an additional midline necrotizing lesion in the raphe (G, Patient 4). Haematoxylin and eosin stain of the oculomotor nucleus (III cranial nerve) in the midbrain shows marked rarefaction of the neuropil with astrogliosis, lipophages, dilated blood vessels and relative sparing of some neuronal cells (H, Patient 3).

blood cells were seen in the cerebral cortex (data not shown), whereas scattered faintly SLC19A2-positive neurons were visible in the deep cerebellar nuclei (Figure 6, B) and in the brainstem.

In the two *SLC19A3*-mutated patients, as well as in the patient with Leigh's syndrome, a stronger immunoreactivity for both SLC19A3 and, to a lesser degree, SLC19A2 was detected in the wall of the blood vessels (Figure 6, C–F). The localization of both transporters was the same as in normal control tissue. In contrast with non-neurological controls, numerous SLC19A3-positive astrocytes were also seen in and around infarct-like lesions in the *SLC19A3*-mutated patients (Figure 6, C and E) and, to a lesser degree, in the patient with Leigh's syndrome (Figure 6, D). Increased SLC19A3 expression was also detected in subpial astrocytes (Figure 6, C).

DISCUSSION

Using MRI pattern recognition we identified a group of young infants with a dramatic, lethal encephalopathy with subtotal brain degeneration. Exome sequencing of one patient and subsequent Sanger sequencing of six patients revealed (presumed) pathogenic mutations in the *SLC19A3* gene. *SLC19A3* encodes the second thiamine transporter and is ubiquitously expressed, including in brain.¹⁶

The cerebral MRI abnormalities of our patients indicate rapid onset and massive neuronal cell death, suggestive of severe energy failure. The white matter abnormalities can be explained by Wallerian degeneration. Different disease phases follow each other rapidly and soon lead to subtotal brain degeneration. Initial diffuse swelling with T₂-hyperintensity of the cerebral cortex and white matter, caudate nucleus, putamen, globus pallidus, thalami, dentate nucleus, cerebellum, pons and midbrain is followed by rarefaction and cystic degeneration of the white matter and progressive cerebral, cerebellar and brainstem atrophy. Deficiency of thiamine pyrophosphate, the active form of thiamine, can explain this energy failure due to its important role as cofactor for three major enzyme systems involved in the tricarboxylic acid cycle. The developing brain is a large energy consumer and can therefore be regarded as one of the most vulnerable organs for thiamine deficiency.

Parallel to the rapidly progressive MRI abnormalities, patients deteriorate dramatically within a few weeks after the first signs and die early. In the majority of the patients the onset of deterioration was preceded by an infection or vaccination, a feature also

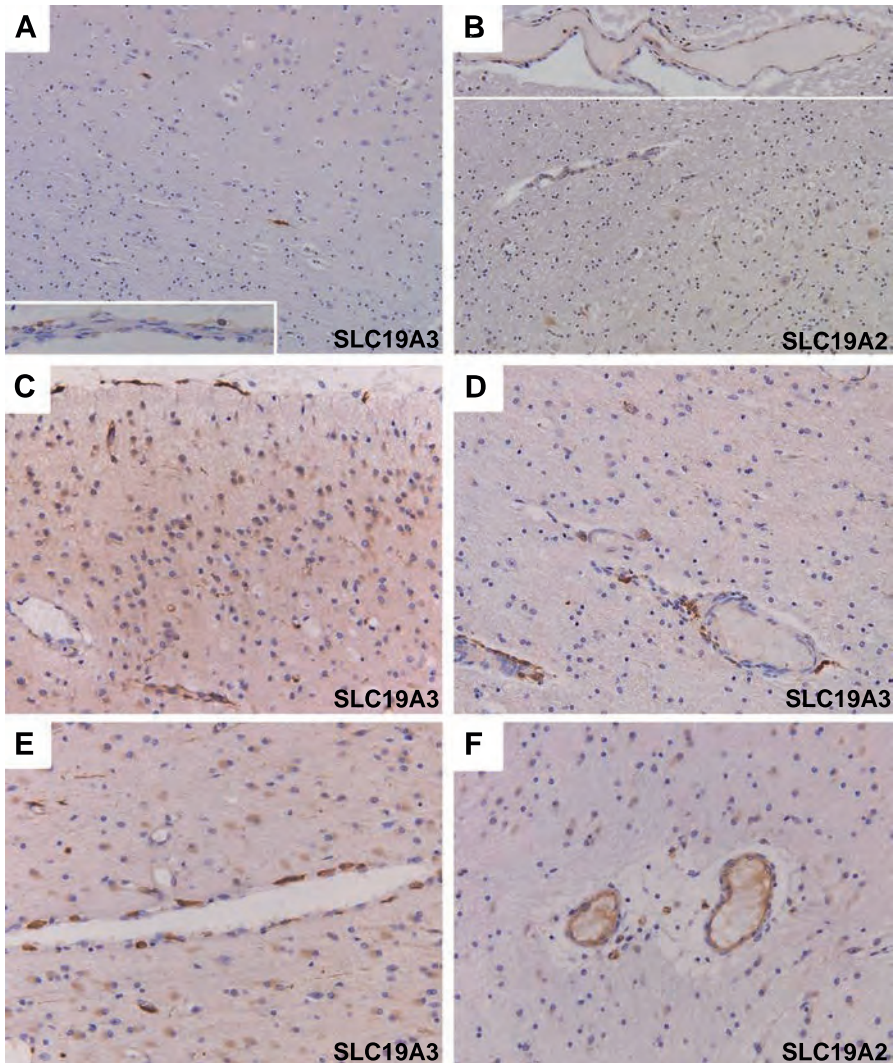


Figure 6. Stain for SLC19A3 in control brain tissue shows scattered strongly immunoreactive neurons in the deeper cerebral cortex (*top right*) and corticosubcortical junction (A). SLC19A3-immunoreactivity is also visible in the wall of blood vessels (A, *inset*) along the basement membrane and in pericytes. Stain for SLC19A2 of the cerebellar white matter shows immunopositivity of the vascular endothelial cells (B, *inset*). Note also a faint immunoreactivity in the neurons of the dentate nucleus (B). Labelling for SLC19A3 of a cortical lesion from Patient 4 shows increased immunoreactivity at the blood vessel walls and immunopositive parenchymal and subpial astrocytes (C). A similar constellation of findings is visible in a grey matter lesion from the age-matched control with Leigh's encephalopathy unrelated to SLC19A3. Note the apparent less pronounced SLC19A3-immunoreactivity in the reactive astrocytes (D). Stain for SLC19A3 of a relatively spared subcortical white matter area in the frontal lobe of Patient 4 shows strong immunoreactivity in the perivascular pericytes and, to a lesser extent, in the reactive astrocytes (E). Labelling for SLC19A2 of the same brain region of the same patient shows increased immunopositivity in the vascular endothelial cells and reactive astrocytes (F).

commonly seen in mitochondrial disorders. Most patients have elevated lactate levels in plasma and on spectroscopy. These findings are consistent with the hypothesis that thiamine deficiency leads to decreased oxidative decarboxylation of pyruvate and α -ketoglutarate acid, resulting in pyruvate accumulation and lactate production.¹⁷

In our patients, brain pathology shows symmetric, bilateral infarct-like lesions with profound loss of neurons, astrogliosis and vascular prominence, comparable to what is observed in Leigh's syndrome.¹⁸ The observation that the crowns of the gyri are less severely affected than the depth of the sulci, as seen both by brain MRI and histologically, is a typical finding in conditions of energy failure.¹⁹ The pathological findings in our patients are, however, more severe and extensive than commonly observed in patients with Leigh's syndrome.¹⁸

The expression of *SLC19A3* and *SLC19A2* has been extensively studied in intestinal and renal epithelial cells,^{20,21} but not in the brain. In our study, we found that both wild-type transporters are differentially expressed within cerebral blood vessels. *SLC19A2* is expressed exclusively at the luminal side, while *SLC19A3* is solely present at the basement membrane and in perivascular pericytes. This distribution differs from that observed in intestinal and renal epithelial cells, where *SLC19A3* is present at the luminal apical side and *SLC19A2* at both the luminal and baso-lateral side.^{20,21} This differential distribution could indicate a different role of both thiamine transporters in thiamine homeostasis. Because the localization of both transporters in the brain is different than observed in renal and intestinal tissue, regulation of thiamine homeostasis could be different for these organs.

Compared with non-neurological controls, both transporters locate to the same position in cerebral blood vessels of the two *SLC19A3*-mutated patients investigated histopathologically. However, their expression is increased. The observation that their expression is also increased in the patient with Leigh's syndrome may imply that the upregulation of the thiamine transporters is not the direct consequence of decreased intracellular thiamine, but of decreased energy availability. In the two investigated *SLC19A3*-mutated patients, however, *SLC19A3* and *SLC19A2* expression was detected in reactive astrocytes to a greater degree than in the patient with Leigh's syndrome. This suggests that the intracellular thiamine level affects the expression of both transporters in this cell type. The increased *SLC19A3* and *SLC19A2* expression is possibly due to a regulatory feedback mechanism. We could not determine whether this is specific for the brain or also concerns the thiamine transporters located in other organs, like the intestine and the kidney, because no intestinal or renal material from patients was available in which we could investigate the expression of the transporters. Plasma

thiamine levels were not measured, so it remains unknown if thiamine absorption in the intestine or kidney is affected in these patients. It also remains to be investigated whether increased brain *SLC19A3* and *SLC19A2* expression is a general feature observed in patients with *SLC19A3* mutations.

3

Until now, *SLC19A3* mutations have been associated with three different clinical variants (see Supplementary Table 5 for an overview of all patients reported with *SLC19A3* mutations): basal ganglia disease (MIM#607483), Wernicke-like encephalopathy (MIM#607483) and a more generalized encephalopathy.^{14,22-25} Patients with basal ganglia disease have a childhood or adolescent onset encephalopathy, mainly characterized by epilepsy, confusion, dysarthria, dysphagia and extrapyramidal symptoms. MRI shows focal lesions predominantly in the putamen and caudate nucleus. Patients improve on biotin or thiamine medication.^{14,23,25} Patients with Wernicke-like encephalopathy have an adolescent onset encephalopathy, clinically resembling Wernicke syndrome. MRI also shows the typical abnormalities involving the peri-aqueductal grey and medial thalamus. These patients improved on thiamine medication.²² The patients with the more generalized encephalopathy have an infantile onset and a more severe phenotype, characterized by infantile spasms and psychomotor retardation. Besides focal lesions in the basal nuclei, their brain MRI also shows cerebral atrophy.²⁴ The effect of biotin or thiamine could not be determined in the latter patients. Overall, these three phenotypes have a milder clinical course and a different MRI pattern with more limited abnormalities than our patients. Elevated lactate levels as evidence of mitochondrial dysfunction were not reported in any of these cases.

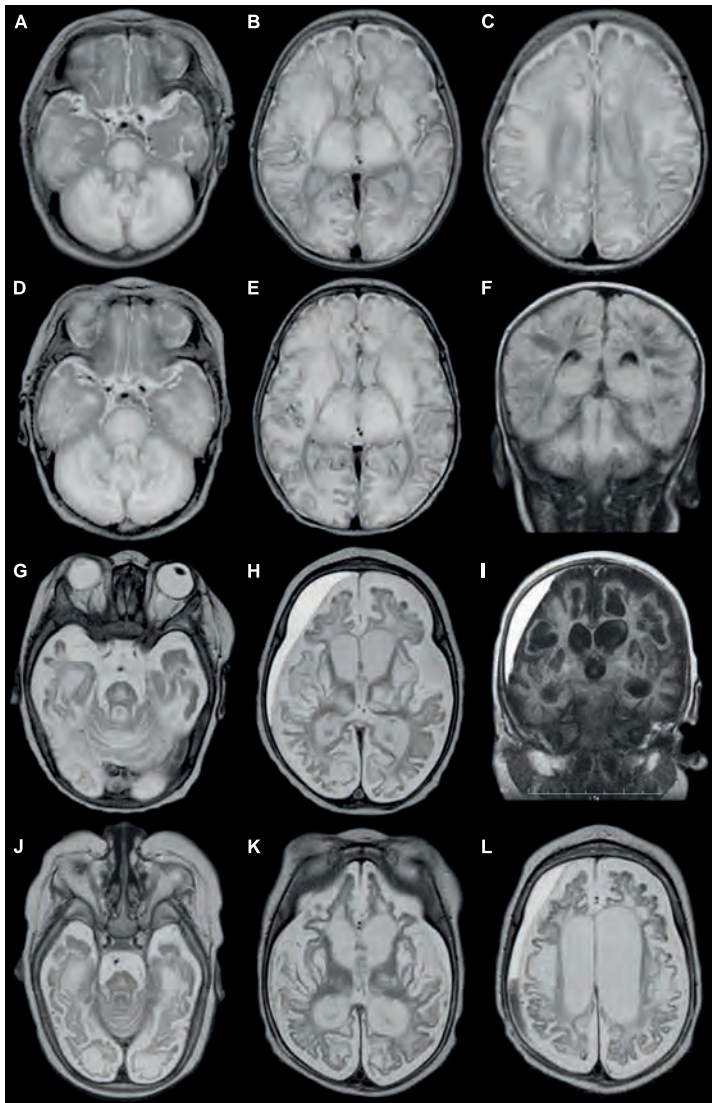
We identified different heterozygous or homozygous missense and nonsense mutations and deletions in *SLC19A3* in our patients. All mutations identified were novel, except for the heterozygous p.Gly23Val mutation in Patient 1 (on the other allele this patient had a deletion of 141 base pairs). This mutation was previously found in homozygous state in two patients from one family with basal ganglia disease.¹⁴ Owing to the small number of patients known, a clear genotype–phenotype relationship cannot be established. The consistent phenotype in multiple affected siblings, however, suggests that the genotype indeed influences the phenotype. It could be that patients with a milder phenotype are less vulnerable to thiamine deficiency due to some remaining function of the mutant protein or due to individual genetic or epigenetic factors, for instance positively influencing the expression of *SLC19A2* or *RFC1*, a potential thiamine monophosphate transporter.^{26,27}

Our findings broaden the phenotypic spectrum of patients with *SLC19A3* mutations. The cause of the clinical heterogeneity associated with mutated *SLC19A3* remains to be elucidated. Recognition of the distinctive MRI pattern associated with the different clinical phenotypes is important as it allows a rapid diagnosis in affected infants. Regarding treatment possibilities, two of our patients received biotin, without thiamine, and had no signs of improvements. The problem with this severe phenotype is that the brain damage is already extensive when patients come to medical attention. At present, the most important implication of the diagnosis for families is in genetic counselling and prenatal diagnosis. Whether antenatal supplementation of thiamine and biotin has any beneficial effect remains to be investigated.

REFERENCES

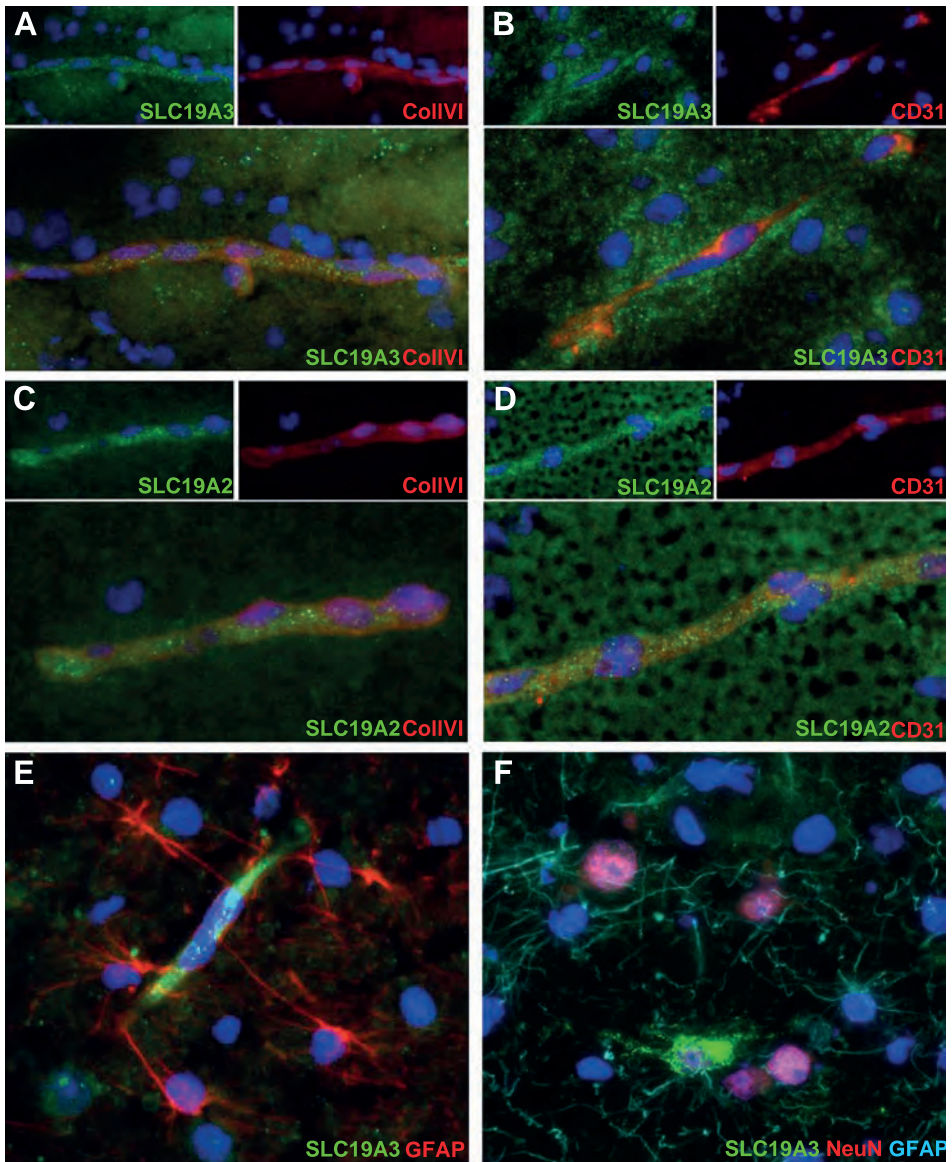
1. Schiffmann R and van der Knaap MS. Invited article: an MRI-based approach to the diagnosis of white matter disorders. *Neurology* 2009;72:750-759.
2. Leegwater PA, Yuan BQ, van der Steen J, et al. Mutations of MLC1 (KIAA0027), encoding a putative membrane protein, cause megalencephalic leukoencephalopathy with subcortical cysts. *Am J Hum Genet* 2001;68:831-838.
3. Leegwater PA, Vermeulen G, Konst AA, et al. Subunits of the translation initiation factor eIF2B are mutant in leukoencephalopathy with vanishing white matter. *Nat Genet* 2001;29:383-388.
4. Zara F, Biancheri R, Bruno C, et al. Deficiency of hyccin, a newly identified membrane protein, causes hypomyelination and congenital cataract. *Nat Genet* 2006;38:1111-1113.
5. Scheper GC, van der Klok T, van Andel RJ, et al. Mitochondrial aspartyl-tRNA synthetase deficiency causes leukoencephalopathy with brain stem and spinal cord involvement and lactate elevation. *Nat Genet* 2007;39:534-539.
6. Steenweg ME, Vanderver A, Ceulemans B, et al. Novel infantile-onset leukoencephalopathy with high lactate level and slow improvement. *Arch Neurol* 2012;69:718-722.
7. Steenweg ME, Ghezzi D, Haack T, et al. Leukoencephalopathy with thalamus and brainstem involvement and high lactate 'LTBL' caused by EARS2 mutations. *Brain* 2012;135:1387-1394.
8. Ku CS, Naidoo N, Pawitan Y. Revisiting Mendelian disorders through exome sequencing. *Hum Genet* 2011;129:351-370.
9. van der Knaap MS, Breiter SN, Naidu S, Hart AA, Valk J. Defining and categorizing leukoencephalopathies of unknown origin: MR imaging approach. *Radiology* 1999;213:121-133.
10. Li H and Durbin R. Fast and accurate short read alignment with Burrows-Wheeler transform. *Bioinformatics* 2009;25:1754-1760.
11. Koboldt DC, Chen K, Wylie T, et al. VarScan: variant detection in massively parallel sequencing of individual and pooled samples. *Bioinformatics* 2009;25:2283-2285.
12. Wang K, Li M, Hakonarson H. ANNOVAR: functional annotation of genetic variants from high-throughput sequencing data. *Nucleic Acids Res* 2010;38:e164.
13. Adzhubei IA, Schmidt S, Peshkin L, et al. A method and server for predicting damaging missense mutations. *Nat Methods* 2010;7:248-249.
14. Zeng WQ, Al-Yamani E, Acierno JS, Jr., et al. Biotin-responsive basal ganglia disease maps to 2q36.3 and is due to mutations in *SLC19A3*. *Am J Hum Genet* 2005;77:16-26.
15. den Dunnen JT and Antonarakis SE. Nomenclature for the description of human sequence variations. *Hum Genet* 2001;109:121-124.
16. Rajgopal A, Edmondson A, Goldman ID, Zhao R. *SLC19A3* encodes a second thiamine transporter ThTr2. *Biochim Biophys Acta* 2001;1537:175-178.
17. Jhala SS and Hazell AS. Modeling neurodegenerative disease pathophysiology in thiamine deficiency: consequences of impaired oxidative metabolism. *Neurochem Int* 2011;58:248-260.
18. Powers JM and de Vivo DC. Peroxisomal and mitochondrial disorders. In: Greenfield's Neuropathology. New York: Arnold Press; 2002.
19. van der Knaap MS and Valk J. *Magnetic Resonance of Myelination and Myelin Disorders*. Heidelberg: Springer; 2005.
20. Said HM, Balamurugan K, Subramanian VS, Marchant JS. Expression and functional contribution of hTHTR-2 in thiamin absorption in human intestine. *Am J Physiol Gastrointest Liver Physiol* 2004;286:G491-G498.
21. Ashokkumar B, Vaziri ND, Said HM. Thiamin uptake by the human-derived renal epithelial (HEK-293) cells: cellular and molecular mechanisms. *Am J Physiol Renal Physiol* 2006;291:F796-F805.
22. Kono S, Miyajima H, Yoshida K, Togawa A, Shirakawa K, Suzuki H. Mutations in a thiamine-transporter gene and Wernicke's-like encephalopathy. *N Engl J Med* 2009;360:1792-1794.
23. Debs R, Depienne C, Rastetter A, et al. Biotin-responsive basal ganglia disease in ethnic Europeans with novel *SLC19A3* mutations. *Arch Neurol* 2010;67:126-130.
24. Yamada K, Miura K, Hara K, et al. A wide spectrum of clinical and brain MRI findings in patients with *SLC19A3* mutations. *BMC Med Genet* 2010;171-11.
25. Serrano M, Rebollo M, Depienne C, et al. Reversible generalized dystonia and encephalopathy from thiamine transporter 2 deficiency. *Mov Disord* 2012;27:1295-1298.

26. Zhao R, Gao F, Wang Y, Diaz GA, Gelb BD, Goldman ID. Impact of the reduced folate carrier on the accumulation of active thiamin metabolites in murine leukemia cells. *J Biol Chem* 2001;276:1114-1118.
27. Zhao R, Gao F, Goldman ID. Reduced folate carrier transports thiamine monophosphate: an alternative route for thiamine delivery into mammalian cells. *Am J Physiol Cell Physiol* 2002;282:C1512-C1517.



Supplementary Figure 1.

Axial T₂-weighted images (A-C, D and E, G and H, J-L) and coronal FLAIR images (F and I) in patient 5, illustrating all four disease phases. MRI images at 2.2 months (A-C) demonstrate the acute phase, characterised by severe swelling and T₂-hyperintensity of the cerebral and cerebellar white matter, basal nuclei and thalami. In the post-acute phase (2.4 months), cystic degeneration and rarefaction of white matter evolves (F). In this patient swelling of abnormal white matter is still evident at this stage (D and E). MRI images at 7.2 months (G-I) illustrate the intermediate phase. Severe atrophy of the cerebral white matter, thalami and basal nuclei is already noted. Cystic-like structures are present throughout the brain (H and I). At 10.9 months there is advanced cerebral atrophy that characterised the end-stage (J-L). Note the decreasing signal abnormalities of the brainstem during the subsequent phases (A, D, G, and J).



Supplementary figure 2.

Double labelling for SLC19A3 in control brain tissue with collagen IV (A) or CD31 (B) shows SLC19A3 immunoreactivity in the wall of a blood vessels where it co-localizes with the basement membrane marker collagen IV. Double stain for SLC19A2 with collagen IV (C) or CD31(D) shows SLC19A2 immunopositivity co-localizing with the endothelial cell marker CD31. Double labelling for SLC19A3 and the glial fibrillary acidic protein (GFAP) shows that the SLC19A3 immunoreactivity is restricted to the blood vessel wall. Note one faintly SLC19A3-positive neuron in the left lower corner of the picture (E). Triple stain for SLC19A3 with the neuronal marker NeuN and glial fibrillary acidic protein shows one neuron expressing SLC19A3 at the surface of the perikarion and proximal dendrites (F).

Supplementary Table 1. MRI-findings

		B: Post-acute phase MRIs						
		5: 2(2.4)	6: 2(2.9)	7: 1(4.3)	5: 1(2.2)	1: 1(3.0)	5: 1(2.2)	
Patient nr: MRI nr (age in months)								
Overall conclusion		cystic degeneration	ongoing degeneration	cystic degeneration	swollen brain	swollen brain	swollen brain	
Signal abnormality of:								
Cerebral WM	+	+	+	+	+	+	+	
Predominance WM abn.		diffuse cerebral	diffuse cerebral	diffuse cerebral	diffuse cerebral	diffuse cerebral	diffuse cerebral	
Cerebral cortex	+	+	+	+	+	+	+	
Cerebellar WM	+, diffuse	+, diffuse	+, diffuse	+, diffuse	+, diffuse	+, diffuse	+, diffuse	
Cerebellar cortex	+	+	+	+	+	+	+	
Corpus callosum	+, mild atrophy	+, mild atrophy	+, mild atrophy	+, mild atrophy	+, mild atrophy	+, mild atrophy	+, mild atrophy	
Thalamus	+, swollen	+, swollen	+, swollen	+, swollen	+, swollen	+, swollen	+, swollen	
Putamen	+	+	+	+	+	+	+	
Caudate nucleus	+	+	+	+	+	+	+	
Globus pallidus	+	+	+	+	+	+	+	
Dentate nucleus	+	+	+	+	+	+	+	
Midbrain	+	+	+	+	+	+	+	
Pons	+	+	+	+	+	+	+	
Medulla	-	-	-	-	-	-	-	
Swelling of abn. WM	+	swelling, mild atrophy	swelling, mild atrophy	swelling, mild atrophy	+	+	+	
Depth of sulci cerebral cortex	+	+	+	+	+	+	+	
predominantly affected		-	-	-	-	-	-	
Depth of sulci cerebellar cortex	+				+	+	+	
predominantly affected		-	-	-	-	-	-	
Cerebral atrophy	-	-	mild	mild	-	-	-	
Cerebellar atrophy	-	-	-	-	-	-	-	
Rarefaction		cerebral & cerebellar WM	cerebral WM subcortical	cerebral subcortical WM	deep cerebral WM, putamen	deep cerebral WM, putamen	deep cerebral WM, putamen	
Cystic degeneration	-	cerebral parieto-occipital WM	-	cerebral parietal WM	-	-	-	
Gradient echo/SWI signal abn.	n.d.	n.d.	n.d.	n.d.	-	n.d.	n.d.	
Restricted diffusion	n.d.	areas of cerebral cortex, WM, basal nuclei, thalamus, brainstem, cerebellar WM	areas of cerebral cortex, cerebellar WM, basal nuclei, thalamus, brainstem, cerebellar WM	areas of cerebral cortex, cerebellar WM, CC, basal nuclei, thalamus, brainstem, cerebellar WM	areas of cerebral cortex, cerebellar WM, CC, basal nuclei, thalamus, brainstem, cerebellar WM	areas of cerebral cortex, cerebellar WM, CC, basal nuclei, thalamus, brainstem, cerebellar WM	areas of cerebral cortex, cerebellar WM, CC, basal nuclei, thalamus, brainstem, cerebellar WM	
Lactate in MRS	n.d.	elevated	n.d.	n.d.	n.d.	n.d.	n.d.	
Contrast enhancement	n.d.	-	-	-	n.d.	n.d.	n.d.	

C: Intermediate phase MRIs							
Patient nr: MRI nr (age in months)	2: 1 (3.8)	3: 1 (2.3)	4: 1 (4.7)	5: 3 (7.2)	6: 2 (4.7)	7: 2 (4.4)	
Overall conclusion	ongoing atrophy	ongoing atrophy	ongoing atrophy	cystic degeneration and ongoing atrophy	ongoing atrophy	ongoing atrophy	ongoing atrophy
Signal abnormality of:							
Cerebral WM	+	+	+	+	+	+	+
Predominance WM abn.	diffuse cerebral	diffuse cerebral	diffuse cerebral	diffuse cerebral	diffuse cerebral	diffuse cerebral	diffuse cerebral
Cerebral cortex	+, thinning	+, thinning	+, thinning	+, thinning	+, thinning	+, thinning	+, thinning
Cerebellar WM	+	+	+	+	+	+	+
Cerebellar cortex	+	+	+	+	+	+	+
Corpus callosum	n.e., moderate atrophy	n.e., severe atrophy	n.e., mild atrophy	n.e., severe atrophy	n.e., severe atrophy	n.e., severe atrophy	+, moderate atrophy
Thalamus	+, swollen	+, mild atrophy, cystic	+, pulvinar rel. spared	+, moderate atrophy, cystic	+, moderate atrophy, cystic	+, severe atrophy	+, moderate atrophy
Putamen	+, moderate atrophy	+, mild atrophy, cystic	+, mild atrophy	+, severe atrophy, cystic	+, severe atrophy	+, severe atrophy	+, moderate atrophy
Caudate nucleus	+, moderate atrophy	+, mild atrophy	+, mild atrophy	+, severe atrophy, cystic	+, severe atrophy	+, severe atrophy	+, moderate atrophy
Globus pallidus	+, moderate atrophy	+, mild atrophy	+, mild atrophy	+, severe atrophy, cystic	+, severe atrophy	+, severe atrophy	+, moderate atrophy
Dentate nucleus	+	-	-	-	-	-	-
Midbrain	+	+	+	+, mild atrophy	+, mild atrophy	+, mild atrophy	+, mild atrophy
Pons	+	+	+	+, mild atrophy	+, mild atrophy	+, mild atrophy	+
Medulla	+	-	-	+	-	-	-
Swelling of abn. WM	-	-	-	-	-	-	-
Depth of sulci cerebral cortex predominant affected	+	+	+	+	-	-	-
Depth of sulci cerebellar cortex predominant affected	-	+	-	-	-	-	-
Cerebral atrophy	moderate	moderate	moderate	severe	severe	moderate	moderate
Cerebellar atrophy	-	-	-	mild	severe	-	-
Rarefaction	cerebral and cerebellar WM, thalami	-	subcortical cerebral WM	cerebral and cerebellar WM	severe	-	-
Cystic degeneration	-	cerebral WM, basal nuclei and thalami	-	cerebral and cerebellar WM, basal nuclei, thalami	-	-	-
Gradient echo/SWI signal abn.	n.d.	n.d.	n.d.	n.d.	n.d.	n.d.	n.d.
Restricted diffusion	n.d.	n.d.	n.d.	-	-	-	-
Lactate in MRS	n.d.	n.d.	n.d.	n.d.	elevated	elevated	elevated
Contrast enhancement	n.d.	n.d.	n.d.	-	n.d.	n.d.	n.d.

D: End phase MRI	3: 2 (11.7)	4: 2 (9.5)	5: 4 (10.9)	6: 3 (62.3)	7: 3 (8.9)
Overall conclusion	cerebral destruction	cerebral destruction	cerebral destruction	cerebral destruction	cerebral destruction
Signal abnormality of:					
Cerebral WM	+	+	+	+	+
Predominance WM abn.	diffuse cerebral	diffuse cerebral	diffuse cerebral	diffuse cerebral	diffuse cerebral
Cerebellar WM	+, diffuse	+, diffuse	+, diffuse	+, diffuse	+, diffuse
Cerebral cortex	+, thinning	+, thinning	+, thinning	+, thinning	+, thinning
Cerebellar cortex	+	+	+	+	+
Corpus callosum	-, moderate atrophy	n.e., severe atrophy	n.e., severe atrophy	n.e., severe atrophy	n.e., severe atrophy
Thalamus	+, severe atrophy, cystic	-, moderate atrophy	+, severe atrophy, cystic	-, severe atrophy	+, severe atrophy
Putamen	+, severe atrophy, cystic	n.e., moderate atrophy	n.e., severe atrophy, cystic	n.e., severe atrophy	+, severe atrophy
Caudate nucleus	+, severe atrophy	n.e., moderate atrophy	n.e., severe atrophy, cystic	n.e., severe atrophy	+, severe atrophy
Globus pallidus	+, severe atrophy	n.e., moderate atrophy	n.e., severe atrophy, cystic	n.e., severe atrophy	+, severe atrophy
Dentate nucleus	+	-	-, atrophy	-, atrophy	-
Midbrain	+	+, mild atrophy	-, mild atrophy	-, moderate atrophy	+, mild atrophy
Pons	+	+, mild atrophy	+, mild atrophy	+, moderate atrophy	+, mild atrophy
Medulla	-	-, mild atrophy	-, mild atrophy	-	+
Swelling of abn. WM	-	-	-	-	-
Cerebral atrophy	severe	severe	severe	severe	severe
Cerebellar atrophy	-	mild	moderate	severe	-
Depth of sulci cerebral/cerebellar cortex predominant affected	+	-	-	-	-
Rarefaction	subcortical cerebral WM	-	cerebral and cerebellar WM	-	-
Cystic degeneration	cerebellar WM, basal nuclei, thalami	-	cerebral WM, cerebellar WM, basal nuclei, thalami	-	cerebral parietal WM
Gradient echo/SWI signal abn.	n.d.	n.d.	-	n.d.	n.d.
Restricted diffusion	n.d.	n.d.	-	-	-
Lactate in MRS	elevated	elevated	n.d.	elevated	elevated
Contrast enhancement	n.d.	n.d.	n.d.	n.d.	n.d.

+ = present; - = absent; n.d = not done; n.e = not evaluate; abn. = abnormal/abnormalities; rel. = relative/relatively; WM = white matter; CC = corpus callosum; MRS = magnetic resonance spectroscopy; SWI susceptibility-weighted imaging ✕ Signal abnormality assessed on CT-scan. A low density is regarded as abnormal.

Supplementary Table 2. Clinical findings

Patient number	1	2 ^a	3	4 ^a	5 ^b	6	7 ^b
Patient and family characteristics:							
Gender	female	female	male	female	female	male	male
Year of birth	1993	1998	1999	2000	2002	2006	2010
Siblings (affected/unaffected/ otherwise affected)	0/0/1	1/1/0	0/2/0	1/1/0	1/0/1	0/1/0	1/0/1
Consanguinity of the parents	no	no	no	no	yes	yes	yes
Past history:							
Pregnancy/delivery	uncomplicated	uncomplicated	uncomplicated	uncomplicated	forceps delivery	uncomplicated	Caesarean section (elective)
Abnormalities neonatal period after birth		colic from 3 weeks	feeding difficulties	no	jaundice	no	withdrawal syndrome (oxycontin)
Initial motor development	normal	normal	normal	normal	delayed	normal	delayed
Initial mental development	normal	normal	normal	normal	delayed	normal	delayed
Presentation:							
Age at presentation (months)	2.5	2.5	2	3	2	2	5.5
Signs at presentation	irritability, loss of smile & social interaction, loss of head control, feeding difficulties, failure to thrive	irritability, arching posture	irritability, infantile spasms, feeding difficulties	irritability, loss of milestones, suspect seizures	developmental delay, loss of eye contact, lethargy, seizures	irritability, loss of eye contact, myoclonic jerks	irritability, lethargy, developmental delay, suspected seizures
Preceding event	not evident	vaccination at 2 months	respiratory tract infection at 3.5 weeks	vaccination at 3 months	infection	vaccination at 2 months	infection at 5 months
Signs of further deterioration	progressive spasticity, deterioration of eye contact and feeding, respiratory failure	progressive spasticity, deterioration of eye contact and feeding, respiratory failure	progressive spasticity, deterioration of eye contact and feeding, respiratory failure	progressive spasticity, intractable seizures, deterioration of eye contact and feeding, respiratory failure	progressive spasticity, deterioration of eye contact and feeding, respiratory failure	progressive spasticity, deterioration of eye contact and feeding, no development	progressive spasticity, deterioration of eye contact and feeding, respiratory failure
Course over time:							
Further episodes of regression	no	no	no	no	no	no	no
Behavioural problems	irritability	irritability	irritability, improved	irritability	irritability	irritability	irritability
Epilepsy	no	no	yes, increasing	yes, increasing	yes	yes	yes
Outcome	death	death	death	death	death	death	death
Age death (months)	15.6	4.0	12	11	18	58	20

Patient number	1	2 ^a	3	4 ^a	5 ^b	6	7 ^b
Latest examination:							
Age at latest examination (months)	14	4	11.5	9	6	63	8
Dysmorphic features	no	no	no	no	no	no	thin upper lip
Internal organs	normal	normal	normal	normal	normal	normal	normal
Head circumference	-1.5 SD	0 SD	-2.5 SD	0 SD	0 SD	-1 SD	-2SD
Eyes, vision and movements	no visual contact	no visual contact	no visual contact, upward gaze, ptosis	no visual contact	no visual contact	no visual contact	no visual contact
Highest motor response	spontaneous movements of limbs	spontaneous movements, extensor spasms	spontaneous movements of limbs	withdraw to pain	spontaneous movements of limbs	spontaneous movements of limbs	spontaneous movements of limbs
Highest verbal response	no interactive response	grunting	vocalises and smiles	no interactive response	no interactive response	sounds	no interactive response
Dysphagia, tube feeding	tube feeding	tube feeding	tube feeding	tube feeding	tube feeding	tube feeding	tube feeding
Respiration	ventilator support	ventilator support	spontaneous breathing	ventilator support	spontaneous breathing	spontaneous breathing	ventilator support
Axial tone	low	low	low	low	low	low	low
Arms	Intentional movements	none	none	none	none	none; continuous myoclonia	none
Tone	increased	increased	increased	increased	decreased	increased	increased
Reflexes	increased	increased	increased	increased	brisk	increased	increased
Spasticity	yes	yes	yes	yes	yes	yes	yes
Extrapyramidal signs	no	no	no	no	no	no	no
Legs	Intentional movements	none	none	none	none	none; continuous myoclonia	none
Tone	increased	increased	increased	increased	decreased	increased	increased
Reflexes	increased	increased	increased	increased	brisk	increased	increased
Babinski signs	yes	yes	yes	yes	yes	yes	no
Spasticity	yes	yes	yes	yes	yes	yes	yes
Extrapyramidal signs	no	no	no	no	no	no	no
Ophthalmologic investigation	pale optic nerve	pale optic nerve	not done	optic atrophy	optic atrophy	normal	optic atrophy

^asiblings; ^bsiblings; SD = standard deviation

Supplementary table 3. Laboratory Findings

Patient number	1	2 ^a	3	4 ^a	5 ^b	6	7 ^b
Routine haematology and biochemistry panel	normal	normal	normal	normal	normal	normal	normal
Plasma lactate	3.3 mmol/l (elevated; at first presentation, no follow-up)	3.6 mmol/l (elevated; one measurement two days before death)	4.6 mmol/l (elevated at first presentation with subsequent decline)	3.3 mmol/l (elevated; at first presentation then normal)	normal	3.4 mmol/l (elevated; at first presentation with gradual decline)	normal
Plasma lactate/pyruvate ratio	53 (normal 10-20)	n.d.	n.d.	n.d.	n.d.	28 (normal 10-20)	n.d.
CSF lactate	2.36 mmol/l (borderline; in acute phase, no follow-up)	2.6 mmol/l (elevated; one measurement two days before death)	normal	n.d.	normal	normal	normal
Plasma amino acids	alanine mildly elevated	alanine, glycine and ornithine slightly elevated	normal	normal	normal	alanine mildly elevated	normal
Urine organic acids	normal	normal	normal	normal	normal	normal	normal
Acylcarnitine profile	n.d.	n.d.	n.d.	normal	normal	normal	normal
Galactocerebrosidase	normal	normal	normal	normal	n.d.	n.d.	normal
Muscle							
Electron microscopy	slight increase in lipid and glycogen (not membrane bound)	slight increase in lipid and glycogen	increase in glycogen (not membrane bound)	slight increase in lipid and glycogen	normal	n.d.	normal
Respiratory chain enzyme activity	all complexes slightly low	ratio of all complexes to citrate synthase slightly low	normal	n.d.	n.d.	n.d.	ratio of complexes II and III to citrate synthase slightly low
Fibroblast							
Respiratory chain enzyme activity	normal	normal	normal	normal	n.d.	n.d.	normal
PDHc activity	normal	normal	normal	n.d.	n.d.	n.d.	normal
Lactate/pyruvate ratio	normal	normal	normal	normal	n.d.	n.d.	n.d.
Genetics							
	n.d.	narp/leigh 8993 9176 in muscle negative; mtDNA ratio 61% depleted in muscle	NARP/Leigh 8993 negative	n.d.	n.d.	MELAS 3243, MERRF 8344, NARP/Leigh 8993; negative	mtDNA genome sequencing and targeted mutation analysis of MELAS 3243, 3271, MERRF 8344, NARP/Leigh 8993, LON 11778 normal

n.d. = not done; CSF = cerebrospinal fluid; PDHc = pyruvate dehydrogenase complex; MELAS = Mitochondrial Encephalopathy, Lactic acidosis and Stroke-like episodes; MERRF = Myoclonic Epilepsy with Ragged Red Fibers; LON = Leber Hereditary Optic Neuropathy; NARP = Neuroopathy, Ataxia and Retinitis Pigmentosa; mtDNA = mitochondrial DNA; nDNA = nuclear DNA^a = siblings, ^b = sibs.

Supplementary Table 4. Statistics and variants identified in patient 2 by whole-exome sequencing

Sequencing statistics				
Reads	Reads on target		Percentage	
44.569.944	28.806.015		64.63%	
Target bases with dept:	>10x	>15x	>20x	30X
	94.39%	90.7%	85.96%	73.38%
Variant filtering				
Total single nucleotide variants and insertions or deletions			19.715	
Excluding segmental duplications and single nucleotide variants/insertions or deletions on X-chromosome			16.728	
Novelty filter				
Not present in 1000 Genomes				
Not present in dbSNP132			285	
Not present in in-house exomes ^a				
Inheritance pattern ^b				
≥2 single nucleotide variants/ insertions or deletions per gene			8 genes	
Pathogenicity filter				
Both variants change amino acid or splice site			3 genes (<i>SLC19A3</i> ; <i>SLC34A1</i> ; <i>OBSL1</i>)	

^aIn-house control exomes included 17 subjects with disease phenotypes different than the index patient.

^bSince there is no consanguinity reported our hypothesis was that the mutations are present in a heterozygous state in the patient.

Supplementary Table 5. Overview of published patients with SLC19A3 mutations

Clinical phenotype	nr. of pat	Mutation	Exon	State	Effect	Onset	Brain MRI abnormalities	Biotin	Thiamine	Outcome	Reference
Family 1 (Canadian) Early-infantile lethal encephalopathy	1	c.68G>T; p.Gly23Val	2	het.	missense	2.5 mo	diffuse GM&WM abn., rapid brain atrophy	-	n.e.	death: 15.6 mo	This paper
Family 2 (Lebanese) Early-infantile lethal encephalopathy	2	r.1173_1314del; p.Gln393*	5	het.	exon deletion	pat 1: 2 mo pat 2: 5.5 mo	diffuse GM&WM abn., rapid brain atrophy	n.e.	n.e.	death pat 1: 18 mo pat 2: 20 mo	This paper
Family 3 (European) Early-infantile lethal encephalopathy	2	c.541T>C; p.Ser181Pro	3	het.	missense	pat 1: 2.5 mo pat 2: 3.0 mo	diffuse GM&WM abn., rapid brain atrophy	n.e.	n.e.	death pat 1: 4.0 mo pat 2: 11 mo	This paper
Family 4 (European) Early-infantile lethal encephalopathy	1	c.527C>A; p.Ser176Tyr	3	het.	missense	2 mo	diffuse GM&WM abn., rapid brain atrophy	-	n.e.	death: 12 mo	This paper
Family 5 (Moroccan) Early-infantile lethal encephalopathy	1	c.507C>Gp.Tyr169*	3	het.	missense	2 mo	diffuse GM&WM abn., rapid brain atrophy	n.e.	n.e.	death: 58 mo	This paper
Family 6 (Japanese) Infantile generalized encephalopathy	4	c.1332C>G; p.Ser444Arg	6	hom.	missense	1- 11 mo	diffuse GM&WM abn., rapid brain atrophy	pat 1-3: n.e.; pat 4: -	n.e.	2 severe MR 2 death (12 y,9 y)	Yamada et al.,2010
Family 7 (Yemen) Basal ganglia disease	1	c.958G>C; p.Glu320Gln	3	hom.	missense	1 y	basal nuclei, thalamus, brain atrophy	+	n.e.	Normal	Zeng et al.,2010
Family 8 (Yemen) Basal ganglia disease	1	c.68G>T; p.Gly23Val	2	hom.	missense	n.e.	n.e.	n.e.	n.e.	n.e.	Zeng et al.,2010
Family 9 (Saudi) Basal ganglia disease	1	c.1264A>G; p.Thr422Ala	5	hom.	missense	6 y	caudate, putamen	+	n.e.	Normal	Zeng et al.,2010
Family 10 (Saudi) Basal ganglia disease	2	c.1264A>G; p.Thr422Ala	5	hom.	missense	pat 1: 3 y pat 2: 5 y	caudate, putamen; pat 2 additional scattered central WM lesions	+	pat 1: n.e. pat 2: -	pat 1: normal pat 2: MR	Zeng et al.,2010
Family 11 (Saudi) Basal ganglia disease	2	c.1264A>G; p.Thr422Ala	5	hom.	missense	pat 1: 7 y pat 2: 9 y	caudate, putamen	+	pat 1: n.e. pat 2: +	Normal	Zeng et al.,2010
Family 12 (European) Basal ganglia disease	2	c.74dupT; p.Ser26Leufs*19 c.980-144>G; p.Gly327Apsfs*8	2 intron 3	het. het.	nonsense nonsense	pat 1: 7 y pat 2: 20 y	caudate, putamen, midbrain, lesions cortical-subcortical junction	pat 1: + pat 2: -	pat 1: n.e. pat 2: +	Normal	Debs et al.,2010
Family 13 (European) Basal ganglia disease	2	c.74dupT; p.Ser26Leufs*19 c.980-144A>G; p.Gly327Apsfs*8	2 intron 3	het. het.	nonsense nonsense	pat 1: 8 y pat 2: 4 y	caudate, putamen, medial thalamus; in pat 1 also lesions cortical-subcortical junction	pat 1: - pat 2: n.e.	+	Normal	Serrano et al.,2012
Family 14 (Japanese) Wernicke-like encephalopathy	2	c.130A>G; p.Lys44Glu c.958G>C; p.Glu320Gln	2 3	het. het.	missense missense	> 10 y	bilateral medial thalamus, periaqueductal region	n.e.	+	Normal	Kono et al.,2009

nr. = number; mo = months; y = year; pat = patient; n.e. = not examined; het. = heterozygous; hom. = homozygous; hom. = homozygous; GM = gray matter; WM = white matter; MR = magnetic resonance imaging; - = not responsive; + = responsive

Chapter 3.2

Reply: Infantile Leigh-like syndrome caused by *SLC19A3* mutations is a treatable disease

Marjo S. van der Knaap and Sietske H. Kevelam

Brain. 2014 Sep;137(Pt 9):e297.



Sir,

We are grateful for the opportunity to respond to the correspondence from Haack *et al*¹ and thank the authors for their interest in our recent paper on seven patients with early-infantile, lethal encephalopathy caused by *SLC19A3* mutations.² In their letter, the authors present two brothers with an early onset Leigh-like clinical presentation.¹ The first boy died at the age of 2 months. The second was treated with thiamine and biotin from the day he presented (18 days old), with striking clinical improvement. Before treatment MRI showed bilateral signal abnormalities in limited areas of the cerebral cortex and in the basal nuclei, thalami and brainstem (Figure 1, A). With treatment, the signal abnormalities disappeared, although significant cerebral atrophy was seen on the MRI at the age of 4 months (Figure 1, C). The atrophy as shown in Figure 1 is more severe than suggested by the text of the letter (compare Figure 1, C and D).¹

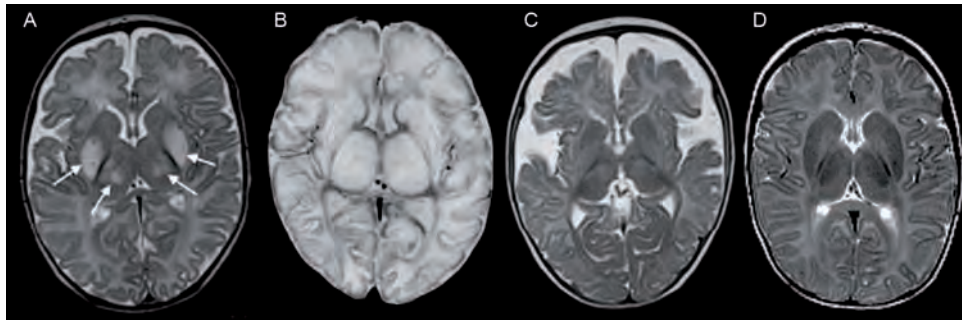


Figure 1. Cerebral MRI images illustrating the differences between the patient of Haack *et al.* (2014), one of our patients² and a healthy infant.

Axial T₂-weighted images, obtained at presentation, show localized abnormalities in Patient 75709 (arrows in A), whereas extensive involvement of virtually the whole brain is seen in our patient (B). Axial T₂-weighted images of Patient 75709, obtained 3 months after starting treatment, show disappearance of the signal abnormalities but also significant brain atrophy (C) as compared to the age-matched control (D).

These findings are, of course, highly promising. Our study concerned the retrospective diagnosis in seven patients, who had all died before the study was performed.² Because of the retrospective nature of our study, we were not able to assess the effects of early treatment in our cases. Considering the severe encephalopathy and the impressive MRI abnormalities showing near-complete grey matter degeneration in all areas of the brain at presentation (Figure 1, B), we were rather pessimistic about the possible beneficial effects of thiamine and biotin in such cases and considered that treatment soon after presentation may already be too late to prevent severe permanent brain damage. Two

of our patients had received biotin without clinical effects. But perhaps we should revise our concerns.

Although it is important to avoid therapeutic negativism and not give up on patients who have a treatable condition, it is equally important to avoid the devastating neurological handicap associated with treatment that has been started too late. We would like to stress that the clinical severity of the encephalopathy and MRI findings at presentation should be considered. Evidently, our patients were even more severely affected than the brothers described in the present letter.^{1,2} They had more extensive MRI abnormalities with virtually diffuse cerebral cortical involvement and also more extensive grey matter abnormalities elsewhere (compare Figure 1, A and B). We do not know what the outcome would be if thiamine and biotin treatment was started in such patients. But we also do not know what the outcome of the present patient will be.¹ Considering the fact that the follow-up was only up to the age of 4 months and MRI at 4 months shows significant cerebral atrophy (Figure 1, C), we are concerned about the long-term outcome. We would like to invite Haack *et al.* to describe the outcome of their patient again after 6 and 18 years.

The present title of the paper, 'Infantile Leigh-like syndrome caused by *SLC19A3* mutations is a treatable disease' suggests complete or almost complete recovery upon treatment, which must still be proven. As such, we would have preferred a more cautious title of the letter.

REFERENCES

1. Haack TB, Klee D, Strom TM, et al. Infantile Leigh-like syndrome caused by *SLC19A3* mutations is a treatable disease. *Brain* 2014;137:e295.
2. Kevelam SH, Bugiani M, Salomons GS, et al. Exome sequencing reveals mutated *SLC19A3* in patients with an early-infantile, lethal encephalopathy. *Brain* 2013;136:1534-1543.

Chapter 4

***LAMA2* mutations in adult-onset muscular dystrophy with leukoencephalopathy**

Sietske H. Kevelam, Baziel G.M. van Engelen, Carola G.M. van Berkel, Benno Küsters, and Marjo S. van der Knaap

Muscle Nerve. 2014 Apr;49(4):616-617.



LETTER TO THE EDITOR

In 1992, van Engelen *et al.* reported a familial, adult-onset muscular dystrophy with distal weakness and leukoencephalopathy.¹ Apart from adult onset, the combination of muscle disease and leukoencephalopathy was reminiscent of congenital muscular dystrophies (CMD).² The investigators suspected that this family may have an adult-onset variant of a subtype of CMD, probably with an allelic mutation at a CMD locus.¹ The MRI findings (Figure 1, A-C) would be compatible with merosin ($\alpha 2$ -chain of laminin-2) deficient congenital muscular dystrophy (now called MDC1A),³ but other variants would also be possible.³ Immunocytochemical staining of a muscle biopsy was performed using an anti- $\alpha 2$ -chain antibody (clone Mer2/22B2; Novocastra), which probably recognizes the LG3 or LG4 domain of the laminin- $\alpha 2$ chain; normal staining was found (Figure 1, D and E). Because of lack of further information regarding the possible mutation, no DNA analysis was performed.

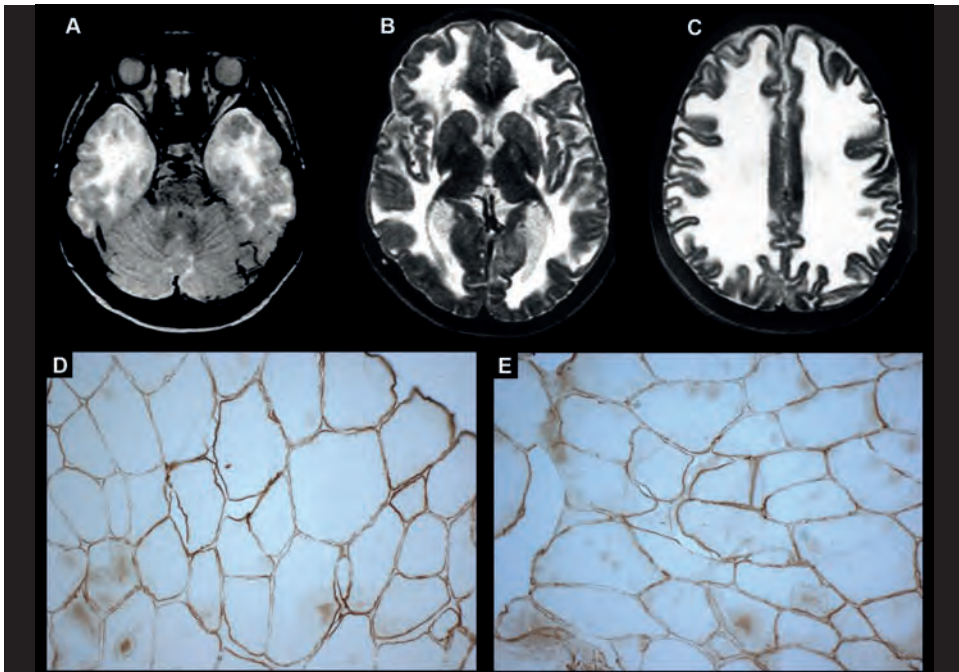


Figure 1. Brain MRI (A–C) shows diffuse cerebral white matter abnormalities with mild swelling of the abnormal white matter (C). The cerebellar white matter (A) and corpus callosum (B) are spared. Immunocytochemical labeling of spectrin as control and laminin- $\alpha 2$ in the muscle biopsy (collected in 2001) from a patient (D, E). Note the normal level of laminin $\alpha 2$ expression using an antibody directed against merosin (clone Mer2/22B2; Novocastra) (E) as compared with the control (D). Original magnification: $\times 125$.

Using whole-exome sequencing we recently identified 2 novel compound heterozygous mutations in the *LAMA2* gene in the 3 affected siblings: 4516T>A missense mutation predicting p.Cys1506Ser located in exon 31 (protein domain IIIA) and 6466C>T nonsense mutation predicting p.Arg2156* located in exon 46 (protein domain I/G). Both mutations were not present in public control databases [dbSNP132 (http://www.ncbi.nlm.nih.gov/projects/SNP/snp_summary.cgi?build_id=132), NHLBI GO Exome Sequencing Project (<http://evs.gs.washington.edu/EVS/>), and 1000 Genomes (<http://www.1000genomes.org/home>)], and the missense mutation was predicted to be deleterious by the Sorting Tolerant From Intolerant program (<http://sift.jcvi.org/>) and Polyphen-2 (<http://genetics.bwh.harvard.edu/pph2/>). These mutations were confirmed by Sanger sequencing.

LAMA2 mutations are the cause of MDC1A. Some mutations in *LAMA2* result in complete deficiency of the laminin- α 2 chain and are associated predominantly with a severe CMD.⁴ Other mutations result in partial laminin- α 2 chain deficiency, a group that is clinically more heterogeneous.^{4,5} The latter group also contains a few patients with an adult-onset muscular dystrophy, mainly affecting the proximal muscles (limb-girdle distribution).⁵ Using the NCL-antibody we did not detect partial deficiency of laminin α 2 in our family. However, we cannot exclude the possibility that we would detect partial deficiency of laminin- α 2 using a more sensitive antibody, directed against the N-terminal 300-kDa fragment.⁶ The observed mild phenotype would be compatible with the compound heterozygosity between a nonsense and missense mutation that we found. The missense change results in loss of a conserved cysteine residue on the short arm of laminin- α 2 that probably plays a role in disulfide cross-linking. The important G-domain of the protein that interacts with the membrane receptors alpha-dystroglycan and integrin α 7 β 1⁷ is not affected by the missense mutation, which could possibly explain the mild phenotype. The late onset of the disease and the predominantly distal muscle weakness in our patients extends the clinical spectrum associated with *LAMA2* mutations.

REFERENCES

1. van Engelen BG, Leyten QH, Bensen PL, et al. Familial adult-onset muscular dystrophy with leukoencephalopathy. *Ann Neurol* 1992;32:577-580.
2. Banker BQ. Congenital muscular dystrophy. In: Engel AG and Banker BQ. *Myology*. New York: McGraw-Hill; 1986. p. 1367-1382.
3. van der Knaap MS, Smit LM, Barth PG, et al. Magnetic resonance imaging in classification of congenital muscular dystrophies with brain abnormalities. *Ann Neurol* 1997;42:50-59.
4. Geranmayeh F, Clement E, Feng LH, et al. Genotype-phenotype correlation in a large population of muscular dystrophy patients with LAMA2 mutations. *Neuromuscul Disord* 2010;20:241-250.
5. Gavassini BF, Carboni N, Nielsen JE, et al. Clinical and molecular characterization of limb-girdle muscular dystrophy due to LAMA2 mutations. *Muscle Nerve* 2011;44:703-709.
6. He Y, Jones KJ, Vignier N, et al. Congenital muscular dystrophy with primary partial laminin alpha2 chain deficiency: molecular study. *Neurology* 2001;57:1319-1322.
7. Miyagoe-Suzuki Y, Nakagawa M, Takeda S. Merosin and congenital muscular dystrophy. *Microsc Res Tech* 2000;48:181-191.

Chapter 5

Absent thalami caused by a homozygous *EARS2* mutation: expanding disease spectrum of LTBL

Sietske H. Kevelam,* Femke C.C. Klouwer,* Johanna M. Fock,
Gajja S. Salomons, Marianna Bugiani, and Marjo S. van der Knaap

*These authors share first authorship.

Neuropediatrics. 2016 Jan;47(1):64-67.



ABSTRACT

Leukoencephalopathy with thalamus and brainstem involvement and high lactate (LTBL) is caused by autosomal recessive *EARS2* mutations. Onset is most often in infancy, but in severe cases in the neonatal period. Patients typically have magnetic resonance imaging (MRI) signal abnormalities involving the thalamus, brainstem and deep cerebral white matter. Most signal abnormalities resolve, but in severe cases at the expense of tissue loss. Here we report a patient with an encephalopathy of antenatal onset. His early MRI at 8 months of age showed signal abnormalities in the deep cerebral white matter that improved over time. The thalami were absent with the configuration of a developmental anomaly, without evidence of a lesion. We hypothesized that this was a case of LTBL in which the thalamic damage occurred antenatally and was incorporated in the normal brain development. The diagnosis was confirmed by a novel homozygous *EARS2* mutation. Our case adds to the phenotypic and genetic spectrum of LTBL.

INTRODUCTION

In 2012, the novel disease “leukoencephalopathy with thalamus and brainstem involvement and high lactate” (LTBL) was defined based on a distinctive magnetic resonance imaging (MRI) pattern.¹ Patients typically have symmetrical signal abnormalities in the thalamus, brainstem and deep cerebral white matter that improve over time in the majority (70%) of the originally identified cases.² The underlying genetic defect of this disorder was identified shortly thereafter. All patients have autosomal recessive mutations in the gene *EARS2*, encoding mitochondrial glutamyl tRNA synthetase.^{1,2} Although the core neurological and MRI phenotype was similar, a wide variability in clinical severity was seen in this group, ranging from infantile-onset disease followed by evident clinical improvement or a more severe neonatal-onset encephalopathy with stabilization, but no improvement.² The patient discussed here has an earlier, antenatal-onset encephalopathy with in addition a novel feature on brain MRI.

CASE REPORT

An 18-year-old male with a leukoencephalopathy of unknown cause was referred for second opinion. He was born full term after an uneventful pregnancy with a birth weight of 3,600 g. He was the second child to healthy Dutch parents without known consanguinity. From birth on, hypotonia, poor visual contact and total lack of achievement of any developmental milestones were noted. He did not show behavioural problems or signs of distress. He experienced severe feeding difficulties, which led to percutaneous endoscopic gastrostomy tube feeding at 12 years of age. His neurological picture was stable and there were no periods of clinical regression. He developed tonic-clonic seizures at age 18 years. Laboratory investigations, including serum lactate and extensive screening for metabolic diseases, were unrevealing. Lumbar puncture was not performed. Physical examination at 18 years revealed a young man with a severe microcephaly (-4 SD). He had a divergent squint and offered no eye contact. No head control was present. He had hyperreflexia and hypertonia with contractures of arms and legs. He had no intentional movements.

His initial brain MRI, performed at 8 months of age, showed disfiguration and moderate enlargement of the lateral ventricles and confluent, symmetrical signal abnormalities in the deep cerebral white matter with sparing of a periventricular rim and the directly subcortical white matter (Figure 1, B and C). The corpus callosum was complete, but

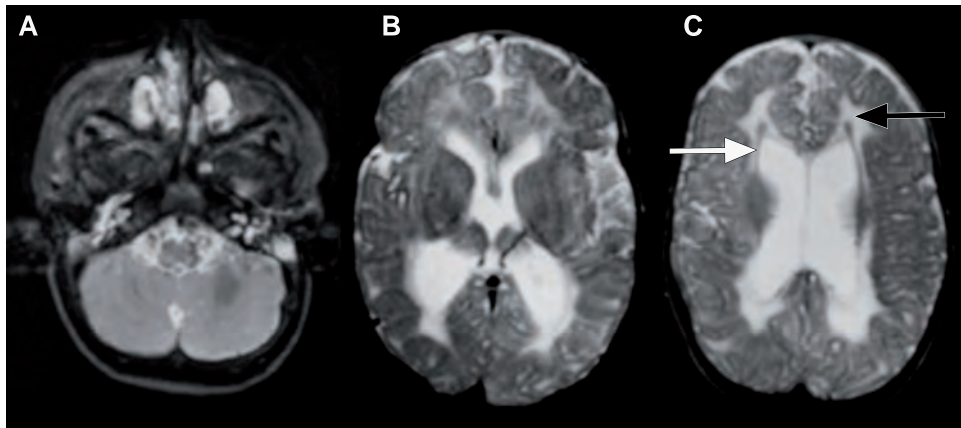


Figure 1. (A-C) Axial T2-weighted MR images of the patient at age 8 months. (A) The brain stem and cerebellum have a normal T2 signal intensity. (B) The lateral ventricles are moderately enlarged and disfigured. (C) The deep white matter contains confluent T2 signal abnormalities (black arrow) sparing a periventricular rim (white arrow). MR, magnetic resonance.

thin, especially the posterior part and showed T2 signal abnormalities throughout. The basal nuclei, brainstem, and cerebellar white matter had a normal signal (Figure 1, A). Follow-up MRIs, at 3 and 18 years of age showed partial resolution of the signal abnormalities in the cerebral white matter and corpus callosum (Figure 2, B). The basal nuclei, brainstem and cerebellar white matter still had a normal signal. We noticed that the remarkable disfiguration of the lateral and third ventricles was caused by absence of the thalami (Figure 2, A-D). There were no signal abnormalities in this region suggesting a lesion and there was smooth lining of the ventricles (Figure 2, C). In retrospect, the absence of the thalami was also visible on his previous MRI (Figure 1).

We argued that *EARS2* mutations could be the cause of the disorder (see discussion) and thus performed DNA analysis of the *EARS2* gene, which revealed a homozygous in-frame deletion of three base pairs (c.454_456del), causing a deletion of the highly conserved amino acid lysine at position 152 (p.[Lys152del]). This mutation has not been reported in public databases (1,000 Genomes [release of February 2012], dbSNP137 [available at: <http://www.ncbi.nlm.nih.gov/projects/SNP>], and NHLBI Exome Sequencing Project, ESP6500 release [available at: <http://evs.gs.washington.edu/EVS/>]). Parents both carried the mutation. Subsequent detailed analysis of their pedigrees revealed consanguinity with a common ancestor in the 17th century, eight generations back.

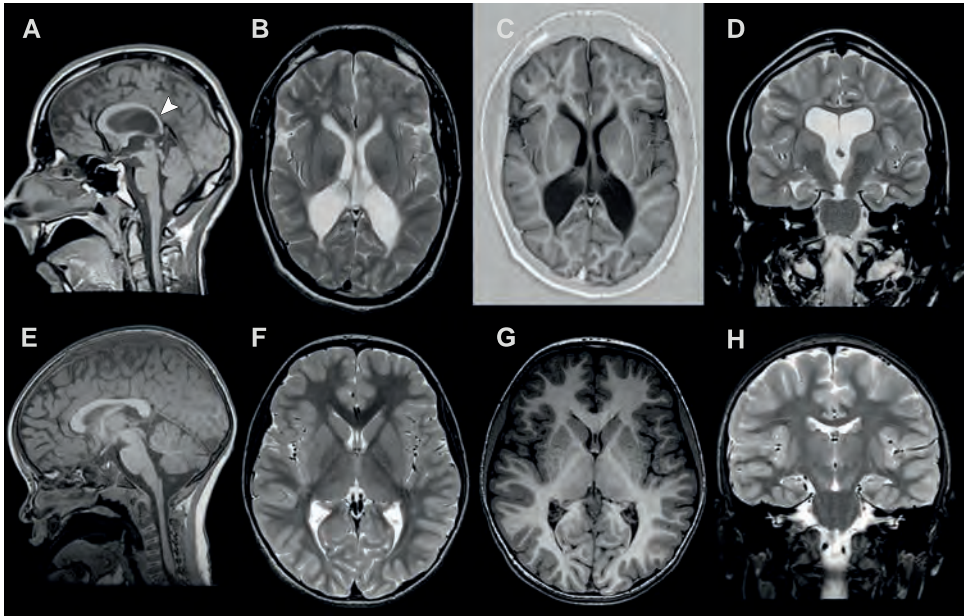


Figure 2. (A) Sagittal T1-weighted, (B) axial and (D) coronal T2-weighted, and (C) axial inversion recovery MR images of the patient at age 18 years. (E) Sagittal and (G) axial T1-weighted and (F) axial and (H) coronal T2-weighted images of a normal person. The apparent absence of the thalami is shown in A-D in three different planes (compare with control images E-H). There is smooth lining along the ventricles (C). The posterior part of the corpus callosum is thin (A, arrowhead). MR, magnetic resonance.

DISCUSSION

The patient described here presented shortly after birth with a severe but stable encephalopathy with lack of all development and spastic tetraparesis. These features are in themselves nonspecific and with the apparent a- or hypoplasia of the thalami they would suggest a genetically determined developmental anomaly of the brain. However, mutations analysis showed that this patient had a novel homozygous one amino acid deletion in the gene *EARS2* associated with the disease LTBL.²

Patients with LTBL were initially described in 2012.^{1,2} These patients could be divided into two clinical groups: (1) patients with neurological regression at 6 to 12 months of age and subsequent stabilization and improvement on follow-up, and (2) patients with a neonatal or early infantile onset severe encephalopathy with seizures and spastic paraparesis with subsequent stabilization but no clinical improvement.^{1,2} None of these patients had a second period of regression. The MRI early in the disease course showed symmetrical signal abnormalities and swelling of the deep cerebral white matter with

sparing of a periventricular rim and the directly subcortical white matter. Additional signal abnormalities were present in deep gray matter structures, most prominently involving the thalami. The corpus callosum, brainstem and cerebellar white matter were affected as well. Proton MR spectroscopy showed elevated lactate in the affected white matter. Follow-up MRI showed improvement and partial to complete resolution of signal abnormalities and normalization of lactate. In the severe cases, however, part of the affected structures was apparently damaged beyond repair and displayed atrophy, especially the thalami and cerebral white matter, with remaining evidence of scarring. In some patients the posterior corpus callosum was abnormally thin or completely absent.²

5

The evidence available until now suggests that the phenotype of patients with *EARS2* mutations results from a single episode of deterioration early in life. The degree of damage is thought to be determined by the timing and the severity of this episode.² Superficial inspection of our patient's MRIs suggested a developmental anomaly with a- or hypoplasia of the thalamus and smooth lining of the ventricles, without evidence at all suggesting a previous lesion and scarring. Closer examination of the MRI, however, showed absence of thalamic nuclei originating from both the thalamus dorsalis and ventralis, which are separated nuclear zones along the diencephalic wall of the neural tube during fetal development,³ and no involvement of other derivatives as the habenula or pineal gland. This is more compatible with a very early disruptive event. Damage early during fetal life is incorporated into normal development, making the final configuration look like a developmental anomaly. A comparable phenomenon is seen in schizencephaly, which is characterized by clefts spanning the cerebral hemisphere from the pial surface to the lateral ventricle.⁴⁻⁶ Interestingly, the walls of the defect are subsequently lined with ectopic and dysplastic gray matter.⁶ The presence of this gray matter lining indicates that the induced injury, caused by vascular disruption or exogenous environmental factors, occurs prior to termination of neuronal migration with the consequence that the defect is incorporated within further brain development.⁶ A similar scenario could be envisioned for LTBL. Keeping in mind the possibility of an expanding disease spectrum, we hypothesize that the MRI features of our patient could reflect a very early hit resulting in an early antenatal onset of LTBL with disappearance of the thalamus. Some special MRI features supported our hypothesis of LTBL, including abnormalities in the deep cerebral white matter with sparing of a periventricular rim, the improvement of the white matter abnormalities over time and the thin posterior corpus callosum. We considered other early antenatal events disrupting the thalami, such as infection or ischemia, but in view of the special MRI features supporting LTBL, we tested *EARS2* first. Indeed, our hypothesis was confirmed by detection of a homozygous *EARS2*

mutation in our patient. Interestingly, in some of the early onset, severely affected LTBL patients described by Steenweg et al, the posterior part and rostrum of the corpus callosum were absent (see Figure 3, C in Steenweg et al, 2013²), and this was ascribed to a developmental anomaly.² With the new information, this interpretation should be revised. The corpus callosum abnormality is more likely also the result of an early injury disrupting further development of the corpus callosum rather than a developmental anomaly per se. This revised interpretation indicates two episodes of deterioration in those patients, one early fetal and one early infantile.

Since the discovery of recessive *EARS2* mutations in LTBL patients, three more patients with *EARS2* mutations were reported.⁷⁻⁹ For one patient no detailed clinical features were reported.⁹ The patient described by Talim et al., presented with a severe infantile multisystem disease involving the brain and the liver with a very early death at three months of age due to necrotizing bronchopneumonia. Also this patient had absence of the posterior part of the corpus callosum.⁸ The patient reported by Biancheri et al., had an intermediate clinical phenotype, with an early-onset disease, but subsequent clinical improvement. His MRI, however, showed new lesions in the left caudate nucleus and globus pallidus during follow-up at age 5 years and 10 months, indicating that there could be more than one episode of regression.⁷ This is in line with the new view that there can be more than one episode of deterioration. Based on the patients published so far, there is no clear genotype-phenotype correlation.

With the identification of the patient described here we illustrate that an early antenatal “hit” may give rise to a severe clinical phenotype and a specific MRI pattern characterized by absence of the thalami, which expands the disease spectrum associated with *EARS2* mutations. Additionally, new evidence indicates that there can be more than one episode of deterioration. It is to be expected that whole-exome sequencing and whole-genome sequencing will lead to a further expansion of the known disease spectrum of LTBL.

REFERENCES

1. Steenweg ME, Vanderver A, Ceulemans B, et al. Novel infantile-onset leukoencephalopathy with high lactate level and slow improvement. *Arch Neurol* 2012;69:718-722.
2. Steenweg ME, Ghezzi D, Haack T, et al. Leukoencephalopathy with thalamus and brainstem involvement and high lactate 'LTBL' caused by *EARS2* mutations. *Brain* 2012;135:1387-1394.
3. Martinez-Ferre A and Martinez S. Molecular regionalization of the diencephalon. *Front Neurosci* 2012;6:73.
4. Yakovlev PI and Wadsworth RC. Schizencephalies; a study of the congenital clefts in the cerebral mantle; clefts with hydrocephalus and lips separated. *J Neuropathol Exp Neurol* 1946;5:169-206.
5. Yakovlev PI and Wadsworth RC. Schizencephalies; a study of the congenital clefts in the cerebral mantle; clefts with fused lips. *J Neuropathol Exp Neurol* 1946;5:116-130.
6. Hayashi N, Tsutsumi Y, Barkovich AJ. Morphological features and associated anomalies of schizencephaly in the clinical population: detailed analysis of MR images. *Neuroradiology* 2002;44:418-427.
7. Biancheri R, Lamantea E, Severino M, et al. Expanding the Clinical and Magnetic Resonance Spectrum of Leukoencephalopathy with Thalamus and Brainstem Involvement and High Lactate (LTBL) in a Patient Harboring a Novel *EARS2* Mutation. *JIMD Rep* 2015;23:85-89.
8. Talim B, Pyle A, Griffin H, et al. Multisystem fatal infantile disease caused by a novel homozygous *EARS2* mutation. *Brain* 2013;136:e228.
9. Taylor RW, Pyle A, Griffin H, et al. Use of whole-exome sequencing to determine the genetic basis of multiple mitochondrial respiratory chain complex deficiencies. *JAMA* 2014;312:68-77.



**Novel disease entity
associated with a known gene**

Chapter 6

Novel (ovario) leukodystrophy related to *AARS2* mutations

Cristina Dallabona,* Dario Diodato,* Sietske H. Kevelam,* Tobias B. Haack, Lee-Jun Wong, Gajja S. Salomons, Enrico Baruffini, Laura Melchionda, Caterina Mariotti, Tim M. Strom, Thomas Meitinger, Holger Prokisch, Kim Chapman, Alison Colley, Helena Rocha, Katrin Öunap, Raphael Schiffmann, Ettore Salsano, Mario Savoirdo, Eline M. Hamilton, Truus E. Abbink, Nicole I. Wolf, Ileana Ferrero, Costanza Lamperti, Massimo Zeviani, Adeline Vanderver,** Daniele Ghezzi**, and Marjo S. van der Knaap**

* These authors share first authorship.

** These authors share senior authorship.

ABSTRACT

Objectives

The study was focused on leukoencephalopathies of unknown cause in order to define a novel, homogeneous phenotype suggestive of a common genetic defect, based on clinical and MRI findings, and to identify the causal genetic defect shared by patients with this phenotype.

Methods

Independent next-generation exome-sequencing studies were performed in 2 unrelated patients with a leukoencephalopathy. MRI findings in these patients were compared with available MRIs in a database of unclassified leukoencephalopathies; 11 patients with similar MRI abnormalities were selected. Clinical and MRI findings were investigated.

Results

Next-generation sequencing revealed compound heterozygous mutations in *AARS2* encoding mitochondrial alanyl-tRNA synthetase in both patients. Functional studies in yeast confirmed the pathogenicity of the mutations in one patient. Sanger sequencing revealed *AARS2* mutations in 4 of the 11 selected patients. The 6 patients with *AARS2* mutations had childhood- to adulthood-onset signs of neurologic deterioration consisting of ataxia, spasticity, and cognitive decline with features of frontal lobe dysfunction. MRIs showed a leukoencephalopathy with striking involvement of left-right connections, descending tracts, and cerebellar atrophy. All female patients had ovarian failure. None of the patients had signs of a cardiomyopathy.

Conclusions

Mutations in *AARS2* have been found in a severe form of infantile cardiomyopathy in 2 families. We present 6 patients with a new phenotype caused by *AARS2* mutations, characterized by leukoencephalopathy and, in female patients, ovarian failure, indicating that the phenotypic spectrum associated with *AARS2* variants is much wider than previously reported.

INTRODUCTION

Mutations in genes coding for mitochondrial aminoacyl transfer RNA (tRNA) synthetases, the enzymes that charge a specific tRNA with its cognate amino acid, are recently emerging as a new important cause of mitochondrial disease and have been associated with a wide spectrum of clinical phenotypes.¹⁻³ However, defects in each aminoacyl tRNA synthetase seem to determine rather homogeneous clinical presentations.¹⁻⁵

The use of whole-exome sequencing (WES) has markedly increased efficiency and improved genetic analysis for inherited disorders, allowing gene identification for small groups of patients sharing a phenotype, individual cases with atypical presentation, and disorders lacking consistent genotype-phenotype correlation.⁶⁻⁸

Mutations in the mitochondrial alanyl-tRNA synthetase 2 gene (*AARS2*; OMIM *612035) have been found in severe infantile cardiomyopathy in 2 families.⁹ In the present study, we describe a very different clinical picture determined by *AARS2* genetic defects in 6 patients affected by a progressive leukoencephalopathy and, in females, ovarian failure, a clinical presentation previously described as “ovarioleukodystrophy.”¹⁰

METHODS

Standard protocol approvals, registrations, and patient consents

The study was approved by the Ethical Committees of the Istituto Neurologico Besta, Milan, Italy; the Children’s National Medical Center, Washington, DC; and the VU University Medical Center, Amsterdam, the Netherlands, in agreement with the Declaration of Helsinki. Informed consent was signed by the patients.

Patients

Patients 1 (P1) and 2 (P2) were included in 2 independent next-generation sequencing studies. On the basis of the MRI findings in these 2 patients, we selected 10 patients from 9 families from the Amsterdam database, which contains more than 3,000 cases with an unclassified leukoencephalopathy¹¹ and one patient from the leukoencephalopathy cases of the Istituto Neurologico Besta without genetic diagnosis. Common MRI features were frontal and parietal white matter abnormalities with relative sparing of the central posterior-frontal or frontoparietal region. The anterior part of the corpus callosum and a thin strip in the splenium were affected, with relative sparing of the central region. Most female patients had ovarian failure in addition to the leukoencephalopathy. We

also included 2 patients with unsolved ovarioleukodystrophy, in whom no mutations in *EIF2B1–5* had been found.^{10,12} For all patients, we collected clinical and laboratory data retrospectively. We analyzed available MRIs, as described.¹⁰

Molecular studies

We extracted genomic DNA by standard methods from leukocytes or muscle biopsies. In P1, we performed WES and variant filtering, as described.¹³ For P2, we used a custom probe library for target gene capture (Roche NimbleGen Inc., Madison, WI) designed to capture coding exons plus 20 base pairs into the flanking introns of 500 genes known to be related to mitochondrial disorders, followed by deep sequencing at average coverage depth of 1,000 per base. Because of rapid clinical deterioration of P2, we also initiated clinical WES (Illumina, San Diego, CA). We performed Sanger sequencing of the gene identified by WES in all patients.⁹

Functional studies

We used yeast strains derived from W303-1B.¹⁴ Detailed methods including respiratory activity, cytochrome spectra, in vivo mitochondrial DNA protein synthesis, aminoacylation of mitochondrial tRNA for alanine, cytochrome c oxidase (complex IV) and complex I + III activities, and primers for the preparation of plasmids used in this study are reported in the e-Methods and table e-1 on the *Neurology*[®] Web site at Neurology.org.

RESULTS

Patients and laboratory findings

The clinical features of the patients in whom we found mutations in the gene mentioned below are summarized in table e-2. Herein, we give a brief description.

P1 is a female in whom developmental delay became evident at 2 years of age. She achieved walking without support at 3, but with impaired balance. Her condition remained stable until age 15, when she developed progressive gait ataxia, tremor, cognitive deterioration, and psychosis. At age 18, she developed secondary amenorrhea due to ovarian failure. The latest neurologic examination at age 30 revealed severe cerebellar ataxia with nystagmus, dysarthria, intention tremor, and instable gait. She could walk with support. General physical examination revealed no abnormalities and no evidence of cardiac dysfunction. ECG and cardiac ultrasound were normal.

P2 is a male who came to medical attention in infancy because of congenital nystagmus. In primary school, mild clumsiness and learning difficulties were a concern. In his early teenage years, he developed mild right-sided hemiparesis and ataxia, which was ascribed to periventricular leukomalacia due to periventricular white matter abnormalities on MRI. Around age 17, deterioration set in with bilateral dystonia and spasticity, dysarthria, and cognitive decline. A viral gastroenteritis was followed by abrupt mental decline, unintelligible speech, inability to eat due to choking, recurrent vomiting, and inability to walk because of worsening of ataxia and spasticity, left more than right. General physical examination revealed no abnormalities and no evidence for cardiac dysfunction.

P3 is a female who presented with secondary amenorrhea due to ovarian failure at age 28. At age 33, she developed depression, cognitive deterioration, behavioral problems with signs of frontal dysfunction, and urinary incontinence. Neurologic examination revealed downbeat nystagmus and some postural and appendicular tremor of the arms, but otherwise no motor disability. She developed stereotyped motor behavior and severe apraxia. At age 35, she did not recognize family members anymore. She had to be tube fed. Antiepileptic medication was started because of epileptic seizures. At age 36, she was bedridden and had no interactions with her surroundings.

P4 is a female who was diagnosed with ovarian failure at age 23 years. She developed tremor of her hands at age 24. Because of white matter abnormalities on MRI, she was diagnosed with multiple sclerosis. From age 26, rapid cognitive, behavioral, and motor deterioration became evident. She developed progressive dystonia, cerebellar ataxia, and spasticity, left more than right. General physical examination revealed no abnormalities. She lost speech, became bedridden, and died at age 28.

P5 is a female who had primary amenorrhea due to ovarian failure. From age 40, she developed depression and rapid cognitive deterioration. Neurologic examination revealed no motor dysfunction. General physical examination revealed no abnormalities. She became bedridden and died at age 46.

P6 is a female who was diagnosed with ovarian failure at 20 years of age. At age 22, she presented with gait problems caused by hypertonia of the legs, left more than right. She developed depression but no cognitive regression. Neurologic examination revealed a spastic paraparesis with ataxic signs. The disease was rapidly progressive. At latest examination at age 25, she was wheelchair-bound.

Laboratory findings are summarized in table e-3. None of the patients had elevated blood or CSF lactate. All 5 female patients had primary or secondary amenorrhea due to ovarian failure. P1 and P6 were the only patients extensively investigated for a possible mitochondrial defect. In P1, the Gomori trichrome stain and succinate dehydrogenase

reaction of a skeletal muscle biopsy were normal, whereas the histochemical reaction to cytochrome c oxidase was diffusely reduced (Figure 1, A). Likewise, biochemical assay showed severe isolated cytochrome c oxidase deficiency (15% of residual activity) in muscle homogenate (Figure 1, B), whereas the activities of all respiratory chain complexes, including cytochrome c oxidase, were normal in fibroblasts. Oxygraphic studies performed in patients' fibroblasts, grown in either glucose or galactose medium, showed no defect (not shown). Sequencing of mitochondrial DNA revealed a heteroplasmic variant with a low level of mutation load: m.5979G>A (p.Ala26Thr) in *MTCO1*, reported as a rare single nucleotide polymorphism (<0.1% in Mitomap database) present in haplogroup H45 and deemed not pathogenic. In P6, histologic and histochemical analyses of muscle biopsy revealed diffusely reduced cytochrome c oxidase staining, but no ragged red fibers. Measurement of individual oxidative phosphorylation enzyme activities in muscle homogenate showed reduced cytochrome c oxidase (33% of residual activity) (Figure 1, B). Mitochondrial DNA sequencing revealed no pathogenic point mutations, but several polymorphisms typical of haplogroup T1a1.

MRI abnormalities

The MRI abnormalities are summarized in table e-4 and illustrated in Figures 2 and e-1. In all 6 patients, the cerebral white matter abnormalities were inhomogeneous and patchy, affecting and sparing strips of tissue. In several patients, the signal of small parts of the T2-hyperintense white matter was low on fluid-attenuated inversion recovery images, indicating white matter rarefaction. Typically, the signal abnormalities were predominantly present in the frontal and parietal periventricular and deep white matter, sparing a segment of white matter in between. White matter structures were affected in a tract-like manner, with involvement of left-right connections through the corpus callosum and involvement of descending connections. Depending on the location of the cerebral hemispheric white matter abnormalities, the frontopontine, pyramidal, or parieto-occipitopontine tracts were longitudinally affected. The corpus callosum abnormalities were also dependent on the cerebral hemispheric white matter involvement; they could be limited to a single lesion in the splenium, affect a large part of the anterior corpus callosum and only a narrow strip in the splenium, or involve the entire corpus callosum in an inhomogeneous manner. Diffusion-weighted images showed multiple small areas of restricted diffusion in the cerebral white matter and corpus callosum. The abnormalities were limited to white matter structures and were progressive over time. No contrast enhancement was observed. Cerebellar atrophy was variable and affected the vermis more than the hemispheres. Cerebral atrophy was at most mild.

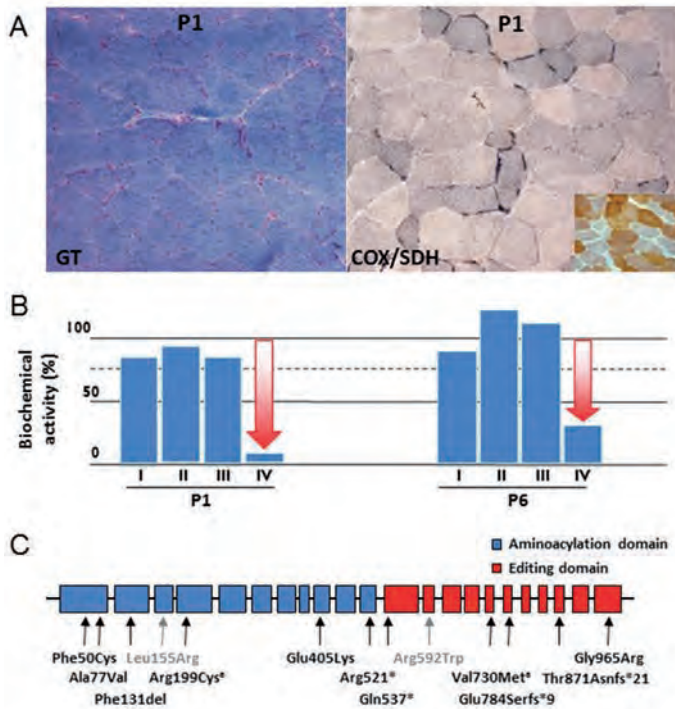


Figure 1. Biochemical and genetic features

(A) Morphologic analysis of muscle biopsy from patient P1: Gomori trichrome (GT) staining and cytochrome c oxidase (COX)/succinate dehydrogenase (SDH) histoenzymatic double staining (COX/SDH). Inset shows the reaction in an age-matched control biopsy. (B) Biochemical activities of mitochondrial respiratory chain complexes in patients P1 and P6 muscle homogenates. All enzymatic activities are normalized for citrate synthase activity and indicated as percentages relative to the mean control value. (C) Genomic structure of *AARS2* with exons coding for the aminoacylation (blue) and editing (red) domains. The arrows indicate the position of mutations identified in this study (black) or previously reported (gray). *The 2 missense variants p.Arg199Cys and p.Val730Met are on the same allele; the latter (rs35623954) is reported to have a frequency >1% in control populations, suggesting that the former is the pathogenic variant.

WES and Sanger sequencing

We performed WES on genomic DNA from P1.⁶ After excluding common single nucleotide polymorphisms (>0.1%), we prioritized the remaining changes according to the presence of homozygous or compound heterozygous mutations, as expected for a recessive inherited trait, and for known or predicted mitochondrial localization of the corresponding protein.¹⁵ This filtering led to the identification of a single outstanding gene entry, *AARS2* (NC_000006.11) in which a missense (c.149T>G, p.Phe50Cys) and a nonsense (c.1561C>T, p.Arg521*) heterozygous variant were present (NM_020745.3) (Figure 1, C, Table 1), segregating within the family.

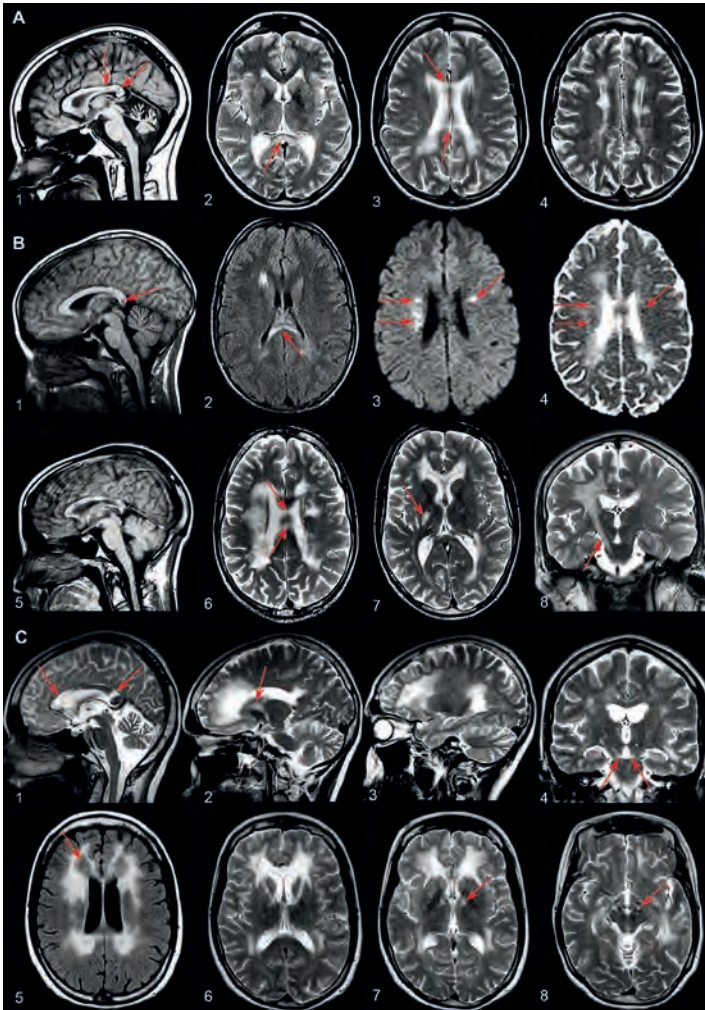


Figure 2. Brain MRI

(A) MRI in P1 at age 28. The sagittal T1-weighted image shows serious cerebellar atrophy and 2 strips of abnormal signal in the splenium (arrows in image 1). The axial T2-weighted images show inhomogeneous areas of abnormal signal in the periventricular white matter. The areas on the left and right are connected signal abnormalities in the corpus callosum (arrows in images 2–4). (B) MRI in P2 at age 14 (images 1 and 2), age 21 (images 3 and 4), and age 23 (images 5–8). At age 14, a lesion is seen in the splenium of the corpus callosum (arrow in image 1) and in the right frontal periventricular white matter. The diffusion-weighted images suggest the presence of multiple small areas of restricted diffusion in the abnormal white matter (arrows in image 3), confirmed by low signal of the corresponding areas on the apparent diffusion coefficient map (arrows in image 4). The most recent MRI shows multiple segments of abnormal signal in the corpus callosum (image 5 and arrows in image 6). More extensive signal abnormalities are seen in the periventricular white matter, especially on the right (images 6 and 7). Signal abnormalities extend downward through the posterior limb of the internal capsule and the pyramidal tracts in the brainstem on the right (arrows in images 7 and 8). (C) MRI in patient 3 at age 35. The midsagittal image shows that the anterior part of the corpus callosum is abnormal, whereas only a strip of signal abnormality is seen in the splenium (arrows in image 1). Images 2 and 3 illustrate that the frontal and parietal white matter is abnormal, whereas the central white matter in between is normal. The tract involvement is evident (arrows in images 2 and 4). The axial fluid-attenuated inversion recovery image shows that the affected white matter is rarefied (arrow in image 5). The axial T2-weighted images illustrate the involvement of the anterior limb of the internal capsule (image 6) and the frontopontine tracts going down into the brainstem (arrows in images 7 and 8).

Table 1. AARS2 mutations found in the patients

Patient	cDNA	Protein	State	Paternal/ Maternal	EVS frequency, % ^a
1	c.149T>G	p.Phe50Cys	heterozygous	M	∅
	c.1561C>T	p.Arg521*	heterozygous	P	∅
2	c.2893G>A	p.Gly965Arg	heterozygous	M	∅
	c.1213G>A	p.Glu405Lys	heterozygous	P	∅
3	c.1609C>T and c.2350del	p.Gln537* and p.Glu784Serfs*9	heterozygous	M	∅
	c.595C>T and c.2188G>A	p.Arg199Cys and p.Val730Met	heterozygous	P	0.008 and 3.1
4	c.230C>T	p.Ala77Val	heterozygous	M	0.008
	c.595C>T and c.2188G>A	p.Arg199Cys and p.Val730Met	heterozygous	P	0.008 and 3.1
5	c.595C>T and c.2188G>A	p.Arg199Cys and p.Val730Met	heterozygous	M	0.008 and 3.1
	c.390_392del	p.Phe131del	heterozygous	P	∅
6	c.595C>T and c.2188G>A	p.Arg199Cys and p.Val730Met	heterozygous	M	0.008 and 3.1
	c.2611dup	p.Thr871Asnfs*21	heterozygous	P	∅

Abbreviations: cDNA = complementary DNA; EVS = Exome Variant Server (varianttools.sourceforge.net/Annotation/EVS/); ∅, not found

We subjected P2 to a gene panel containing 500 genes known to cause mitochondrial disorders and to clinical WES. With both policies, we identified 2 missense mutations in AARS2 (c.2893G>A, p.Gly965Arg and c.1213G>A, p.Glu405Lys).

We performed Sanger sequencing of AARS2 exons and intron-exon boundaries in all patients and found AARS2 mutations in 4 of the 11 patients selected on the basis of MRI features (Table 1). We did not find AARS2 mutations in the 2 patients with ovarioleukodystrophy. All identified nucleotide substitutions with a frequency <0.01% in public databases correspond to amino acid changes predicted to be deleterious (Tables 1 and e-5).

Functional studies

Because no biochemical readout was detected in cell lines of P1, we tested the possible deleterious impact of the AARS2 mutations on oxidative phosphorylation in a *Saccharomyces cerevisiae* yeast model. Phe50 in human AARS2 is highly conserved in phylogenesis, including yeast (figure e-2), in which the ortholog *ala1* gene (NC_001147.6) codes for both the cytosolic and mitochondrial alanyl tRNA synthetase.¹⁶ We disrupted *ala1* by homologous recombination and re-expressed the wild-type cytosolic isoform (supplemental data), thus generating a viable but oxidative phosphorylation-incompetent strain (*ala1^{L-16X}*), which lacked the mitochondrial isoform. In this strain, we expressed either the wild-type *ala1* gene (*ala1^{wt}*), a p.Phe22Cys mutant allele (*ala1^{F22C}*), equivalent to the human p.Phe50Cys variant, or a p.Val500* mutant allele (*ala1^{V500X}*), equivalent to the human p.Arg521* variant.

In contrast to *ala1^{wt}*, the expression of *ala^{V500X}* failed to restore growth on nonfermentable sources (i.e., glycerol). The oxidative growth of the strain expressing *ala1^{F22C}* was similar to the wild-type at 28°C but reduced at 37°C (figure e-3). We obtained similar results from assays evaluating the oxygen consumption (Figure 3, A), the in vivo mitochondrial protein synthesis (Figure 3, B), the activities of the respiratory chain complexes I + III and IV, and the spectra of mitochondrial respiratory chain cytochromes (figure e-3). Finally, we evaluated the charging of the tRNA with alanine; the p.Val500* change determined the complete inability to charge mitochondrial tRNA^{Ala} with its cognate amino acid, whereas the p.Phe22Cys change determined a partial reduction in the amino acid charging at 37°C (Figure 3, C). We analyzed the effects of *ala1^{L125R}*, corresponding to p.Leu155Arg,⁹ and found that in all experiments this missense mutation behaves as a null allele (Figures 3 and e-3). The other known AARS2 mutation, p.Arg592Trp,⁹ could not be tested, because the residue is not conserved in yeast (figure e-2).

The above yeast experiments confirmed that the p.Phe50Cys missense mutation is deleterious only in stress conditions, whereas the truncated protein due to the nonsense mutation is nonfunctional.

DISCUSSION

Defects in several different mitochondrial aminoacyl tRNA synthetases have been associated with specific clinical phenotypes.^{1,3-5} However, these enzymes are ubiquitously expressed and take part in the same process, so this phenotypic segregation is difficult to explain. This conclusion of phenotypic segregation may be based on inclusion bias, because the genes are only analyzed in patients with specific phenotypes. In addition, the number of patients with mutations in different mitochondrial aminoacyl tRNA synthetases is at present too small to provide conclusive evidence of the existence of exclusive genotype-phenotype correlations.

Recently, AARS2 mutations have been reported in 3 subjects as the cause for infantile hypertrophic cardiomyopathy, lactic acidosis, and brain and skeletal muscle involvement, with early fatal outcome.⁹ In contrast, our patients have later-onset neurologic dysfunction due to a leukoencephalopathy and no signs of cardiomyopathy. In P1 and P2, onset was in childhood and initially followed a stable course or very slow disease progression. In all cases, the course after onset of evident deterioration was rather rapid. The neurologic dysfunction comprised motor deterioration, consisting of cerebellar ataxia and spasticity, and cognitive decline with features of frontal lobe

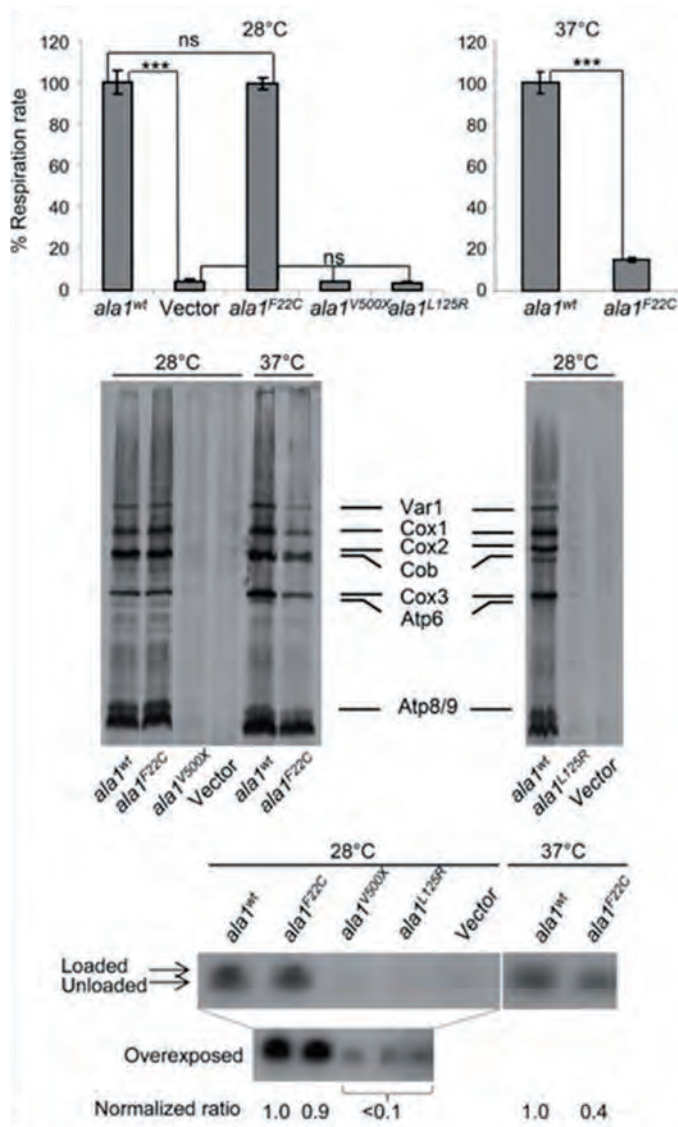


Figure 3. Yeast studies

(A) Oxygen consumption rate of the *ala1^{L16X}* strain transformed with the *ala1^{wt}* allele, the empty vector, and the mutant alleles *ala1^{F22C}*, *ala1^{V500X}*, and *ala1^{L125R}*. Respiratory rates were normalized to the strain transformed with *ala1^{wt}*, in which the respiratory rate was 81.1 nmol min⁻¹ mg⁻¹ at 28°C and 33.4 nmol min⁻¹ mg⁻¹ at 37°C. Values are the mean of 3 independent experiments, each with an independent clone. Two-tailed paired *t* test was applied for statistical significance. ****p* < 0.001. (B) In vivo mitochondrial protein synthesis of the *ala1^{L16X}* strain transformed with the *ala1^{wt}* allele, the empty vector, and the mutant alleles *ala1^{F22C}*, *ala1^{V500X}*, and *ala1^{L125R}*. Mitochondrial gene products were labeled with [³⁵S]-methionine in whole cells in the presence of cycloheximide for 10 minutes at 28°C or 37°C. (C) Mitochondrial tRNA^{Ala} loading of the *ala1^{L16X}* strain transformed with the *ala1^{wt}* allele, the empty vector, and the mutant alleles *ala1^{F22C}*, *ala1^{V500X}*, and *ala1^{L125R}*. Signals were quantified with Quantity 1 (Bio-Rad, Hercules, CA). For each strain, the ratio between the charged tRNA^{Ala} and the uncharged one was calculated and normalized to the *ala1^{wt}* strain. Atp = ATP synthase; Cob = cytochrome b; Cox = cytochrome c oxidase; ns = not significant; Var1 = small mitochondrial ribosome subunit.

dysfunction with poor memory, inactivity and other behavioral changes, as well as depression and other psychiatric features. Comparing clinical and MRI findings, it is clear that the clinical signs of the patients depend on which tracts are affected. P2, P4, and P6 had prominent signs of motor dysfunction and had pyramidal tract involvement on MRI. P3 and P5 mainly had signs of behavioral and cognitive dysfunction and frontopontine tract involvement. The striking white matter tract involvement and presence of spots of restricted diffusion in the cerebral white matter are features shared by another disorder with mutations in a mitochondrial aminoacyl tRNA synthetase: “leukoencephalopathy with brainstem and spinal cord involvement and lactate elevation” (LBSL), caused by mutations in *DARS2* (OMIM *610956). In LBSL, the white matter spots of restricted diffusion are ascribed to myelin vacuolization, a feature frequently seen in mitochondrial leukoencephalopathies.¹⁷

6 In P1 and P6, we detected a profound, isolated defect of complex IV activity, rather than a combination of mitochondrial DNA–related respiratory chain defects, which is the expected consequence of reduced mitochondrial protein synthesis. The pathogenicity of the 2 *AARS2* variants of P1 was proven in a recombinant yeast model. Of note, the yeast p.Phe22Cys mutation, equivalent to p.Phe50Cys found in P1, impairs complex IV activity much more than complex I + III activity, whereas p.Leu125Arg, equivalent to human p.Leu155Arg, a mutation of patients with cardiomyopathy,⁹ decreases them both, suggesting that an isolated defect of complex IV may predominantly depend on specific missense mutations, possibly influencing the main target tissue (brain vs heart). Variable involvement of different respiratory chain complexes and different degrees of defective activities have also been reported for different mutations in other aminoacyl tRNA synthetases.¹⁸

The yeast p.Phe22Cys mutation was only deleterious in stress conditions, while the other tested mutations were highly deleterious in basal conditions, suggesting that the human p.Phe50Cys mutant protein maintains residual activity, which could explain the slow disease of our patient, in contrast to the rapidly fatal outcome of the patients with cardiomyopathy.⁹ While our yeast model enabled us to evaluate the p.Leu155Arg mutation, poor conservation between human and yeast precluded the validation of the p.Arg592Trp substitution in patients with cardiomyopathy.⁹ The latter mutation could impair editing activity of *AARS2*, leading to increased mistranslation of the alanine codon by serine or glycine.⁹ According to this hypothesis, a specific pathogenic mechanism, mistranslation, would lead to cardiomyopathy, while translation deficiency, caused by other aminoacyl tRNA synthetase mutations, is usually not associated with heart damage.³ Of note, hypertrophic cardiomyopathy occurs in subjects with mutations

affecting *MTO1*, encoding an enzyme responsible for tRNA modifications that increase accuracy and efficiency of mitochondrial DNA translation.^{19,20}

A striking feature was the presence of ovarian failure in all female patients with *AARS2* mutations. Mutations in 2 other mitochondrial aminoacyl tRNA synthetase encoding genes, namely *HARS2* (OMIM *600783) and *LARS2* (OMIM *604544), have recently been associated with Perrault syndrome, a disorder characterized by ovarian dysgenesis and sensorineural hearing loss. However, Perrault syndrome is genetically heterogeneous; it can also be caused by mutations in *HSD17B4*, encoding a peroxisomal enzyme involved in fatty acid β -oxidation, and mutations in *CLPP*, encoding a mitochondrial endopeptidase. Mutations in *POLG* (OMIM *174763), the gene encoding DNA polymerase- γ for the replication of human mitochondrial DNA, may also lead to premature menopause²¹ and ovarian failure.²²

Of the 7 patients included in the present study who had similar MRI abnormalities but no *AARS2* mutations, 2 were male and 2 were prepubertal females. Of the 3 adult female patients, one had normal menses until put on contraceptive injections, one had a period of 3 years of amenorrhea but recently started menstruating again, and for one the information is not available. It is therefore not possible to make a definitive conclusion on the presence or absence of ovarian failure in these patients.

The preferential involvement of brain white matter and ovaries is shared by vanishing white matter (OMIM #603896), caused by mutations in any of the 5 genes (*EIF2B1* to *EIF2B5*) encoding subunits of the translation initiation factor eIF2B. Female patients often develop ovarian failure, manifest as primary or secondary amenorrhea.¹² eIF2B impairment leads to a defect in translation initiation for nuclear genes, not affecting translation of the mitochondrial encoded proteins. Hence, even if both *AARS2* and *EIF2B1–5* mutations are likely associated with block or dysregulation of protein synthesis, their targets and site of action (mitochondria vs cytosol) are completely separated and, at present, we have no explanation for the common resulting phenotype. Two patients with ovarioleukodystrophy as well as 7 patients with similar MRI abnormalities had no *AARS2* mutations, suggesting that they have mutations in untranslated regions of the gene or there could be another gene(s) that, when mutated, is associated with the same selective vulnerability.

REFERENCES

1. Rötig A. Human diseases with impaired mitochondrial protein synthesis. *Biochim Biophys Acta* 2011;1807:1198-1205.
2. Yao P and Fox PL. Aminoacyl-tRNA synthetases in medicine and disease. *EMBO Mol Med* 2013;5:332-343.
3. Konovalova S and Tynynismaa H. Mitochondrial aminoacyl-tRNA synthetases in human disease. *Mol Genet Metab* 2013;108:206-211.
4. Scheper GC, van der Kloek T, van Andel RJ, et al. Mitochondrial aspartyl-tRNA synthetase deficiency causes leukoencephalopathy with brain stem and spinal cord involvement and lactate elevation. *Nat Genet* 2007;39:534-539.
5. Steenweg ME, Ghezzi D, Haack T, et al. Leukoencephalopathy with thalamus and brainstem involvement and high lactate 'LTBL' caused by EARS2 mutations. *Brain* 2012;135:1387-1394.
6. Haack TB, Haberberger B, Frisch EM, et al. Molecular diagnosis in mitochondrial complex I deficiency using exome sequencing. *J Med Genet* 2012;49:277-283.
7. Lamperti C, Fang M, Invernizzi F, et al. A novel homozygous mutation in SUCLA2 gene identified by exome sequencing. *Mol Genet Metab* 2012;107:403-408.
8. Hanchard NA, Murdock DR, Magoulas PL, et al. Exploring the utility of whole-exome sequencing as a diagnostic tool in a child with atypical episodic muscle weakness. *Clin Genet* 2013;83:457-461.
9. Götz A, Tynynismaa H, Euro L, et al. Exome sequencing identifies mitochondrial alanyl-tRNA synthetase mutations in infantile mitochondrial cardiomyopathy. *Am J Hum Genet* 2011;88:635-642.
10. Schiffmann R, Tedeschi G, Kinkel RP, et al. Leukodystrophy in patients with ovarian dysgenesis. *Ann Neurol* 1997;41:654-661.
11. van der Knaap MS, Breiter SN, Naidu S, Hart AA, Valk J. Defining and categorizing leukoencephalopathies of unknown origin: MR imaging approach. *Radiology* 1999;213:121-133.
12. Fogli A, Rodriguez D, Eymard-Pierre E, et al. Ovarian failure related to eukaryotic initiation factor 2B mutations. *Am J Hum Genet* 2003;72:1544-1550.
13. Mayr JA, Haack TB, Graf E, et al. Lack of the mitochondrial protein acylglycerol kinase causes Sengers syndrome. *Am J Hum Genet* 2012;90:314-320.
14. Thomas BJ and Rothstein R. Elevated recombination rates in transcriptionally active DNA. *Cell* 1989;56:619-630.
15. Elstner M, Andreoli C, Ahting U, et al. MitoP2: an integrative tool for the analysis of the mitochondrial proteome. *Mol Biotechnol* 2008;40:306-315.
16. Tang HL, Yeh LS, Chen NK, Ripmaster T, Schimmel P, Wang CC. Translation of a yeast mitochondrial tRNA synthetase initiated at redundant non-AUG codons. *J Biol Chem* 2004;279:49656-49663.
17. Steenweg ME, Pouwels PJ, Wolf NI, van Wieringen WN, Barkhof F, van der Knaap MS. Leucoencephalopathy with brainstem and spinal cord involvement and high lactate: quantitative magnetic resonance imaging. *Brain* 2011;134:3333-3341.
18. Rodenburg RJ. Biochemical diagnosis of mitochondrial disorders. *J Inherit Metab Dis* 2011;34:283-292.
19. Ghezzi D, Baruffini E, Haack TB, et al. Mutations of the mitochondrial-tRNA modifier MTO1 cause hypertrophic cardiomyopathy and lactic acidosis. *Am J Hum Genet* 2012;90:1079-1087.
20. Baruffini E, Dallabona C, Invernizzi F, et al. MTO1 mutations are associated with hypertrophic cardiomyopathy and lactic acidosis and cause respiratory chain deficiency in humans and yeast. *Hum Mutat* 2013;34:1501-1509.
21. Luoma P, Melberg A, Rinne JO, et al. Parkinsonism, premature menopause, and mitochondrial DNA polymerase gamma mutations: clinical and molecular genetic study. *Lancet* 2004;364:875-882.
22. Bekheirnia MR, Zhang W, Eble T, et al. POLG mutation in a patient with cataracts, early-onset distal muscle weakness and atrophy, ovarian dysgenesis and 3-methylglutaconic aciduria. *Gene* 2012;499:209-212.

SUPPLEMENTAL DATA

Supplemental methods: Detailed methods for histochemical, biochemical and yeast studies

Supplemental Table e-1: Primers used in this study

Supplemental Table e-2: Clinical characteristics

Supplemental Table e-3: Laboratory findings

Supplemental Table e-4: MRI findings

Supplemental Table e-5: *In silico* prediction of pathogenicity for AARS2 mutations

Supplemental figure e-1: MRI of patients P4 and P5

Supplemental figure e-2: Protein sequence alignment of AARS2 orthologs

Supplemental Figure e-3: OXPHOS growth and biochemical assays in yeast

SUPPLEMENTAL METHODS

Respiratory chain function

Cryostatic cross sections of skeletal muscle biopsies were used for histological and histochemical studies, according to standard techniques. Gomori trichrome staining, succinate dehydrogenase and cytochrome c oxidase activities were performed as previously described.¹ The activities of respiratory chain complexes in muscle homogenates and digitonin-treated fibroblasts were measured using standard spectrophotometric techniques. Micro-oxygraphy was used to measure oxygen consumption rate in fibroblasts, using a SeaHorse FX-96 instrument.² Fibroblasts from P1 were cultured in DMEM glucose medium, or glucose-free 5mM galactose DMEM medium for 72 hours before the analysis.

Yeast strains, plasmids and media

The W303-1B genotype is *Mata ade2-1 leu2-3, 112 ura3-1 trp1-1 his3-11, 15 can1-100*. Strains were grown in YP complete media (1% yeast extract, 2% peptone ForMedium, Norfolk, UK) or SC synthetic defined media (0.19% YNB without aminoacids and NH_4SO_4 powder ForMedium, Norfolk, UK, 0.5% NH_4SO_4) supplemented with 1gr/L dropout mix without uracil and tryptophan.³ Media were supplemented with various carbon sources at 2% (w/v) (Carlo Erba Reagents, Milan, Italy), in liquid phase or after solidification with 20g/L agar (ForMedium, Norfolk, UK).

ala1 was cloned under its natural promoter by PCR-amplification with oligonucleotides ALA1C (Supplementary table 1) and cloning of the *SacI-SphI*-digested *ala1* fragment in pFL36.⁴ The plasmid was inserted in W303-1B through the Li-Ac method.⁵ Since disruption of *ala1* is lethal, we performed disruption of the gene in strain W303-1B harboring pFL36*ala1*. Disruption was performed through one-step gene disruption by PCR-amplification of KanMX4 cassette⁶ with primers ALA1D (Supplementary table 1)

and transformation of the former strain, thus obtaining W303-1B *ala1Δ*/pFL36*ala1*. *ala1* fragment was subcloned from pFL36 to pFL38 and pFL39.⁴ All the mutations were introduced through the *DpnI*-mediated site directed mutagenesis⁷ with appropriate primers (Supplementary table 1). pFL38*ala1* was mutagenized to obtain an isoform of *ala1* encoding the cytoplasmic but not the mitochondrial Ala1 isoform, called *ala1*^{L-16X}, through mutagenesis of codon -16 (respect to the ATG initiator of the cytoplasmic isoform), that was changed to the stop codon TAG, as previously performed by others,⁸ thus obtaining pFL38*ala1*^{L-16X}. pFL39*ala1* was mutagenized with appropriate primers (Supplementary table 1) to obtain mutant alleles pFL39*ala1*^{F22C}, pFL39*ala1*^{L125R} and pFL39*ala1*^{V500X}.

W303-1B *ala1Δ* pFL36*ala1* was co-transformed with pFL38*ala1*^{L-16X}, and each variant of pFL39*ala1*, and then pFL36*ala1* was lost through plasmid-shuffling, thus obtaining strains encoding a cytoplasmic wild type Ala1 isoform and a mutant Ala1 isoform.

Yeast analysis

Respiratory activity and *in vivo* mtDNA protein synthesis were performed as previously described.^{9,10} Reduced vs. oxidized cytochrome spectra of yeast cell cultured for 24hrs at 28°C or 37°C in SC medium supplemented with glucose at non-repressing concentration of 0.6% were recorded (Varian Cary300 UV-VIS Spectrophotometer) at room temperature.

Cytochrome c oxidase and NCCR (complex I+III) activities were measured on a mitochondrial-enriched fraction prepared as previously described^{11,12} after a cellular growth to a concentration of 1.5-2 OD₆₀₀/ml in SC medium supplemented with 2% galactose and 0.2% glucose.

For the *in vivo* determination of charged Ala-tRNA, a mitochondrial-enriched fraction prepared as above was subjected to total RNA extraction in acid condition as previously described¹³ to maintain the acylated tRNAs. Approximately 5 μg of total mitochondrial RNA were loaded in a 20 cm long 12% polyacrylamide (acrylamide:bisacrylamide, 19:1, w/w)/7M urea gel in 0.1M sodium acetate buffer pH 4.6. After approximately 40-hour at 120V at 4°C (partially denaturing conditions), gel was electroblotted onto a Hybond-N+ in TAE buffer (40 mM Tris, 20 mM sodium acetate, 1 mM EDTA, pH 7.4). Northern blot analysis was performed by standard method by using mt-tRNA^{ala} oligo (Supplementary table 1) as a probe, which was 5'-labelled with EasyTides® Adenosine 5'-triphosphate, [γ-32P] (Perkin Elmer) with T4 Polynucleotide Kinase (NEB) in 20 μl. Signals were acquired after different time exposures with Carestream BioMax MS films.

ADDITIONAL REFERENCES:

1. Sciacco M, Bonilla E. Cytochemistry and immunocytochemistry of mitochondria in tissue sections. *Methods Enzymol* 1996;264: 509-521.
2. Invernizzi F, D'Amato I, Jensen PB, Ravaglia S, Zeviani M, Tiranti V. Microscaleoxygraphy reveals OXPHOS impairment in MRC mutant cells. *Mitochondrion* 2012;12:328-335.
3. Baruffini E, Ferrero I, Foury F. In vivo analysis of mtDNA replication defects in yeast. *Methods*. 2010;51:426-36.
4. Bonneaud N, Ozier-Kalogeropoulos O, Li GY, Labouesse M, Minvielle-Sebastia L, Lacroute F. A family of low and high copy replicative, integrative and single-stranded *S. cerevisiae* / *E. coli* shuttle vectors. *Yeast* 1991;7:609–615.
5. Gietz RD, Schiestl RH. High-efficiency yeast transformation using the LiAc/SS carrier DNA/PEG method. *Nat Protoc* 2007;2:31-34.
6. Wach A, Brachat A, Pöhlmann R, Philippsen P. New heterologous modules for classical or PCR-based gene disruptions in *Saccharomyces cerevisiae*. *Yeast* 1994; 10:1793-1808.
7. Fisher CL, Pei GK. Modification of a PCR-based site-directed mutagenesis method. *Biotechniques* 1997;23,570-574.
8. Tang HL, Yeh LS, Chen NK et al. Translation of a yeast mitochondrial tRNA synthetase initiated at redundant non-AUG codons. *J Biol Chem* 2004;279:49656-49663.
9. Goffrini P, Ercolino T, Panizza E, Giachè V, Cavone L, Chiarugi A, Dima V, Ferrero I, Mannelli M. Functional study in a yeast model of a novel succinate dehydrogenase subunit B gene germline missense mutation (C191Y) diagnosed in a patient affected by a glomus tumor. *Hum Mol Genet* 2009;18:1860-1868.
10. Barrientos A. In vivo and in organello assessment of OXPHOS activities. *Methods* 2002;26:307-316.
11. Barrientos A, Fontanesi F, Diaz F. Evaluation of the mitochondrial respiratory chain and oxidative phosphorylation system using polarography and spectrophotometric enzyme assays. *Curr Protoc Hum Genet* 2009;19:19-23.
12. Soto IC, Fontanesi F, Valledor M, Horn D, Singh R, Barrientos A. Synthesis of cytochrome c oxidase subunit 1 is translationally downregulated in the absence of functional F1F0-ATP synthase. *Biochim Biophys Acta* 2009;1793:1776-86.
13. Enriquez JA, Attardi G. Analysis of aminoacylation of human mitochondrial tRNAs. *Methods Enzymol* 1996;264:183-96.
14. Götz A, Tyynismaa H, Euro L et al. Exome sequencing identifies mitochondrial alanyl-tRNA synthetase mutations in infantile mitochondrial cardiomyopathy. *Am J Hum Genet* 2011;88:635-642.

Supplemental Table e-1. Primers used for qPCR and yeast studies

Use	Forward	Reverse
Human AARS2		
RTqPCR-pair1	TGCTTTTTGTCAATGCGGG	GGATCCACGGTGCCCAG
RTqPCR-pair2	TCCAAGCCGCACTGC	CCTACAGCCCCAGTACGTAAACAG
Yeast <i>ala1</i>		
Cloning:ALA1C	gggggGAGCTCgacaatccggtaatgcacac ¹	gggggGCATGCaacagcaaatctttgtccttg ¹
Disruption: ALA1D	atcaactagaaccataatgacgatcgggtgataagcaaaaatggac GCTTCGTACGCTGCAGGTCGACG ²	tcatcaactgcatcctttatagcggctggtttatcacccatacct GATATCATCGATGAATTCGAGC ²
Mutag: L-16X	caactaccggattaaggaactAgactctttcttcaagaagc ³	gcttcctgaagaagagtcTagttccttaatccggtagttg ³
Mutag: F22C	gtccgtaataccttctagactattGcaaatctaaagaacacaag ³	cttggttcttagattgCaatagtctagaaggattacggac ³
Mutag:V500X	caaatcggcagcgccaactGTAaaggtaccatttgaaactgc ³	gcagtttcaaaatggtaccttATCAgttggcctgccgtatttg ³
Mutag:L125R	ggaagctattactactcatggactAGAttgactgaagtatacggc ³	gccgtatactcagtcaaTCTagtcctagagtaagtaatagcttc ³
mt-tRNA ^{ala}	Attggagttaatgagacttgaact	

¹ In upper case the restriction sites

² In upper case the sequences which amplify the KanMX4 cassette

³ Mutagenic primers: in upper case the nucleotide change

Supplemental Table e-2. Clinical characteristics

Patient	1	2	3	4	5	6
Gender	F	M	F	F	F	F
Year of birth	1981	1991	1977	1982	1962	1988
Siblings (affected / unaffected / otherwise affected)	0 / 1 / 0	0 / 1 / 0	0 / 1 / 0	0 / 0 / 1	0 / 1 / 0	0 / 1 / 0
Consanguinity parents	no	no	no	no	no	no
Pregnancy, delivery, neonatal period	normal	normal	normal	normal	normal	normal
Initial motor & cognitive development	normal	normal	normal	normal	normal	normal
Presentation						
age at presentation (y)	3	7	33	24	40	22
Signs at presentation	impaired balance and frequent falls	learning difficulties	depression, cognitive decline	hand tremor, behavioral changes, cognitive decline	memory problems, depression	gait difficulties and impaired balance
Preceding event	no	no	no	no	no	no
Course over time						
regression	yes	yes	yes	yes	yes	yes
Signs of regression	motor & cognitive deterioration	cognitive deterioration, dysarthria, dystonia, ataxia, spasticity	cognitive deterioration, urinary incontinence	motor & cognitive deterioration, spasticity and ataxia	cognitive deterioration	motor deterioration, spasticity and ataxia
Psychiatric	psychosis	no	depression	no	depression	depression
Endocrine	secondary amenorrhea due to ovarian failure	none known	secondary amenorrhea due to ovarian failure	secondary amenorrhea due to ovarian failure	primary amenorrhea due to ovarian failure	secondary amenorrhea due to ovarian failure
Epilepsy	no	no	yes	no	no	no
Outcome	dementia, still walking with support	partial improvement and stabilization	bedridden since age 36	death at 28 years	death at 46 y	wheelchair-bound since age 23
Neurological findings						
age at latest examination (y)	30	21	36	26	43	23
Intelligence	dementia	learning disability	dementia	dementia	dementia	calculation problems
Dysmorphic features	no	no	no	no	no	no
Head circumference	normal	normal	normal	normal	normal	normal
Vision, eye movements	nystagmus	nystagmus	downbeat nystagmus, no tracking	decreased vision, no tracking	normal	nystagmus

Supplemental Table e-2. Clinical characteristics continued

Patient	1	2	3	4	5	6
Hearing	normal	normal	normal	normal	normal	normal
Dysarthria	yes	yes	no speech	no speech	no	no
Arms						
Tone	normal	increased	decreased	increased	normal	normal
Muscle strength	normal	decreased	normal	decreased	normal	normal
Reflexes	increased	brisk	increased	increased	normal	increased
Spasticity	no	yes	no	yes	no	no
Ataxia	yes	yes	yes	yes	no	no
Extrapyramidal signs	no	dystonia >r	no	dystonia left hand	no	no
Sensory problems	no	no	no	no	no	no
Legs						
Tone	increased	increased	decreased	decreased	normal	increased
Muscle strength	normal	decreased	normal	normal	normal	normal
Reflexes	increased	brisk	increased	increased	normal	increased
Babinski signs	yes	yes	no	yes	no	yes
Spasticity	yes	yes	no	yes	no	yes
Ataxia	yes	yes	no	yes	no	yes
Extrapyramidal signs	no	dystonia >r	no	no	no	no
Sensory problems	no	no	no	no	no	no

f, female; m, male; y, year; L, left; R, right

Supplemental Table e-3. Laboratory findings

Patient	1	2	3	4	5	6
Routine hematology and biochemistry	normal	normal	mild leuko- & thrombocytopenia	normal	normal	normal
Endocrine	low estradiol, ↑ FSH & LH	no clinical signs of endocrine dysfunction, n.i.	low estradiol, ↑ FSH & LH	estradiol & prolactine normal, ↑ FSH & LH	↑ FSH, LH and prolactin	low estradiol, normal FSH & LH
Plasma lactate	normal	normal	normal	normal	n.i.	n.i.
CSF lactate	n.i.	normal	normal	normal	n.i.	normal
Plasma amino acids	n.i.	increased alanine	normal	normal	n.i.	normal
Urinary organic acids	n.i.	normal	normal	normal	n.i.	normal
Acylcarnitine profile	n.i.	n.i.	n.i.	n.i.	n.i.	normal
Arylsulfatase A	n.i.	normal	normal	normal	normal	normal
Galactocerebrosidase	n.i.	normal	normal	normal	n.i.	normal
Very long chain fatty acids	n.i.	normal	normal	normal	n.i.	normal
Other		CSF 5-HIAA 47 (nl 67-140), HVA 100 (nl 145-324), neopterin 8 (nl 8-28), tetrahydro-biopterin 11 (nl 10-30), 5-methyltetrahydrofolate 40 (nl 40-120)				
Genetic testing	no mutations in <i>FRDA</i> , <i>APTX</i> and <i>POLG</i> ; no mtDNA mutations in muscle	whole exome sequencing and nuclear mitochondrial panel	n.i.	fragile X: negative, no mutations in <i>EIF2B1-5</i> genes	no mutations in <i>EIF2B1-5</i> genes; normal karyotype	no mutations in <i>EIF2B1-5</i> genes
Muscle biopsy	isolated COX deficiency	n.i.	n.i.	n.i.	n.i.	isolated COX deficiency
EMG/NCV	n.i.	n.i.	n.i.	n.i.	normal	normal
ECG	normal	normal	normal	n.i.	n.i.	normal
Cardiac ultrasound	normal	n.i.	n.i.	n.i.	n.i.	n.i.

n.i., not investigated; CSF, cerebrospinal fluid; nl, normal; 5-HIAA, 5-hydroxyindoleacetic acid; HVA, homovanillic acid; FSH, follicle stimulating hormone; LH, luteinizing hormone; mtDNA, mitochondrial DNA; COX, cytochrome c oxidase; NCV, nerve conducting velocity; EMG, electromyogram; ECG, electrocardiogram

Supplemental Table e-4. MRI findings

Patient	1	2	3	4	5	6
Age first MRI	18 y	14 y	34 y	26 y	42 y	25 y
Predominant location WM abnormalities	periventricular R	periventricular	periventricular, frontal & parietal	periventricular, frontal & parietal	periventricular, frontal & parietal	periventricular
Relative sparing	most WM spared	most WM spared	frontoparietal border area, subcortical WM	subcortical WM	frontoparietal border area, subcortical WM	most WM spared
Aspect WM abnormalities	single small lesion R	confluent, asymmetric (R>L)	largely confluent, partially patchy, symmetric	partially patchy, partially confluent, asymmetric (R>L)	largely confluent, partially patchy, symmetric	largely confluent, symmetric
Corpus callosum genu	-	-	+	+, patchy	+, also atrophic	-
Corpus callosum body	-	-	+, anterior part	+, patchy	+, anterior part	+, focal strip
Corpus callosum splenium	-	+, focal strip	+, focal strip	+, patchy	+, focal strip	-
Internal capsule anterior limb	-	-	+	-	+	-
Internal capsule posterior limb	-	-	+, frontopontine tracts	+, pyramidal and parieto-occipitopontine tracts	+, frontopontine tracts	+
External capsule	-	-	anterior part	anterior part	anterior part	-
WM rarefaction and/or cysts	-	-	+, central frontal and parietal WM	+, central frontal and parietal WM	central frontal WM	-
Cerebral cortex, basal nuclei, thalami	-	-	-	-	-	-
Enlargement lateral ventricles	-	-	-	+, mild	+, mild	-
Enlargement subarachnoid spaces	-	-	-	-	+, frontal, mild	-
Cerebellar WM and peduncles	-	-	-	-	-	-
Cerebellar cortex, dentate nucleus	-	-	-	-	-	-
Cerebellar atrophy	+, mild, vermis > hemisph.	-	+, vermis > hemisph.	+, mild	+, mild	+, mild
Midbrain	-	-	+, frontopontine tracts in cerebral peduncles	+, pyramidal and parieto-occipitopontine tracts	+, frontopontine tracts in cerebral peduncles	+, pyramidal tracts
Pons	-	-	-	-	-	-
Medulla	-	-	-	-	-	+, left pyramid
Contrast enhancement	-	n.d.	-	n.d.	-	-
Restricted diffusion	-	-	n.d.	multifocal WM spots, corpus callosum	n.d.	n.d.
MRS lactate	-	n.d.	n.d.	n.d.	n.d.	not evident

Supplemental Table e-4. MRI findings continued

Patient	1	2	3	4	5	6
Age at most recent MRI	28 y	22 y	35 y			
Predominant location WM abnormalities	periventricular	periventricular, frontal & parietal	periventricular, frontal & parietal			
Relative sparing	most WM	WM in posterior-frontal area L, subcortical WM	frontoparietal border area, subcortical WM			
Aspect WM abnormalities	patchy, more or less symmetric	partially patchy, partially confluent, asymmetric (R>L)	largely confluent, partially patchy, symmetric			
Corpus callosum genu	+, focal strip	+, patchy	+			
Corpus callosum body	-	+, patchy	+, anterior part			
Corpus callosum plenum	+, focal strip	+, patchy	+, focal strip			
Internal capsule anterior limb	-	-	+			
Internal capsule posterior limb	-	pyramidal tracts R>L	+, frontopontine tracts			
External capsule	-	anterior part R>L	anterior part			
WM rarefaction and/or cysts	-	-	+, worse			
Cerebral cortex, basal nuclei, thalami	-	-	-			
Enlargement lateral ventricles	-	-	-			
Enlargement subarachnoid spaces	-	-	-			
Cerebellar WM and peduncles	-	-	-			
Cerebellar cortex, dentate nucleus	-	-	-			
Cerebellar atrophy	+, vermis > hemisph.	+, vermis, slight	+, vermis > hemisph.			
Midbrain	-	+, pyramidal tracts in cerebral peduncles R	+, frontopontine tracts in cerebral peduncles			
Pons	-	+, pyramidal tracts R	-			
Medulla	-	+, pyramid R	-			
Contrast enhancement	-	No	-			
Restricted diffusion	-	multifocal WM areas	n.d.			
MRS lactate	-	n.d.	n.d.			
Change over time	worsening of WM abnormalities and cerebellar atrophy	worsening of WM abnormalities	worsening of WM abnormalities			

WM, white matter; n.d., not done; hemisph., hemisphere(s); R, right; L, left; y, years

Supplemental Table e-5. In silico prediction of pathogenicity for AARS2 mutations

Patient	c.DNA ¹	Protein	State	Mutation Taster ²	SIFT ³	Polyphen2 ⁴	Pmut ⁵	SNP&GO ⁶
1	c.149T>G	p.Phe50Cys	Heterozygous	Disease	0.00	0.999	0.6932	Disease
1	c.1561C>T	p.Arg521*	Heterozygous	Disease	/	/	/	/
2	c.2893G>A	p.Gly965Arg	Heterozygous	Disease	0.00	0.995	0.5952	Disease
2	c.1213G>A	p.Glu405Lys	Heterozygous	Disease	0.00	0.999	0.3374	Disease
3	c.1609C>T and	p.Gln537*	Heterozygous	Disease	/	/	/	/
3	c.2350del	p.Glu784Serfs*9	Heterozygous	Disease	/	/	/	/
3, 4, 5, 6	c.595C>T and	p.Arg199Cys	Heterozygous	Disease	0.02	0.964	0.8301	Disease
3, 4, 5, 6	c.2188G>A	p.Val730Met	Heterozygous	Disease	0.01	0.998	0.3966	Neutral
4	c.230C>T	p.Ala77Val	Heterozygous	Disease	0.02	0.978	0.4018	Disease
5	c.390_392del	p.Phe131del	Heterozygous	Disease	/	/	/	/
6	c.2611dup	p.Thr871Asnfs*21	Heterozygous	Disease	/	/	/	/

¹Nucleotide numbering reflects cDNA numbering starting from the A of the ATG translation initiation codon in the reference sequence NM_020745.3.

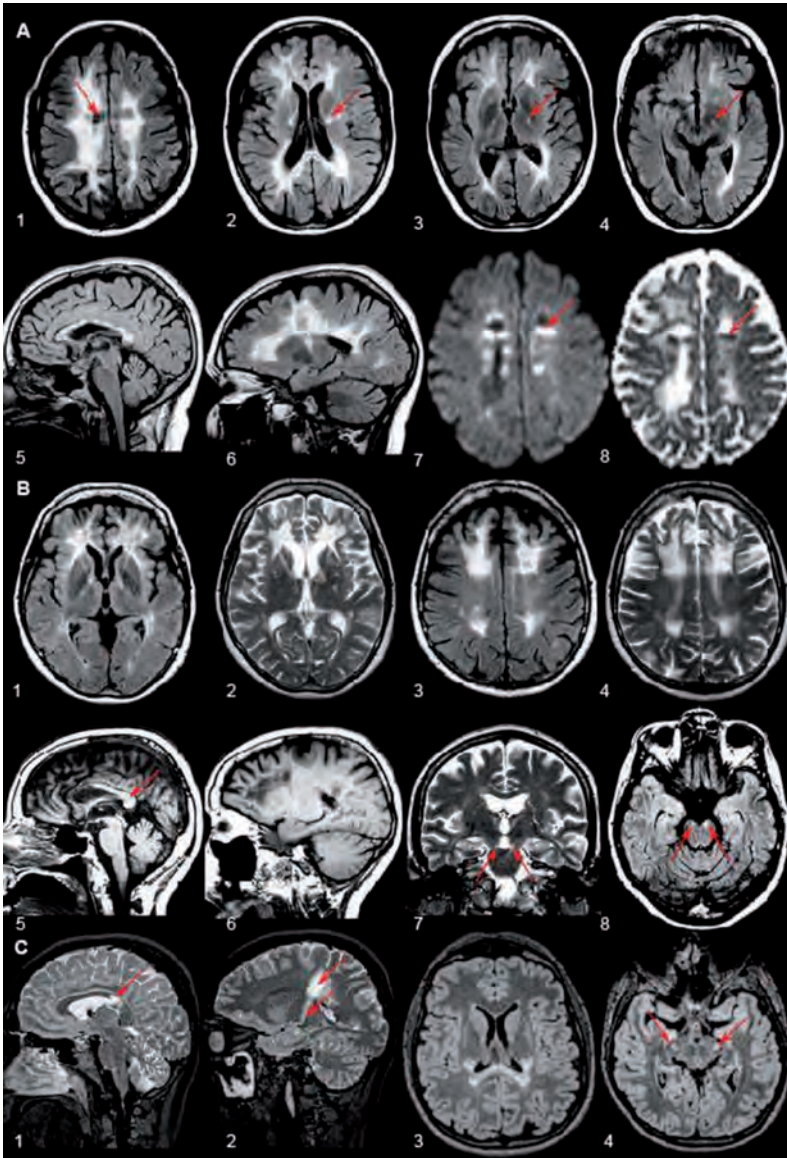
²<http://www.mutationtaster.org/>; Disease: disease-causing variant.

³http://sift.bii.a-star.edu.sg/www/SIFT_seq_submit2.html; SIFT probabilities < .05 are predicted to be deleterious.

⁴<http://genetics.bwh.harvard.edu/pph2/index.shtml>; Humvar pathogenicity scores ranges from 0 (benign) to 1.00 (probably damaging).

⁵<http://mmb.pcb.ub.es/PMut/>; pathogenicity scores ranges from 0 (neutral) to 1 (pathological).

⁶<http://snps-and-go.biocomp.unibo.it/snps-and-go/>; Neutral: Neutral Polymorphism, Disease: Disease related Polymorphism.

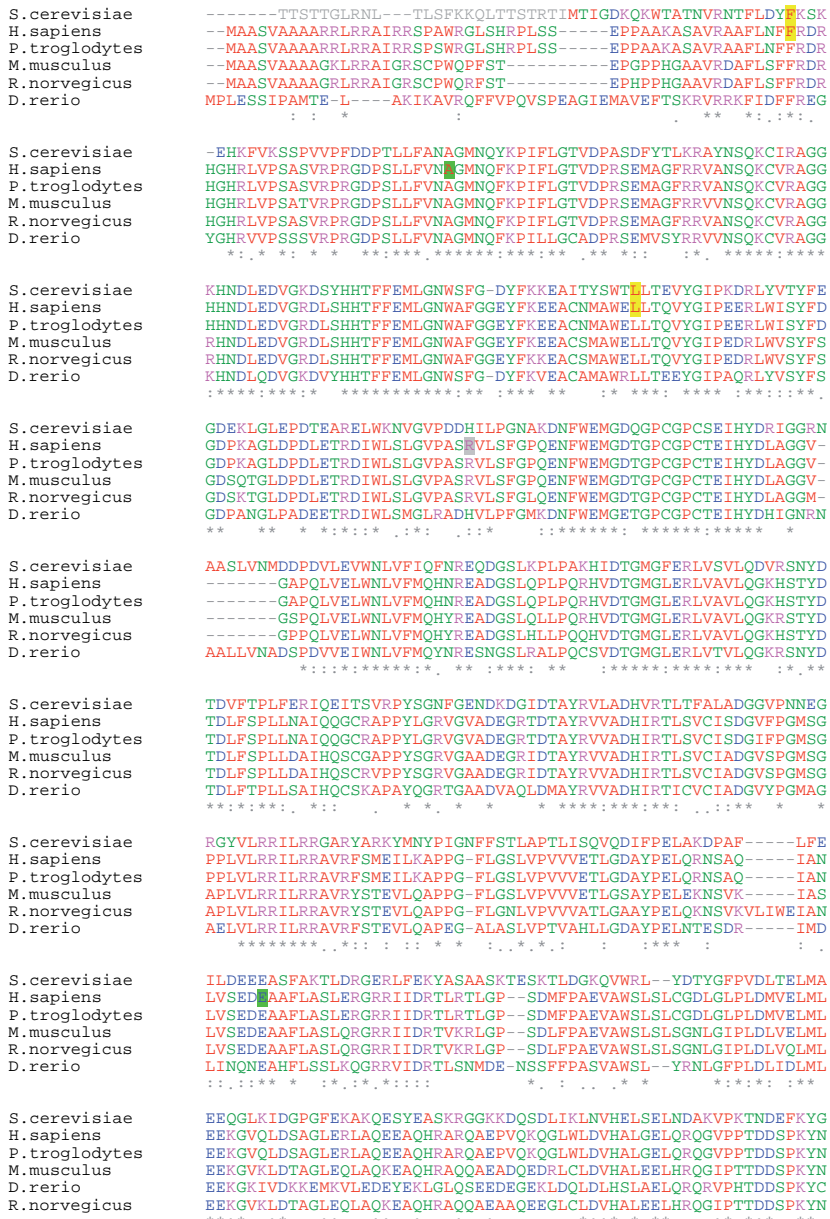


Supplemental Figure e-1. MRI in patients P4, P5 and P6

A. MRI in P4 at age 26. The axial FLAIR image shows areas of white matter rarefaction (arrow in image 1). The frontopontine tracts are affected (arrows in images 2-4). The corpus callosum contains multiple lesions (image 5). Note the tract involvement under the rarefied area (image 6). Multifocal areas of diffusion restriction are present (images 7 and 8).

B. MRI in P5 at age 42. The frontal white matter is most prominently affected (images 1 and 2) and partially rarefied (image 1). The middle section of the brain is spared (images 3, 4 and 6). The anterior corpus callosum is affected, the middle part is spared and a strip in the splenium is affected (arrow in image 5). The frontopontine tracts are affected (arrows in images 7 and 8).

C. MRI in P6 at age 25. The pyramidal tracts are affected from the motor cortex through the posterior limb of the internal capsule (arrows in image 2) into the brain stem (arrows in image 4). The lesions are connected through the corpus callosum (arrow in image 1 and image 3).



Supplemental Figure e-2. Protein sequence alignment of AARS2 orthologs obtained by Clustal-Omega

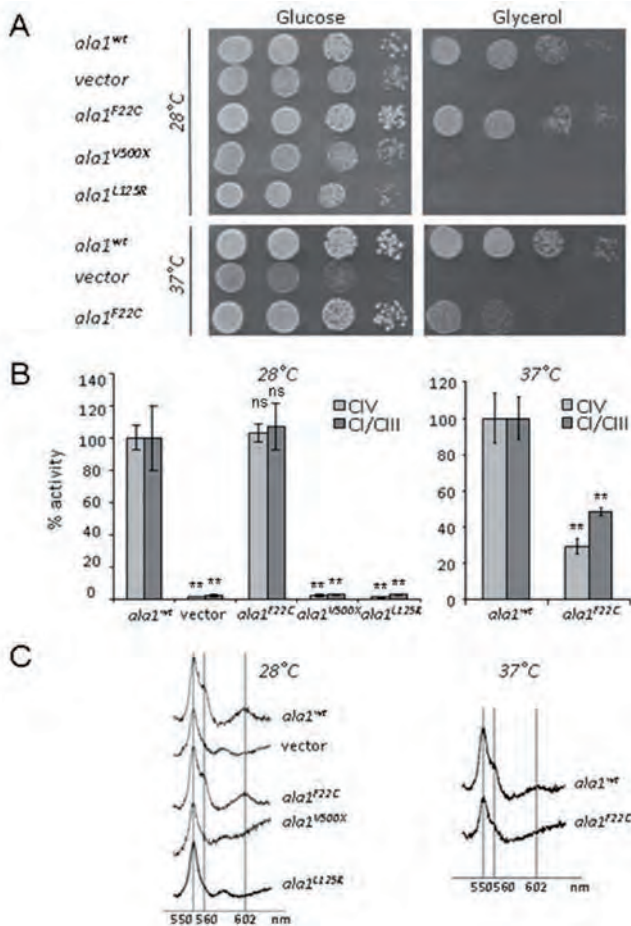
The amino-acids corresponding to AARS2 missense mutations identified in P1 or previously reported (F50C, this study, and L155R¹⁴) and studied in yeast are highlighted in yellow. The positions of other missense mutations affecting amino acid conserved in yeast are highlighted in green, whereas those not conserved in yeast (including the previously reported R592W¹⁴) are highlighted in gray.

```

S.cerevisiae      SAN-----VEGTILKLDHGTNFVDEITPEPKKYYGILLDKTCFYAEQGGQBYDITGK
H.sapiens        YSLRPSGSSYEFPTCEAQLVQLYTEDGTAVASVGGKQRCGLLLDRTNFYAEQGGQASDRGY
P.troglodytes    YSLRPSGSSYEFPTCEAQLVQLYTEDGTAVASVGGKQRCGLLLDRTNFYAEQGGQASDRGY
M.musculus       YTLHPNGDYEFGLCEARVLQLYSETGTAVASVGGKQRCGLLLDRTNFYAEQGGQASDRGY
R.norvegicus     YSLRHPNGDYEFGLCEAQLVQLYSETGTAVASVGGKQRCGLLLDRTNFYAEQGGQASDRGY
D.rierio         YSVGSDGQYVFEPCASVLALYCD-GALVSEVRQQQHCAVILLDQTSFYAEQGGQANDQGG
:               : : * * : : * : : * * * * * * * * * * * *
S.cerevisiae      IVIDDA--AEFNVENVQLYNGFVFPHTGSLEEKLSVGDKI IASFDELRRFPKNNHTGTH
H.sapiens        LVRAGQEDVLPVPAEQVCGGFILHEAVA-PECLRLGDQVQLHVDEAWRLGCMKHTATH
P.troglodytes    LVRAGQEDVLPVPAEQVCGGFILHEAVA-PECLRLGDQVQLHVDEAWRLGCMKHTATH
M.musculus       LVRAGQEDVLPVPAEQVCGGFILHEAMA-PERLQVGDVQLVYDKAWRMGCMVKHTATH
R.norvegicus     LVRAGQEDVLPVPAEQVCGGFILHEAMA-PECLQVGDVQLVYDKAWRMGCMVKHTATH
D.rierio         FTKDLQDVLFPVKVRLAGGYVHKVTA-AETLRTGDQVHLHVDEAWRLGCMINHTATH
:               : : * * : : * : : * * * * * * * * * * * *
S.cerevisiae      ILNFALKETLGNVDQKGSVLAPEKLRDFSHKKAHSVNEELKKVEDICNEQIKENLQVYF
H.sapiens        LLNWLARQTLGPGTTEQQGSHLNPEQLRLDVTQTPLTPEQLRAVENTVQEAQVGGDEAVYM
P.troglodytes    LLNWLARQTLGPGTTEQQGSHLNPEQLRLDVTQTPLTPEQLRAVENTVQEAQVGGDEAVYM
M.musculus       LLSWALRQTLGPTTTEQRGSHLNPERLRFVATQTLTTEQLRVTVESYVQEVVGGDKPVFM
R.norvegicus     LLNWLARQTLGPTTTEQRGSHLNPERLRFVATQTLTTEQLRVTVESYVQEAQVGGDKPVFM
D.rierio         LLNFALRELLGPIVSRQGSCHSANLRDFSVKGLTIVSELQVVEVLVLIIRQNADVHV
:               : : * * * * * * * * * * * * * * * * * * * * * *
S.cerevisiae      KEIPLDLAKSIDGVRVAFGETYDPVPRVSVGKPIEELLANPANEEWTKYSIEFCGGTHV
H.sapiens        EEVPLALTAQVPLRSL-DEVYPDPVPRVSVGVPVAHALD-PASQAALQTSVELCCGTHL
P.troglodytes    EEVPLALTAQVPLRSL-DEVYPDPVPRVSVGVPVAHALD-PASQAALQTSVELCCGTHL
M.musculus       EEVPLAHTARIPGLRSL-DEVYPDPVPRVSVGVPVAHALD-PASQAAMHTSVELCCGTHL
R.norvegicus     EEVPLAHTARIPGLRSL-DEVYPDPVPRVSVGVPVAQALA-PASQAALQTSVELCCGTHL
D.rierio         EEVPLSSAKQIAGLRTV-DELYPDPVPRVSVAVPVSDDLAA---SERAEQTSVELCCGTHL
:               : : * * * * * * * * * * * * * * * * * * * * * *
S.cerevisiae      NKTGDIKYFVILEESGIAGKIRRIVAVTGTAEFAEQRLAEQFADLDAADKL-PFSP-IK
H.sapiens        LRTGAVGDLVLIIGDRQLSKGTRLLAVTGEQAQQARELGSQAQEVKAATERLSGSRD
P.troglodytes    LRTGAVGDLVLIIGDRQLSKGTRLLAITGEQAQQARELGSQAQEVKAATERLSGSRD
M.musculus       LSTGAVGDLVLIIGERLVKGI TRLLAITGEQAQQAREVGGSLQEVAAERLSGSRD
R.norvegicus     LSTGAVGDLVLIIGDRLVKGI TRLLAITGEQAQQAREVGGSLQEVVAVSERLSGSRD
D.rierio         LRTGAIRDVAVVSRQMMKGVCRIVAFGTDDAKAREAGALQEELESLEARMGLSNTLS
:               : : * * * * * * * * * * * * * * * * * * * * * *
S.cerevisiae      E---KKLKELGVLGQLSISVITK---NELKQKFNKIEKAVKDEVKSRACKENKQTLDE
H.sapiens        VAEALRLSKDIGRLIEAVETAVMPQWRRELLATVKMLQRR---ANTAIRKLMQGAQAKK
P.troglodytes    VAEALRLSKDIGRLIEAVETAVMPQWRRELLATVKMLQRR---ANTAIRKLMQGAQAKK
M.musculus       LPEAHLRLSKDIGRLIEAVESAVIPQWRQELQTTLKMQLRR---ANTAIRKLEKQATEK
R.norvegicus     LLEAHLRLSKDIGRLIEFTESAVIPQWRQEQTTLKMQLRR---ANTAIRKLEKQATEK
D.rierio         IQEAKRLSKVGHILNAVDTIPMPQWRLELQTRKAKMLK---SNNSIRKLEIKAEALK
:               : : * * * * * * * * * * * * * * * * * * * * * *
S.cerevisiae      VKTFEFTNENAPYLKVFIDISPNAKAITEAINYMKSNDSVVKDKSIYLLAGNDPEGRVAHG
H.sapiens        TQELLERHSKGPLIVDTVSAESLSVLKVVVRQ---LCEQAPSTSVLLLSP-QPMGKVLCA
P.troglodytes    TQELLERHSKGPLIVDTVSAESLSVLKVVVRQ---LCEQAPSTSVLLLSP-QPMGKVLCA
M.musculus       SQELLKRHSEGPLIVDTVSAESLSVLKVVVRQ---LCKQAPSTSVLLLSP-QPTGSQLCA
R.norvegicus     SQELLKRHSEGPLIVDTVSAQSLSVLKVVVRQ---LCKQAPSTSVLLLSP-QPTGSQLCA
D.rierio         AKELLDKHSNKPVVVDLIQDTSISVLMKTVVQ---LSKSTPKSLVLMFLSHWESSGKLLCA
:               : : * * * * * * * * * * * * * * * * * * * * * *
S.cerevisiae      CYISNAALAKGIDGSALAKKVVSSIIIGKAGGKGNVFGMGDKPAAIKDAVDLDE---SLF
H.sapiens        CQVAQGM-PTFTAEEAWALAVCSHMGGKAWGSRVVAQGTSTTDL-EAAL---SIAQTYA
P.troglodytes    CQVAQGM-PTFTAEEAWALAVCSHMGGKAWGSRVVAQGTSTTDL-EAAL---SIAQTYA
M.musculus       CQVAQDAT-PTFTAEEAWALAVCSHMGGKAWGSRVVAQGTGHTADL-EAAL---GTARAYA
R.norvegicus     CQVAQCAT-PTFTAEEAWALAVCSHMGGKAWGSPVVAQGTGHTADL-EAAL---RTARAYA
D.rierio         CLVPGKST-GG-SAI EWALVCSRLGGNAEGAKDTAKGVGNAVKV-EDVAELIHWAEFEFA
:               : : * * * * * * * * * * * * * * * * * * * * * *
S.cerevisiae      KEKLSI-----
H.sapiens        LSQ-----
P.troglodytes    LSQ-----
M.musculus       LSQ-----
R.norvegicus     LNQL-----
D.rierio         HNKLRNVPRTD
:               : :

```

Supplemental Figure e-2. continued



Supplemental Figure e-3. OXPHOS growth and biochemical assays in yeast

A. Growth of the *ala1Δ* strain expressing the wild-type cytosolic isoform (*ala1*^{L-16X}) transformed with the *ala1*^{wt} allele, the empty vector, or the mutant alleles *ala1*^{F22C}, *ala1*^{V500X}, *ala1*^{L125R} on YP medium supplemented with 2% glucose or 2% glycerol. Cells were pre-grown on YP-glucose medium and plated after serial dilutions to obtain spots of 5x10⁴, 5x10³, 5x10² and 5x10¹ cells/spot. Plates were incubated at 28°C or 37° C.

B. Cytochrome c oxidase (CIV) activity and complex I-III activity of the *ala1*^{L-16X} strain transformed with the *ala1*^{wt} allele, the empty vector, and the mutant alleles *ala1*^{F22C}, *ala1*^{V500X}, *ala1*^{L125R}. Activities were normalized to the strain transformed with *ala1*^{wt}. Values are the mean of three independent experiments, each with an independent clone. Two-tail, unpaired t test was applied for statistical significance of comparison between the activities of the mutant strains and the activity of *ala1*^{wt} strain. ** p<0.01; ns: not significant.

C. Cytochrome spectra profiles of the *ala1*^{L-16X} strain transformed with the *ala1*^{wt} allele, the empty vector, and the mutant alleles *ala1*^{F22C}, *ala1*^{V500X}, *ala1*^{L125R}. The peaks at 550, 560 and 602 nm (vertical bars) correspond to cytochromes c, b and aa3 respectively. Cytochromes b is a component of complex III, aa3 of complex IV. The height of each peak relative to the baseline of each spectrum is an index of cytochrome content.

Chapter 7

Acute intermittent porphyria-related leukoencephalopathy

Sietske H. Kevelam, Rochus A. Neeleman, Quinten Waisfisz,
Edith C.H. Friesema, Janneke G. Langendonk, and Marjo S. van der Knaap

Accepted for publication.



ABSTRACT

Objective

To identify the genetic etiology of a distinct leukoencephalopathy with autosomal recessive inheritance in a single family.

Methods

We analyzed available magnetic resonance images (MRIs) and retrospectively reviewed clinical information and laboratory investigations. We performed whole-exome sequencing (WES) to find the causal gene variants.

Results

We identified 3 family members with a similar MRI pattern characterized by symmetrical signal abnormalities in the periventricular and deep cerebral white matter, thalami, and central part of the pons. Cerebellar atrophy was noted in advanced disease stages. Clinical features were childhood-onset slowly progressive spastic paraparesis, cerebellar ataxia, peripheral neuropathy and in 2 patients optic atrophy as well as vertical gaze and convergence palsies and nystagmus. WES revealed compound heterozygous missense variants in the *HMBS* gene, both associated with the autosomal dominant disorder acute intermittent porphyria (AIP). Sanger sequencing of 6 healthy siblings confirmed the bi-allelic location of the variants and segregation with the disease. Patients had a slight and moderate increase in urinary and plasma porphobilinogen and 5'-aminolevulinic acid respectively and a 50-66 % decrease in hydroxymethylbilane synthase enzyme activity compared to normal.

Conclusions

Bi-allelic *HMBS* variants have been reported before as cause of severe encephalopathy with early childhood fatality in AIP. Our cases demonstrate childhood onset, but milder and slower disease progression in middle-aged patients. With this, a novel phenotype can be added to the disease spectrum associated with bi-allelic *HMBS* variants: a leukoencephalopathy with early onset, slowly progressive neurological symptomatology and long life expectancy.

INTRODUCTION

Acute intermittent porphyria (AIP) is characterized by attacks of severe abdominal pain with nausea, vomiting and hypertension and can be accompanied by psychiatric symptoms including anxiety, psychosis, and hallucinations.^{1,2} Attacks, which are caused by liver derived accumulation of 5'-aminolevulinic acid (ALA) and porphobilinogen (PBG), can be precipitated by drugs, alcohol, fasting, menarche, and stress.^{1,2} Without treatment acute porphyria attacks can progress to life-threatening hyponatremia, paralysis, epilepsy, coma, and death.^{1,2}

AIP is an autosomal dominant disorder caused by variants in the *HMBS* gene, encoding hydroxymethylbilane synthase (HMBS, EC 2.5.1.61), also named porphobilinogen deaminase (PBGD), the third enzyme in the heme biosynthesis pathway.³ The carrier frequency in European countries is estimated at one in 75.000 people, but less than 10% of the carriers actually develop acute porphyric attacks.^{1,4}

Reports of bi-allelic AIP are extremely rare and only 5 patients have been published so far.⁵⁻¹⁰ We report 3 siblings from a single family with a childhood-onset slowly progressive neurological disorder of unknown origin and a distinct leukoencephalopathy on MRI. Whole-exome sequencing (WES) revealed bi-allelic *HMBS* variants segregating with the disease. We describe the phenotype, biochemical tests results, and genotype of all tested siblings, and we compare the patients' phenotype with the published cases of bi-allelic *HMBS* variants.

PATIENTS AND METHODS

Patients

Three siblings from 1 family shared a distinct pattern of MRI abnormalities. S.H.K. and M.S.v.d.K. evaluated the MRIs as previously described.¹¹ We reviewed the clinical information and laboratory investigations retrospectively. With 6 healthy siblings and non-consanguineous parents, who never had signs or symptoms of neurological dysfunction, we considered the pedigree suggestive of an autosomal recessive disorder. We included all 6 healthy siblings for genetic segregation analysis, and 2 of them for further biochemical studies upon identification of the candidate gene. The parents were deceased and no DNA was available.

Standard protocols, registration and patient consents

The ethical standards committee approved our gene identification studies on patients with unclassified leukoencephalopathies at the VU University Medical Center in Amsterdam, the Netherlands. We received written consent from all individuals participating in this study.

Whole-exome sequencing

We performed WES in 2 affected (patient 1 and 2) and 1 unaffected sibling. We extracted genomic DNA by standard methods. We enriched exonic targets with SeqCap EZ Human Exome Library v3.0 kit (Nimblegen). We performed sequencing with 100 bp paired-end reads on a HiSeq2000 (Illumina). For data analysis we used an in-house pipeline previously described.¹² We performed variant filtering under the hypothesis of an autosomal recessive inheritance pattern assuming that the variant had a minor allele frequency of < 1% in the dbSNP137 (<http://www.ncbi.nlm.nih.gov/projects/SNP>), NHLBI Exome Sequencing Project (ESP6400 release) (<http://evs.gs.washington.edu/EVS/>), 1000genomes project (release February 2012), and GoNL database¹³ and was not present in-house control exomes. We excluded synonymous variants that were not located adjacent to the consensus splice site.

Segregation and validation of candidate variants

We performed Sanger sequencing in the 3 patients for confirmation of the 2 variants in *HMBS* (NM_000190.3) and in the 6 healthy siblings for segregation analysis. Primer sequences are available on request.

Measurement of ALA and PBG in urine and plasma

We collected urine and plasma samples for patients 1 and 2, and 2 healthy siblings following standard protocols during outpatient clinic visits in the National Porphyria Center in the Erasmus MC, Rotterdam, the Netherlands, after the outcome of the WES analysis. The samples were analyzed within 24 hours or stored at -80° Celsius for later examination. Methods for measuring ALA and PBG in urine and plasma have been published.¹⁴ In short, urinary ALA and PBG are separated by ion-exchange chromatography. At pH 6–6.5, ALA is a cation and PBG an anion. The urine is passed through an anion-exchanger on top of a cation exchanger, after which interfering substances are removed by washing the columns. ALA and PBG are then eluted separately. Reaction with Ehrlich's reagent gives a red condensation product that can be measured spectrophotometrically. In plasma, ALA is converted enzymatically to PBG by added ALA-dehydratase. PBG, present in plasma or formed from ALA by the addition of ALA-dehydratase, is subsequently converted to uroporphyrinogen I by the

addition of HMBS. Both ALA-dehydratase and HMBS are present in control red blood cell lysate, from which they are derived making use of their difference in sensitivity to heat denaturation. Following oxidation of the uroporphyrinogen to uroporphyrin using ultraviolet light, the latter is measured by fluorometric assay.

Hydroxymethylbilane synthase in erythrocytes

HMBS catalyzes the formation of hydroxymethylbilane from 4 molecules of PBG. The tetrapyrroles are converted to uroporphyrinogen III by uroporphyrinogen cosynthase (an essential step in the synthesis of heme) or nonenzymatically cyclized to uroporphyrinogen I. We incubated erythrocyte lysate with PBG. We measured the formed porphyrins by specific fluorescence detection. We used a coproporphyrin standard as a reference.

Literature search

We performed a literature search to identify published cases with compound bi-allelic AIP. A PubMed search in November 2015 with the terms, “Porphyrias”[Mesh] AND compound heterozygous (33 hits), “Porphyrias”[Mesh] AND ‘homozygous’ (169 hits), “Porphyrias”[Mesh] AND ‘encephalopathy’ (32 hits) resulted in 234 articles. Available publications with descriptions of homozygous or compound heterozygous AIP patients were included. All papers mentioned in the OMIM database for the *HMBS* gene were checked for other cases with bi-allelic variants. Furthermore, the reference lists of the selected articles and review articles on acute porphyria, that resulted from our literature search were scanned with this objective. Case reports without definitive diagnosis, as defined by decreased enzyme activity or gene mutation, were excluded from the case series.

RESULTS

Patients, laboratory findings and neurophysiological investigations

Patient 1, the first child, was born after an uneventful pregnancy and delivery. He had a congenital deafness, for which he received a unilateral cochlear implant at age 53 years. Initial development was unremarkable. In his teenage years he developed a slowly progressive spastic paraparesis. At latest follow-up, 58 years old, he had a normal cognition, and his vision was normal with glasses. His neurological examination showed a spastic paraparesis and a distal peripheral neuropathy of his legs. He was able to walk using a walking aid. He was independent regarding activities of daily living (ADL).

Patient 2, the second child, was born after an uneventful pregnancy and delivery. Her

gross motor development was mildly delayed; she achieved walking at 2 years. During childhood she experienced a progressive spastic paraparesis, which caused loss of unsupported walking and wheelchair dependency at the age of 4 years. She had a gradually progressive loss of vision due to optic atrophy. In the course of decades she experienced a slowly progressive neurological deterioration with also mild cognitive impairment. The latest neurological examination at age 63 years revealed clinical evidence of a peripheral neuropathy in arms and legs. She had a severe cerebellar ataxia and apraxia. Ophthalmological examination demonstrated an almost complete loss of vision, a pendular nystagmus and vertical gaze and convergence palsies. She was completely ADL dependent and lived in a nursing home. She could participate in simple conversations.

Patient 3, the third child, was also born after an uneventful pregnancy and delivery. He achieved walking at 18 months, but was never able to run. From 4 years of age, he experienced progressive vision loss due to optic atrophy and from 12 years of age he developed progressive gait problems leading to wheelchair dependency at 35 years. He developed mild cognitive impairment. At latest follow-up, at 57 years, he had a spastic paraparesis, a distal peripheral neuropathy of legs and arms, cerebellar ataxia and also apraxia. He had an almost complete loss of vision, pendular nystagmus and vertical gaze palsy. He was partially ADL dependent and could participate in simple conversations.

After identification of the *HMBS* gene variants, the 3 patients and the 6 healthy siblings were questioned for AIP-related symptoms; none were reported.

Preceding WES analysis routine hematologic and biochemistry tests and extensive metabolic testing were performed in urine, blood, and cerebrospinal fluid (CSF) and were unrevealing. Patient 2 and 3 had once a mildly elevated CSF lactate. Mitochondrial DNA screening in blood and muscle revealed no pathogenic point variants or deletions. Measurement of oxidative phosphorylation enzyme activities in fresh muscle biopsy was normal. Nerve conduction studies of patient 2 (at age 55 years) and patient 3 (at age 38 years) showed normal sensory and motor conduction velocities. A reduced amplitude of compound muscle action potentials was seen in patient 2, suggestive of axonal neuropathy. Somatosensory-evoked potentials of the tibial and median nerve showed no cortical response in patient 3. Two successive sural nerve biopsies performed in patients 1 and 3 revealed progressive loss of both thick and thin nerve fibers.

MRI abnormalities

For patient 1, one MRI was available, performed at age 43 years; patients 2 and 3 had two available MRIs, obtained at age 51 and 59 years for patient 2, and at 36 and 57 years for patient 3. The most recent MRIs are shown in Figure 1. All 3 patients had extensive,

confluent, symmetrical signal abnormalities in the periventricular and deep cerebral white matter with relative sparing of the U-fibers (Figure 1, A-L and O). In patients 2 and 3 the abnormalities were most extensive. The thalami were affected, but the basal nuclei, internal capsule and corpus callosum were spared (Figure 1, B, F and J). All patients had mild widening of the lateral ventricles and subarachnoid spaces. Patients 2 and 3 had signal abnormalities in the central part of the pons. In both patients 2 and 3, the cerebellar atrophy was more severe on recent MRIs (Figure 1, E, I, N, P) than on earlier MRIs (not shown). At most mild cerebellar atrophy was observed in patient 1 (Figure 1, M). The white matter abnormalities progressed very slowly over time.

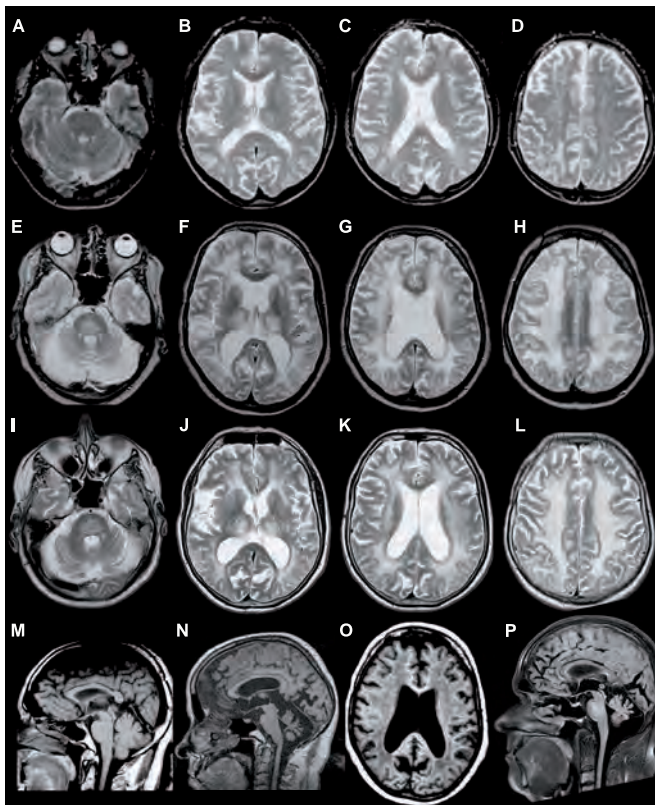


Figure 1. MRI characteristics.

Axial T2-weighted images of patient 1 (A-D, 43 years), patient 2 (E-H, 59 years), and patient 3 (I-L, 57 years); sagittal T1-weighted images of patient 1 (M), sagittal and axial T1-weighted images of patient 2 (N, O); sagittal fluid-attenuated inversion recovery (FLAIR) image of patient 3 (P). Confluent, symmetrical T2 signal abnormalities are seen in the pons (A and E) and periventricular and deep cerebral white matter (B-D, F-H and J-L). The thalami are symmetrically affected (B, F and J). The axial T1-weighted image of patient 2 (O) shows that the corpus callosum and U-fibers are relatively spared. Cerebellar atrophy is seen in patients 2 and 3 (N and P), but is at most mild in patient 1 (M). Diffuse mild cerebral atrophy, with widening of the ventricles and subarachnoid spaces is present in all cases (B-D, F-H and J-L).

Genetic analysis

After filtering of the variants obtained by WES a single candidate gene remained. The 2 patients carried two heterozygous missense variants in *HMBS*: c.500G>A (p.(Arg167Gln)), c.674G>A (p.(Arg225Gln)), located in exon 10 and exon 12 respectively. Both variants are known pathogenic variants associated with AIP.^{15,16} Segregation analysis of the variants confirmed the bi-allelic location of the variants and the presence of both variants in all 3 patients, while the 6 healthy siblings were heterozygous for one of the variants or carried 2 wild-type alleles. No other candidate genes were identified with WES using the filtering steps described.

Biochemical analysis

Detailed results of the biochemical studies are outlined in Table 1. Patients had moderately increased values of ALA and PBG in plasma and urine, and *HMBS* enzyme activity was decreased within the reference range for heterozygous carriers of AIP. The healthy siblings, both carriers of the c.674G>A mutation, had normal urine ALA and PBG values, near-normal plasma ALA and PBG values and *HMBS* enzyme activity.

Table 1. Biochemical analysis

	Patient 1	Patient 2	Sib 1	Sib 2
Urine				
ALA/creatinine umol/mmol (N < 4.6)	2.4	2.6	2.5	2.3
PBG/creatinine umol/mmol (N < 1.3)	3.2	3.6	0.7	0.7
Plasma				
ALA nmol/l (N < 74)	72	158	98	77
PBG nmol/L (N < 12)	293	176	22	4
<i>HMBS</i> enzyme activity in % of normal mean in erythrocytes	55	67	105	83
<i>HMBS</i> variants	c.500G>A c.674G>A	c.500G>A c.674G>A	c.674G>A	c.674G>A

Abbreviations: ALA = 5'-aminolevulinic acid; PBG = porphobilinogen; N = normal reference range; *HMBS* = hydroxymethylbilane synthase

Literature search bi-allelic *HMBS* variants

Five patients with 2 pathogenic bi-allelic *HMBS* gene variants have been reported previously. All cases, including our patients, are summarized in Table 2.^{5-10,17} A patient published in 1977 by Gregor *et al.*, who presented with a severe neurological disease and increased porphyrin precursors in urine presumably had bi-allelic *HMBS* variants, but no genotype was described and this patient was not included.¹⁸ Three of the 5 proven bi-allelic *HMBS* patients presented with an infantile-onset chronic, progressive neurological disease,^{5,9,10} two others had an onset during early childhood.⁸ They all

showed signs of psychomotor retardation and at least 4 died at an early age.^{5,8,9} All had an increased excretion of urinary ALA and PBG, up to a 100 fold increase relative to upper limits of the normal range, which was reflected in abnormally colored urine in all cases except for the patients reported by Llewellyn *et al.*⁸ All had a severely decreased erythrocyte HMBS enzyme activity (1%-17% of normal).⁵⁻¹⁰ Despite these findings, symptoms associated with acute porphyric attacks were not reported in any of the patients. Neurological features included a peripheral neuropathy (mixed axonal and demyelinating), cerebellar ataxia, reduced tendon reflexes and positive bilateral Babinski signs.^{5-9,17} MRI findings of 1 patient showed extensive signal abnormalities of the periventricular and deep white matter, sparing the thalami and pons.⁹

DISCUSSION

To our surprise, WES revealed bi-allelic variants in *HMBS*, known to be associated with autosomal dominant AIP, in 3 siblings with a leukoencephalopathy. All patients had a similar MRI pattern characterized by extensive symmetrical signal abnormalities in the periventricular and deep white matter, the thalami and the central part of the pons, with slow progression and late cerebellar atrophy. The clinical phenotype of the siblings, presently between 58 and 64 years old, was characterized by a childhood-onset very slowly progressive spastic paraparesis, cerebellar ataxia, peripheral neuropathy, and in 2 patients near-total vision loss due to optic atrophy. In the literature 5 other patients with bi-allelic *HMBS* variants have been reported. These patients also had neurological signs, but the onset of the disease was considerably earlier, the course more severe and the outcome less favorable (see table 2). One patient was reported to have white matter abnormalities, but without further details; the specific MRI pattern observed in our patients was not reported.⁹ Strikingly, similar to the 5 previously reported children with bi-allelic *HMBS* variants, our 3 affected siblings did not experience acute porphyric attacks.

Both variants, found in our patients, have been reported in heterozygous patients with a deleterious effect on enzyme function and occurrence of acute porphyric attacks. *In vitro* studies in *Escherichia coli* showed that the c.500G>A variant in homozygosity is associated with a residual HMBS enzyme activity of less than 2%,⁹ and X-ray crystallization studies indicated disturbances of pyrrole polymerization.¹⁹ The c.674G>A variant was previously reported in 3 family members from Sweden, one of whom was symptomatic. This woman had intermittent periods of abdominal pain and pain in shoulders and limbs. Urinary ALA and PBG ranged from normal to mildly increased.¹⁶ The authors argue

that this variant would lead to severe disruption of the enzyme structure and activity due to its importance for the conformation of the enzyme.¹⁶ In light of this information we found the biochemical results in our patients remarkable. Both urinary and plasma ALA and PBG levels were slightly to moderately increased with an 55-67% erythrocyte HMBS enzyme activity of normal, values similar to heterozygous carriers of *HMBS* gene variants outside episodes of AIP.

Previously reported patients with bi-allelic *HMBS* variants had HMBS enzyme activity levels of 1-17% of normal, with an excessive excretion of porphyrin precursors.⁵⁻¹⁰ This would implicate that our family has a new disease phenotype, caused by bi-allelic *HMBS* variants, with milder neurological features than the other bi-allelic cases and biochemical results in the range of heterozygous carriers. The latter would indicate that either the reduced enzyme activity with elevated ALA and PBG levels does not cause chronic leukoencephalopathy in our patients or that the enzyme activity in erythrocytes is not comparable with brain activity.

During attacks, heterozygous carriers of *HMBS* variants frequently experience neurological manifestations, most commonly motor neuropathy, but seizures, pyramidal signs, cerebellar dysfunction, transient blindness, and decreased consciousness have also been reported.^{4,20} Clinical presentation can mimic the Guillain-Barré syndrome.²¹ Chronic axonal neuropathy is seen both in heterozygous carriers of *HMBS* with active AIP and in individuals with latent AIP.^{22,23}

Several hypotheses have been proposed to explain the acute and chronic neurological dysfunction in AIP.²⁴ First, it has been suggested that high levels of ALA are directly neurotoxic because of the structural similarity of ALA with gamma-aminobutyric acid (GABA), a potent inhibitor of neuronal synaptic activity. The neurotoxicity of ALA has been hypothesized to be due to direct interaction with GABA-receptors or by inhibiting glutamate uptake.^{25,26} However, mice partially deficient for HMBS (25-30% rest activity) develop a chronic, progressive motor neuropathy in the presence of normal or only slightly elevated plasma and urinary levels of ALA, and no acute attacks.²⁷ This suggests that at least for the chronic neurological symptoms alternative pathomechanisms would play a role.²⁷ Another hypothesis concerns the effect of a long-term relative shortage of heme in neurons. Heme is an important molecule involved in a variety of biological processes such as oxygen, electron transport and cytochrome p450 system. If patients with AIP have a relative chronic heme deficiency because of the disruption in the heme biosynthesis pathway, this might disrupt axonal transport leading to axonal degeneration.²⁷ This explanation would be in line with the evidence that acute porphyric attacks can be precipitated by drugs increasing Cyp450, in this way depleting the hepatic heme pool, as heme is a substrate for Cyp450. Via a negative feedback loop

Table 2. Overview patients with bi-allelic HMBS variants

	Villeneuve et al., 1964	Llewellyn et al., 1992	Llewellyn et al., 1992	Solis et al., 2004	Hessels et al., 2004	This report (patient 1)	This report (patient 2)	This report (patient 3)
Ethnicity	Caucasian	British	British	Spanish	Turkish	Caucasian	Caucasian	Caucasian
Gender	female	female	male	male	male	male	female	male
HMBS variants (c.DNA)	c.500G>A c.518G>A	c.499C>T c.500G>A	c.499C>T c.500G>A	c.499C>T c.499C>T	c.242T>C c.242T>C	c.500G>A c.674G>A	c.500G>A c.674G>A	c.500G>A c.674G>A
Age of onset	8 months	18 months	18 months-18 years	3 months	birth	during teens	4 years	4 years
Age last follow-up	8 years†	8 years†	10 years	3 years and 3 months†	7 years	58 years	63 years	57 years
Neurological signs	spasticity with contractures of arms and legs	ataxia, dysarthria, nystagmus	spasticity, ataxia, dysarthria, peripheral neuropathy (at age 8 years)	decreased muscle tone and reflexes, Babinski signs, peripheral neuropathy	developmental delay	spastic paraparesis legs and symmetrical neuropathy	spastic paraparesis legs and symmetrical axonal neuropathy	spastic paraparesis legs and symmetrical axonal neuropathy
Ophthalmological signs	n.a.	bilateral cataract; optic nerve atrophy	normal	bilateral cataract	n.a.	normal vision with classes	optic atrophy with vision loss (2/60 OD; 1/60 OS), fine peripheral cortical cataract, nystagmus	optic atrophy with vision loss (3/300), nystagmus
Acute porphyric attacks	no	no	no	no	no	no	no	No
Course and outcome, age of death	progressive, death due to seizure (8 years)	progressive, death due to chronic illness (8 years)	progressive, severe debilitated during sleep at 3 years	progressive, sudden death during sleep at 3 years	stable, attended school for mentally handicapped children	slowly progressive, walking with walker and ADL independent at age 58 years	slowly progressive, wheelchair at age 4 years; ADL dependent at age 63 years	slowly progressive, wheelchair at age 35 years. ADL dependent at age 57 years.
MRI WM abnormalities	n.a.	n.a.	n.a.	yes	n.a.	yes	yes	yes
Urine ALA levels	11-68 fold	n.a.	n.a.	14 fold	10 fold	normal	normal	normal
Urine PBG levels	9-45 fold	54 fold	3-11 fold	33 fold	128 fold	4 fold	2 fold	n.a.
HMBS enzyme activity (% of normal)	n.a.	14%	17%	1%	2-4%	55%	67%	n.a.

Abbreviations: ALA = 5'-aminolevulinic acid; PBG = porphobilinogen; HMBS = hydroxymethylbilane synthase; n.a. = not available; AIP = acute intermittent porphyria; ADL = daily life quality; OD, = oculus dextrus; OS, = oculus sinister; WM = white matter; y = years; † = deceased

restoration of the hepatic heme pool occurs by increasing 5' aminovulinate synthase enzyme production. With a decreased capacity to convert PBG to hydroxymethylbilane in patients with HMBS enzyme deficiency, accumulation of porphyrin precursors ALA and PBG occurs.^{1,2,4}

In patient 3, however, the normal oxidative phosphorylation enzyme activities in muscle provide evidence against a chronic heme deficiency, as these enzymes are heme dependent. Also, heme deficiency cannot explain the complete resolution of acute and neurological symptoms in heterozygous AIP patients after liver transplantation, a curative treatment performed in very severe cases.²⁸ Although the exact pathomechanism remains unsolved, the presented family adds new insight into the complex pathophysiology of acute porphyrias. Our family suggests that pain and neuropathy during attacks have a different pathomechanism than the progressive spastic paraparesis and leukoencephalopathy in AIP patients with bi-allelic variants.

As illustrated by this study, the unbiased approach of WES analysis may lead to unexpected and insightful results. In the case of our patients, the genetic findings also have direct implications for the 'healthy' siblings who are heterozygous carriers; they have an approximately 10% lifetime risk for AIP attacks, comparable to other heterozygous carriers. With this knowledge, measures can be taken to limit the risk of the potential life-threatening porphyric attacks. In addition, long-term complications of AIP like hypertension, chronic kidney disease, and hepatocellular carcinoma should be monitored in these patients and the family members who are carriers.²⁹ Due to the increasing use of next-generation sequencing studies in patients with an unexplained neurological disorder we expect that more patients with bi-allelic *HMBS* variants will be identified.

REFERENCES

1. Sassa S. Gene-environmental interactions: Lessons from porphyria. *Environ Health Prev Med* 2003;7:254-263.
2. Pischik E and Kauppinen R. An update of clinical management of acute intermittent porphyria. *Appl Clin Genet* 2015;8:201-14.
3. Grandchamp B, Picat C, Mignotte V, et al. Tissue-specific splicing mutation in acute intermittent porphyria. *Proc Natl Acad Sci U S A* 1989;86:661-664.
4. Puy H, Gouya L, Deybach JC. Porphyrias. *Lancet* 2010;375:924-937.
5. Villeneuve de V, Wadman S K, Heuvel van de JM. Een kind met een bijzondere vorm van porfyrie. *Maandschrift voor de kindergeneeskunde* 1964;731-742.
6. Picat C, Delfau MH, de Rooij FW, et al. Identification of the mutations in the parents of a patient with a putative compound heterozygosity for acute intermittent porphyria. *J Inherit Metab Dis* 1990;13:684-686.
7. Beukeveld GJ, Wolthers BG, Nordmann Y, Deybach JC, Grandchamp B, Wadman SK. A retrospective study of a patient with homozygous form of acute intermittent porphyria. *J Inherit Metab Dis* 1990;13:673-683.
8. Llewellyn DH, Smyth SJ, Elder GH, Hutchesson AC, Rattenbury JM, Smith MF. Homozygous acute intermittent porphyria: compound heterozygosity for adjacent base transitions in the same codon of the porphobilinogen deaminase gene. *Hum Genet* 1992;89:97-98.
9. Solis C, Martinez-Bermejo A, Naidich TP, et al. Acute intermittent porphyria: studies of the severe homozygous dominant disease provides insights into the neurologic attacks in acute porphyrias. *Arch Neurol* 2004;61:1764-1770.
10. Hessels J, Voortman G, van der Wagen A, van der Elzen C, Scheffer H, Zuijderhoudt FM. Homozygous acute intermittent porphyria in a 7-year-old boy with massive excretions of porphyrins and porphyrin precursors. *J Inherit Metab Dis* 2004;27:19-27.
11. van der Knaap MS, Breiter SN, Naidu S, Hart AA, Valk J. Defining and categorizing leukoencephalopathies of unknown origin: MR imaging approach. *Radiology* 1999;213:121-133.
12. Wolf NI, Salomons GS, Rodenburg RJ, et al. Mutations in RARS cause hypomyelination. *Ann Neurol* 2014;76:134-139.
13. The genome of the Netherlands Consortium. Whole-genome sequence variation, population structure and demographic history of the Dutch population. *Nat Genet* 2014;46:818-825.
14. De Rooij FFW, Edixhoven A, and Wilson JHP. Porphyria: a diagnostic approach. In: *Porphyria Handbook*. USA: Elsevier Science; 2003. p. 211-245.
15. Delfau MH, Picat C, de Rooij FW, et al. Two different point G to A mutations in exon 10 of the porphobilinogen deaminase gene are responsible for acute intermittent porphyria. *J Clin Invest* 1990;86:1511-1516.
16. Floderus Y, Shoolingin-Jordan PM, Harper P. Acute intermittent porphyria in Sweden. Molecular, functional and clinical consequences of some new mutations found in the porphobilinogen deaminase gene. *Clin Genet* 2002;62:288-297.
17. Sheppard L and Dorman T. Anesthesia in a child with homozygous porphobilinogen deaminase deficiency: a severe form of acute intermittent porphyria. *Paediatr Anaesth* 2005;15:426-428.
18. Gregor A, Kostrzewska E, Prokurat H, Pucek Z, Torbicka E. Increased protoporphyrin in erythrocytes in a child with acute intermittent porphyria. *Arch Dis Child* 1977;52:947-950.
19. Gill R, Kolstoe SE, Mohammed F, et al. Structure of human porphobilinogen deaminase at 2.8 Å: the molecular basis of acute intermittent porphyria. *Biochem J* 2009;420:17-25.
20. Kuo HC, Huang CC, Chu CC, et al. Neurological complications of acute intermittent porphyria. *Eur Neurol* 2011;66:247-252.
21. Schutte CM, Van der Meyden CH, Van NL, et al. Severe porphyric neuropathy - importance of screening for porphyria in Guillain-Barre syndrome. *S Afr Med J* 2015; 20;106:44-47.
22. Wikberg A, Andersson C, Lithner F. Signs of neuropathy in the lower legs and feet of patients with acute intermittent porphyria. *J Intern Med* 2000;248:27-32.
23. Wu CL, Ro LS, Jung SM, et al. Clinical presentation and electrophysiological findings of porphyric neuropathies: a follow-up study. *Muscle Nerve* 2015;51:363-369.
24. Straka JG, Rank JM, Bloomer JR. Porphyria and porphyrin metabolism. *Annu Rev Med* 1990;41:457-69.:457-469.

25. Brennan MJ and Cantrill RC. Delta-aminolaevulinic acid is a potent agonist for GABA autoreceptors. *Nature* 1979;280:514-515.
26. Brennan MJ, Cantrill RC, Kramer S. Effect of delta-aminolaevulinic acid on GABA receptor binding in synaptic plasma membranes. *Int J Biochem* 1980;12:833-835.
27. Lindberg RL, Martini R, Baumgartner M, et al. Motor neuropathy in porphobilinogen deaminase-deficient mice imitates the peripheral neuropathy of human acute porphyria. *J Clin Invest* 1999;103:1127-1134.
28. Singal AK, Parker C, Bowden C, Thapar M, Liu L, McGuire BM. Liver transplantation in the management of porphyria. *Hepatology* 2014;60:1082-1089.
29. Stewart MF. Review of hepatocellular cancer, hypertension and renal impairment as late complications of acute porphyria and recommendations for patient follow-up. *J Clin Pathol* 2012;65:976-980.

Chapter 8

Cathepsin A-related arteriopathy with strokes and leukoencephalopathy (CARASAL)

Marianna Bugiani,* Sietske H. Kevelam,* Hannah S. Bakels, Quinten Waisfisz,
Chantal Ceuterick-de Groote, Hans W.M. Niessen, Truus E. M. Abbink, **
Saskia A.M.J. Lesnik Oberstein,** and Marjo S. van der Knaap

* These authors share first authorship.

** These authors share senior authorship.

Accepted for publication.

ABSTRACT

Objective

To characterize the clinical and MRI features of 2 families with adult-onset dominant leukoencephalopathy and strokes and identify the underlying genetic cause.

Methods

We applied MRI pattern recognition, whole-exome sequencing (WES) and neuropathology.

Results

Based on brain imaging, 13 family members of 40 years or older from 2 families were diagnosed with the disease; in 11 family members of the same age, MRI was normal. In the affected family members, MRI showed a leukoencephalopathy that was disproportionately severe compared to the clinical disease. The clinical picture was dominated by ischemic and hemorrhagic strokes, slow and late cognitive deterioration and therapy-resistant hypertension. With WES we identified 1 variant shared by both families and segregating with the disease: c.973C>T in *CTSA*. Haplotype analysis revealed a shared 1145 kb interval encompassing the *CTSA* variant on chromosome 20q13.12, suggesting a common ancestor. Brain autopsy of 3 patients showed a leukoencephalopathy that was disproportionately extensive compared to the vascular abnormalities. *CTSA* encodes cathepsin A. Recessive *CTSA* mutations cause galactosialidosis. One of the numerous cathepsin A functions is to degrade endothelin-1. In the patients, striking endothelin-1 immunoreactivity was found in white matter astrocytes, correlating with increased numbers of pre-myelinating oligodendrocyte progenitors. This finding supports a role for endothelin-1 in the leukoencephalopathy through inhibition of oligodendrocyte progenitor maturation.

Conclusions

Cathepsin A-related arteriopathy with strokes and leukoencephalopathy (CARASAL) is a novel hereditary adult-onset cerebral small vessel disease. Interestingly, next to the cerebral vascular abnormalities, endothelin-1 may play a role in the pathogenesis of the extensive leukoencephalopathy.

INTRODUCTION

Vascular brain white matter abnormalities are common among adults, especially elderly. Most are attributed to vascular risk factors such as age, hypertension, hypercholesterolemia, diabetes mellitus, and smoking.^{1,2} Only few patients are diagnosed with hereditary small vessel disease (SVD), including cerebral autosomal dominant arteriopathy with subcortical infarcts and leukoencephalopathy (CADASIL),³ cerebral autosomal recessive arteriopathy with subcortical infarcts and leukoencephalopathy (CARASIL),^{4,5} heterozygous *HTRA1* mutations,⁶ defects in collagen IVA1 and IVA2,^{7,8} *TREX1*-related disorders,⁹ and hereditary cerebral amyloid angiopathy (CAA).¹⁰ For several familial SVDs the genetic cause remains unknown.¹¹⁻¹⁴ We report 2 families with adult-onset dominant leukoencephalopathy and ischemic and hemorrhagic strokes, characterized by distinct MRI and pathology findings. Whole-exome sequencing (WES) revealed 1 variant segregating with the disease.

PATIENTS AND METHODS

Patients

We identified a Caucasian Dutch family (F1) with adult-onset leukoencephalopathy by similar brain MRI findings. Family members younger than 40 years without MRI or with normal MRI were considered to have unknown status and were excluded; 22 family members of 40 years or older were included. Based on MRI, 11 were diagnosed with vascular leukoencephalopathy and 11 were unaffected. The pedigree indicated autosomal dominant inheritance (figure e-1). We identified 2 patients from another presumably unrelated, Caucasian Dutch family (F2). The index patient (F2-2) had similar MRI findings to F1 patients. Her father (F2-1) had cerebral white matter hypodensities on CT. No other F2 members were available.

Standard protocol approvals, registrations, and patient consents

We received approval of the ethical standards committee for gene identification studies on patients with unclassified leukoencephalopathies, and written informed consent from all included family members.

Whole-exome sequencing

In F1, we performed WES in 2 patients (F1-IV3 and F1-IV13) and 1 unaffected individual (F1-IV5) using SeqCap EZ Human Exome Library v2.0 kit (Nimblegen) (IV5) and SeqCap EZ Human Exome Library v3.0 kit (Nimblegen) (IV3 and IV13) on HiSeq2000 (Illumina, San

Diego, CA). Data analysis was performed as previously described.¹⁵ Detailed information on WES methods and filtering is provided in the e-appendix on the Neurology® Website at www.neurology.org and in Table 1.

Molecular screening of candidate genes and variants

We performed Sanger sequencing to confirm the 2 candidate variants in *CTSA* (NM_000308.2) and *TTPAL* (NM_024331.3) identified with WES and their segregation with the disease. All included individuals of F1 were tested for the presence of the c.973C>T *CTSA* variant and c.544G>A *TTPAL* variant. All exons and exon-intron boundaries of *CTSA* and *TTPAL* were sequenced in patient F2-2, followed by confirmation of the c.973C>T *CTSA* variant in her father.

Two-point linkage analyses

We performed two-point linkage analysis for the candidate variant using the easyLinkage software package running Superlink v1.6 in F1 (details in e-appendix).

Microsatellite marker analysis

We performed haplotype analysis for F1 and F2-2 using microsatellite markers spanning the region of interest on chromosome 20q13.12 (details in e-appendix).

Neuropathology, immunohistochemical analysis, electron microscopy and Western blots

We obtained brain tissue from patients F1-III1, F1-III2, and F1-IV8 at autopsy. Patient F1-IV8 also underwent body autopsy. For control studies, we obtained brain samples from 2 individuals (ages 27 and 57 years) without neurological complaints and confounding neuropathology, 2 individuals (78 and 79 years) with hypertension-related sporadic SVD, 1 individual with sporadic capillary CAA (75 years) and 1 individual with CADASIL (69 years).

We stained sections for Hematoxylin & Eosin, Periodic Acid Schiff (PAS), Kluver-PAS, Gomori trichrome and elastin van Gieson. For immunostaining, we used antibodies against cathepsin A (CathA), glial fibrillary acidic protein (GFAP), endothelin-1 (ET-1), amyloid beta, phosphorylated tau, oligodendrocyte transcription factor 2 (olig2) and platelet derived growth factor alpha receptor (PDGFR α).¹⁶ We quantified the degree of vessel wall changes by calculating the sclerotic index, which is the ratio of lumen diameter / external diameter, representing the degree of lumen narrowing. We performed electron microscopy (EM) on white matter from 3 patients. We counted the percentage of olig2/PDGFR α double-positive pre-myelinating oligodendrocyte progenitor cells (OPCs) in white matter of patients, controls with sporadic SVD and non-

neurological controls. We compared results with one-way Anova analysis of variance with subsequent Bonferroni multiple comparisons test. We performed Western blotting and SDS-PAGE of CathA and myelin basic protein (MBP) in white matter of patients, sporadic SVD controls and non-neurological controls. Details of immunohistochemistry, EM, Western blotting and SDS-PAGE are provided in the e-appendix.

Cathepsin A activity assessment

We measured carboxypeptidase, β -galactosidase and neuraminidase-1 activity in leukocytes in patients F1-IV3 and F1-IV13, using standard clinical testing.

Results

MRI findings

MRI abnormalities were similar for F1 and F2 patients (Figure 1; details in table e-1). The MRI pattern was characterized by signal changes in the frontoparietal periventricular and deep white matter that were patchy in younger patients (Figure 1, A-H), and became diffuse with increasing age (Figure 1, I-L). The temporal white matter was relatively spared and the temporal poles were not affected. Small multifocal areas of signal abnormality were seen in basal nuclei, thalami, internal and external capsules, brainstem (especially pons and around midbrain red nuclei), which were more confluent in older patients (Figure 1, A-C, E-G and I-K). Seven patients had infarcts in basal nuclei, brainstem, cerebellum or cerebral hemispheres (Figure 1, M and N). Some infarcts were acute with restricted diffusion (Figure 1O). Three patients had microbleeds and 1 a small hemorrhage (Figure 1P). Infarcts and microbleeds were more prominent in older patients. Medial temporal lobe atrophy score was 0 (normal) for all except the oldest patient F1-III2, who had a score of 1. All unaffected individuals had a normal brain MRI.

Clinical and laboratory findings

Detailed information is provided in table e-2. First symptoms, ranging from headaches, migraines and gait problems to strokes, were noted in the 3rd to 5th decade. Most patients had signs of vascular disease with hypertension requiring multiple drugs, strokes and transient ischemic attacks. Many complained of mild cognitive impairment. None of the unaffected family members had similar complaints. Only 2 had hypertension, which was controlled with a single drug. Smoking and alcohol consumption were similar between patients and unaffected individuals. Patients also had more non-neurological complaints than unaffected family members, including dry mouth with difficulty swallowing, dry eyes and muscle cramps. Physical examination of patients showed at most mild neurological abnormalities.

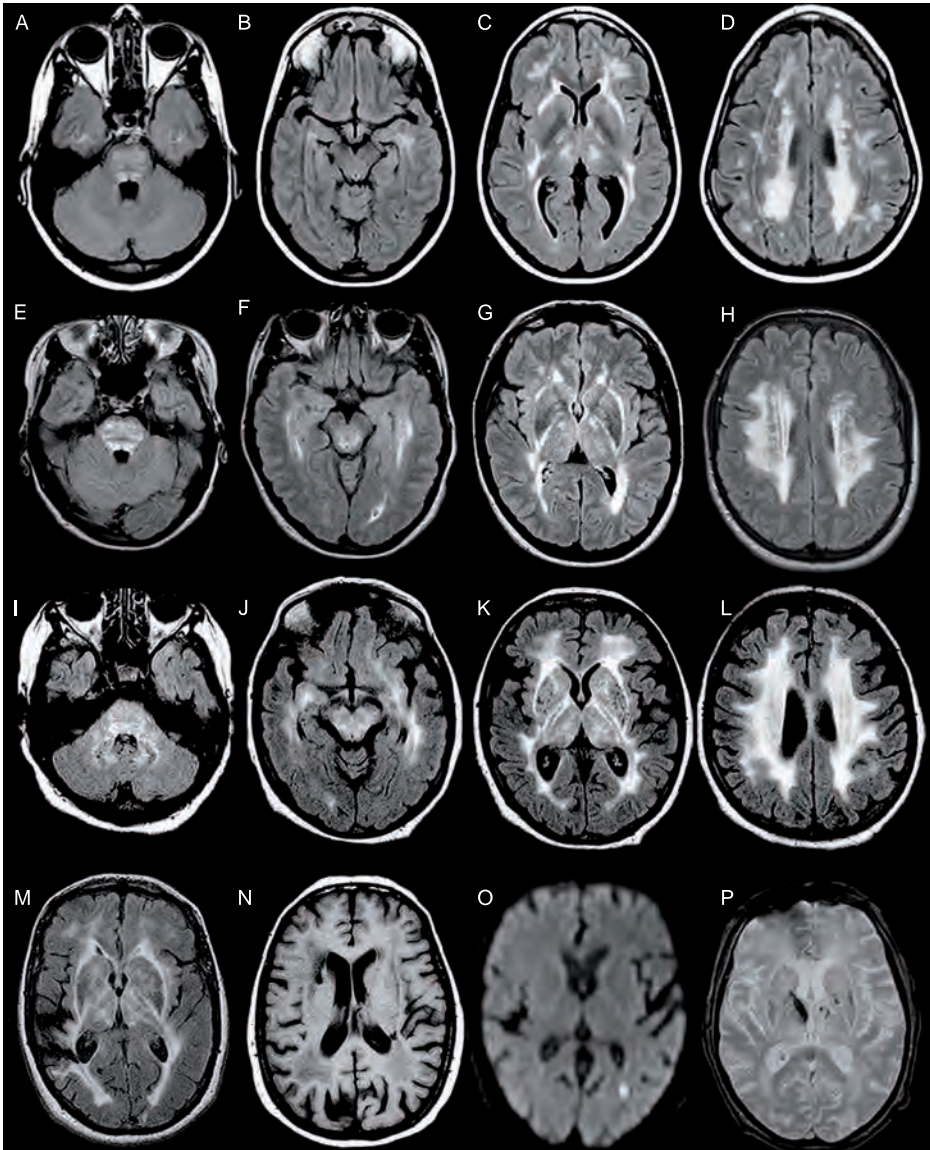


Figure 1. MRI findings.

Axial fluid-attenuated recovery (FLAIR) images of patient F2-2 (39 years) (A-D), patient F1-IV6 (46 years) (E-H), patient F1-III1 (67 years) (I-L) and patient F1-III5 (69 years) (M); T1-weighted image of patient F1-III4 (73 years) (N); diffusion weighted image (DWI) of patient F1-IV8 (53 years) (O); gradient echo image of patient F1-III2 (P). MR images show the multifocal to confluent white matter abnormalities located predominantly in the frontoparietal deep and periventricular white matter (B-D, F-H, J-L), the basal nuclei, thalamus and the internal and external capsule (C, G, K). The pons shows multifocal T2-hyperintensities, even at an early age (A and E). The white matter abnormalities are more extensive in the elder patients (compare figures A-H and I-L). Patient F1-III5 had a large infarct located in the right temporo-parietal region (M). Small cystic infarcts are seen in the periventricular white matter (N). Some infarcts are acute, as indicated by a high signal on DWI (O), and a low signal on apparent diffusion coefficient maps (not shown). Microbleeds and a small hemorrhage are seen in the basal nuclei and thalamus (P).

Laboratory findings, including β -galactosidase, neuraminidase-1 and carboxypeptidase activity in leukocytes were unremarkable. Sanger sequencing of all *NOTCH3* exons and exon-intron boundaries, except the non-coding exon 1, did not identify pathogenic variants in 3 F1 patients and the F2-2 patient. *COL4A1* and *COL4A2* were sequenced in F2-2 and showed no pathogenic variants. In F1 patients IV3 and IV13, additional Sanger sequencing of exon 1, which was not sufficiently covered by WES, revealed no pathogenic *HTRA1* variants.

Genetic analysis

WES in 3 family members of F1, 2 affected and 1 unaffected, revealed 2 heterozygous candidate variants in 2 genes: c.973C>T, p.(Arg325Cys) in *CTSA* and c.544G>A, p.(Gly182Arg) in *TTPAL*, both located on chromosome 20q13.12 (Table 1). *CTSA* encodes CathA; *TTPAL* encodes tocopherol (alpha) transfer protein-like (TTPAL). Both unknown variants segregated with the disease in F1 (e-figure 1). Only the same heterozygous *CTSA* variant was found in patient F2-2 and her father, leaving *CTSA* as the only shared candidate gene. The c.973C>T *CTSA* variant (NP_000299; p. (Arg325Cys)), is absent from public databases, including dbSNP, 1000 genomes project, Exome variant server and genome of the Netherlands (GoNL¹⁷) database, and the Exome Aggregation Consortium (ExAC), Cambridge, MA (URL: <http://exac.broadinstitute.org>) [March 2016 accessed]. *In silico* programs predict the mutation to be damaging.

Two-point linkage analysis for the *CTSA* variant in F1 showed a maximal LOD score of 5.4953 at theta 0 for the variant.

Haplotype analysis around the *CTSA* locus

Using 13 consecutive microsatellite markers, we identified among F1 patients a shared haplotype of 8 consecutive markers flanked by markers D20S46 and D20S891 (physical genomic location Hg 19 chr20: 41334729-45929596) (not shown), which was not shared by any of the unaffected F1 individuals. Marker analysis for patient F2-2 showed that she shared identical alleles for 2 adjacent markers close to *CTSA* (see table e-3), suggestive of common ancestry of the allele. The smallest putative shared region was 1145 kb, flanked by microsatellite markers D20S481 and D20S836 (Hg19 chr20: 43768281-44940373). This interval contains 58 genes (24 with OMIM annotation), including *CTSA* but not *TTPAL*.

Table 1. WES variant filtering and candidate gene identification

Total identified variants in sequenced family members								
	IV3 patient	IV5 healthy sib	IV13 patient					
Total variants^a	22274	19135	21666					
Variant filtering								
	IV3	IV5	IV13					
<i>Excluding segmental duplications & variants located on X-chromosome</i>	18826	16296	18268					
<i>Frequency filter:^b</i>								
Excluding variants with MAF > 0.001 (0.1%) in 1000 Genomes database, EVS database and dbSNP137 database	989	871	944					
<i>Inheritance</i>								
Excluding variants without autosomal dominant inheritance pattern ^c		63						
<i>In-house control</i>								
Excluding variants present in our in-house control database ^d		3						
<i>Pathogenicity</i>								
Excluding synonymous variants not adjacent to splice site		2 (see below)						
Identified candidate variants								
Gene	c. DNA ^e	Protein	Effect	Chromosome	Conservation	Pathogenicity ^f	ExAC ^g database	Confirmed ^h
CTSA	c. 922C>T	Arg308Cys	missense	20q13	up to c. elegans	damaging	not present	yes
TTPAL	c. 544G>A	Gly182Arg	missense	20q13	up to fruit fly	damaging	not present	yes

Nomenclature according to Human Genome Variation Society (HGVS, <http://www.hgvs.org/mutnomen>). MAF, minor allele frequency.

^aIncluding both detected insertions and deletions and single nucleotide variants.

^bThree public variant databases were used: 1) dbSNP137 (<http://www.ncbi.nlm.nih.gov/projects/SNP>), 2) 1000 Genomes Project (release of February 2012), 3) Exome Variant Server (EVS), National Heart, Lung, and Blood Institute GO Exome Sequencing Project (ESP5400 release) (<http://evs.gs.washington.edu/EVS/>).

^cAutosomal dominant inheritance was defined as a heterozygous variant ($\geq 32\%$ and $\leq 69\%$ of the reads harboured the alternative allele) present in both affected family members IV3 and IV13 and absent in a heterozygous or homozygous state in the unaffected individual IV5. Variants with a minimal coverage of 5 reads in both affected individuals were considered.

^dThe in-house control database contained 21 exomes.

^eCTSA reference sequence: NM_000308.2, TTPAL reference sequence: NM_024331.3.

^fPathogenicity prediction of variants was calculated with SIFT, PolyPhen-2 and MutationTaster.

^gThe Exome Aggregation Consortium (ExAC), Cambridge, MA (URL: <http://exac.broadinstitute.org>) [March, 2016 accessed].

^hInvestigated with Sanger sequencing.

Neuropathologic findings

Gross examination (Figure 2A) showed mild cerebral white matter atrophy and scattered small infarcts in subcortical and deep cerebral white matter, basal nuclei, thalami, brainstem, and cerebellum. Microscopy revealed an extensive leukoencephalopathy with myelin pallor, relatively preserved axons, some without myelin, astrogliosis and preserved oligodendrocytic density. Lacunar changes, consisting of perivascular tissue rarefaction with macrophages, focal oligodendrocyte and axonal loss and astrogliosis, were abundant in patients F1-III1 and F1-III2 (Figure 2B), but few in F1-IV8.

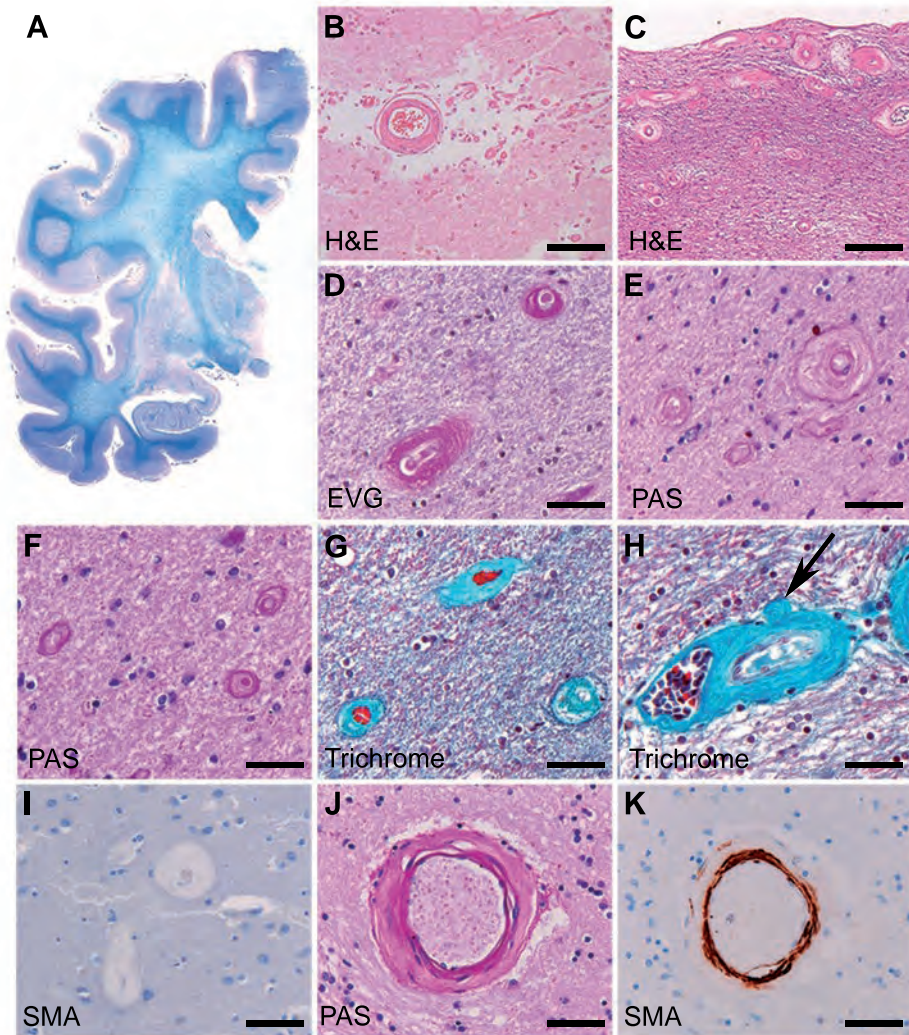


Figure 2. Neuropathological findings.

Whole mount of the right cerebral hemisphere of patient F1-III2 at the level of the anterior hippocampus stained with the Kluver stain for myelin (blue) and periodic acid Schiff (PAS, purple) shows diffuse white matter pallor extending to the internal and external capsules and, in places, the U-fibers. The lateral ventricle is slightly enlarged, indicating mild white matter atrophy. The cortex and hippocampus are not involved (A). Ischemic lesions in the white matter (B, patient F1-III1) appear as areas of enlargement, rarefaction and loosening of the perivascular tissue with presence of foamy macrophages (H&E). The small arterioles along the wall of the lateral ventricle show asymmetric fibrous thickening of the vessel wall with luminal stenosis (C, H&E, patient F1-III2). Similar changes are also visible in the subcortical (D, elastin van Gieson, patient F1-IV8) and deep hemispheric white matter (E, PAS, patient F1-III2) and in white matter bundles in the striatum (F, PAS, patient F1-III1) and pons (G, Gomori trichrome, patient IV8). Note the loss of vascular elastic fibers (D, elastin van Gieson), the absence of PAS-positive material (E and F, PAS) and the asymmetric fibrous thickening of the small arteriolar walls (G, Gomori trichrome). The vasa vasorum of the larger arterioles (arrow) may be totally occluded (H, Gomori trichrome, patient F1-III2). Stain against smooth muscle actin (SMA, I, patient F1-IV8) shows complete degeneration of vascular smooth muscle cells. In sporadic SVD (J and K), small arteries show symmetric thickening of the vessel wall with concentric accumulation of extracellular matrix components (J, PAS) and less severe degeneration of vascular smooth muscle cells (K, SMA). Bars: (B-C) 200 μ m; (D-K) 100 μ m.

In all patients and in the controls with sporadic SVD, arterioles showed diffuse angiosclerosis. There was no accumulation of basophilic, PAS-positive congophilic material. Labelling for amyloid beta was negative (not shown). Strikingly, in *CTSA*-mutated patients but not in the neurological and non-neurological controls, we detected unusual changes involving distal arteriolar branches, consisting of vessel wall fibrous thickening, which was remarkably asymmetric, and loss of smooth muscle cells with near-total occlusion of the lumen. These changes were present throughout the cerebral white matter, basal nuclei and subependymal regions, and also involved vasa vasorum (Figure 2, C-I). Perivascular dystrophic calcifications and inflammatory cells were negligible. These microvascular changes were different from what was found in the neurological controls (Figure 2, J-K). Calculation of the sclerotic index revealed more severe lumen narrowing in our patients (mean 0.55) than in sporadic SVD (mean 0.33) and normal controls (mean 0.27). Patients F1-III1 and F1-III2 also showed mild Alzheimer disease-related changes scored as A1B1C0.¹⁸

EM of white matter blood vessels confirmed absence of granular osmiophilic material close to smooth muscle cells and amyloid. Terminal arterioles showed asymmetrically enlarged tunica adventitia with accumulation of elastic, normal appearing collagen fibrils and, in some vessels, focal thickening of the basal lamina (not shown). In the non-infarcted white matter, EM confirmed the presence of axons without myelin (not shown).

In the non-infarcted cerebral white matter, OPC numbers were higher in *CTSA*-mutated patients than in sporadic SVD ($p < 0.05$), and in both compared to non-neurological controls ($p < 0.01$ and $p < 0.001$, respectively) (Figure 3H). The amounts of the myelin protein MBP were lower in patients than in sporadic SVD controls (Figure 3I).

Body autopsy of patient F1-V8 revealed atherosclerosis in the aorta and larger arteries without ulcerated plaques or signs of major vascular disease, and diffuse glomerulosclerosis in the kidneys.

CathA and ET-1 protein immunoreactivity in the brain

Non-neurological controls showed delicate cytoplasmic CathA-immunoreactivity in neurons and astrocytes at the glia limitans and around blood vessels in gray and white matter. At these sites, increased CathA-labelling was observed in patients and, to a lesser degree, all neurological controls (data not shown). In the white matter of patients and neurological controls, intense cytoplasmic CathA-immunoreactivity was seen in reactive astrocytes. However, in neurological controls, CathA-positive astrocytes were only present around infarcts, whereas in *CTSA*-mutated patients strongly CathA-

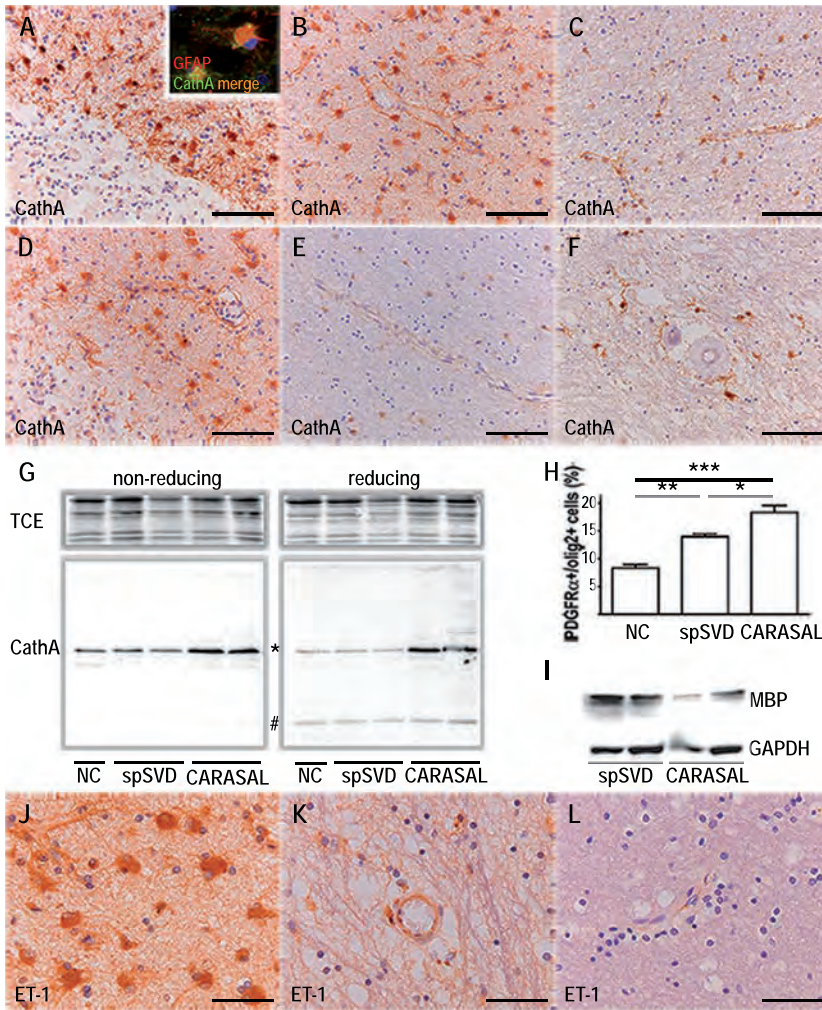


Figure 3. Increased CathA and ET-1 expression correlate with increased OPC numbers and lack of myelin.

Patients (A and B) show increased CathA-immunoreactivity compared to controls with capillary CAA (C), sporadic SVD (D and E) and CADASIL (F) in astrocytes both surrounding infarcts (A and D) and in white matter areas distant from infarcted areas (B, C, E and F). The CathA-positive cells have the morphology of astrocytes and express the astrocyte-specific marker GFAP (inset in A, GFAP in red and CathA in green). Western blotting of white matter lysates in non-reducing (left panel) and reducing SDS-PAGE (right panel) show increased amounts of the CathA precursor protein (*, 54 kDa) in patients F1-III1 and F1-III2 compared to a non-neurological control and 2 controls with sporadic SVD. The amounts of mature CathA protein (#, 20 kDa) are not evidently changed. Note that the additional faint bands of different molecular weight present on both blots are not specific for the patients (G). In white matter areas devoid of lacunar infarcts, the patients' white matter astrocytes (J, F1-patient III2) are more intensely ET-1-immunoreactive than those of controls with sporadic SVD (K). White matter astrocytes of a non-neurological control are ET-1-negative (L). The percentage of PDGFR α -positive pre-myelinating OPCs is significantly higher in the white matter of the patients than of controls with sporadic SVD and the non-neurological control (*: $p < 0.05$; **: $p < 0.01$; ***: $p < 0.001$, H). Western blotting of white matter lysates shows lower amounts of myelin basic protein (MBP, upper panel) in the patients than in controls with sporadic SVD. The lower panel confirms equal protein loading (GAPDH) (I). NC: non-neurological control; spSVD: controls with sporadic SVD; TCE: trichloroethanol, indicating on-blot total protein signal. Bars: (A-F) 100 μ m; (J-L): 50 μ m.

expressing astrocytes were present throughout the white matter (Figure 3, A-F).

We investigated CathA accumulation in reducing and non-reducing SDS-PAGE Western blotting to assess whether the additional cysteine residue causes aberrant disulfide bridge formation and consequent protein misfolding.^{19,20}

Abnormal foldings would only be detected under non-reducing conditions that leave disulfide bridges intact. We did not detect these in patients or controls. However, under all conditions, the CathA 54 kDa precursor protein was increased in *CTSA*-mutated patients compared to neurological and non-neurological controls. Notably, the amounts of CathA precursor protein were similar in sporadic SVD and the non-neurological control. The amounts of the mature 20 kDa CathA product were not significantly changed in *CTSA*-mutated patients (Figure 3G).

ET-1 is a peptide degraded by CathA that has roles in vasoconstriction and OPC maturation.^{21,22} We found ET-1-positive reactive astrocytes around infarcts in patients and all neurological controls. In non-infarcted white matter areas, however, astrocytic ET-1 immunolabelling was strikingly higher in patients than in neurological controls (Figure 3, J and K). Astrocytes in non-neurological controls were ET-1-negative (Figure 3L).

DISCUSSION

We report 2 families with adult-onset dominant “Cathepsin A-related arteriopathy with strokes and leukoencephalopathy” (CARASAL), presenting with therapy-resistant hypertension, ischemic and hemorrhagic strokes and late cognitive deterioration. Complaints of dry eyes and mouth, and muscle cramps are consistent additional features in F1, but not F2. MRI initially shows multifocal signal changes in the cerebral white matter and basal nuclei, thalami, and brainstem, a pattern suggestive of SVD.²³ Over time, the leukoencephalopathy becomes virtually diffuse. As in other SVDs, the leukoencephalopathy on MRI precedes the onset of strokes and is disproportionate to the clinical severity.²⁴

The clinical, MRI and especially pathology phenotypes in our families do not suggest a known autosomal dominant vasculopathy. EM showed no granular osmiophilic material, basal lamina fragmentation or multi-lamination, or amyloid deposition in blood vessels, as seen in CADASIL, defects of collagen IVA1 and IVA2, *TREX1*-related disease and CAA, respectively.^{3,7,8,25-27} *NOTCH3* sequencing was unrevealing and WES showed no known or possible pathogenic variants in *COL4A1*, *COL4A2*, *TREX1* and CAA-related genes, including *APP*, *CST3*, *TTR*, *GSN*, *BRI2* and *PRPN*. No pathogenic *HTRA1* variants were

found in WES and Sanger sequencing of exon 1. The unusual pathology of the terminal arterioles observed in our patients was not present in the investigated patients with CADASIL, CAA and sporadic SVD.

The 2 families were identified independently on the basis of MRI findings. In both, the same *CTSA* variant segregated with the disease. Haplotype analysis showed that an 1145 kb region encompassing the *CTSA* variant is shared by the families, suggesting that the variant originates from a common ancestor. WES revealed no other dominant variants in this region, leaving *CTSA* as the only candidate gene.

Hervé *et al.* reported a French family with autosomal dominant vascular leukoencephalopathy with an MRI pattern similar to CARASAL.¹⁴ Remarkably, the unusual pathologic changes of white matter small arterioles, including the vasa vasorum, were also noted.¹⁴ The French family showed linkage with a 11.2 Mb interval on chromosome 20q13,¹⁴ encompassing the 1145 kb region of the *CTSA* variant,¹⁴ a strong argument for the same disease.

CathA is synthesized as a single-chain precursor of 54 kDa that is converted into a catalytically active heterodimer consisting of 20 and 32 kDa subunits.^{28,29} Mature CathA is mainly found in lysosomes, where it stabilizes a multi-enzyme complex with β -galactosidase and neuraminidase-1. Recessive *CTSA* mutations cause galactosialidosis due to deficiency of β -galactosidase and neuraminidase-1.^{30,31} Heterozygous *CTSA* mutations have hitherto not been associated with disease.

The possible functional role of the *CTSA* mutation in CARASAL is presently unexplained. Considering the dominant inheritance, the Arg325Cys change could have a toxic effect. The extra cysteine could affect stabilization, folding, and structure of the protein due to extra disulfide bonds.¹⁹ Non-reducing SDS-PAGE, however, did not show alternative conformations of mutant CathA. In CARASAL patients, CathA signals in non-reducing and reducing conditions were similar, excluding the possibility of CathA isoforms being too large to enter the gel. These findings do not support misfolding of mutant CathA.

In our patients, CathA-expressing astrocytes were spread over the white matter, whereas in capillary CAA, CADASIL and sporadic SVD they only clustered around infarcts. Reducing SDS-PAGE confirmed increased CathA precursor protein amounts in CARASAL patients only. Notably, CathA was not increased in controls with sporadic SVD and similar degree of vascular lesions and reactive gliosis, indicating that the observed CathA accumulation is not merely a consequence of the small vessel involvement and ischemic pathology.

Leukoencephalopathy is part of the general SVD histopathology phenotype, with loss of oligodendrocytes, myelin and axons centered on abnormal vessels.³² The pathomechanism of SVD-related leukoencephalopathy is complex, also involving chronic hypoperfusion and hypoxia.³² White matter pathology in CARASAL shows paucity of myelin, astrogliosis and increased OPC numbers extending *beyond* the ischemic pathology, also present in patient F1-IV8 who had no infarcts and few lacunae. The discrepancy between extensive white matter involvement and relatively mild vascular lesions in CARASAL suggests that additional pathomechanisms besides ischemia contribute to the leukoencephalopathy.

We investigated ET-1, a peptide with roles in vasoconstriction²¹ and OPC maturation,²² which is degraded by CathA carboxypeptidase and other proteases.^{33,34} We found strikingly increased ET-1 immunoreactivity in CARASAL white matter astrocytes, also compared to other vascular leukoencephalopathies. Astrocyte-derived ET-1 may contribute to long-lasting vasoconstriction and hypoxia.³⁵ Transgenic mice with selective inactivation of CathA carboxipeptidase have hypertension due to reduced ET-1 degradation,³⁶ a feature shared by CARASAL patients. In CARASAL, ET-1 overexpression coincides with increased numbers of pre-myelinating OPCs, decreased MBP amounts and abundance of axons without myelin, features of re-myelination failure. Findings in multiple sclerosis (MS) indicate that astrocyte-derived ET-1 may inhibit OPC maturation.²² Strikingly, in MS ET-1-expressing astrocytes are found only within demyelinating lesions,²² whereas in CARASAL they are present throughout the non-infarcted white matter. It is tempting to speculate that ET-1 accumulates in CARASAL because of the *CTSA* mutation. This would imply that CathA carboxypeptidase activity is reduced in patients' brain, although reduced activity was not found in leukocytes. In this scenario, ET-1 would contribute to the leukoencephalopathy in CARASAL and explain the extensive white matter abnormalities far beyond the vascular injury.

Arterial hypertension with cortical-subcortical infarctions has been reported in a single galactosialidosis patient.³⁷ Parents of galactosialidosis patients, who are obligatory *CTSA* mutation carriers, are not known to have increased risk for hypertension and SVD. However, since galactosialidosis is rare and hypertension and hypertension-related white matter lesions are common, such association may have easily been overlooked. Similar oversights have occurred before.^{38,39} It is long known that Gaucher disease is caused by recessive mutations in *GBA1*, encoding glucocerebrosidase. Only recently it has become clear that heterozygous carriers of *GBA1* mutations have an increased risk of Parkinson disease and Lewy bodies dementia.³⁸ It is worthwhile to investigate if heterozygous *CTSA* mutations are associated with an increased risk of SVD in families

of galactosialidosis patients. Further studies should elucidate whether only the p.(Arg325Cys) variant in *CTSA* is associated with CARASAL or whether the risk of an SVD is also seen in other mutations.

Vascular leukoencephalopathies are common in elderly individuals. With CARASAL a new phenotype is added to the spectrum. We suspect that the genetic origin of adult-onset vascular leukoencephalopathies is often overlooked.

REFERENCES

1. Sahathevan R, Brodtmann A, Donnan GA. Dementia, stroke, and vascular risk factors; a review. *Int J Stroke* 2012;7:61-73.
2. Roman GC, Erkinjuntti T, Wallin A, Pantoni L, Chui HC. Subcortical ischaemic vascular dementia. *Lancet Neurol* 2002;1:426-436.
3. Joutel A, Corpechot C, Ducros A, et al. Notch3 mutations in CADASIL, a hereditary adult-onset condition causing stroke and dementia. *Nature* 1996;383:707-710.
4. Hara K, Shiga A, Fukutake T, et al. Association of HTRA1 mutations and familial ischemic cerebral small-vessel disease. *N Engl J Med* 2009;360:1729-1739.
5. Tikka S, Baumann M, Siitonen M, et al. CADASIL and CARASIL. *Brain Pathol* 2014;24:525-544.
6. Verdura E, Herve D, Scharrer E, et al. Heterozygous HTRA1 mutations are associated with autosomal dominant cerebral small vessel disease. *Brain* 2015;138:2347-2358.
7. Gould DB, Phalan FC, van Mil SE, et al. Role of COL4A1 in small-vessel disease and hemorrhagic stroke. *N Engl J Med* 2006;354:1489-1496.
8. Verbeek E, Meuwissen ME, Verheijen FW, et al. COL4A2 mutation associated with familial porencephaly and small-vessel disease. *Eur J Hum Genet* 2012;20:844-851.
9. Richards A, van den Maagdenberg AM, Jen JC, et al. C-terminal truncations in human 3'-5' DNA exonuclease TREX1 cause autosomal dominant retinal vasculopathy with cerebral leukodystrophy. *Nat Genet* 2007;39:1068-1070.
10. Revesz T, Holton JL, Lashley T, et al. Genetics and molecular pathogenesis of sporadic and hereditary cerebral amyloid angiopathies. *Acta Neuropathol* 2009;118:115-130.
11. Verreault S, Joutel A, Riant F, et al. A novel hereditary small vessel disease of the brain. *Ann Neurol* 2006;59:353-357.
12. Ding XQ, Hagel C, Ringelstein EB, et al. MRI features of pontine autosomal dominant microangiopathy and leukoencephalopathy (PADMAL). *J Neuroimaging* 2010;20:134-140.
13. Low WC, Junna M, Borjesson-Hanson A, et al. Hereditary multi-infarct dementia of the Swedish type is a novel disorder different from NOTCH3 causing CADASIL. *Brain* 2007;130:357-367.
14. Herve D, Chabriet H, Rigal M, et al. A novel hereditary extensive vascular leukoencephalopathy mapping to chromosome 20q13. *Neurology* 2012;79:2283-2287.
15. Kevelam SH, Bugiani M, Salomons GS, et al. Exome sequencing reveals mutated SLC19A3 in patients with an early-infantile, lethal encephalopathy. *Brain* 2013;136:1534-1543.
16. Bugiani M, Boor I, van KB, et al. Defective glial maturation in vanishing white matter disease. *J Neuropathol Exp Neurol* 2011;70:69-82.
17. The genome of the Netherlands Consortium. Whole-genome sequence variation, population structure and demographic history of the Dutch population. *Nat Genet* 2014;46:818-825.
18. Montine TJ, Phelps CH, Beach TG, et al. National Institute on Aging-Alzheimer's Association guidelines for the neuropathologic assessment of Alzheimer's disease: a practical approach. *Acta Neuropathol* 2012;123:1-11.
19. Thornton JM. Disulphide bridges in globular proteins. *J Mol Biol* 1981;151:261-287.
20. Duering M, Karpinska A, Rosner S, et al. Co-aggregate formation of CADASIL-mutant NOTCH3: a single-particle analysis. *Hum Mol Genet* 2011;20:3256-3265.
21. Kiely DG, Cargill RI, Struthers AD, Lipworth BJ. Cardiopulmonary effects of endothelin-1 in man. *Cardiovasc Res* 1997;33:378-386.
22. Hammond TR, Gadea A, Dupree J, et al. Astrocyte-derived endothelin-1 inhibits remyelination through notch activation. *Neuron* 2014;81:588-602.
23. Wardlaw JM, Smith EE, Biessels GJ, et al. Neuroimaging standards for research into small vessel disease and its contribution to ageing and neurodegeneration. *Lancet Neurol* 2013;12:822-838.
24. Chabriet H, Joutel A, Dichgans M, Tournier-Lasserre E, Bousser MG. Cadasil. *Lancet Neurol* 2009;8:643-653.
25. van der Knaap MS, Smit LM, Barkhof F, et al. Neonatal porencephaly and adult stroke related to mutations in collagen IV A1. *Ann Neurol* 2006;59:504-511.
26. Plaisier E, Gribouval O, Alamowitch S, et al. COL4A1 mutations and hereditary angiopathy, nephropathy, aneurysms, and muscle cramps. *N Engl J Med* 2007;357:2687-2695.
27. Kolar GR, Kothari PH, Khanlou N, Jen JC, Schmidt RE, Vinters HV. Neuropathology and genetics of cerebroretinal vasculopathies. *Brain Pathol* 2014;24:510-518.

28. Rudenko G, Bonten E, d'Azzo A, Hol WG. Three-dimensional structure of the human 'protective protein': structure of the precursor form suggests a complex activation mechanism. *Structure* 1995;3:1249-1259.
29. Kolli N and Garman SC. Proteolytic activation of human cathepsin A. *J Biol Chem* 2014;289:11592-11600.
30. d'Azzo A, Andria G, Strisciuglio P, Galjaard H. Galactosialidosis. 2001;8th:3811.
31. Strisciuglio P, Parenti G, Giudice C, Lijoi S, Hoogeveen AT, d'Azzo A. The presence of a reduced amount of 32-kd "protective" protein is a distinct biochemical finding in late infantile galactosialidosis. *Hum Genet* 1988;80:304-306.
32. Jellinger KA. The enigma of vascular cognitive disorder and vascular dementia. *Acta Neuropathol* 2007;113:349-388.
33. Itoh K, Kase R, Shimmoto M, Satake A, Sakuraba H, Suzuki Y. Protective protein as an endogenous endothelin degradation enzyme in human tissues. *J Biol Chem* 1995;270:515-518.
34. Pshezhetsky AV and Hinek A. Serine carboxypeptidases in regulation of vasoconstriction and elastogenesis. *Trends Cardiovasc Med* 2009;19:11-17.
35. Zhang WW, Badonic T, Hoog A, et al. Structural and vasoactive factors influencing intracerebral arterioles in cases of vascular dementia and other cerebrovascular disease: a review. Immunohistochemical studies on expression of collagens, basal lamina components and endothelin-1. *Dementia* 1994;5:153-162.
36. Seyrantepe V, Hinek A, Peng J, et al. Enzymatic activity of lysosomal carboxypeptidase (cathepsin) A is required for proper elastic fiber formation and inactivation of endothelin-1. *Circulation* 2008;117:1973-1981.
37. Nordborg C, Kyllerman M, Conradi N, Mansson JE. Early-infantile galactosialidosis with multiple brain infarctions: morphological, neuropathological and neurochemical findings. *Acta Neuropathol* 1997;93:24-33.
38. Siebert M, Sidransky E, Westbroek W. Glucocerebrosidase is shaking up the synucleinopathies. *Brain* 2014;137:1304-1322.
39. Tetreault M, Gonzalez M, Dicaire MJ, et al. Adult-onset painful axonal polyneuropathy caused by a dominant NAGLU mutation. *Brain* 2015;138:1477-1483.

APPENDIX E-1

E-METHODS

Magnetic resonance imaging pattern recognition analysis

All included individuals from F1 and patient F2-2 underwent at least 1 brain MRI. MRIs studies included sagittal T1-weighted spin-echo images, and axial T1-weighted, T2-weighted and Fluid-Attenuated Inversion Recovery (FLAIR) images. MRIs were evaluated according to a previously published protocol (SHK and MSvdK).^{e1} Medial temporal lobe atrophy (MTA) was scored using the Scheltens visual rating scale.^{e2} Gradient echo images were available in 7 individuals (of whom 6 patients) and used to identify microbleeds. Diffusion-weighted images and apparent diffusion coefficient (ADC) maps, available in 14 individuals (of whom 9 patients), were used to assess the presence of restricted diffusion. Patient F2-1 had 2 successive CT-scans.

Whole-exome sequencing

Whole-exome sequencing (WES) was performed in 2 patients (F1-IV3 and F1-IV13) and 1 unaffected family member (F1-IV5) using SeqCap EZ Human Exome Library v2.0 kit (Nimblegen) (IV5) and SeqCap EZ Human Exome Library v3.0 kit (Nimblegen) (IV3 and IV13) on HiSeq2000 (Illumina, San Diego, CA). Read alignment to the human genome assembly hg19 was performed with Burrows-Wheeler Aligner tool (v0.5.9) (<http://bio-bwa.sourceforge.net>).^{e3} Single-nucleotide variants and small insertions and deletions were called with VarScan v2.2.5 (<http://varscan.sourceforge.net>)^{e4} and annotated with Annovar (<http://www.openbioinformatics.org/annovar>).^{e5} Variant filtering was executed under the hypothesis of an autosomal dominant inheritance pattern assuming that the variant had a minor allele frequency (MAF) of $\leq 0.1\%$ in public variant databases including dbSNP132 (<http://www.ncbi.nlm.nih.gov/projects/SNP>), the 1000 Genomes project (release February 2012), the National Heart, Lung, and Blood Institute Exome Sequencing Project (<http://evs.gs.washington.edu/EVS/>); the variant was absent from our in-house exome database. Synonymous variants that were not located adjacent to the consensus splice site were excluded. *In silico* prediction programs: SIFT (<http://sift.jcvi.org/>),^{e6} PolyPhen-2 (<http://genetics.bwh.harvard.edu/pph2/index.shtml>)^{e7} and MutationTaster (<http://www.mutationtaster.org/>)^{e8} were used to assess predicted pathogenicity scores of identified variants.

Two-point linkage analyses

Upon identification of the candidate variant, two-point linkage analyses using the the easyLinkage software package running Superlink v1.6 was performed. The following settings were used: autosomal dominant pattern of inheritance, disease allele frequency of 0.001 with a penetrance of 0.9 and equal distribution between males en females.

Microsatellite genotyping

We investigated the common affected haplotype segregating in F1 by using 13 microsatellite markers (D20S108, D20S46, D20S96, D20S861, D20S454, D20S119, D20S481, D20S838, D20S856, D20S836, D20S891, D20S866 and D20S75) spanning chromosome 20q13.12 (physical genomic location on Hg19 range from 40830457- 47690674). We tested all 22 included F1 family members. We compared the common affected haplotype segregating in F1 with patient F2-2 using 10 microsatellite markers (D20S46, D20S96, D20S861, D20S454, D20S119, D20S481, D20S838, D20S856, D20S836, D20S891). PCR products were analyzed with an Applied Biosystems Genetic Analyzer 3730 with GS-500-Liz as a size standard. Control DNA from CEPH individual 1347-01 was used as a reference. GeneMapper v3.7 software was used to analyze the data.

Neuropathology, immunohistochemical analysis and electron microscopy

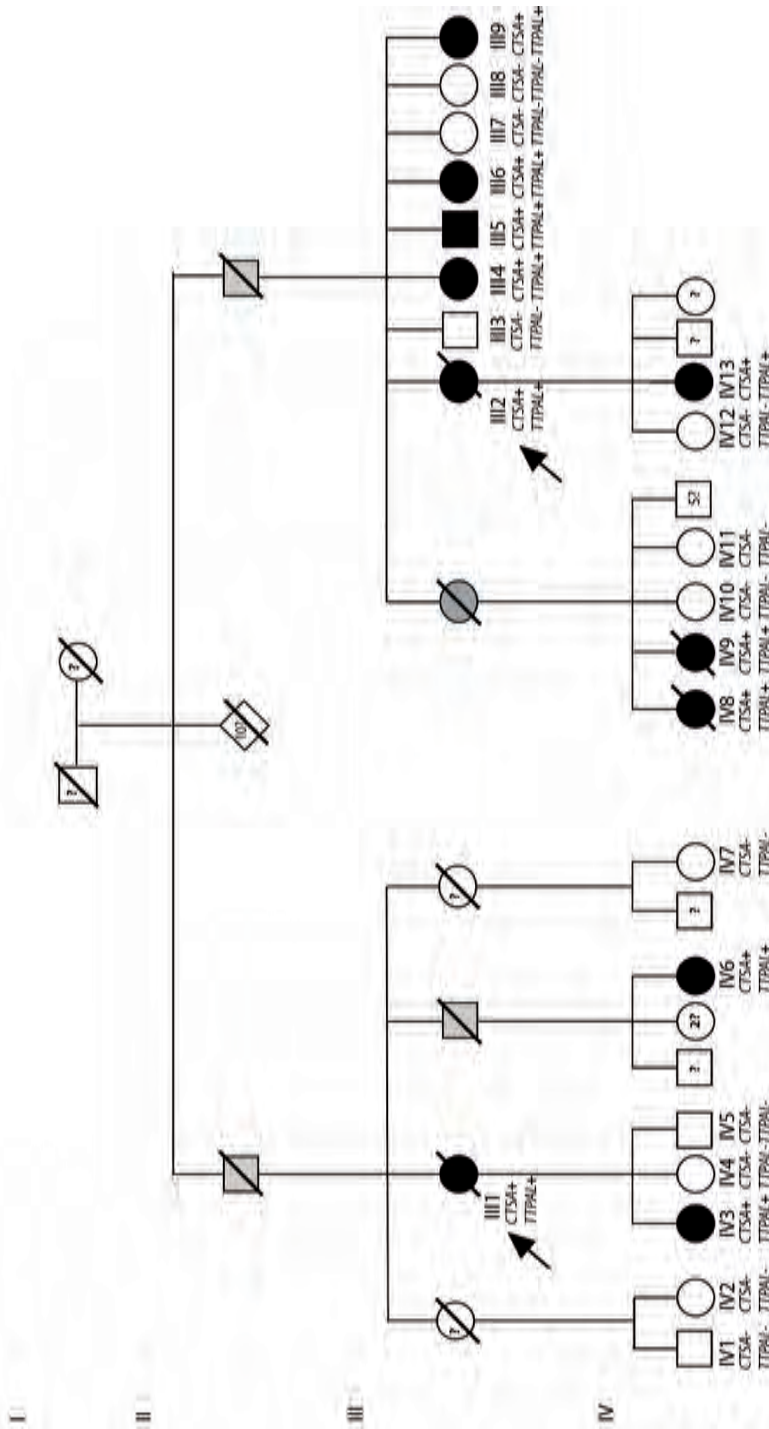
We obtained brain tissue from patients F1-III1, F1-III2, and F1-IV8 at autopsy. Patient F1-IV8 also underwent body autopsy. For control studies, we obtained brain samples from 2 subjects (ages 27 and 57 years) without neurological complaints and confounding neuropathology, 2 individuals (78 and 79 years) with hypertension-related sporadic SVD, 1 individual with sporadic capillary CAA (75 years) and 1 individual with CADASIL (69 years). Postmortem time was 3-6 hours for all subjects.

We stained 6- μ m-thick formalin-fixed, paraffin-embedded tissue sections with Hematoxylin & Eosin (H&E), Periodic Acid Schiff (PAS), Kliver-PAS, Gomori trichrome, and elastin van Gieson according to standard methods. For immunohistochemistry, sections were deparaffinized and rehydrated. Endogenous peroxidase activity was quenched by incubating the slides in 0.3% hydrogen peroxide in methanol. We performed heat-induced antigen retrieval with citric acid (pH6) using microwave irradiation for 15 min on low setting. Tissue sections were then incubated overnight with primary antibodies against cathepsin A (CathA) (Sigma-Aldrich, HPA031068, 1:25); glial fibrillary acidic protein (GFAP) (Millipore Ab5541, 1:1000); endothelin-1 (ET-1) (Meridian Life Science H54085M, 1:100); amyloid beta (Dako clone 6F3D, 1:100); phosphorylated tau (Innogenetics 90206, 1:200); smooth muscle actin (Dako M0851, 1:200); oligodendrocyte transcription factor 2 (olig2) (Millipore AB9610, 1:400); and platelet derived growth factor alpha receptor (PDGFR α) (BD Pharmingen 556001, 1:100). We verified specificity of the immunolabelling by omitting the primary antibody or by staining with isotype IgGs. Specificity of the CathA antibody was confirmed on fibroblasts from 2 infantile-onset galactosialidosis patients and 2 controls (not shown). Immunopositivity was detected with 3,3'-diaminobenzidine as chromogen or with fluorescent secondary antibodies (Alexa 488-, and 568-tagged; Molecular Probes,

1:400) followed by counterstaining with 4',6-diamidino-2-phenylindole (DAPI) (10 ng/ml, Molecular Probes). Sections were photographed using a Leica DM6000B microscope (Leica Microsystems BV). Morphometric analysis of vessel wall changes was performed calculating the sclerotic index (internal luminal diameter / external vessel diameter). A ratio of 0.2 to 0.3 is considered to denote healthy vessels, a ratio of 0.3 to 0.5 to be diseased and a ratio over 0.5 as severe.^{e9} In the frontal white matter of patients, controls with sporadic SVD and non-neurological controls, we counted the percentage of Olig2/PDGFR α double-positive pre-myelinating oligodendrocyte progenitor cells (OPCs) on the total number of nuclei in 10 fields using a 20x objective lens. Results were compared with one-way Anova analysis of variance with subsequent Bonferroni multiple comparisons test. For electron microscopy (EM) analysis, specimens were fixed in 4% glutaraldehyde, post-fixed in osmium tetroxide and further conventionally processed. Ultrathin sections were stained with uranyl acetate and lead citrate and analyzed at 60kV with a FEI CM10 transmission electron microscope.

SDS-PAGE and Western blotting

To obtain cytoplasmic lysates of patients, controls with sporadic SVD and non-neurological controls, we homogenized approximately 0.5 mg of white matter in lysis buffer containing 20mM Tris (pH 7.4), 100mM potassium acetate, 3mM magnesium acetate, 1.5% IGEPAL (NP-40), 0.2mM EDTA, 1.5% sodium deoxycholate, 20mM N-ethylmaleimide, and protease inhibitors (Roche). Samples were centrifuged (10,000xg, 10 minutes, 4°C) and the supernatant was transferred into a pre-chilled 1.5 ml eppendorf tube. We performed Bradford assays to quantify total protein per sample. Samples for reducing and non-reducing SDS-PAGE were prepared by mixing 100ug of total protein and Laemmli sample buffer with or without beta-mercapto-ethanol. Samples were heated (5 minutes, 56°C) and loaded onto 10% polyacrylamide gels prepared with 0.5% 2,2,2-trichloroethanol (TCE,^{e10}). We visualized proteins in the gel by ultraviolet exposure, which initiates a TCE-dependent tryptophan photoreaction (ChemiDoc, Bio-Rad). We assessed protein integrity of the sample and quantified the signal as a measure for total protein amount (loading control; Image Lab 3.0 software). Gels were transferred overnight at 30V (0.10A) onto Immobilon-P membranes (Millipore). Membranes were blocked in Tris-buffered saline with 5% non-fat milk and 0.1% Tween at room temperature and incubated with primary antibodies overnight. Immunoreactive proteins were visualized with an HRP-conjugated secondary antibody and SuperSignal Femto kit (Pierce) using an ODYSSEY Fc Dual-mo imaging system (LI-COR; chemiluminescence channel). Immunoreactive protein bands were quantified and the signal corrected for the amount of TCE signal on the membrane. The myelin basic protein (MBP) (Millipore MAB387, 1:50) Western blot was performed as previously described.^{e11}



e-figure 1. Simplified pedigree of family F1

The 22 individuals included in this study are indicated by a pedigree number. The 2 arrows point to the index patients. Solid black symbols indicate patients diagnosed by MRI. Open symbols, without a question mark indicate unaffected individuals. Gray symbols indicate individuals in whom no brain MRI was available but who showed clinical signs of the disease. A question mark means an unknown status. A number in a symbol indicates multiple individuals. A deceased individual is indicated by a symbol with a stripe. Segregation of the CTS and TPAL variant is shown by - (absence of the variant) and + (presence of the variant).

Table e-1. MRI characteristics

Patient number	F1-III1 ^a	F1-III2 ^a	F1-III4	F1-III5	F1-III6	F1-III9
Year of birth, gender	1935, f	1935, f	1937, f	1941, m	1945, f	1954, f
Age most recent MRI (years)	67	71	73	69	65	56
Cerebral WM abnormalities	confluent	confluent	mainly confluent	confluent	confluent and multifocal	confluent and multifocal
Predominance WM abnormalities	frontoparietal, periventricular & deep	frontoparietal, periventricular & deep	frontoparietal, periventricular & deep	frontoparietal, periventricular & deep	frontoparietal, periventricular & deep	frontoparietal, periventricular & deep
T2 signal abnormalities of:						
Anterior temporal WM	only periventricular	only periventricular	only periventricular	only periventricular	only periventricular	only periventricular
Corpus callosum	inner blade	inner blade	inner blade	inner blade	inner blade	inner blade
Internal capsule	+	+	+	+	+	+, only posterior limb
External capsule	+	+	+	+	+	+
Cerebral cortex	-	-	- apart from infarct	- apart from infarct	-	-
Thalamus	+	+	+	+	+	+
Putamen	+	+	+	+	+, few foci	+
Caudate nucleus	+	+	+	+	+, few foci	+
Globus pallidus	+	+	+	+	+, few foci	+
Cerebellar WM	+, hilus of the dentate nucleus and deep WM	+, hilus of the dentate nucleus and deep WM	-	-	-	-
Cerebellar cortex	-	-	-	-	-	-
Dentate nucleus	-	-	-	-	-	-
Midbrain	+	+	+	+	+	+
Pons	+	+	+	+	+	+
Medulla	+	+	-	+	-	-
Atrophy:						
Enlargement lat. ventricles	+, mild	+, mild	+, mild	-	+, mild	+, mild
Enlargement subarachnoid Spaces	+, mild	+, mild	+, mild	+, right parietal	+, mild	-
Enlarged perivascular spaces	+, basal nuclei and dentate nucleus	+, basal nuclei	+, basal nuclei	-	+, basal nuclei, thalami	+, basal nuclei
Microbleeds ^b	n.i.	14, cerebellum, pons, midbrain, basal nuclei, thalami, cerebral WM	n.i.	4, thalamus, deep white matter, basal nuclei	n.i.	-

Table e-1. MRI characteristics continued

Patient number	F1-III1*	F1-III2*	F1-III4	F1-III5	F1-III6	F1-III9
Small cystic infarct	-	2, basal nuclei left, cerebral WM right	2, basal nuclei left, cerebral WM right	1, cerebral WM right	-	-
Larger infarct	1, cerebellum right (small)	-	1, occipital right	2, temporoparietal right and occipital left (small)	-	-
Hemorrhage	-	1, basal nuclei right	-	-	-	-
Restricted diffusion ^c	n.i.	n.i.	-	-	-	-
Contrast enhancement	-	n.i.	n.i.	-	n.i.	n.i.
Magnetic resonance angiogram	n.i.	n.i.	n.i.	n.i.	n.i.	n.i.
MTA score ^d	n.i. (probably 0) ^e	1	0	0	n.i. (probably 0) ^e	0

Table e-1. MRI characteristics continued

Patient number	F1-IV3	F1-IV8 ^a	F1-IV9	F1-IV13	F1-IV6	F2-2
Year of birth, gender	1955, f	1958, f	1959, f	1961, f	1964, f	1975, f
Age most recent MRI	55	53	51	48	46	39
Cerebral WM abnormalities	mainly confluent	confluent and multifocal	mainly confluent	confluent and multifocal	confluent and multifocal	confluent and multifocal
Predominance WM abnormalities	frontoparietal, periventricular & deep	frontoparietal, periventricular & deep	frontoparietal, periventricular & deep	frontoparietal, periventricular & deep	frontoparietal, periventricular & deep	frontoparietal, periventricular & deep
T2 signal abnormalities of:						
Anterior temporal WM	only periventricular	only periventricular	only periventricular	only periventricular	only periventricular	only periventricular
Corpus callosum	-	inner blade	inner blade	inner blade	-	inner blade
Internal capsule	+, only posterior limb	+, only posterior limb	+	+, only posterior limb	+, only posterior limb	+, only posterior limb
External capsule	+	+	+	+	+	+
Cerebral cortex	-	-	-	-	-	-
Thalamus	+, mild	+	+, mild	+	+, mild	+, mild
Putamen	+, mild	+, mild	+, mild	+	+, mild	+, mild
Caudate nucleus	+, mild	+, mild	+, mild	+	+, mild	+, mild
Globus pallidus	+, mild	+, mild	+, mild	+	+, mild	+, mild
Cerebellar white matter	-	-	+, hilus of the dentate nucleus	-	-	-
T2 signal abnormalities of:						
Cerebellar cortex	-	-	-	-	-	-
Dentate nucleus	-	-	-	-	-	-
Midbrain	+	+	+	+	+	+
Pons	+	+	+	+	+	+
Medulla	-	+	+	-	-	-
Atrophy:						
Enlargement lat. ventricles	-	+, mild	+, mild	+, mild	-	+, mild
Enlargement subarachnoid Spaces	-	+, mild	-	-	-	-

Table e-1. MRI characteristics continued

Patient number	F1-IV3	F1-IV8 ^a	F1-IV9	F1-IV13	F1-IV6	F2-2
Enlarged perivascular spaces	+; basal nuclei, thalami, cerebral WM	+; a few in the basal nuclei	+; basal nuclei	+; a few in the basal nuclei	-	-
Microbleeds ^b	n.i.	1, basal nuclei left	n.i.	-	n.i.	-
Small cystic infarct	-	1, recent, deep parietal WM left	-	1, parietal WM right	-	-
Larger infarct	1, cerebellum right (small)	-	-	-	-	-
Hemorrhage	-	-	-	-	-	-
Restricted diffusion ^c	n.i.	+; deep parietal WM left	-	-	-	-
Contrast enhancement	n.i.	-	n.i.	n.i.	n.i.	-
Magnetic resonance angiogram	n.i.	n.i.	n.i.	normal	n.i.	n.i.
MTA score ^d	0	0	0	1	0	0

^aDecreased and pathology information available. ^bDecreased and pathology information available

^bGradient-echo images were used to identify microbleeds.

^cDiffusion-weighted images and apparent diffusion coefficient maps were used to assess the presence of restricted diffusion. ^dMTA = Medial temporal lobe atrophy score based on Scheltens visual rating scale. ^eNo coronal images available for scoring. WM = white matter; n.i.=not investigated; + = T2 signal abnormality; - = normal T2 signal; f = female; m = male; lat. = lateral; F1 = Family 1; F2 = Family 2

Table e-2. Clinical characteristics

Patient number	F1-III1	F1-III2	F1-III4	F1-III5	F1-III6	F1-III9	F1-IV3	F1-IV8	F1-IV9	F1-IV13	F1-IV6	F2-1	F2-2	Total in patients ^b	Total in healthy family members ^b
Year of birth	1935	1935	1937	1941	1945	1954	1955	1958	1959	1961	1964	1952	1975	mean 1949	mean 1958
Gender	female	female	female	male	female	female	female	female	female	female	female	male	female	85% female	70% female
History															
Initial motor and cognitive development	normal	normal	normal	normal	normal	normal	normal	normal	normal	normal	normal	normal	normal	13/13	10/10
Onset															
Age at first complaints (y)	65	51	69	68	42	58	unknown	32	30	47	44	42	38	49	none
Signs/symptoms	vertigo, balance problems	brain hemorrhage	brain infarct	small brain infarct	TIA, memory deficit	eye infarction	headache	headache, balance problems	lack of energy, stiffness	sinus thrombosis	hypertension	brain infarct	migraine/headache		
Symptoms															
Age at interview (y)	deceased	deceased	74	70	66	61	56	53	52	50	48	42	40	61	54
Neurological															
Clinical stroke/TIA	no/no	yes/yes	yes/no	yes/no	no/yes	no/no	no/no	no/no	no/no	no/no	no/no	yes/yes	no/no	5/13	0/10
Migraine with aura	yes	no	no	no	no	no	yes	no	no	no	yes	no	yes	4/13	1/10
Cognitive complaints ^c	memory and concentration problems, disorientation, apraxia	memory and concentration problems, apraxia	concentration problems	no	mild memory problems	no	no	mild memory and concentration problems	memory problems	mild memory and concentration problems	mild memory and concentration problems	no	no	8/13	0/10
Dysphasia	no	no	no	no	no	no	no	no	no	no	no	no	no	0/13	0/10
Balance problems	yes	yes	no	no	no	no	no	yes	yes	yes	no	no	no	5/13	0/10
Other motor Problems	no	no	no	no	no	no	no	no	no	no	no	no	no	0/13	0/10
Epilepsy	no	no	no	no	no	no	no	no	no	no	no	no	no	0/13	1/10
Psychological complaints ^c	loss of interest, depression	depression	emotional lability, loss of interest	no	no	emotional lability	no	depression	no	depression, loss of interest	no	no	no	7/13	2/10

Table e-2. Clinical characteristics continued

Patient number	F1-III1	F1-III2	F1-III4	F1-III5	F1-III6	F1-III9	F1-IV3	F1-IV8	F1-IV9	F1-IV13	F1-IV6	F2-1	F2-2	Total in patients ^b	Total in healthy family members ^b
Symptoms															
Vascular															
Hypertension	yes	yes	yes	no	yes	yes	yes	yes	yes	yes	yes	yes	yes	12/13	2/10
Number of drugs to control blood pressure	2	2	2	none	2	0	1	2	2	1	3	1	1	2	1
Thrombosis/Pulmonary Embolism	no/no	no/no	no/no	no/no	no/no	yes/no	no/no	yes/no	yes/yes	yes/no	no/no	yes/no	no/no	5/13	0/10
Venous insufficiency	varicosities legs	no	no	mild edema ankles	no	varicosities legs	varicosities legs	varicosities legs	varicosities, edema legs	mild varicosities	mild edema legs	varicosities legs	no	9/13	4/10
Internal organs															
Dry mouth with swallowing problems	yes	no	no	no	yes	no	yes	yes	yes	yes	yes	no	no	7/13	0/10
Renal dysfunction	renal insufficiency	no	kidney stones, unilateral nephrectomy	kidney stones	kidney stones, unilateral nephrectomy	no	no	no	no	kidney stones	no	renal insufficiency	no	6/13	1/10
Cardiac															
Infarct	myocardial infarct	no	no	no	no	no	no	no	no	no	no	no	no	2/13	0/10
Other	no	no	no	no	no	no	no	no	no	no	no	no	no	0/13	1/10

Table e-2. Clinical characteristics continued

Patient number	F1-III1	F1-III2	F1-III4	F1-III5	F1-III6	F1-III9	F1-IV3	F1-IV8	F1-IV9	F1-IV13	F1-IV6	F2-1	F2-2	Total in patients ^b	Total in healthy family members ^b
Ophthalmologic															
Dry eyes	yes	yes	yes	no	yes	no	yes	yes	yes	yes	yes	no	no	9/13	0/10
Other	no	no	no	no	no	infarct	no	no	no	no	no	no	no	1/13	0/10
Muscle/skeletal cramps/spasm	legs	fingers, legs	no	legs	fingers	legs	fingers	legs	legs	fingers, legs	no	no	no	9/13	0/10
Follow-up															
Slow regression	yes	yes	yes	no	no	no	yes	yes	yes	yes	no	yes	no	8/13	0/10
Death, y, (cause)	75 (myo-cardial infarct)	75 (chronic illness)	no	no	no	no	no	55 (hepatitis)	52 (cancer)	no	no	62 (pons hemorrhage)	no	5/13	0/10
Vascular risk factors															
Diabetes mellitus type 2	yes	yes	no	no	no	no	no	yes	no	no	no	DM1	no	3/13	0/10
Smoking (pack-years)	yes (50)	yes (n.a.)	yes (30)	no	yes (41)	yes (8)	yes (20)	yes (n.a.)	n.a.	no	yes (25)	no	no	8/12	5/10
Cholesterol	normal	normal	n.d.	slightly elevated	n.d.	elevated	normal	normal	normal	elevated	slightly elevated	n.d.	normal	4/10	0/10
Alcohol consumption (max. units per week)	no	no	yes (14)	no	yes (14)	no	yes (21)	yes (14)	n.a.	no	yes (14)	no	no	5/12	8/10
Laboratory tests															
β-galactosidase activity ^c (normal range 150-330 nmol/h/mg protein)	n.i.	n.i.	n.i.	n.i.	n.i.	n.a.	247	n.i.	n.i.	246	n.i.	n.i.	n.i.	n.a.	n.a.
Neuraminidase-1 activity ^c (normal range 800-2800 pmol/h/mg protein)	n.i.	n.i.	n.i.	n.i.	n.i.	n.a.	540	n.j.	n.i.	1240	n.i.	n.i.	n.i.	n.a.	n.a.
Carboxypeptidase activity ^c (normal range 72-166 nmol/min/mg protein)	n.i.	n.i.	n.i.	n.i.	n.i.	n.a.	118	n.i.	n.i.	121	n.i.	n.i.	n.i.	n.a.	n.a.

Table e-2. Clinical characteristics continued

Patient number	F1-III1	F1-III2	F1-III4	F1-III5	F1-III6	F1-III9	F1-IV3	F1-IV8	F1-IV9	F1-IV13	F1-IV6	F2-1	F2-2
Age at latest physical examination (y)	70	n.i.	74	68	66	n.i.	56	53	52	50	47	n.i.	40
Performance tests													
MMSE (max. 30)	n.i.	n.i.	30	30	27	n.i.	30	22	n.i.	26	29	n.i.	30
Cranial nerves													
Fundus, vision, eye movements	normal	n.i.	normal	normal	normal	n.i.	normal	normal	normal	normal	normal	n.i.	normal
Central VII paresis	no	n.i.	no	no	no	n.i.	no	yes	no	yes	no	n.i.	no
Hearing	normal	n.i.	normal	normal	normal	n.i.	normal	normal	normal	normal	normal	n.i.	normal
Dysarthria	no	n.i.	no	no	no	n.i.	no	yes	no	no	no	n.i.	no
Arms													
Tone	normal	n.i.	normal	normal	normal	n.i.	normal	normal	normal	normal	normal	n.i.	normal
Reflexes	normal	n.i.	normal	normal	normal	n.i.	normal	low	normal	normal	normal	n.i.	normal
Spasticity	no	n.i.	no	no	no	n.i.	no	no	no	no	no	n.i.	no
Muscle weakness	no	n.i.	no	no	no	n.i.	no	no	no	no	no	n.i.	no
Ataxia	no	n.i.	no	no	no	n.i.	no	no	mild tremor	no	no	n.i.	no
Extrapyramidal signs	no	n.i.	no	no	no	n.i.	no	no	no	no	no	n.i.	no
Sensory functions	normal	n.i.	normal	normal	normal	n.i.	normal	decreased gnostic sensibility	normal	decreased gnostic sensibility	normal	n.i.	normal
Legs													
Tone	normal	n.i.	normal	normal	normal	n.i.	normal	normal	normal	normal	normal	n.i.	normal
Reflexes	normal	n.i.	left > right	left > right	right > left	n.i.	normal	low	low	normal	normal	n.i.	normal
Babinski signs	yes	n.i.	no	no	no	n.i.	no	no	no	no	no	n.i.	no
Spasticity	no	n.i.	no	no	no	n.i.	no	no	no	no	no	n.i.	no

Table e-2. Clinical characteristics continued

Patient number	F1-III1	F1-III2	F1-III4	F1-III5	F1-III6	F1-III9	F1-IV3	F1-IV8	F1-IV9	F1-IV13	F1-IV6	F2-1	F2-2
Legs													
Muscle weakness	mild global decrease	n.i.	no	no	no	n.i.	no	global decrease	no	no	no	n.i.	no
Ataxia	no	n.i.	no	no	no	n.i.	no	no	mild tremor	no	no	n.i.	no
Extrapyramidal signs	no	n.i.	no	no	no	n.i.	no	no	no	no	no	n.i.	no
Sensory functions	decreased gnostic sensibility	n.i.	decreased gnostic sensibility	normal	normal	n.i.	normal	decreased gnostic sensibility	mildly decreased gnostic sensibility	mildly decreased gnostic sensibility	normal	n.i.	normal
Gait	unstable; only with support	n.i.	normal	normal	normal	n.i.	normal	wheel-chair dependent	stiff and unstable	mildly unstable	normal	n.i.	normal
General													
Lack of periorbital fat	n.i.	n.i.	yes	yes	yes	n.i.	yes	yes	yes	yes	yes	n.i.	yes
Venectasies fingers	n.i	n.i.	yes	no	yes	n.i.	minimal	yes	yes	yes	no	n.i.	no
Varicosities legs	n.i.	n.i.	no	no	no	n.i.	yes	yes	yes	yes	no	n.i.	no

*Subjective assessment. No formal neuropsychological test was performed. ^b Only family members of whom clinical information was available were included in this column. ^cMeasured in patients' leukocytes. ^dPhysical examination for healthy family members was normal and is not shown. F1= family 1; F2 = family 2; y = year; TIA = transient ischemic attack; max. = maximal; n.i.= not investigated; n.a. = not available; MMSE = minimal mental state examination; nmol = nanomole; min = minute; mg = milligram

Table e-3. Smallest haplotype shared by family 1 (F1) and patient F2-2

Microsatellite marker	Hg19, physical position	F1	F2-2
	Chromosome 20		
D20S46	41334729	194	194-184
D20S96	42095436	145	145-133
D20S861	42607372	113	n.a.
D20S454	43340833	203	188-200
D20S119	43649051	316	316-318
D20S481	43768281	240	236-236
D20S838	44637396	125	125-138
D20S856	44652722	179	179-174
D20S836	44940373	172	176-166
D20S891	45929596	231	231-231

Results of 10 consecutive microsatellite markers.

For F1 the smallest haplotype with the corresponding microsatellite markers segregating with the affected family members is shown (flanked by microsatellite markers D20S46 and D20S891). For patient F2-2 markers for both alleles are shown.

The smallest putative haplotype shared by F1 and patient F2-2 is bracketed by two double horizontal lines (D20S481-D20S836, physical genomic location 43768281 - 44940373).

Physical genomic location *CTSA* gene: 44519591 - 44527459, and *TTPAL* gene: 43104526 - 43123244

n.a. = not available

E-REFERENCES

- e1. van der Knaap M S, Breiter SN, Naidu S, Hart AA, Valk J. Defining and categorizing leukoencephalopathies of unknown origin: MR imaging approach. *Radiology* 1999;213:121-133.
- e2. Scheltens P, Leys D, Barkhof F, et al. Atrophy of medial temporal lobes on MRI in "probable" Alzheimer's disease and normal ageing: diagnostic value and neuropsychological correlates. *J Neurol Neurosurg Psychiatry* 1992;55:967-972.
- e3. Li H and Durbin R. Fast and accurate short read alignment with Burrows-Wheeler transform. *Bioinformatics* 2009;25:1754-1760.
- e4. Koboldt D C, Chen K, Wylie T, et al. VarScan: variant detection in massively parallel sequencing of individual and pooled samples. *Bioinformatics* 2009;25:2283-2285.
- e5. Wang K, Li M, Hakonarson H. ANNOVAR: functional annotation of genetic variants from high-throughput sequencing data. *Nucleic Acids Res* 2010;38:e164
- e6. Ng P C and Henikoff S. Predicting deleterious amino acid substitutions. *Genome Res* 2001;11:863-874.
- e7. Adzhubei I, Jordan DM, Sunyaev SR. Predicting functional effect of human missense mutations using PolyPhen-2. *Curr Protoc Hum Genet* 2013;Chapter 7:Unit7.20.
- e8. Schwarz J M, Cooper DN, Schuelke M, Seelow D. MutationTaster2: mutation prediction for the deep-sequencing age. *Nat Methods* 2014;11:361-362.
- e9. Craggs LJJ, Yamamoto Y, Deramecourt V, Kalaria RN. Microvascular pathology and morphometrics of sporadic and hereditary small vessel disease in the brain. *Brain pathol* 2014;24:495-509.
- e10. Ladner CL, Yang J, Turner RJ, Edwards RA. Visible fluorescent detection of proteins in polyacrylamide gels without staining. *Anal Biochem* 2004;326:13-20.
- e11. Bugiani M, Postma N, Polder E, et al. Hyaluronan accumulation and arrested oligodendrocyte progenitor maturation in vanishing white matter disease. *Brain* 2013;136:209-222.



**Novel disorder associated with
a gene previously not linked to
a human disorder or clear phenotype**

Chapter 9

***NUBPL* mutations in patients with complex I deficiency and a distinct MRI pattern**

Sietske H. Kevelam, Richard J. Rodenburg, Nicole I. Wolf, Patrick Ferreira, Rolineke J. Luning, Leo G. Nijtmans, Anne Mitchell, Hugo A. Arroyo, Dietz Rating, Adeline Vanderver, Carola G. M. van Berkel, Truus E. M. Abbink, Peter Heutink, and Marjo S. van der Knaap

Neurology. 2013 Apr;80(17):1577-1583.



ABSTRACT

Objective

To identify the mutated gene in a group of patients with an unclassified heritable white matter disorder sharing the same, distinct MRI pattern.

Methods

We used MRI pattern recognition analysis to select a group of patients with a similar, characteristic MRI pattern. We performed whole-exome sequencing to identify the mutated gene. We examined patients' fibroblasts for biochemical consequences of the mutant protein.

Results

We identified 6 patients from 5 unrelated families with a similar MRI pattern showing predominant abnormalities of the cerebellar cortex, deep cerebral white matter, and corpus callosum. The 4 tested patients had a respiratory chain complex I deficiency. Exome sequencing revealed mutations in *NUBPL*, encoding an iron-sulfur cluster assembly factor for complex I, in all patients. Upon identification of the mutated gene, we analyzed the MRI of a previously published case with *NUBPL* mutations and found exactly the same pattern. A strongly decreased amount of *NUBPL* protein and fully assembled complex I was found in patients' fibroblasts. Analysis of the effect of mutated *NUBPL* on the assembly of the peripheral arm of complex I indicated that *NUBPL* is involved in assembly of iron-sulfur clusters early in the complex I assembly pathway.

Conclusion

Our data show that *NUBPL* mutations are associated with a unique, consistent, and recognizable MRI pattern, which facilitates fast diagnosis and obviates the need for other tests, including assessment of mitochondrial complex activities in muscle or fibroblasts.

INTRODUCTION

There are many rare childhood leukoencephalopathies and currently a high percentage of cases remain without a specific diagnosis.¹ Consequently, the diagnostic process is challenging. In mitochondrial leukoencephalopathies, elevated lactate in body fluids often points in the right direction, generally followed by analysis of respiratory chain function in muscle tissue, and DNA analysis guided by the results. The extreme clinical and genetic heterogeneity of mitochondrial disorders, however, makes the final diagnosis frequently hard or impossible to achieve.²⁻⁴ MRI pattern recognition can greatly facilitate this diagnostic process by providing a rapid diagnosis in patients with known white matter disorders¹ and allowing identification of groups of patients with the same novel disorder among the unsolved cases.⁵ Formerly, definition of novel disorders was followed by genetic linkage studies if numerous patients or highly informative families were available.⁶⁻⁹ The recent introduction of whole-exome sequencing has created the opportunity to identify the mutated gene in small groups of patients with a rare mendelian disorder.¹⁰⁻¹²

METHODS

Patients

We identified 6 patients from 5 unrelated families from our MRI database of more than 3,000 cases with an unclassified leukoencephalopathy using MRI pattern recognition analysis.⁵ Patients 3 and 4 are affected siblings. Inclusion criteria were 1) extensive cerebellar cortex signal abnormalities; 2) signal abnormalities in the corpus callosum; and 3) absence of signal abnormalities in the basal ganglia, thalami, and cerebral cortex. Patient 2 was previously published by Wolf et al.¹³ In none of the patients a molecular diagnosis was achieved.

S.H.K. and M.S.v.d.K. evaluated the MRIs according to a previous protocol.⁵ We retrospectively reviewed the clinical information and laboratory investigations. Upon identification of the mutated gene, we included the MRI of a previously published case (patient 7) in our analysis to confirm consistency of our findings.^{14,15}

Standard protocol approvals, registrations, and patient consents.

We received approval of the ethical standards committee for our research on patients with unclassified leukoencephalopathies. We received written informed consent for exome sequencing from all guardians of the patients participating in the study.

Whole-exome sequencing

We performed whole-exome sequencing in DNA of patients 2 and 4, using SeqCap EZ Human Exome Library v3.0 kit (Nimblegen) on HiSeq2000 (Illumina, San Diego, CA; detailed information in e-Methods on the *Neurology*[®] Web site at www.neurology.org).

NUBPL mutation analysis

We amplified the 11 exons and intron-exon junctions of the human *NUBPL* gene (NG_028349.1) by PCR using suitable primers (available upon request) and analyzed these by Sanger sequencing.

Biochemical analysis

Skin fibroblasts of patients 2, 3, 4, and 6 were available and cultured in M199 medium supplemented with 10% fetal calf serum and antibiotics. We measured the enzyme activity of complexes I, II, III, IV, and V, and citrate synthase spectrophotometrically in mitochondria-enriched fractions isolated from fibroblasts and muscle as described.¹⁶⁻¹⁸ We performed biochemical analysis of *NUBPL* and complex I assembly with the fibroblasts of patients 3 and 4. We performed 10% sodium dodecyl sulfate (SDS)-polyacrylamide gel electrophoresis (PAGE) and 1- and 2-dimensional 5% to 15% blue native (BN)-PAGE as previously described.¹⁹ Lanes were loaded with 40 μg (SDS analysis) or 80 μg (BN analysis) of solubilized mitochondrial protein. After electrophoresis, the gels were further processed for in-gel activity assays and Western blotting, as described.¹⁹ We incubated the Western blots using antibodies against *NUBPL* (kind gift of Prof. R. Lill, Marburg, Germany), complex I subunits *NDUFA9* and *NDUFS3*, and complex II subunit *SDHA*/70 kDa (MitoSciences, Eugene, OR).

RESULTS

MRI findings

Detailed MRI findings are provided in table e-1 and illustrated in Figure 1. Initial MRIs (Figure 1, A–D, patient 7; I–L, patient 4) of patients 2, 4, 5, 6, and 7, obtained early in the disease course, showed confluent or multifocal cerebral white matter lesions, predominantly affecting the deep frontal and parietal white matter and sparing the U-fibers, internal and external capsules, and central part of the corona radiata under the pericentral cortex. Early MRIs showed prominent signal abnormalities and swelling of the corpus callosum. Callosal fibers connecting the pericentral cortex were relatively preserved (Figure 1, D). Extensive signal abnormalities were present in the cerebellar cortex and subcortical white matter, whereas the cerebellar deep white matter and

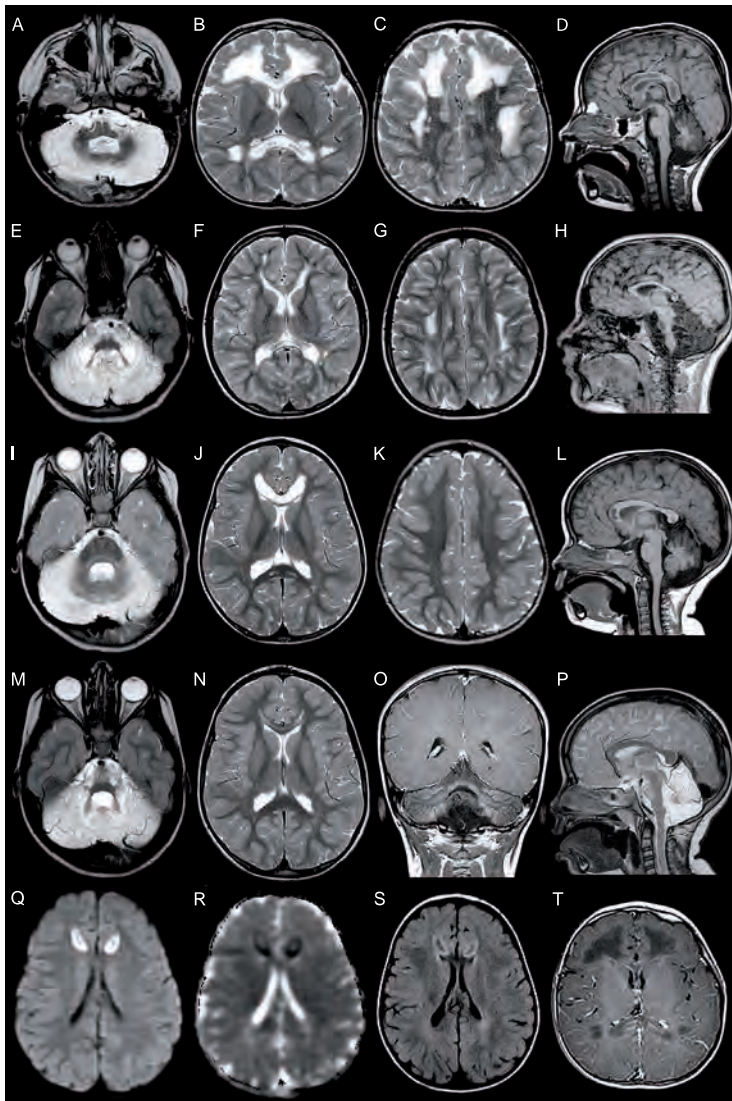


Figure 1. Illustrations of the characteristic MRI pattern.

MRIs of patient 7 (A–D, T), patient 2 (E–H), and patient 4 (I–S) obtained in the early (A–D, I–L, Q–T) and late stages (E–H, M–P) are shown. Axial T2-weighted images (A–C, E–G, I, J, M, N), sagittal T1-weighted (D, H, L) and T2-weighted (P) images, contrast-enhanced coronal (O) and axial (T) T1-weighted images, axial diffusion-weighted image (DWI) (Q), apparent diffusion coefficient (ADC) (R), and fluid-attenuated inversion recovery (S) images are shown. The initial MRIs (A, D, I, L) show diffuse signal abnormalities of the cerebellar cortex with sparing of the cerebellar deep white matter and pons, T2 hyperintensity of the corpus callosum with swelling (B, J), and variable deep cerebral white matter abnormalities (C, K). The inferior part of the cerebellum is relatively less affected (D, L) and the callosal fibers connecting the pericentral sulcus are spared (D). Contrast enhancement is seen in the corpus callosum (T). DWI and ADC images show restricted diffusion at the edges of the corpus callosum lesions (Q, R). The abnormal cerebral white matter is rarefied surrounded by a rim of abnormal but solid tissue (S). The late MRIs (F, G, N, P) show significant improvement or disappearance of the corpus callosum and deep white matter changes. The cerebellar abnormalities worsen and there are additional signal changes in the cerebellar deep white matter and basis pontis (E, H, M, P). Contrast enhancement is seen in the cerebellar cortex (O).

hilus of the dentate nucleus were spared (Figure 1, A, D, I, and L). The inferior part of the cerebellum was less severely affected (Figure 1, D and L). The corpus callosum and abnormal cerebral hemispheric white matter were rarefied (Figure 1, S). Contrast enhancement was seen in small areas of the abnormal cerebral white matter and corpus callosum (Figure 1, T). Restricted diffusion was present at the edges of the affected cerebral white matter and corpus callosum (Figure 1, Q and R).

Late MRIs (Figure 1, E–H, patient 2; M–P, patient 4) were available in patients 1, 2, 3, and 4. In patients 2 and 4, substantial improvement of the cerebral white matter and corpus callosum abnormalities were seen with decrease in both white matter swelling and extent of the white matter abnormalities, whereas the cerebellar abnormalities had worsened (Figure 1, E–H, M, N, and P). In patients 1 and 3, only a late MRI was available. In patient 3, subtle signal changes were exclusively seen in the corpus callosum; patient 1 had severe atrophy of the corpus callosum and limited cerebral white matter abnormalities. The cerebellar white matter and cortex were now extensively affected and atrophic in all patients. Prominent lesions were present in the basis pontis and pyramids of the medulla (Figure 1, E, H, M, and P). Contrast enhancement was seen in the pons and cerebellar cortex (Figure 1, O). No diffusion restriction was observed.

Clinical profiles and laboratory results

Detailed clinical characteristics and laboratory results are provided in tables e-2 and e-3. In contrast to the other patients, patient 7 was the only patient in which the early motor development was delayed. Patients presented with insufficient gain or loss of motor skills and signs of cerebellar dysfunction at the end of the first or in the second year of life. On follow-up, signs of continuing development were observed in most patients. Patient 1 experienced continuous slow regression; patients 4, 6, and 7 had episodes of regression of speech and mobility with partial recovery. Five patients developed spasticity. At the most recent clinical follow-up, patients 2 and 3 were able to walk without support. All patients had motor problems due to ataxia. Patient 1 died at 9 years of age of respiratory complications. Cognitive capabilities varied between normal and significantly deficient. No involvement of internal organs was noted.

Plasma and CSF lactate was elevated in most patients. Respiratory chain enzyme assays in muscle and fibroblasts revealed a complex I deficiency in all tested patients, ranging between 27% and 83% of the lowest reference value. The other respiratory chain complexes and complex V showed a normal activity in all patients (tables e-3 and e-4). The diagnosis of complex I deficiency was accomplished between 6 months and 2.5 years after the first MRI.

Genetic analysis

We performed whole-exome sequencing in DNA of patients 2 and 4. After filtering of the raw data under the hypothesis of a mitochondrial disorder, *NUBPL* (MIM*613621), encoding a Fe/S protein involved in complex I assembly, was the only remaining candidate gene with mutations (table e-5). Both patients harbored a heterozygous c.166G>A transition, predicting p.Gly56Arg. Patient 4 also harbored a c.313G>T change, predicting p.Asp105Tyr. Manual analysis of the intron data additionally revealed a heterozygous c.815–27T>C change in both patients. Sanger sequencing confirmed these mutations and revealed a frameshift mutation in patient 2: c.667_668insCCTTGTGCTG/p. Glu223Alafs*4. Subsequently, we identified *NUBPL* mutations in all 4 other patients (see table 1 for all identified *NUBPL* mutations). The c.166G>A missense mutation and the intronic c.815–27T>C branch-site mutation were present on the same allele in all patients. These 2 mutations were previously reported in patient 7 of this report by Calvo et al.¹⁴ within a large exome sequencing project of complex I-deficient patients. We analyzed all identified exonic missense mutations with Polyphen-2, which showed prediction scores of ≥ 0.99 . The amino acids involved are moderately to highly conserved. The mutations were therefore presumed to be pathogenic. The intronic c.815–27T>C mutation was previously shown to cause aberrant splicing of *NUBPL* mRNA.¹⁵ This mutation is found in the heterozygous state in 1 of 60 controls in the 1000 Genomes database. None of the other identified mutations are present in the public single nucleotide polymorphism databases, including the dbSNP (<http://www.ncbi.nlm.nih.gov/projects/SNP>) and 1000 Genomes database.

Table 1. Overview of *NUBPL* mutations^a

Patient	Country of origin	c.DNA ^b	Protein	Exon	State	Inheritance
1	Argentina	c.166G>A	p.Gly56Arg	2	Homozygous ^c	Unknown
		c.815-27T>C ^d		Intron 9	Homozygous ^c	Unknown
2	Germany	c.166G>A	p.Gly56Arg	2	Heterozygous	Paternal
		c.667_668insCCTTGTGCTG	p.Glu223Alafs*4	8	Heterozygous	Maternal
		c.815-27T>C ^d		Intron 9	Heterozygous	Paternal
3 and 4 (sibs)	Canada	c.166G>A	p.Gly56Arg	2	Heterozygous	Paternal
		c.313G>T	p.Asp105Tyr	4	Heterozygous	Maternal
		c.815-27T>C ^d		Intron 9	Heterozygous	Paternal
5	United States	c.166G>A	p.Gly56Arg	2	Heterozygous	Paternal
		693+1G>A ^e	p.?	Intron 8	Heterozygous	Unknown ^f
		815-27T>C ^d		Intron 9	Heterozygous	Paternal
6	Netherlands	c.166G>A	p.Gly56Arg	2	Heterozygous	Maternal
		c.579A>C	p.Leu193Phe	7	Heterozygous	Paternal
		c.815-27T>C ^d		Intron 9	Heterozygous	Maternal
7 ^g	Australia	c.166G>A	p.Gly56Arg	2	Heterozygous	Paternal
		240 kb deletion (exon 1-4); 137 kb duplication (exon 7)		1-4 and 7	Heterozygous	Maternal
		c.815-27T>C ^d		Intron 9	Heterozygous	Paternal

^a Nomenclature according to HGVS (<http://www.hgvs.org/mutnomen>)

^b *NUBPL* reference sequence: NM_025152.2.

^c We could not confirm if this mutation was homozygous or hemizygous because no parental DNA or fibroblasts of the patient was available for study.

^d For the three transcripts generated in the presence of the c.815-27T>C mutation see Tucker et al., 2012.¹⁵

^e Affects an essential nucleotide of the splice donor site, which probably leads to skipping of exon 10.

^f Maternal DNA not available.

^g Previously published patient.^{14,15}

Biochemical analysis

We performed biochemical analysis of *NUBPL* and complex I assembly with the fibroblasts of patients 3 and 4. The *NUBPL* signals obtained in both patients were severely decreased as compared with the control (Figure 2, A). Both complex I in-gel activity and the amount of fully assembled complex I were decreased in both patients as compared with the control (Figure 2, B), which is compatible with the 50% to 60% reduction of complex I activity measured spectrophotometrically (table e-4). We performed 2-dimensional BN/SDS-PAGE analysis to investigate the effect of mutated *NUBPL* on the assembly of the peripheral arm of complex I, which contains the Fe-S clusters. We observed that the amount of fully assembled complex I was decreased in both patients (Figure 2, C), consistent with the findings from the BN analysis (Figure 2, B). Moreover, no subassemblies of the peripheral arm of complex I were present in the patients' fibroblasts, in contrast to the control cells (Figure 2, C).

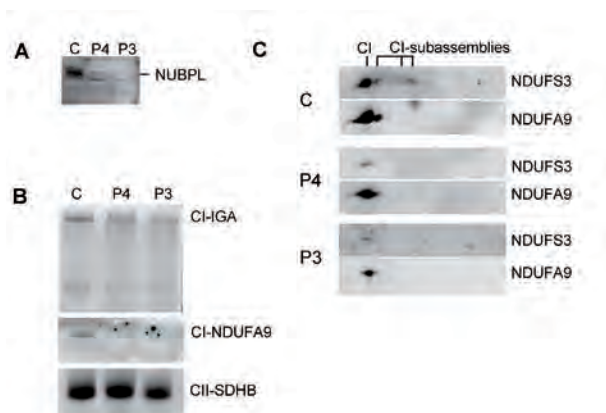


Figure 2. Biochemical analysis of mutated *NUBPL*.

NUBPL and complex I protein levels and assembly were analyzed in fibroblasts of patients 3 (P3) and 4 (P4) and control (C). Western blot analysis showed a decreased amount of *NUBPL* in patients' fibroblasts (A). Complex I analysis in patients' fibroblasts by in-gel activity assay (CI-IGA) (upper panel) and BN-PAGE, by using an antibody against complex I subunit NDUF9 (middle panel), or against complex II subunit SDHB, serving as a loading control (lower panel). Patients had a reduced activity of complex I compared with controls (upper panel), and a reduced amount of complex I (middle panel) (B). Analysis of complex I assembly by 2-dimensional BN/SDS-PAGE in fibroblasts of the patients and control, using complex I antibodies against NDUF3 and NDUF9. Fully assembled complex I (CI) was reduced in the patients. Complex I assembly intermediates (CI-subassemblies) of the peripheral arm were not detected in the patients, in contrast to the control (C). BN = blue native; PAGE = polyacrylamide gel electrophoresis; SDS = sodium dodecyl sulfate.

DISCUSSION

In this study, we show that the combination of disease definition by MRI pattern analysis and whole-exome sequencing can provide a rapid molecular diagnosis in a small group of patients with the same rare, unclassified leukoencephalopathy of suspected mitochondrial origin. All of our patients harbor mutations in *NUBPL*, involved in mitochondrial respiratory chain complex I assembly.^{20,21}

The MRI pattern observed in the present patients is unique and has not been described in any other disorder of mitochondrial or other origin.²² The early stages are characterized by a combination of abnormalities involving the cerebellar cortex and deep cerebral white matter and corpus callosum. On follow-up, the corpus callosum and cerebral white matter abnormalities improve and disappear in some patients. In contrast, the cerebellar abnormalities are progressive and brainstem abnormalities appear. One patient with *NUBPL* mutations has been published before with little clinical information and no MRIs (patient 7).¹⁴ We were able to retrieve his MRI and confirmed that the abnormalities fit perfectly within the pattern observed in the other patients. While preparing this manuscript, an additional patient with *NUBPL* mutations was published.²³ His MRI at 23 years showed severe cerebellar abnormalities and signal changes of the

basis pontis and pyramids of the medulla, characteristic for the late disease stage.²³

We used whole-exome sequencing as a first genetic approach to identify the associated gene. Although highly sensitive in detecting genetic variants, filtering and interpretation of gene variants remain challenging. To selectively reduce the number of variants, specific clues can be used for choosing the correct filters. In our patients, MRI features suggested a mitochondrial disease: multifocal and confluent white matter lesions, rarefied at the center, surrounded by a rim of abnormal but solid tissue, restricted diffusion in these solid rims, additional gray matter abnormalities, patchy contrast enhancement, and elevated lactate in affected brain areas.²² Our suspicion was substantiated by biochemical evidence of complex I deficiency in all tested patients. In suspected mitochondrial disorders, public mitochondrial databases, such as mitocarta,²⁴ can substantially reduce the number of candidate genes. However, filtering should be done with caution because not all variants may be detected, such as the insertion of patient 2. Our filter included all genes that contained just one or more variants in both patients. If the filter had been more stringent, *NUBPL* would have been missed.

Besides the c.166G>A missense mutation, the intronic c.815–27T>C branch-site mutation was present on the same allele in all patients. Functional in vitro studies have shown that the c.815–27T>C variant possesses more pathogenic qualities than the c.166G>A missense mutation. Overexpression of *NUBPL* protein carrying the missense mutation is able to fully complement complex I activity in an *NUBPL*-deficient cell line, while the intronic branch-site variant results in aberrant splicing of *NUBPL* mRNA,¹⁵ which was also confirmed by us (data not shown). The intronic branch-site variant has been found in approximately 1 of 60 controls (1000 Genomes database). Considering the rarity of the disease, it remains inconclusive whether the c.815–27T>C variant is pathogenic in its own right, or acts in synergy with the c.166G>A variant.

All tested patients have a complex I deficiency in muscle and fibroblasts, ranging between 83% and 27% of the lowest reference value. There appears to be no correlation between the residual complex I activity levels and the severity of the clinical phenotype, as has been documented before for other complex I defects.³

Protein analysis of fibroblasts of patients 3 and 4 shows that the mutations in *NUBPL* result in severely decreased *NUBPL* protein levels. Furthermore, consistent with the proposed role in complex I assembly, the decreased *NUBPL* protein levels result in a decreased complex I activity. *NUBPL* is a chaperone involved in the iron-sulfur cluster assembly in complex I.²⁰ Complex I contains 7 iron-sulfur clusters, associated with 5 different subunits (NDUFS1, -S7, -S8, -V1, and -V2), which are located in the peripheral

arm of the complex.²⁵ NDUF57 and -S8 assemble relatively early in the assembly pathway, and defects in these subunits usually do not result in accumulation of assembly intermediates, in contrast to defects in NDUFV1, -V2, and -S1. We observed no accumulation of assembly intermediates of the peripheral arm in our patients and conclude that NUBPL is at least involved in early assembly of the iron-sulfur clusters within the subunits NDUF57 or -S8 in the peripheral arm of complex I.

The 2 previously reported patients with *NUBPL* mutations were published as single cases with little clinical information and in the first case without MRIs.^{14,23} The consequence of such publications is that the disease phenotype remains uncertain and diagnosis in new patients is difficult. In this study, we demonstrate that *NUBPL* mutations are associated with a consistent and recognizable MRI pattern that is pathognomonic for the disease. If present in a new patient, no further studies are warranted; sequence analysis of *NUBPL* is the single necessary test.

REFERENCES

1. Schiffmann R and van der Knaap MS. Invited article: an MRI-based approach to the diagnosis of white matter disorders. *Neurology* 2009;72:750-759.
2. Loeffen JL, Smeitink JA, Trijbels JM, et al. Isolated complex I deficiency in children: clinical, biochemical and genetic aspects. *Hum Mutat* 2000;15:123-134.
3. Distelmaier F, Koopman WJ, van den Heuvel LP, et al. Mitochondrial complex I deficiency: from organelle dysfunction to clinical disease. *Brain* 2009;132:833-842.
4. Tucker EJ, Compton AG, Calvo SE, Thorburn DR. The molecular basis of human complex I deficiency. *IUBMB Life* 2011;63:669-677.
5. van der Knaap MS, Breiter SN, Naidu S, Hart AA, Valk J. Defining and categorizing leukoencephalopathies of unknown origin: MR imaging approach. *Radiology* 1999;213:121-133.
6. Leegwater PA, Vermeulen G, Konst AA, et al. Subunits of the translation initiation factor eIF2B are mutant in leukoencephalopathy with vanishing white matter. *Nat Genet* 2001;29:383-388.
7. Leegwater PA, Yuan BQ, van der Steen J, et al. Mutations of MLC1 (KIAA0027), encoding a putative membrane protein, cause megalencephalic leukoencephalopathy with subcortical cysts. *Am J Hum Genet* 2001;68:831-838.
8. Scheper GC, van der Kloot T, van Andel RJ, et al. Mitochondrial aspartyl-tRNA synthetase deficiency causes leukoencephalopathy with brain stem and spinal cord involvement and lactate elevation. *Nat Genet* 2007;39:534-539.
9. Zara F, Biancheri R, Bruno C, et al. Deficiency of hyccin, a newly identified membrane protein, causes hypomyelination and congenital cataract. *Nat Genet* 2006;38:1111-1113.
10. Steenweg ME, Ghezzi D, Haack T, et al. Leukoencephalopathy with thalamus and brainstem involvement and high lactate 'LTBL' caused by EARS2 mutations. *Brain* 2012;135:1387-1394.
11. Steenweg ME, Pouwels PJ, Wolf NI, van Wieringen WN, Barkhof F, van der Knaap MS. Leukoencephalopathy with brainstem and spinal cord involvement and high lactate: quantitative magnetic resonance imaging. *Brain* 2011;134:3333-3341.
12. Ku CS, Naidoo N, Pawitan Y. Revisiting Mendelian disorders through exome sequencing. *Hum Genet* 2011;129:351-370.
13. Wolf NI, Seitz A, Harting I, et al. New pattern of brain MRI lesions in isolated complex I deficiency. *Neuropediatrics* 2003;34:156-159.
14. Calvo SE, Tucker EJ, Compton AG, et al. High-throughput, pooled sequencing identifies mutations in NUBPL and FOXRED1 in human complex I deficiency. *Nat Genet* 2010;42:851-858.
15. Tucker EJ, Mimaki M, Compton AG, McKenzie M, Ryan MT, Thorburn DR. Next-generation sequencing in molecular diagnosis: NUBPL mutations highlight the challenges of variant detection and interpretation. *Hum Mutat* 2012;33:411-418.
16. Janssen AJ, Trijbels FJ, Sengers RC, et al. Spectrophotometric assay for complex I of the respiratory chain in tissue samples and cultured fibroblasts. *Clin Chem* 2007;53:729-734.
17. Janssen AJ, Trijbels FJ, Sengers RC, et al. Measurement of the energy-generating capacity of human muscle mitochondria: diagnostic procedure and application to human pathology. *Clin Chem* 2006;52:860-871.
18. Rodenburg RJ. Biochemical diagnosis of mitochondrial disorders. *J Inher Metab Dis* 2011;34:283-292.
19. Calvaruso MA, Smeitink J, Nijtmans L. Electrophoresis techniques to investigate defects in oxidative phosphorylation. *Methods* 2008;46:281-287.
20. Sheftel AD, Stehling O, Pierik AJ, et al. Human ind1, an iron-sulfur cluster assembly factor for respiratory complex I. *Mol Cell Biol* 2009;29:6059-6073.
21. Bych K, Kerscher S, Netz DJ, et al. The iron-sulphur protein Ind1 is required for effective complex I assembly. *EMBO J* 2008;27:1736-1746.
22. van der Knaap MS and Valk J. *Magnetic Resonance of Myelination and Myelin Disorders*. Heidelberg: Springer; 2005.
23. Tenisch EV, Lebre AS, Grevent D, et al. Massive and exclusive pontocerebellar damage in mitochondrial disease and NUBPL mutations. *Neurology* 2012;79:391-
24. Pagliarini DJ, Calvo SE, Chang B, et al. A mitochondrial protein compendium elucidates complex I disease biology. *Cell* 2008;134:112-123.
25. Sazanov LA and Hinchliffe P. Structure of the hydrophilic domain of respiratory complex I from *Thermus thermophilus*. *Science* 2006;311:1430-1436.

SUPPLEMENTAL MATERIAL METHODS

Whole-Exome sequencing

Genomic DNA was extracted by standard methods. Exonic targets were enriched by using the SeqCap EZ Human Exome Library v3.0 kit (Nimblegen), and subsequently sequenced as 100 base pair paired-end reads on a HiSeq2000 (Illumina, San Diego, CA). The BWA tool (v 0.5.9) (<http://bio-bwa.sourceforge.net>) was used for read alignment to the human genome assembly hg19. Detection of single-nucleotide variants (SNVs) and small insertions and deletions (indels) was performed with Varscan v2.2.5 (<http://varscan.sourceforge.net>). Variants were annotated with Annovar (<http://www.openbioinformatics.org/annovar>). Novelty of variants was determined using public single nucleotide polymorphism databases, including dbSNP132 (<http://www.ncbi.nlm.nih.gov/projects/SNP>) and the 1000 Genomes project (release November 2010). Pathogenicity of variants was predicted with Polyphen-2(<http://genetics.bwh.harvard.edu/pph2/index.shtml>).

Table e-1. MRI Findings

Patient number	1	2	3	4	5	6	7 ^{a1}
MRIs (ages in years)	1 (8)	3 (1½, 2½, 12)	1 (7)	3 (2, 2½, 5½)	1 (1½)	1 (1)	
Early MRI	no early MRI		no early MRI				
Cerebral WM abn ^a , aspect		+, extensive, both confluent and multifocal		+, limited, confluent	+, extensive, both confluent and multifocal	+, extensive, both confluent and multifocal	+, extensive, both confluent and multifocal
Predominance cerebral WM abn.		frontoparietal, deep		frontal, deep	frontoparietal, deep	frontoparietal, deep	frontal, deep
Sparing cerebral WM		periventricular and subcortical WM rim, occipital and temporal WM, central part corona radiata		almost all cerebral WM spared	periventricular and subcortical rim, occipital and temporal WM, central part corona radiata	periventricular and subcortical WM, occipital and temporal areas	periventricular and subcortical WM, parietal, occipital and temporal areas incl. central part corona radiata
Corpus callosum genu abn.		+		+	+	+	+
Corpus callosum body abn.		+, except fibers connecting pericentral cortex		-	+, except fibers connecting pericentral cortex	+	+, except fibers connecting pericentral cortex
Corpus callosum splenium abn.		+, except central fibers		+, only central fibers	+	+	+, except central fibers
Internal/external capsule abn.		-		-	-	-	-
Swelling of abn. WM		+		+	+	+	+
Rarefaction of abn. WM ^b		+		+, abn. frontal WM and genu	small areas in abn. WM	+, all areas in abn. WM	no FLAIR
Cysts ^c		-		-	-	-	no FLAIR
Cerebral cortex signal abn.		-		-	-	-	-
Basal nuclei signal abn.		-		-	-	-	-
Thalamus signal abn.		-		-	-	-	-
Cerebral atrophy		-		-	-	-	-
Cerebellar WM signal abn.		+, subcortical WM		+, subcortical WM	+, subcortical WM	+, directly subcortical WM	+, subcortical WM

Table e-1. MRI Findings continued

Patient number	1	2	3	4	5	6	7 ^{ei}
Hilus dentate nucleus abn.	-	-	-	-	-	-	-
Cerebellar cortex signal abn.	+ , inf. part relatively spared	+ , inf. part relatively spared	-	+ , inf. part relatively spared	+ , inf. part relatively spared	+ , inf. part relatively spared	+
Dentate nucleus signal abn.	-	-	-	-	-	-	-
Cerebellar atrophy	-	-	-	-	-	-	-
Cerebellar peduncles abn.	-	-	-	-	-	-	+ , only middle
Midbrain signal abn.	-	-	-	-	-	-	-
Pons signal abn.	-	-	-	-	-	-	-
Medulla signal abn.	-	-	-	-	-	-	-
Brain stem atrophy	-	-	-	-	-	-	-
Abnormal myelination	-	-	-	-	-	+ , delayed	-
Contrast enhancement	-	multiple small areas in cerebral WM	-	-	-	no contrast given	multiple small areas in cerebral WM and corpus callosum
Restricted diffusion ^d	-	no diffusion-weighted images	-	borders of genu and frontal WM lesions	mainly edges of WM lesions	cerebellar cortex, hippocampus, abn. cerebral WM, incl. corpus callosum	not done
Elevated lactate in MRS	-	elevated lactate in abn. WM	-	not done	not done	elevated lactate abn. WM	not done

Table e-1. MRI Findings continued

Patient number	1	2	3	4	5	6	7 ^{a1}
Most recent MRI (late MRI)							
Cerebral WM abn ^a , aspect	+, limited, multifocal	+, limited, multifocal	-	+, limited to one strip			
Predominance cerebral WM abn.	frontoparietal, deep	frontoparietal, deep	-	frontal, deep			
Sparing cerebral WM	subcortical WM	central part corona radiata, periventricular and subcortical WM	all cerebral WM is spared	remainder of cerebral WM is spared			
Corpus callosum genu abn.	severe atrophy	+, mild	-	+, only central strip affected			
Corpus callosum body abn.	severe atrophy	-	-	-			
Corpus callosum splenium abn.	severe atrophy	+, central part affected, rim not affected	subtle abn.	-			
Internal/external capsule abn.	-	-	-	-			
Atrophy of affected WM	+, corpus callosum	+, corpus callosum	-	-			
Rarefaction of affected WM ^b	+, abn. WM	no FLAIR	-	-			
Cysts ^c	+, abn. WM	no FLAIR	-	-			
Cerebral cortex signal abn.	-	-	-	-			
Basal nuclei signal abn.	-	-	-	-			
Thalamus signal abn.	-	-	-	-			
Cerebral atrophy	-	-	-	-			
Cerebellar WM signal abn.	+	+	+	+			
Hilus dentate nucleus signal abn.	+	-	-	-			
Cerebellar cortex signal abn.	+	+	+, inf. part. relatively spared	+			
Dentate nucleus signal abn.	+	+	+	+			
Cerebellar atrophy	+, severe	+, severe	+	+			

Table e-1 . MRI Findings continued

Patient number	1	2	3	4	5	6	7 ^{a1}
Cerebellar peduncles signal abn.	+, inferior, middle and superior	+, only middle	+, middle and inferior	+, only middle			
Midbrain signal abn.	+, anterior part	-	-	-			
Pons signal abn.	+, basis pontis	+, basis pontis	+, basis pontis	+, basis pontis			
Medulla signal abn.	+, pyramids	-	+, pyramids	+, pyramids			
Brain stem atrophy	+, pons	+, basis pontis	+, basis pontis	+, pons			
Abnormal myelination	-	-	-	-			
Contrast enhancement	not done	not done	-	cerebellar cortex and basis pontis			
Restricted diffusion ^d	not done	not done	-	-			
Elevated lactate in MRS	not done	not done	elevated lactate affected cerebellar WM	elevated lactate affected cerebellar WM			

^a Signal abnormalities were defined as an abnormally high signal on T₂-weighted images.

^b White matter rarefaction was defined as T₂-hyperintense white matter areas with low signal on FLAIR or proton density, but not as low as cerebrospinal fluid.

^c Cysts were defined as T₂-hyperintense white matter areas with low signal on FLAIR or proton density, as low as cerebrospinal fluid.

^d Restricted diffusion was assessed using the apparent diffusion coefficient to avoid false positive results due to the shine-through effect.

^e Calvo *et al.*, 2010

WM = white matter; abn = abnormalities; ant = anterior part; F = frontal; P = parietal; excl = excluding; inf = inferior; MRS = magnetic resonance spectroscopy; FLAIR = fluid-attenuated inversion recovery.

Table e-2. Clinical Findings

Patient number	1	2	3 ^a	4 ^a	5	6	7 ^{a1}
Patient and family characteristics:							
Gender	m	m	f	f	f	f	m
Year of birth	1994	1997	2002	2004	2005	2008	2001
Siblings (affected/unaffected/otherwise affected)	1/0/0	0/0/0	1/2/0	1/2/0	0/0/0	0/0/0	0/2/0
Consanguinity of the parents	no	no	no	no	no	no	no
Pregnancy/delivery	normal	CS due to breech position	CS due to fetal distress	elective CS	normal	cocaine use	normal
Abnormalities neonatal period	no	no	no	no	no	no	no
Initial motor development	normal	normal	normal	normal	normal	normal	delayed
Initial mental development	normal	normal	normal	normal	normal	normal	normal
Unsupported walking (years)	never	yes (1,3 years)	yes (8 years)	never	never	never	never
Presentation							
Age at presentation (months)	8	8	13	13	21	10	24
Signs at presentation	loss of motor abilities	instable sitting, truncal ataxia	inability to walk	inability to walk	loss of cruising, truncal instability, decreased speech, abnormal eye movements	loss of head control, frequent falling, ataxia, feeding difficulties	delay in sitting and crawling
Preceding event	no	no	no	no	immunization	viral infection 4 weeks before onset of regression	no
Course over time							
Further signs	ataxia increasing spasticity, flexion contractures	progressive ataxia, dysarthria, mild spasticity	ataxia, dysarthria	ataxia, dysarthria	ataxia, dysarthria, leg spasticity, loss of smooth pursuit, rotatory nystagmus	ataxia, dysarthria, increasing spasticity of legs	ataxia, speech problems, increasing spasticity, myopathy, flexion contractures, increasing difficulties feeding and swallowing

Table e-2. Clinical Findings continued

Patient number	1	2	3 ^a	4 ^a	5	6	7 ^{a1}
Episodes of regression	continuous regression at onset	no	no	transient loss of motor and speech skills, swallowing difficulties following gastroenteritis	no	transient loss of motor and speech skills and increased epileptic activity	periods of regression of speech and mobility
Continuing development	no	yes	yes	Yes	yes	yes	yes
Behavioral problems	no	no	mild anxiety, obsessional	anxiety, obsessional, oppositional, tantrums	anxiety	initially irritable, later normal	no
Epilepsy	no	no	no	No	no	suspected at disease onset; at the time of regression bilateral central epileptic discharges	suspected, but EEG normal
Outcome	deceased at 9 years	several steps without support, low-normal cognitive capability	unsupported walking, fine motor delay; functioning at close to normal level at school	walking with support, fine motor delay; functioning 2-3 years behind normal school level	walking with support, functioning at near normal cognitive level	walking with support, 3-4 word sentences	no unsupported walking

Table e-2. Clinical Findings continued

Patient number Physical examination	1	2	3 ^a	4 ^a	5	6	7 ^{a1}
Age at latest examination (years)	9	11.6	8.6	7.1	7.25	4.2	11.5
Intelligence	very low level	low-normal	Full Scale WISC-IV 5 th percentile	Full Scale WISC-IV 1 st percentile	normal	very low level	normal
Dysmorphic features	no	no	no	No	no	no	no
Internal organs	normal	normal	normal	Normal	normal	normal	normal
Head circumference	+ 2 SD	-1 SD	0 SD	0 SD	0 SD	0.5 SD	0 SD
Height	n.d.	< -2.5 SD	-3 SD	-2 SD	-2 SD	0.6 SD	0 SD
Vision, eye movements	no eye contact, alternating esotropia, nystagmus, left facial palsy	normal, rotatory nystagmus	normal, nystagmus, strabismus	normal, nystagmus, strabismus	normal, rotatory nystagmus absence of smooth pursuit	normal, normal	normal, vertical and horizontal nystagmus
Hearing	n.e.	normal	normal	Normal	normal	normal	normal
Language	no	normal	normal	short sentences	normal	4-word sentences	normal
Dysarthria	n.a.	yes	yes	Yes	yes	yes	yes
Dysphagia, tube feeding	yes	no	no	in the past	no	yes, tube feeding	yes, PEG
Axial tone	decreased	decreased	mildly decreased	Decreased	decreased	decreased	decreased
Arms							
Tone	increased	decreased	mildly decreased	Decreased	mildly increased	increased	decreased
Reflexes	brisk	increased	mildly increased	Increased	increased	increased	decreased
Spasticity	yes	mild	no	No	mild	no	yes
Ataxia	no	yes	yes	Yes	yes	yes	yes
Extrapyramidal signs	no	no	no	No	no	no	no
Legs							
Tone	increased	increased	mildly decreased	mildly decreased	mildly increased	increased	decreased
Reflexes	brisk	increased	mildly increased	Increased	increased	increased	decreased
Babinski signs	yes	yes	yes	Indeterminate	yes	yes	no
Spasticity	yes	mild	no	No	mild	yes	yes
Ataxia	yes	yes	yes	Yes	yes	yes	yes
Extrapyramidal signs	no	no	no	No	no	no	no
Highest motor milestone	unsupported sitting	walking without support	walking, running without support	walking with support	walking with support	walking with support	no unsupported walking
Quality of walking	n.a.	severely ataxic	ataxic	severely ataxic	ataxic and spastic	ataxic and spastic	ataxic and spastic

^aSiblings

^{a1}Calvo *et al.*, 2010

m = male; f = female; n.d = not done; n.e = not evaluable; n.a = not applicable; CS = caesarian section; PEG = percutaneous endoscopic gastrostomy



Table e-3. Laboratory Results

Patient number	1	2	3 ^a	4 ^a	5	6	7 ^{a,1}
Laboratory general & metabolic							
Routine hematology panel	normal	normal	normal	normal	normal	normal	normal
Routine biochemistry panel	normal	normal	normal	normal	normal	normal	normal
Plasma lactate	normal	inconsistently elevated (2.13-3.0 mmol/L)	normal	borderline (2.0-2.6mmol/L)	elevated (4.7 mmol/L)	inconsistently elevated (1.5 - 6.0 mmol/L)	normal
CSF lactate	not done	elevated (4.89 mmol/L)	not done	elevated (5.4 mmol/L)	not done	elevated (3.6 mmol/L)	elevated (5.2 mmol/ and 2.7 mmol/L)
Plasma amino acids	not done	not done	normal	normal	normal	normal	normal
Urine organic acids	normal	normal	normal	normal	normal	normal	normal
Lysosomal enzymes (if yes, which)	not done	ASA, β-gal, Hex A, Hex A+B normal	hexosaminidase normal	not done	ASA, β-gal, Hex A, Hex A+B, B mannosidase, fucosidase normal	not done	normal
Muscle							
LM, EM	LM: Fiber type 2 atrophy Slight increased lipids in fiber type 1 Minimally increased subsarcolemmal oxidative activity	normal	normal	normal	not done	normal	20% RRF
Respiratory chain complexes (1-5)							
Respiratory chain complexes (1-5)	not done	not done	normal	complex I deficiency	not done	complex I deficiency ^b	complex I deficiency
Fibroblasts							
Respiratory chain complexes (1-5)	not done	complex I deficiency 27% of the lowest reference value ^b	complex I deficiency 64% of the lowest reference value ^b	complex I deficiency 56% of the lowest reference value ^b	not done	complex I deficiency 83% of the lowest reference value ^b	complex I deficiency
Pyruvate dehydrogenase complex	not done	normal ^b	normal ^b	borderline low ^b	not done	normal ^b	not done

Table e-3. Laboratory Results continued

Patient number	1	2	3 ^a	4 ^a	5	6	7 ^{a1}
Genetics	not done	mtDNA sequencing in muscle and blood; <i>NDUFS1</i> , <i>NDUFS2</i> , <i>NDUFS7</i> , <i>NDUFS8</i> : normal	mtDNA sequencing in muscle: normal	mtDNA sequencing not done	mtDNA sequencing in blood; <i>NDUFV1</i> , <i>NDUFS4</i> , <i>NDUFS8</i> , <i>NSUFS1</i> , <i>NSUFS7</i> , <i>POLG1</i> : normal	mtDNA sequencing in muscle: normal	normal male karyotype

^a Siblings

^{a1} Detailed phosphorylation measurements are outlined in table e-4. ^{a1} Calvo *et al.*, 2010

EM = electron microscopy; LM = light microscopy; ASA = arylsulfatase A; β -gal = β -galactosidase; Hex A, β = hexosaminidase A; Hex B = β -hexosaminidase A+B;

mtDNA = mitochondrial DNA; RRF = ragged red fibers

Table e-4. Oxidative Phosphorylation Measurements in Fibroblasts and Muscle

fibroblasts	complex I ^a	complex II ^a	complex III ^a	complex II-III ^b	complex IV ^b	complex V ^c			
patient 2	75	888	1050	575	784	750			
patient 3	179	746	1552	463	554	1478			
patient 4	156	810	1286	551	642	1299			
patient 6	232	889	1242	495	825	1192			
reference values	279-1076	375-2692	623-3534	269-781	288-954	480-2705			
muscle	complex I ^b	complex II ^b	complex III ^b	complex II-III ^b	complex IV ^b	complex V ^c	ATP production ^d	1- ¹⁴ C-pyruvate + malate oxidation ^e	1- ¹⁴ C-pyruvate + carnitine oxidation ^f
patient 6	67	331	2630	327	1185	293	10,6	1,15	2,53
reference values	100-401	335-749	2200-6610	300-970	810-3120	161-711	34,5-67,5	3,90-6,94	3,89-7,28

Measurements were performed in mitochondria-enriched fractions of cultured fibroblasts (patients 2-4,6) or a muscle biopsy (patient 6) using spectrophotometry and radiochemical detection. All fibroblasts showed an isolated complex I deficiency. In the muscle biopsy of patient 6, the oxidation rate of pyruvate in the presence of malate was stronger reduced than in the presence of carnitine, which is indicative of a primary oxidative phosphorylation deficiency. In this muscle sample, a complex I deficiency was present. In addition, complex II activity was near the lowest reference value, while complex II-III was within the reference range. The latter excludes a primary complex II deficiency. All other enzyme activities were normal. Normalization was as follows: ^a, mU/U complex I; ^b, mU/U complex II; ^c, mU/U citrate synthase; ^d, mU/h.mU citrate synthase.

Table e-5. Whole-Exome Sequencing Statistics and Variant Filtering

Sequencing statistics								
	Patient 2				Patient 4			
Reads	81339929				66851011			
Reads on target	51525484				43191717			
Percent	63.35%				64.61%			
Target bases with dept:	>10x	>15x	>20x	30X	>10X	>15X	>20X	30X
	97.6%	95.9%	94%	86%	96.6%	94.3%	90.9%	79.9%
Variant filtering								
	Patient 2				Patient 4			
Total SNVs and indels	22.207				21.776			
Excluding segmental duplications	19.063				18.607			
Novelty filter ^a								
Excluding variant frequency < 0.01 in 1000 Genomes project					636			
Excluding variants present in dbSNP132					534			
Mitochondrial localization								
Variants in genes present in MitoCarta database ^b					14			
Inheritance								
Genes with ≥ 1 variants present in both patients 2 and 4					1 gene: <i>NUBPL</i>			
Identified genes								
Gene	Patient	c.DNA ^c	Protein	Conservation ^d	Pathogenicity ^e			
<i>NUBPL</i>	2	c.166G>A ^f	p.Gly56Arg	Up to <i>C. elegans</i>	probably damaging			
<i>NUBPL</i>	4	c.166G>A ^f	p.Gly56Arg	Up to <i>C. elegans</i>	probably damaging			
		c.313G>T	p.Asp105Tyr	Up to <i>C. elegans</i>	probably damaging			

Nomenclature according to HGVS (<http://www.hgvs.org/mutnomen>)

^a Novelty of variants was determined using public single nucleotide polymorphism databases, including dbSNP132 (<http://www.ncbi.nlm.nih.gov/projects/SNP>) and the 1000 Genomes project (release November 2010).

^b The MitoCarta human inventory (<http://www.broadinstitute.org/pubs/MitoCarta/index.html>) is a collection of 1013 nuclear and mtDNA genes encoding proteins with strong support of mitochondrial localization based on homolog to mouse MitoCarta genes.^{e2}

^c *NUBPL* reference sequence NM_025152.

^d Conservation was analyzed in 12 species, including human, chimp, macaque, rat, mouse, dog, cow, chicken, frog, tetraodon, fruit fly, *C. elegans*.

^e Pathogenicity of variants was predicted with Polyphen-2 (<http://genetics.bwh.harvard.edu/pph2/index.html>).

^f The c.166G>A transition in *NUBPL* was previously reported in a patient with complex I deficiency. This patient harbored a 240 Kb deletion spanning exon 1-4 and a 137 Kb duplication involving exon 7 on the other allele.^{e1, e3} This patient was subsequently included in this study (patient 7).

SNVs = single-nucleotide variants; indels = insertion and deletions.

E-REFERENCES

- e1. Calvo SE, Tucker EJ, Compton AG et al. High-throughput, pooled sequencing identifies mutations in *NUBPL* and *FOXRED1* in human complex I deficiency. *Nat Genet.* 2010;42:851-858.
- e2. Pagliarini DJ, Calvo SE, Chang B et al. A mitochondrial protein compendium elucidates complex I disease biology. *Cell.* 2008;134:112-123.
- e3. Tucker EJ, Mimaki M, Compton AG et al. Next-generation sequencing in molecular diagnosis: *NUBPL* mutations highlight the challenges of variant detection and interpretation. *Hum Mutat.* 2012;33:411-4.

Chapter 10

Recessive *ITPA* mutations cause an early-infantile encephalopathy

Sietske H. Kevelam, Jürgen Bierau, Ramona Salvarinova, Shakti Agrawal, Tomas Honzik, Dennis Visser, Marjan M. Weiss, Gajja S. Salomons, Truus E.M. Abbink, Quinten Waisfisz, and Marjo S. van der Knaap

Ann Neurol 2015;78:649–658.



ABSTRACT

Objective

To identify the etiology of a novel, heritable encephalopathy in a small group of patients.

Methods

Magnetic resonance imaging (MRI) pattern analysis was used to select patients with the same pattern. Homozygosity mapping and whole exome sequencing (WES) were performed to find the causal gene mutations.

Results

Seven patients from 4 families (2 consanguineous) were identified with a similar MRI pattern characterized by T_2 signal abnormalities and diffusion restriction in the posterior limb of the internal capsule, often also optic radiation, brainstem tracts, and cerebellar white matter, in combination with delayed myelination and progressive brain atrophy. Patients presented with early infantile onset encephalopathy characterized by progressive microcephaly, seizures, variable cardiac defects, and early death. Metabolic testing was unrevealing. Single nucleotide polymorphism array revealed 1 overlapping homozygous region on chromosome 20 in the consanguineous families. In all patients, WES subsequently revealed recessive predicted loss of function mutations in *ITPA*, encoding inosine triphosphate pyrophosphatase (ITPase). ITPase activity in patients' erythrocytes and fibroblasts was severely reduced.

Interpretation

Until now *ITPA* variants have only been associated with adverse reactions to specific drugs. This is the first report associating *ITPA* mutations with a human disorder. ITPase is important in purine metabolism because it removes noncanonical nucleotides from the cellular nucleotide pool. Toxicity of accumulated noncanonical nucleotides, leading to neuronal apoptosis and interference with proteins normally using adenosine triphosphate/guanosine triphosphate, probably explains the disease. This study confirms that combining MRI pattern recognition to define small, homogeneous patient groups with WES is a powerful approach for providing a fast diagnosis in patients with an unclassified genetic encephalopathy.

10

INTRODUCTION

The diagnostic process of rare childhood encephalopathies is challenging, and numerous cases remain without a specific diagnosis.¹ Inborn errors of metabolism are among the main causes of childhood encephalopathies.² Screening for metabolic disorders in blood, urine, and cerebrospinal fluid may lead to clues for a specific metabolic defect.^{3,4} However, not all metabolic defects cause measurable metabolite abnormalities. Because of this, in combination with the heterogeneous presentations, rarity of these disorders, and unidentified underlying genetic defects for several metabolic disorders, a definitive diagnosis is often delayed or not established.^{3,5} The utilization of next generation sequencing techniques facilitates the discovery of new genes for unclassified disorders, but also allows the identification of new phenotypes related to known gene defects.⁶⁻⁸

In this study, we used MRI pattern analysis to define a phenotypically homogeneous group of 7 patients from 4 families with a novel, early onset, devastating encephalopathy. Extensive metabolic tests did not pinpoint a specific inborn metabolic defect in these patients. By means of whole exome sequencing (WES), we ascertained the mutated gene. The gene encodes an enzyme central in purine metabolism that was not known to be associated with a human metabolic disorder.

PATIENTS AND METHODS

Patients

Seven patients from 4 unrelated families were included, who shared a distinct pattern of magnetic resonance imaging (MRI) abnormalities. These patients were identified from our MRI database of >3,000 cases with an unclassified leukoencephalopathy using MRI pattern recognition analysis.⁹ Inclusion criteria were striking T₂ hyperintensity and diffusion restriction of the posterior limb of the internal capsule in young infants. S.H.K. and M.S.v.d.K. evaluated the MRIs according to a previously published protocol.⁹ The MRIs were obtained at different centers, on different magnetic resonance machines and with different protocols, precluding quantitative analyses. Clinical information and laboratory investigations were retrospectively reviewed.

Informed consent

We received approval from the ethical standards committee for our gene identification research on patients with unclassified leukoencephalopathies at the VU University Medical Center in Amsterdam. All guardians of the patients participating in this study gave written consent.

Single nucleotide polymorphism array analysis

Parents of 2 of the 4 families were consanguineous. Two affected (Patients 2 and 3) and 2 unaffected children from 1 consanguineous family and 1 affected child (Patient 4) from the second consanguineous family were subjected to single nucleotide polymorphism (SNP) array analysis (CytoScan HD array; Affymetrix, Santa Clara, CA) according to the manufacturer's protocol, to identify homozygous overlapping regions using Nexus version 7 (BioDiscovery, Hawthorne, CA).

WES

WES was performed on DNA from Patients 3, 4, and 5, using a SeqCap EZ Human Library v3.0 kit (Roche NimbleGen, Madison, WI) on a HiSeq2000 (Illumina, San Diego, CA). Data analysis was performed as previously described.¹⁰ Coverage of at least 30× was reached for > 89% of the targeted regions. Average sequencing depth ranged between 91 and 99.5 reads. Variant filtering was executed under the hypothesis of an autosomal recessive inheritance model. All rare variants with a minor allele frequency (MAF) of <1% in public databases, including dbSNP137 (<http://www.ncbi.nlm.nih.gov/projects/SNP>), 1000 Genomes Project (release of February 2012), and Exome Variant Server (EVS), NHLBI Exome Sequencing Project (ESP5400 release; <http://evs.gs.washington.edu/EVS/>) and absent from our in-house exome control database, that were present in at least 2 patients and located in the identified overlapping homozygous region, were selected. Synonymous variants that were not located adjacent to the consensus splice site were excluded.

Validation and detection of *ITPA* variants

Validation and segregation of the identified *ITPA* variants (NM_033453.3) with WES were performed using the standard Sanger sequencing protocol. Primers were designed using Primer 3, V.0.4.0.¹¹ In Patient 6, all 8 exons and exon–intron boundaries of the human *ITPA* gene were amplified by polymerase chain reaction using suitable primers (available upon request) and analyzed by Sanger sequencing.

Inosine triphosphate pyrophosphatase activity and nucleotides in patients' erythrocytes and fibroblasts

Inosine triphosphate pyrophosphatase (ITPase or ITPA) activity was investigated in erythrocytes of Patient 7 as previously described.¹² Briefly, 15 μ l of erythrocyte lysate was incubated with 40mM inosine triphosphate (ITP), 1mM $MgCl_2$ in 100mM Tris pH 8.5 in a final volume of 200 μ l. The formation of inosine monophosphate (IMP) from ITP was quantified by using ion pair ultra-performance liquid chromatography method with ultraviolet (UV) detection. ITPase activity was expressed as moles of IMP formed from ITP in 1 hour per mole of hemoglobin. ITPase activity in cultured fibroblasts was investigated for Patients 2, 5, and 6. The cell pellets were lysed in MilliQ water by sonication. After centrifugation, the supernatant was used for the enzyme activity assay described above. Measurement of protein content was determined using the bicinchoninic acid assay.

Nucleotides were measured in cultured fibroblasts of Patients 2, 5, and 6. Briefly, cells were harvested by trypsinization and washed once with phosphate-buffered saline. The cell pellet was resuspended in 200 μ l 0.4M ice cold perchloric acid and left to stand on melting ice for 10 minutes. The lysate was then cleared by centrifugation and the supernatant was neutralized by adding 8 μ l 5M K_2CO_3 and centrifuged after standing for 10 minutes on melting ice. The protein pellet was dissolved in 2M KOH overnight at ambient temperature and used for protein determination. The supernatant was stored at $-80^\circ C$ until analysis. Prior to analysis, the supernatant was thawed and cleared using a SpinX centrifuge filter. Packed erythrocytes of Patient 7 were extracted in a similar way. Nucleotides were quantified using an ion-pairing reverse-phased ultra-performance liquid chromatography method on a LC-18 column and a buffer system consisting of 25mM $di-NH_4PO_4$ and 8mM tetrabutylammonium bisulfate with acetonitrile. Detection was done using UV detection, and a single point calibration was used.

RESULTS

Radiological findings

Detailed MRI findings are provided in Supplementary Table 1 and illustrated in Figure 1. Early MRIs, obtained at ≤ 2 months of age, did not show any abnormalities apart from lack of the normal T_2 -hypointense spot representing the myelinated pyramidal tracts in the posterior limb of the internal capsule. MRIs performed between 4 and 8 months showed delayed myelination and mild to moderate cerebral atrophy. On all MRIs, the pyramidal tracts in the posterior limb of the internal capsule or the entire posterior

limbs were strikingly T₂ hyperintense (see Figure 1). Several patients showed additional involvement of the pyramidal tracts in the midbrain, middle and inferior cerebellar peduncles, and cerebellar white matter. Diffusion-weighted images and apparent diffusion coefficient maps, obtained in all patients except Patient 1, invariably showed restricted diffusion in the posterior limb of the internal capsule and in some patients also in the optic radiation and midbrain. One patient also had restricted diffusion in the medulla oblongata and deep cerebellar white matter. Later follow-up images, obtained at 13, 16, 19, and 31 months, revealed severely delayed cerebral myelination and progressive cerebral atrophy. The T₂ signal abnormalities of the posterior limb of the internal capsule and the diffusion restriction improved.

Clinical presentation

Detailed clinical characteristics and laboratory findings are provided in Supplementary Table 2. Most patients were rather small for gestational age at birth. All patients presented shortly after birth with a severe and progressive microcephaly, seizures, and failure to achieve developmental milestones. After disease onset, no or very little further cognitive and motor development occurred. All patients continued to have epilepsy, and in 2 patients the epilepsy became refractory. Three patients had cardiac involvement, either a dilated cardiomyopathy or electrocardiographic abnormalities. The 3 patients of Family I had cataract. At last clinical examination, head circumference of all patients was far below –2 standard deviations from normal, and height and weight were below normal in most patients.

All patients had a severe encephalopathy with hypotonia and swallowing difficulties, requiring tube feeding in 3 patients. Six patients died; age at death was between 10 months and 2.5 years. Patient 2 died due to cardiac failure, and Patients 3, 4, 5, and 7 due to respiratory insufficiency, caused by a respiratory tract infection in Patients 3, 4, and 5, and status epilepticus in Patient 7. Patient 6, currently 3 years old, is still alive. Extensive metabolic testing in blood and urine, including purine and pyrimidine urinary excretion profiles using high-performance liquid chromatography, showed no abnormalities. Genetic tests for several mitochondrial disorders revealed no pathogenic mutations. A muscle biopsy in Patients 2 and 3 showed inconclusive abnormalities in respiratory chain function.

Genetic analysis

A large overlapping homozygous region on the tip of chromosome 20 (genomic coordinates 0–6.832.683; hg19) was identified by SNP array analysis (data not shown). Subsequently, WES with additional variant filtering led to the identification of a single candidate gene located in this region: *ITPA* [MIM 147620] encoding the enzyme ITPase,

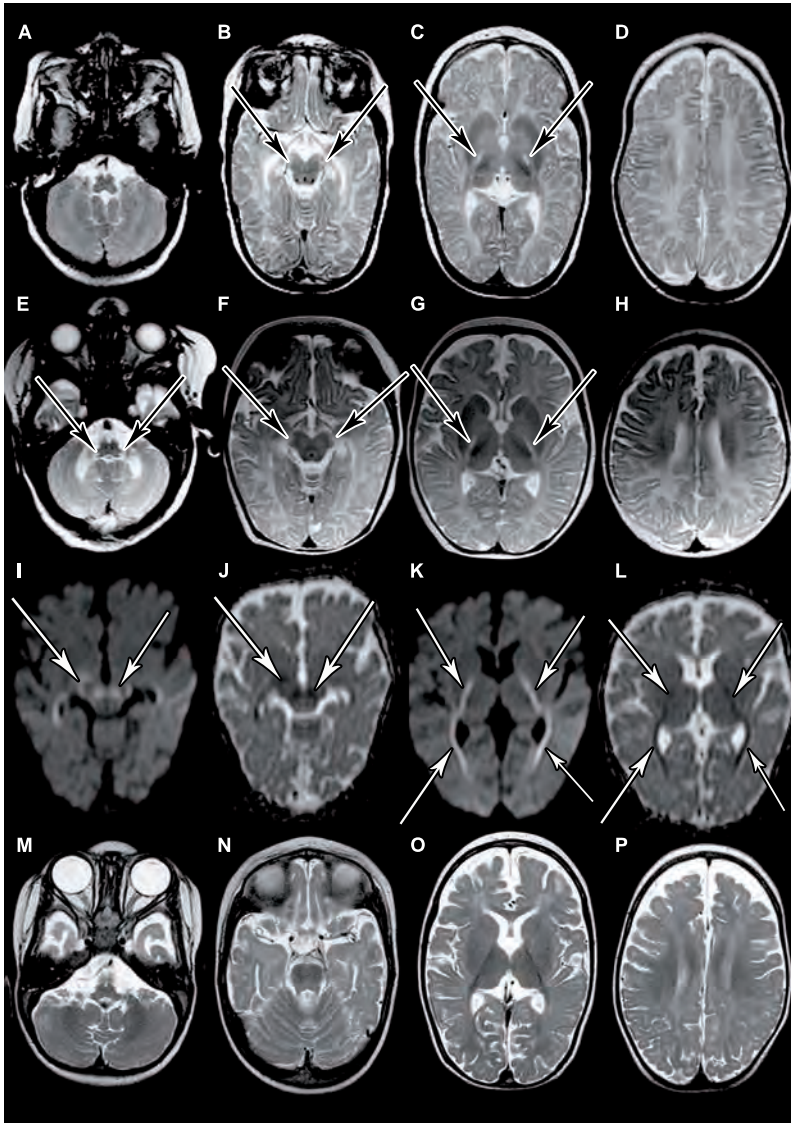


Figure 1. Illustration of the typical magnetic resonance imaging (MRI) pattern.

(A–L) Initial axial T_2 -weighted magnetic resonance (MR) images of Patient 2 (A–D, age=6 months) and Patient 4 (E–H, age=4 months), and diffusion-weighted images (DWIs; I, K) and apparent diffusion coefficient (ADC) images of Patient 4 (J, L). (M–P) Late follow-up MR images of Patient 6 (age=16.5 months). On initial MR images, overall myelination is delayed and there is mild cerebral atrophy (A–H). Patients show T_2 hyperintensity of the pyramidal tracts in the posterior limb of the internal capsule (C, arrows), or whole posterior limb of the internal capsule (G, arrows). Involvement of the cerebral peduncles and pyramidal tracts within the cerebral peduncles is shown in B and F, respectively (arrows). Signal abnormalities can also be observed in the pyramids of the medulla, inferior cerebellar peduncles (E, arrows), and deep cerebellar white matter (E). The DWIs show an increased signal in the cerebral peduncles (I, left arrow) and decussation of the superior cerebellar peduncles (I, right arrow) in the midbrain (I), and posterior limb of the internal capsule and optic radiation (K, arrows), with a corresponding low signal on the ADC images (J and L, arrows), indicating restricted diffusion of these areas. Follow-up MR images show resolution of the T_2 signal abnormalities (M–O), but increasing cerebral atrophy and severe delayed cerebral myelination (O, P).

in which all patients had a rare or novel homozygous variant (summarized in Table 1). The 3 affected siblings of Family I harbored a novel homozygous deletion of 1,874 base pairs (bp), spanning exon 5, and extending both in intron 4 and intron 5 (c. 264-607_295 + 1267del). The deletion of exon 5 is predicted to result in an out-of-frame transcript. Patients 4 and 7 (siblings) both had a homozygous nonsense mutation: c.452G>A predicting a premature stop codon, p.(Trp151*). This variant has been reported once in a single heterozygous carrier in the EVS database (MAF of 0.009%). Patient 5 was homozygous for the c.532C>T; p.(Arg178Cys) missense mutation. This mutation is predicted to be deleterious by the 3 prediction software programs used, and the amino acid arginine is highly conserved at this position. Sanger sequencing was used to confirm each mutation and additionally revealed in Patient 6 a homozygous duplication of 8bp, c.359_366dupTCAGCACC, resulting in a frameshift (p.[Gly123Serfs*104]). This frameshift mutation is predicted to result in an extended protein of 225 amino acids instead of 194 amino acids. This mutation has been found in a heterozygous state in 1 Bulgarian individual with an ITPase activity of 30% measured in erythrocytes.¹³ The locations of the Arg178Cys and the Trp151* mutation in the dimeric crystal structure of ITPA are shown in Figure 2, A. In all patients, analysis of parental DNA confirmed that both parents carried 1 mutant allele.

ITPase activity and nucleotides in patients' erythrocytes and fibroblasts

ITPase activity in erythrocytes of Patient 7 was severely decreased (0.02 mol IMP/[mol Hb/h]), corresponding to 0.4% residual activity. This corresponds to the residual activity found in erythrocytes of *ITPA* c.94C>A homozygous individuals.¹⁴ There was evident accumulation of ITP, but also of inosine diphosphate (IDP), the latter likely to be the result of spontaneous degradation of ITP during transport of the sample (Table 2). The fibroblasts of all 3 tested patients (2, 5, and 6) showed severely decreased ITPase activity, corresponding to 0.3 to 5.3% of residual activity compared to control fibroblasts, without accumulation of ITP or IDP (see Table 2). No changes were observed for adenosine triphosphate (ATP), guanosine triphosphate (GTP), uridine triphosphate, and cytidine triphosphate. The intracellular concentrations of the diphosphates adenosine diphosphate (ADP), guanosine diphosphate, uridine diphosphate, and cytidine diphosphate were higher than in the controls; however, no change in the adenine energy charge ($[ATP + 0.5 ADP]/[ATP + ADP + \text{adenosine monophosphate}]$) was observed.

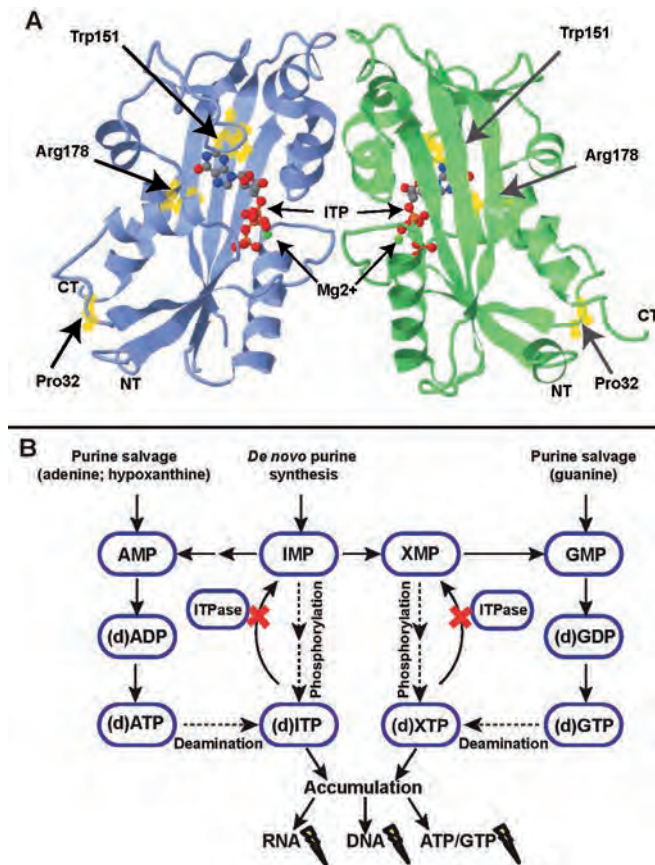


Figure 2. Inosine triphosphate pyrophosphatase (ITPase) structure and its function within purine metabolism.

(A) Dimeric structure of human ITPase with bound substrate. The monomers are shown in blue and green, with the dimer interface located in the center of the figure. The helices, β -sheets, and loops are shown as ribbons, arrows, and threads, respectively. The locations of N- and C-termini are labeled (NT, CT, respectively). Inosine triphosphate (ITP) is shown as red, gray, brown, and blue spheres. The 2 magnesium molecules are depicted as green spheres. The mutated residues Trp151 and Arg178 present in ITPA encephalopathy patients and the residue Pro32 are highlighted as yellow spheres. Note that both the Trp151 and Arg178 residues are in a crucial position at the substrate binding site. The Pro32 residue is located in the loop connecting the helix α 1 and β -strand. This figure was generated with FirstGlance in Jmol using data from the Protein Database (PDB code 2J4E²⁷). Mg²⁺ = magnesium molecule. (B) Purine metabolism and formation of the noncanonical nucleotides (deoxy)inosine triphosphate (ITP) and (deoxy)xanthosine triphosphate (XTP). In the purine metabolic pathway, purine nucleosides and nucleotides can be synthesized by 2 different routes; by de novo synthesis via inosine monophosphate (IMP) or by recycling of the components (salvage pathway).³ Regardless of which pathway is used, the result is that adenosine mono- and triphosphate (AMP/ATP), guanosine mono- and triphosphate (GMP/GTP), and their deoxy forms dAMP/dATP and dGMP/dGTP are formed. The noncanonical nucleotides ITP and xanthosine triphosphate XTP are produced as byproducts due to deamination of ATP and GTP and by phosphorylation of IMP and xanthosine monophosphate (XMP). ITPase plays a central role in conversion of ITP and XTP back to IMP/XMP. Absence of ITPase leads to accumulation of ITP and XTP. The same cycle is seen for the deoxy forms inosine triphosphate dITP and dXTP. Accumulation of these noncanonical nucleotides can potentially cause damage to DNA and RNA and interfere with enzymes that normally use ATP or GTP.^{23,25} An event or enzyme is indicated with an arrow. The putative pathways for deamination and phosphorylation producing (d)ITP/XTP are shown with dotted arrows. Gray arrows indicate pathways not present in erythrocytes. ADP = adenosine diphosphate; GDP = guanosine diphosphate.

Table 1. Overview of ITPA mutations

Family	Patient number	Ethnic background	c.DNA	Type of mutation	Deduced effect	Exon	State	SIFT (score 0-1) ^a	PolyPhen-2 (score 0-1) ^b	Mutation Taster ^c (score 0-1)	Minor allele Frequency in controls ^d
I	1, 2, 3	Moroccan	c. 264-607_295+1267del	deletion	p.?	5	homozygous	n.a.	n.a.	n.a.	not reported
II	4, 7	Pakistani	c.452G>A	nonsense	p.(Trp151*) ^e	7	homozygous	n.a	n.a.	n.a.	0.009% ^f
III	5	First Nation, Canada	c.532C>T	missense	p.(Arg178Cys)	8	homozygous	deleterious (0.0)	probably damaging (1.0)	disease causing (0.99)	not reported
IV	6	Roma	c.359_366dup TCAGCACC	frameshift	p.(Gly123Serfs*104)	6	homozygous	n.a.	n.a.	n.a.	1 Bulgarian (heterozygous) ^g

^a SIFT score: 0 = deleterious, 1 = benign.

^b PolyPhen-2 score: 0 = benign, 1 = probably damaging.

^c MutationTaster score = probability of the prediction. Probability close to 1 indicates high security of the prediction.

^d Minor allele frequency determined using the 1000 Genome database, Exome Variant Server database, and dbSNP137 database (see Patients and Methods).

^e Nonsense RNA-mediated decay.

^f This mutation has been reported once in a heterozygous individual in the EVS database (total tested individuals = 5,379).

^g Mutation reported in 1 Bulgarian individual in heterozygous state.¹³

n.a. = not applicable; SIFT = Sorting Intolerant From Tolerant.

Table 2. Inosine triphosphate pyrophosphatase activity and accumulation of nucleotides in erythrocytes and fibroblasts

Genotype (homozygous)	Erythrocytes		Fibroblasts	
	mol IMP/ (mol Hb x hour)	Residual activity (%)	ITP (μmol/mmol Hb)	IDP (μmol/g protein)
c.452G>A	0.02	0.4	11.43	2.8
Controls (n=5)	5.23 ± 2.04 SD	100	not detectable	not detectable
c.94C>A	0.00 ± 0.05 SD ¹⁴			
Genotype (homozygous)	mmol IMP/ (mg x hour)	Residual activity (%)	ITP (μmol/g protein)	IDP (μmol/g protein)
c.264-607_295+1267del	0.02	0.3	not detectable	not detectable
c.532C>T	0.36	5.3	not detectable	not detectable
c.359_366dupTCAGCACC	0.23	2.9	not detectable	not detectable
Controls (n=5)	6.86 ± 2.51 SD	100	not detectable	not detectable

Hb = hemoglobin; IDP = Inosine diphosphate; IMP = inosine monophosphate; ITP = Inosine triphosphate; SD = standard deviation.

DISCUSSION

This study shows that recessive mutations in *ITPA* are associated with a human disorder that we call ITPA encephalopathy. The patients have a devastating encephalopathy, characterized by progressive microcephaly, lack of development, and seizures, in combination with variable cardiac abnormalities and cataract. The patients share a distinct brain MRI pattern characterized by a high T₂ signal and restricted diffusion in the posterior limb of the internal capsule in combination with delayed myelination and progressive cerebral atrophy. More variable are T₂ signal abnormalities and diffusion restriction in the optic radiation, mesencephalic pyramidal tracts or entire cerebral peduncles, hilus of the dentate nucleus, cerebellar peduncles, and cerebellar white matter.

Patients with Krabbe disease share essential features of this MRI pattern, including early and striking signal abnormalities in the pyramidal tracts in the posterior limb of the internal capsule and hilus of the dentate nucleus.¹⁵ These patients, however, typically have a stripelike pattern in the affected cerebral hemispheric white matter and do not show restricted diffusion of the same tracts as seen in ITPA encephalopathy patients.¹⁵ Clinically, they have more prominent motor dysfunction, no or less severe epilepsy, and no cardiac involvement. Galactocerebrosidase enzyme activity was normal in our patients, ruling out Krabbe disease. The combination of restricted diffusion and involvement of the brainstem could be considered suggestive for a mitochondrial disorder. Extensive metabolic testing, however, did not pinpoint a specific mitochondrial defect in our patients.

Using WES in combination with homozygosity mapping, we identified 4 different very rare or novel homozygous mutations in *ITPA*, encoding ITPase, in all 7 included patients. This enzyme has an important function in purine metabolism by removing noncanonical triphosphate purines ITP and xanthosine triphosphate (XTP) and their deoxy forms (dITP/dXTP) from the cellular pool.¹⁶⁻¹⁸ The metabolic pathway of purine metabolism is represented in Figure 2, B. Inborn errors of purine metabolism are rare, and currently 13 enzyme defects in purine synthesis, catabolism, and salvage have been identified, causing very different disorders.³

Until now, *ITPA* mutations have not been associated with a human disorder. However, several polymorphisms have been identified in *ITPA*, most of which result in a partial or even complete loss of ITPase activity in erythrocytes.¹⁹⁻²² The variant of highest interest is a missense mutation in exon 2, c.94C>A (p.[Pro32Thr], rs1127354), because individuals

homozygous for this mutation have undetectable ITPase activity and accumulation of ITP in erythrocytes.^{19,22} This lack of ITPase activity in erythrocytes is not associated with a clinical disease, but may cause adverse drug reactions to thiopurine prodrugs, mercaptopurines, and methotrexate, with signs such as leukopenia, pancreatitis, influenzalike symptoms, and rash.^{23,24} In striking contrast, *Itpa* knockout mice have a severe neurological and cardiac phenotype with early demise.²⁵

The *ITPA* mutations observed in our patients cause a severe reduction of ITPase activity in erythrocytes and fibroblasts compared to controls, with accumulation of ITP in erythrocytes, but not in fibroblasts. These results are comparable to those obtained in *Itpa* knockout mice, where ITP accumulation was found in erythrocytes only and not in the organs, including the clinically affected heart.²⁵ Behmanesh et al hypothesized that accumulating ITP is spent in its incorporation into RNA by the process of transcription, which does not occur in erythrocytes; this hypothesis was supported by the detection of accumulation of IMP in mouse heart RNA.²⁵ Also, de novo purine synthesis and conversion of IMP to guanosine monophosphate is not possible in erythrocytes.²⁶ Consequently, the p.(Pro32Thr) variant and the *ITPA* encephalopathy-associated mutations cannot be discriminated by their effects on ITPase activity and accumulation of nucleotides in fibroblasts and erythrocytes. Like our patients, *Itpa* null mice have a severe disorder, with motor dysfunction, growth retardation, abnormal breathing, cardiomyopathy, and a maximum life span of 2 weeks.²⁵ Considering that the p.(Pro32Thr) variant is not associated with a clinical disease outside increased sensitivity for specific drugs, it is unlikely that p.(Pro32Thr) abolishes ITPase activity in all cell types. The explanation for the apparent discrepancy between similar loss of ITPase activity in erythrocytes in *ITPA* encephalopathy patients, *Itpa* knockout mice, and homozygous p.(Pro32Thr) individuals and dissimilar clinical phenotype may be that *ITPA* expression¹⁸ and the effect of the mutations vary between tissues. Lack of availability of tissue from *ITPA* encephalopathy patients and *Itpa* knockout mice (personal communication) precluded further studies. It should, however, be noted that the *ITPA* encephalopathy-associated mutations and the p.(Pro32Thr) variant have markedly different predicted effects on the ITPase protein. Three of the *ITPA* encephalopathy mutations (c. 264-607_295 + 1267del, c.359_366dupTCAGCACC, and c.452G>A) are predicted to result in loss of the C-terminal part of ITPase affecting the conserved NTPase/HAM1 domain. The fourth mutation, a c.532C>T missense change, replaces the amino acid arginine at position 178 by a cysteine. In the ITPase crystal structure, arginine178 is located in the binding pocket at a crucial position to allow substrate specificity.²⁷ In vitro studies confirmed that arginine178 is essential for normal ITPase activity and substrate specificity.²⁸ By contrast, the p.(Pro32Thr) variant is located in the loop connecting helix α 1 and β -strand 2, far

10

away from the active site and binding pocket of ITPase (see Figure 2, A). Numerous studies have focused on the putative pathogenic mechanism of the p.(Pro32Thr) variant on ITPase functioning, but no definitive answer has been established.²⁹⁻³² In vitro studies revealed that the p.(Pro32Thr) mutated enzyme is catalytically active.^{31,32} Splicing studies of *ITPA* and structural analysis of the p.(Pro32Thr) ITPase protein showed that a combination of mis-splicing of exon 2 and 3, chaperone binding, and proteasomal degradation of the unstable ITPase protein could cause the reduced ITPase enzyme activity in erythrocytes.^{29,30}

ITPA is highly expressed in brain, with the highest levels in neurons.³³ In normal cells, the noncanonical nucleotides ITP/XTP and their deoxy forms dITP/dXTP are present at low levels as byproducts generated by deamination of ATP/GTP and dATP/dGTP or by phosphorylation of IMP (see Figure 2, B). Removal of ITP/XTP and dITP/dXTP by ITPase is crucial for normal cell function; if not converted, they accumulate and can be incorporated into DNA and RNA instead of the canonical nucleotides, which causes genetic damage and programmed cell death.^{25,34} In the case of ITPase deficiency, accumulation of ITP/dITP or XTP/dXTP could be toxic for neurons and result in neuronal apoptosis. Additionally, because ITP possesses a molecular structure similar to that of ATP and GTP, it could interfere with enzymes normally utilizing ATP or GTP, like the cardiac sarcomeres and G-proteins.^{23,34,35} Inappropriate regulation of G-protein signal transduction can influence a variety of cellular processes in the brain, including neural plasticity, neurotransmitter release, and astrocyte glucose metabolism.^{35,36}

A question is how to unify this information with our patient phenotypes. Whereas the initial MRI abnormalities involve white matter structures, the subsequent prominent cerebral atrophy suggests a neuronal degenerative disease process. The clinical picture with the severe epilepsy and total lack of development also indicates a neuronal degenerative disorder rather than a leukodystrophy. The best explanation fitting both clinical and MRI findings is early onset neuronal degeneration with Wallerian degeneration of the associated white matter tracts. Wallerian degeneration is associated with diffusion restriction in the early stages.³⁷ Strikingly, in ITPA encephalopathy patients, early myelinating structures are preferentially affected, including the posterior limb of the internal capsule, brainstem tracts, and tracts to the primary visual cortex and motor cortex. Tracts become myelinated when they become functionally active. So, early myelinating tracts attached to the most active neurons are most susceptible for ITPase deficiency.

Most of our patients with *ITPA* encephalopathy had homozygous predicted loss of function mutations, and it is therefore not surprising that their clinical phenotype is similar to that of *Itpa* knockout mice.²⁵ *ITPA*-related disease is most likely a spectrum, with the now described disease at the most severe end of the spectrum and the p.(Pro32Thr) variant-related phenotype at the mildest end of the spectrum. This implies that phenotypes of intermediate severity are to be expected with milder, slower, and perhaps more selective neuronal loss and less severe cardiac disease. We expect that WES and whole genome sequencing will identify more patients with *ITPA* mutations and that the gap between these two extremes will be filled.

In conclusion, this study shows that MRI pattern recognition in combination with WES is a powerful tool to provide a rapid diagnosis in patients with an unknown, rare, neurological disorder of metabolic origin, when screening of metabolites in body fluids fails. It also shows the strength of focusing on groups of patients, although small, over focusing on single patients or single families for WES, as the *ITPA* gene variants of our patients would not have been considered pathogenic based on the known lack of clinical effect of the p.(Pro32Thr) variant in the presence of zero enzyme activity in erythrocytes. The recognition of possible future *ITPA* encephalopathy patients remains difficult, because the characteristic MRI pattern with striking T₂ hyperintensity and diffusion restriction of the posterior limb of the internal capsule is present for a few months only and may be lacking in milder phenotypes, and assessment of ITPase activity and ITP accumulation in erythrocytes does not discriminate between benign and pathogenic mutations.

REFERENCES

- Schiffmann R and van der Knaap MS. Invited article: an MRI-based approach to the diagnosis of white matter disorders. *Neurology* 2009;72:750-759.
- Vanderver A. Tools for diagnosis of leukodystrophies and other disorders presenting with white matter disease. *Curr Neurol Neurosci Rep* 2005;5:110-118.
- Bierau J and Šebesta I. Purine and Pyrimidine disorders. In: *Physician's guide to the Diagnosis, Treatment, and Follow-up of Inherited Metabolic Diseases*. Berlin Heidelberg: Springer; 2014. p. 641-660.
- Saudubray J and Charpentier C. Clinical Phenotypes: Diagnosis/Algorithms. In: *The Online Metabolic & Molecular Bases of Inherited Disease*. McGraw-Hill Companies; 2014.
- Balasubramaniam S, Duley JA, Christodoulou J. Inborn errors of purine metabolism: clinical update and therapies. *J Inher Metab Dis* 2014;37:669-686.
- Dallabona C, Diodato D, Kevelam SH, et al. Novel (ovario) leukodystrophy related to AARS2 mutations. *Neurology* 2014;82:2063-2071.
- Kevelam SH, Rodenburg RJ, Wolf NI, et al. NUBPL mutations in patients with complex I deficiency and a distinct MRI pattern. *Neurology* 2013;80:1577-1583.
- Simons C, Wolf NI, McNeil N, et al. A de novo mutation in the beta-tubulin gene TUBB4A results in the leukoencephalopathy hypomyelination with atrophy of the basal ganglia and cerebellum. *Am J Hum Genet* 2013;92:767-773.
- van der Knaap MS, Breiter SN, Naidu S, Hart AA, Valk J. Defining and categorizing leukoencephalopathies of unknown origin: MR imaging approach. *Radiology* 1999;213:121-133.
- Wolf NI, Salomons GS, Rodenburg RJ, et al. Mutations in RARS cause hypomyelination. *Ann Neurol* 2014;76:134-139.
- Koressaar T and Remm M. Enhancements and modifications of primer design program Primer3. *Bioinformatics* 2007;23:1289-1291.
- Bierau J, Bakker JA, Lindhout M, van Gennip AH. Determination of ITPase activity in erythrocyte lysates obtained for determination of TPMT activity. *Nucleosides Nucleotides Nucleic Acids* 2006;25:1129-1132.
- Atanasova S, Shipkova M, Svinarov D, et al. Analysis of ITPA phenotype-genotype correlation in the Bulgarian population revealed a novel gene variant in exon 6. *Ther Drug Monit* 2007;29:6-10.
- Bierau J, Bakker JA, Schippers JA, et al. Erythrocyte inosine triphosphatase activity is decreased in HIV-seropositive individuals. *PLoS One* 2012;7:e30175.
- van der Knaap MS and Valk J. Globoid cell leukodystrophy (krabbe disease). In: *Magnetic Resonance of Myelination and Myelin Disorders*. Heidelberg: Springer; 2005.
- Vanderheiden BS. Purification and properties of human erythrocyte inosine triphosphate pyrophosphohydrolase. *J Cell Physiol* 1979;98:41-47.
- Holmes SL, Turner BM, Hirschhorn K. Human inosine triphosphatase: catalytic properties and population studies. *Clin Chim Acta* 1979;97:143-153.
- Lin S, McLennan AG, Ying K, et al. Cloning, expression, and characterization of a human inosine triphosphate pyrophosphatase encoded by the itpa gene. *J Biol Chem* 2001;276:18695-18701.
- Sumi S, Marinaki AM, Arenas M, et al. Genetic basis of inosine triphosphate pyrophosphohydrolase deficiency. *Hum Genet* 2002;111:360-367.
- Maeda T, Sumi S, Ueta A, et al. Genetic basis of inosine triphosphate pyrophosphohydrolase deficiency in the Japanese population. *Mol Genet Metab* 2005;85:271-279.
- Shipkova M, Lorenz K, Oellerich M, Wieland E, von Ahsen N. Measurement of erythrocyte inosine triphosphate pyrophosphohydrolase (ITPA) activity by HPLC and correlation of ITPA genotype-phenotype in a Caucasian population. *Clin Chem* 2006;52:240-247.
- Bakker JA, Lindhout M, Habets DD, van den Wijngaard A, Paulussen AD, Bierau J. The effect of ITPA polymorphisms on the enzyme kinetic properties of human erythrocyte inosine triphosphatase toward its substrates ITP and 6-Thio-ITP. *Nucleosides Nucleotides Nucleic Acids* 2011;30:839-849.
- Simone PD, Pavlov YI, Borgstahl GE. ITPA (inosine triphosphate pyrophosphatase): from surveillance of nucleotide pools to human disease and pharmacogenetics. *Mutat Res* 2013;753:131-146.
- Zelinkova Z, Derijks LJ, Stokkers PC, et al. Inosine triphosphate pyrophosphatase and thiopurine s-methyltransferase genotypes relationship to azathioprine-induced myelosuppression. *Clin Gastroenterol Hepatol* 2006;4:44-49.

25. Behmanesh M, Sakumi K, Abolhassani N, et al. ITPase-deficient mice show growth retardation and die before weaning. *Cell Death Differ* 2009;16:1315-1322.
26. Dudzinska W, Hlynczak AJ, Skotnicka E, Suska M. The purine metabolism of human erythrocytes. *Biochemistry (Mosc)* 2006;71:467-475.
27. Stenmark P, Kursula P, Flodin S, et al. Crystal structure of human inosine triphosphatase. Substrate binding and implication of the inosine triphosphatase deficiency mutation P32T. *J Biol Chem* 2007;282:3182-3187.
28. Gall AD, Gall A, Moore AC, et al. Analysis of human ITPase nucleobase specificity by site-directed mutagenesis. *Biochimie* 2013;95:1711-1721.
29. Arenas M, Duley J, Sumi S, Sanderson J, Marinaki A. The ITPA c.94C>A and g.IVS2+21A>C sequence variants contribute to missplicing of the ITPA gene. *Biochim Biophys Acta* 2007;1772:96-102.
30. Simone PD, Struble LR, Kellezi A, et al. The human ITPA polymorphic variant P32T is destabilized by the unpacking of the hydrophobic core. *J Struct Biol* 2013;182:197-208.
31. Stepchenkova EI, Tarakhovskaya ER, Spitler K, et al. Functional study of the P32T ITPA variant associated with drug sensitivity in humans. *J Mol Biol* 2009;392:602-613.
32. Herting G, Barber K, Zappala MR, Cunningham RP, Burgis NE. Quantitative in vitro and in vivo characterization of the human P32T mutant ITPase. *Biochim Biophys Acta* 2010;1802:269-274.
33. Behmanesh M, Sakumi K, Tsuchimoto D, et al. Characterization of the structure and expression of mouse Itpa gene and its related sequences in the mouse genome. *DNA Res* 2005;12:39-51.
34. Pang B, McFaline JL, Burgis NE, et al. Defects in purine nucleotide metabolism lead to substantial incorporation of xanthine and hypoxanthine into DNA and RNA. *Proc Natl Acad Sci U S A* 2012;109:2319-2324.
35. Dong JH, Chen X, Cui M, Yu X, Pang Q, Sun JP. beta2-adrenergic receptor and astrocyte glucose metabolism. *J Mol Neurosci* 2012;48:456-463.
36. Hein L. Adrenoceptors and signal transduction in neurons. *Cell Tissue Res* 2006;326:541-551.
37. van der Knaap MS and Valk J. Wallerian Degeneration and Myelin Loss Secondary to Neuronal and Axonal Degeneration. In: *Magnetic Resonance of Myelination and Myelin Disorders*. Heidelberg: Springer; 2005. p. 832-838.

Table e-1. MRI characteristics

Patient / family	1 / I	2 / I	3 / I	4 / II	5 / III	6 / IV	7 / II
Early MRI (≤ 2 months)	not done	1.5 months	not done	10 days	not done	2 months	2 months
Myelination		normal		normal		delayed	delayed
T ₂ signal abnormality of:							
Cerebral white matter		+ , mild swelling, especially in the anterior temporal region		-		+ , mild swelling and inhomogeneous signal	+ , mild swelling
Corpus callosum		-		-		-	-
Internal capsule anterior limb		-		-		-	-
Internal capsule poster limb		no low signal in region of pyramidal tracts		no low signal in region of pyramidal tracts		no low signal in region of pyramidal tracts	no low signal in region of pyramidal tracts
Cerebellar white matter		-		-		-	-
Hilus of the dentate nucleus		+ , hyperintense		+ , hyperintense		+ , hyperintense	+ , hyperintense
Superior cerebellar peduncles		-		-		-	-
Middle cerebellar peduncles		-		-		-	-
Inferior cerebellar peduncles		-		-		-	-
Midbrain		-		-		-	+ , cerebral peduncles
Pons		-		-		-	-
Medulla		-		-		-	+ , pyramids
Cerebral cortex		-		-		-	-
Cerebellar cortex		-		-		-	-
Basal nuclei & thalami		-		-		-	-
Cerebral atrophy		no		no		no	no
Cerebellar atrophy		no		no		no	no
Diffusion restriction		not done		not done		no	pyramidal tracts posterior limb internal capsule
Contrast abnormalities		not done		not done		not done	not done
Magnetic resonance spectroscopy		not done		not done		not done	not done
Extra features		subependymal pseudocyst right		no		no	no

Table e-1. MRI characteristics continued

Patient / family	1 / I	2 / I	3 / I	4 / II	5 / III	6 / IV	7 / II
Intermediate MRI (4-8 months)	8 months	6 months	4.5 months	4 months	4.5 months	8 months	not done
Myelination	delayed	delayed	delayed	delayed	delayed	severe delayed	
T ₂ signal abnormality of:							
Cerebral white matter	-	-	-	-	-	-	-
Corpus callosum	thin	thin	thin	thin	thin	thin	
Internal capsule anterior limb	-	-	-	-	-	-	
Internal capsule posterior limb	+, hyperintense	+, hyperintense	+, hyperintense	+, hyperintense	+, hyperintense	+, pyramidal tracts hyperintense	
Cerebellar white matter	+, hyperintense	-	+, hyperintense	+, hyperintense	-	-	
Hilus of the dentate nucleus	-	+, hyperintense	-	-	-	-	
Superior cerebellar peduncles	-	-	-	-	-	-	
Middle cerebellar peduncles	+, hyperintense	-	+, hyperintense	+, hyperintense	-	-	
Inferior cerebellar peduncles	+, hyperintense	-	+, hyperintense	+, hyperintense	-	-	
Midbrain	+, cerebral peduncles hyperintense	+, cerebral peduncles hyperintense	+, cerebral peduncles hyperintense	+, cerebral peduncles hyperintense	-	-	
Pons	-	-	-	-	-	-	
Medulla	-	-	-	-	-	-	
Cerebral cortex	-	-	-	-	-	-	
Cerebellar cortex	-	-	-	-	-	-	
Basal nuclei & thalami	-	-	-	-	-	-	
Cerebral atrophy	moderate	mild	no	moderate	no	moderate	
Cerebellar atrophy	no	no	no	no	no	no	
Diffusion restriction	not done	posterior limb internal capsule, cerebellar peduncles midbrain	optic radiation, posterior limb internal capsule, pyramidal tracts midbrain, cerebellar white matter	optic radiation, posterior limb internal capsule, cerebellar white matter	optic radiation, posterior limb internal capsule	optic radiation, posterior limb internal capsule, decussation of the superior cerebellar peduncles in the midbrain	
Contrast abnormalities	not done	not done	not done	not done	not done	no	
Magnetic resonance spectroscopy	not done	not done	no lactate elevation	not done	not done	not done	
Extra features	no	no	no	no	no	no	

Table e-1. MRI characteristics continued

Patient / family	1 / I	2 / I	3 / I	4 / II	5 / III	6 / IV	7 / II
Late MRI (> 8 months)	not done	13 months	19 and 31 months	not done	not done	16 months	not done
Myelination		severely delayed	severely delayed			severely delayed	
T ₂ signal abnormality of:							
Cerebral white matter	-	-	-	-	-	-	-
Corpus callosum		thin	thin			thin	
Internal capsule anterior limb	-	-	-	-	-	-	-
Internal capsule posterior limb		+, hyperintense	+, hyperintense at 19 months; - at 31 months			-	
Cerebellar white matter	-	-	-	-	-	-	-
Hilus of the dentate nucleus	-	-	-	-	-	-	-
Superior cerebellar peduncles	-	-	-	-	-	-	-
Middle cerebellar peduncles	-	-	-	-	-	-	-
Inferior cerebellar peduncles	-	-	-	-	-	-	-
Midbrain	-	-	+, cerebral peduncles hyperintense at 19 months; - at 31 months	-	-	-	-
Pons	-	-	-	-	-	-	-
Medulla	-	-	-	-	-	-	-
Cerebral cortex	-	-	-	-	-	-	-
Cerebellar cortex	-	-	-	-	-	-	-
Basal nuclei & thalami	-	-	-	-	-	-	-
Cerebral atrophy		severe	severe			moderate	
Cerebellar atrophy		slight	no at 19 months, mild at 31 months			no	
Diffusion restriction		no	no			no	
Contrast enhancement		not done	not done			no	
Magnetic resonance spectroscopy		no lactate elevation	no lactate elevation			not done	
Extra features		no	no			no	

+ indicates abnormal T₂ signal; - indicates no T₂ signal abnormalities.

Table e-2. Clinical characteristics

Patient / family	1 / I	2 / I	3 / I	4 / II	5 / III	6 / IV	7 / II
Gender	male	male	male	female	male	female	male
Year of birth	1998	2000	2003	2010	2010	2012	2014
Siblings (affected / unaffected/ otherwise affected)	3/2/0	3/2/0	3/2/0	1/0/0	0/0/1	0/2/0	1/0/0
Consanguinity parents	yes	yes	yes	yes	no	unknown	yes
Pregnancy, delivery, neonatal period admission at 2 weeks due to feeding problems	admission at 2 weeks due to feeding problems	intrauterine growth retardation	intrauterine growth retardation	admissions due to feeding problems; clieromegaly and low cortisol in neonatal period, temporary hydrocortisone treatment	preclampsia, intrauterine growth retardation, decreased fetal movements	intrauterine growth retardation, after birth no sucking reflex, tube feeding	spontaneous premature delivery (35 weeks)
Birth weight (SD for gestational age)	3.3 kg (-0.5 SD)	2.4 kg (<2 SD)	2.9 kg (-1.8 SD)	3.3 kg (-0.5 SD)	2.3 kg (-1.5 SD)	2.4 kg (-1.8 SD)	2.2 kg (-0.5 SD)
Head circumference at birth	unknown	33 cm (-2 SD)	33.8 cm (-1.5 SD)	34 cm (-1 SD)	unknown	33 cm (-1.5 SD)	32 cm (-0.5 SD)
Presentation							
Age at presentation (months)	5	3	4	3	4.5	at birth	2
Signs at presentation	microcephaly, developmental delay	microcephaly, seizures, developmental delay	microcephaly, seizures	microcephaly, seizures, developmental delay	microcephaly, seizures, developmental delay, hypotonia	irritable, tremors of limbs, high pitched voice, failure to thrive	seizures manifesting as apneas, developmental delay
Preceding event	no	no	no	no	no	no	no
Course over time							
Developmental progress	no	no	no	no	minimal	no	not available
Other signs	hypotonia	hypotonia	hypotonia	hypotonia	hypotonia	microcephaly, hypotonia	hypotonia
Feeding problems	yes	yes, also vomiting	yes, also vomiting	severe, nasogastric tube	severe, PEG-tube	severe, PEG-tube at 3 months	no
Epilepsy	severe	severe	severe	severe, refractory	severe	severe, refractory from 5 months	severe
Ophthalmologic problems	cataract	cataract	cataract	no	cone dystrophy, flat looking macula with atrophic area around it	no	not investigated
Cardiac involvement	not investigated	dilated cardiomyopathy	abnormal axis and repolarization defect on ECG	ECG normal, no cardiac ultrasound performed	mild pulmonary stenosis; slightly prolonged QT interval	normal ECG and cardiac ultrasound	normal cardiac ultrasound
Outcome	death at 10 months, specific cause unknown	death at 2.5 years due to dilated cardiomyopathy	death at 2.11 years due to respiratory infection	death at 6 months due to respiratory infection	death at 2 years 2 months due to seizures and respiratory infection	alive	death at 10 months due to respiratory failure secondary to status epilepticus

Table e-2. Clinical characteristics continued

Patient / family	1 / I	2 / I	3 / I	4 / II	5 / III	6 / IV	7 / II
Age latest examination (months)	8	28	30	5	26	25	3 (corrected age 2)
Head circumference (SD)	40.5 cm (-3.5 SD)	43.5 cm (-4 SD)	40.5 cm (-5.5 SD)	36.5 cm (-4 SD)	43.8 cm (-3.5 SD)	39 cm (-6 SD)	34.8 cm (-3.5 SD)
Weight (SD)	6.6 kg (-2.5 SD)	13 kg (0 SD)	12.5 kg (-0.5 SD)	5.4 kg (-2 SD)	7.9 kg (-3.9 SD)	6.5 kg (-5.1 SD)	2.8 kg (-6.5 SD)
Height (SD)	68 cm (-1.5 SD)	unknown	87 cm (-1.5 SD)	unknown	76.6 cm (-4 SD)	78 cm (-2.5 SD)	unknown
Dysmorphic features	no	no	no	no	hypotelorism	large and low set ears, micrognathia	no
Development	severely delayed	severely delayed	severely delayed	severe delayed	severely delayed	severely delayed	severely delayed
Vision, eye movements	no eye contact; nystagmus	minimal eye contact; no tracking, convergent strabismus	minimal eye contact, no tracking	never fixed or followed	could follow, myopia, astigmatism	no eye contact, strabismus	never fixed or followed
Hearing	normal	normal	normal	normal	normal	impaired (BAEP)	normal
Axial tone	low, no head control	low, no head control	low, no head control	low	low	low	low
Extremities							
Tone	low	low	low	low	low	low	low
Muscle strength	decreased	no evident paresis	no evident paresis	decreased	decreased	decreased	decreased
Reflexes	normal	areflexia	low	low	brisk	low	normal
Spasticity	no	no	no	no	no	no	lower limbs
Extrapyramidal signs	no	choreoatiform movements	no	choreoatiform movements	no	no	no
Laboratory results							
Plasma lactate	not done	normal	slightly elevated	normal	normal	normal	normal
CSF lactate	not done	normal	not done	normal	normal	normal	normal
Plasma amino acids	normal	not done	normal	normal	normal	normal	normal
Urine organic acids	normal	normal	normal	normal	normal	normal	normal
Lysosomal enzymes	not done	arylsulfatase A, B, galactocerebrosidase, β -galactosidase, α -galactosidase-A, α -glucosidase, sphingomyelinase, chitrosidase: normal	not done	not done	arylsulfatase A, galactocerebrosidase, β -Hexoaminidase, β -galactosidase, α -glucosidase: normal	arylsulfatase-A, galactocerebrosidase, β -Hexoaminidase A, β -galactosidase, chitrosidase: normal	not done

Table e-2. Clinical characteristics continued

Patient / family	1 / I	2 / I	3 / I	4 / II	5 / III	6 / IV	7 / II
Acylcarnitine profile	not done	normal	not done	normal	abnormal consistent with mild CPT-1 deficiency	normal	normal
Transferrin iso-electric focusing	Normal	normal	not done	normal	normal	normal	not done
Very long-chain fatty acids	Normal	normal	not done	slight increase in C24 fatty acids and phytanic acid	normal	normal	normal
Urine purines, pyrimidines (HPLC)	normal	not done	not done	not done	normal	normal	not done
Urine uric acid	not done	not done	normal	not done	not done	normal	not done
Muscle biopsy	not done	yes	yes	not done	yes	not done	not done
Microscopy		normal	normal		nonspecific myopathic abnormalities; type 2 fiber atrophy		
Oxidative phosphorylation		decreased substrate oxidation rates and production of ATP and creatine phosphate; reduced activity of all complexes	mildly decreased substrate oxidation rates and production of ATP and creatine phosphate; mildly reduced complex I and II activity		respiratory chain complexes I, II and IV normal		
Mitochondrial DNA Testing		no abnormalities mitochondrial DNA	no abnormalities mitochondrial DNA				
Fibroblasts							
Oxidative phosphorylation	not done	normal	normal	not done	not done	not done	not done
Genetic testing	normal chromosomes	no pathogenic mutations mitochondrial DNA	not done	no pathogenic mutations mitochondrial DNA, <i>DARS2</i> and <i>Aicardi-Goutières</i> gene panel	no mutations <i>EIF2B1-EIF2B5</i> , <i>GCH1</i> , <i>SPR</i> ; homozygous p.P479L variant in <i>CPT1</i>	MLPA 22q11.1; normal; no mutations <i>NBS1</i> and no pathogenic mutations mitochondrial DNA	no pathogenic mutations in mitochondrial DNA

SD = standard deviation; cm = centimeter; kg = kilogram; PEG = percutaneous endoscopic gastrostomy; ECG = electrocardiogram; CSF = cerebrospinal fluid; MLPA = multiplex ligation dependent probe amplification; HPLC = high performance liquid chromatography; BAEP = brain stem auditory evoked potentials

IV

Update on leukodystrophies

Chapter 11

Update on leukodystrophies: origin, evolution and two revolutions

Sietske H. Kevelam,* Marjan E. Steenweg,* Siddharth Srivastava,
Guy Helman, Sakkubai Naidu, Raphael Schiffmann, Susan Blaser,
Adeline Vanderver, Nicole I. Wolf, and Marjo S. van der Knaap

* These authors share first authorship.

Accepted for publication.



SUMMARY

When we initiated our studies of leukodystrophies in the nineteen eighties, a limited number of disorders were known and no associated gene defects. We estimated then that over 60% of the cases were unclassified. In the following two decades MRI pattern recognition revolutionized the field, allowing definition of numerous novel leukodystrophies. Their genetic defects were usually identified by genetic linkage studies. This process required substantial numbers of cases and many rare disorders remained unclassified. As recently as 2010, 50% of the leukodystrophy patients remained unclassified. Soon after, whole-exome sequencing caused another revolution with an exponential increase in numbers of distinct, genetically determined, ultra-rare leukodystrophies. Results from our retrospective studies concerning three historical cohorts of unclassified leukodystrophy patients indicate that currently at least 80% of the patients can now be molecularly classified. Based on the original definition of leukodystrophies, numerous defects in proteins important in myelin structure, maintenance and function were expected. By contrast, a high percentage of the newly identified gene defects affect the housekeeping process of mRNA translation, shedding new light on white matter pathobiology. With this new information, a myelin focused definition of leukodystrophies is outdated; we propose a further adaption of the definition.

PATHOLOGY ERA

Research on brain white matter disorders started in the eighteen thirties, when the first pathology descriptions of brain disorders appeared. In the subsequent 150 years, diagnosis and classification of brain white matter disorders remained almost exclusively based on pathology. 'Multiple sclerosis' was first defined,^{1,2} after 60 years followed by the definition of 'diffuse sclerosis' to distinguish disorders with diffuse abnormality of the brain white matter from those with multifocal abnormalities.³ The word 'leukodystrophy' was introduced in 1928 for metachromatic leukodystrophy (MLD).⁴ 'Leukodystrophy' comes from the Greek roots leuko= white, dys=lack of, and trophy=growth. Consensus on the definition of leukodystrophies emerged in the nineteen eighties. They were defined as disorders primarily affecting myelin, either directly or through involvement of oligodendrocytes, caused by a genetic defect, and clinically progressive.^{5,6} So, the initial definition of leukodystrophy was myelin-focused. As of today it is this definition that most physicians have in mind when using the word. 'Leukoencephalopathy' is a more neutral term for any brain white matter disorder, genetic or acquired.

MRI ERA

In the nineteen seventies, the advent of CT scanning provided the first opportunity to visualize leukoencephalopathies *in vivo*, but due to the low sensitivity and tissue differentiation CT was unable to distinguish between most different disorders.⁷ In the early nineteen eighties, the advent of MRI had a major impact on studies of leukoencephalopathies. It was immediately clear that MRI had a very high sensitivity for white matter abnormalities,⁸ but the specificity of these findings was considered as low.^{9,10}

When we started to study leukoencephalopathies in the late nineteen eighties, a limited number of disorders and no genes associated with a leukodystrophy were known. The diagnosis depended on metabolic investigations (metabolites in body fluids and enzyme activities) for most disorders¹¹ and pathology findings for a few.^{12,13} MRI changed the diagnostic approach entirely and caused a revolution in the white matter field. We noticed that patients with a diagnosis that was verifiable by laboratory testing presented with distinct patterns of MRI abnormalities, shared by patients with the same diagnosis, but different from the patterns observed in patients with other diagnoses.¹⁴ This observation prompted the development of MRI pattern recognition to enhance the specificity of MRI interpretation.¹⁵

For the diagnosis of leukoencephalopathies known at that time, MRI pattern recognition worked well.¹⁶ In the early nineties it became, however, clear that in substantial numbers of leukoencephalopathy cases no specific diagnosis could be established. We estimated that over 60% of the leukoencephalopathy cases remained unsolved.¹⁷ The heavy load of unclassified leukoencephalopathies impelled us to work on them and define novel disorders by their distinct MRI patterns.¹⁷ In this way, new disease entities as megalencephalic leukoencephalopathy with subcortical cysts (MLC),¹⁸ vanishing white matter (VWM),¹⁹⁻²¹ hypomyelination and atrophy of the basal ganglia and cerebellum (H-ABC),²² leukoencephalopathy with brainstem and spinal cord involvement and lactate elevation (LBSL),²³ hypomyelination, hypodontia and hypogonadotropic hypogonadism (4H syndrome),²⁴⁻²⁶ leukoencephalopathy and thalamus and brainstem involvement and high lactate (LTBL),²⁷ and hypomyelination of early myelinating structures (HEMS)²⁸ were defined and criteria were drafted for MRI-based diagnoses.

GENETIC LINKAGE ERA

The first genes associated with known leukodystrophies were identified at the end of the nineteen eighties, initially mainly by a candidate gene approach directed at the likely genetic defect. Examples are *PLP1* for Pelizaeus-Merzbacher disease,²⁹ *ARSA* for MLD,³⁰ *ASPA* for Canavan disease,³¹ and *GALC* for Krabbe disease.³² Later, genes were identified by genetic linkage, e.g. *ABCD1* for X-linked adrenoleukodystrophy.³³

Validation of the concept that novel leukodystrophies could be defined by their MRI pattern came in 2001, when the first genes mutated in MRI-defined disorders were identified: *EIF2B1-5* for VWM^{34,35} and *MLC1* for MLC.³⁶ Soon many other genes mutated in newly MRI-defined disorders were identified.³⁷⁻⁴¹ Linkage analysis using positional cloning to pinpoint the chromosomal location of the candidate gene and subsequent narrowing of the candidate region, followed by sequential analysis of candidate genes in the region by Sanger sequencing were the main techniques used. This approach required substantial numbers of patients at all stages. Several patients with the same MRI pattern were necessary to define the disease and multiple genetically informative families were needed for genetic linkage. For most patients with an unclassified or defined, but molecularly undetermined leukodystrophy, this technique did not succeed, mainly due to the rarity of the disorders or dominant *de novo* inheritance.

Despite the fact that the most prevalent novel leukodystrophies had been identified between 1990 and 2010 and their gene defect had been elucidated, it was found that 50% of leukodystrophy patients still remained without a specific diagnosis in 2010.⁴²

EXOME SEQUENCING ERA

The advent of next-generation-sequencing technology in 2005 caused a second revolution in the leukodystrophy field. It created a paradigm shift in the approach of gene discovery for rare Mendelian disorders.⁴³ Massive parallel sequencing of the protein-coding part of the genome is referred to as whole-exome sequencing (WES).⁴³ In 2011, the first genetic defect for a leukodystrophy without known molecular cause, 'hereditary diffuse leukoencephalopathy with spheroids' (HDLS), was identified using WES, which revealed dominant mutations in *CSF1R*.⁴⁴ Soon thereafter WES revealed recessive mutations in *EARS2* in patients with LTBL,⁴⁵ and dominant de novo mutations in *TUBB4A* in the sporadic disease H-ABC.⁴⁶ The number of novel genes associated with new or previously defined Mendelian disorders identified between 2011 and 2016 using WES has been enormous and illustrates the high potential of this technique for gene finding.^{47,48} Additionally, WES has proven to greatly facilitate a molecular diagnosis for disorders associated with numerous different gene defects, such as hypomyelination and respiratory chain defects, in which sequential gene analysis is costly and time consuming.

Although extremely successful, one of the biggest challenges of WES is interpretation of the data. From the approximately 20.000-25.000 variants identified in each individual exome, a single candidate gene has to be selected. WES approaches using small groups of patients with presumably the same MRI-defined novel leukodystrophy are quite successful in gene identification.^{45,46,49-56} and appears much more powerful than performing WES in large, unselected patient groups. We have had a success rate of 80-90% for gene identification by WES in small, homogeneous patient groups from the Amsterdam database of unclassified leukoencephalopathy cases, whereas several larger WES studies have reported success rates of 42% for mixed leukodystrophy cases⁵⁷ and 16-53% for unselected patients.⁵⁸⁻⁶⁰ The most important advantage of WES in homogeneous patient groups is that the patients validate each other in that the conclusion on pathogenicity of identified variants does not only depend on knowledge of gene function or predicted effect of the variant, but also on whether variants in the same gene are observed in other patients.

Percentage of unsolved cases

In 2010, 50% of the leukodystrophy cases remained unclassified.⁴² We suspected that with WES the percentage has decreased substantially. To confirm this we conducted a retrospective study of three different historical cohorts including a total of 430 patients with an unclassified leukoencephalopathy despite extensive available diagnostic work-up.

The first and oldest cohort, cohort 1, was published in 1999 and contains 92 leukoencephalopathy patients from 82 families, including both inherited and acquired disorders, evaluated at the Kennedy Krieger Institute in Baltimore during 1990-1996.¹⁷ Follow-up for outcomes was executed in October 2015. A specific diagnosis had been established in 40 of the 82 families: 27 through DNA-confirmation, 10 based on established MRI criteria (four MLC and six Alexander disease), and three based on pathology (Alexander disease and HDLS). For the latter 13 patients the diagnosis could not be confirmed molecularly because of lack of available DNA. The percentage of almost 50% of the cases with a specific diagnosis is an underestimation. As expected for such an old cohort, many cases were lost to follow-up and most cases never had the genetic work-up that would now be state-of-the-art. Additionally, a part of the patients may not have a genetic disease.¹⁷

The second and third cohorts consist of cases from the MRI database of the Center for Childhood White Matter Disorders in Amsterdam that contains over 3000 unclassified leukoencephalopathy cases. In 2011, cases from this database were entered on lists if they presumably had a leukodystrophy, but no molecular diagnosis, and had hypomyelination (cohort 2) or were suspected of a mitochondrial defect (cohort 3). Hypomyelination was defined as evidence of stable lack of myelin on two successive MRIs with an interval of at least six months and the second MRI after one year of age.⁶¹ A 'suspected mitochondrial leukodystrophy' was determined by the MRI pattern, showing features as cystic lesions in the abnormal white matter, additional gray matter lesions, restricted diffusion, contrast enhancement, and elevated lactate on magnetic resonance spectroscopy of the brain.^{62,63} Outcomes were assessed in December 2015 and exclusively based on presence or absence of a molecular diagnosis. Counting siblings as one, a total of 181 cases were present in cohort 2 and 167 in cohort 3. For cohorts 2 and 3, 67 (37%) and 61 (37%) of the cases were lost to follow-up leaving 114 and 106 cases, respectively (Table 1). For these remaining cases, a molecular diagnosis was established in 60/114 (53%) for cohort 2 and 69/106 (65%) for cohort 3 (Table 1), and 129/220 (59%) for the overall group.

It is important to realize that the patients included in the present retrospective study represent the 60% (cohort 1) or 50% (cohorts 2 and 3) patients in whom no diagnosis could be established 17 or 5 years ago, respectively. A positive molecular diagnosis in these cases results in an estimated decrease of the unclassified group to approximately 20%. This is still an underestimation of the percentage of classifiable leukodystrophy cases. Most of the remaining unclassified leukodystrophy patients did not undergo WES (50/54 cases for cohort 2 and 34/37 cases for cohort 3). With WES applied in all patients, the percentage of unclassified cases would be even lower.

Table 1. Outcome for cohort 2 and cohort 3

	Cohort 2 – hypomyelination	Cohort 3 – suspected mitochondrial leukodystrophy
	Number of cases (%)	Number of cases (%)
Informative cases	114 (100%)	106 (100%)
Diagnosis	60/114 (53%)	69/106 (65%)
No diagnosis, WES unrevealing	4/114 (4%)	3/106 (3%)
No diagnosis, no WES performed	50/114 (43%)	34/106 (32%)
Lost to follow-up	67	61
Total cases	181	167

GENETIC DEFECTS AND LEUKODYSTROPHY CONCEPTS

Figure 1 presents the reported genetic defects in cohorts 2 and 3. An intriguing finding is that only three myelin- or oligodendrocyte-specific protein defects were found: *PLP1* for HEMS,⁵⁵ *GJC2* for Pelizaeus-Merzbacher-like disease⁶⁴ and *GJB1* for brain manifestations of X-linked Charcot-Marie-Tooth disease.⁵⁰ Based on the original definition of leukodystrophies, numerous defects in proteins important in myelin build-up, maintenance, structure and function would be expected, but instead a high percentage of the newly identified gene defects affect the housekeeping process of mRNA translation (Figure 1).

mRNA translation is a highly complex process and numerous proteins are involved, including proteins mediating activation, initiation, elongation or termination of mRNA translation; aminoacyl tRNA synthetases; ribosomal proteins; as well as cofactors and modifying proteins.⁶⁵ VWM was the first example of a leukodystrophy caused by a defect in mRNA translation.^{34,66} In our cohorts many patients had a defect in one of the mitochondrial or cytosolic aminoacyl tRNA synthetases. These are housekeeping enzymes that attach amino acids to their cognate tRNA molecules as essential step in protein synthesis.⁶⁷ Furthermore, a large group of patients had mutations in genes encoding subunits of RNA polymerase POLR3 (*POLR3A*, *POLR3B*, and *POLR1C*). Strikingly, POLR3-related disorders prove to be among the most prevalent hypomyelinating leukodystrophies.⁶⁸

It is intriguing that several defects in mRNA translation result in distinctly different leukodystrophies, whereas other, similar defects in mRNA translation genes are associated with non-neurological phenotypes.⁶⁵ Each disease has its own cell type- and tissue-specificity. In line with the housekeeping function of the affected proteins,

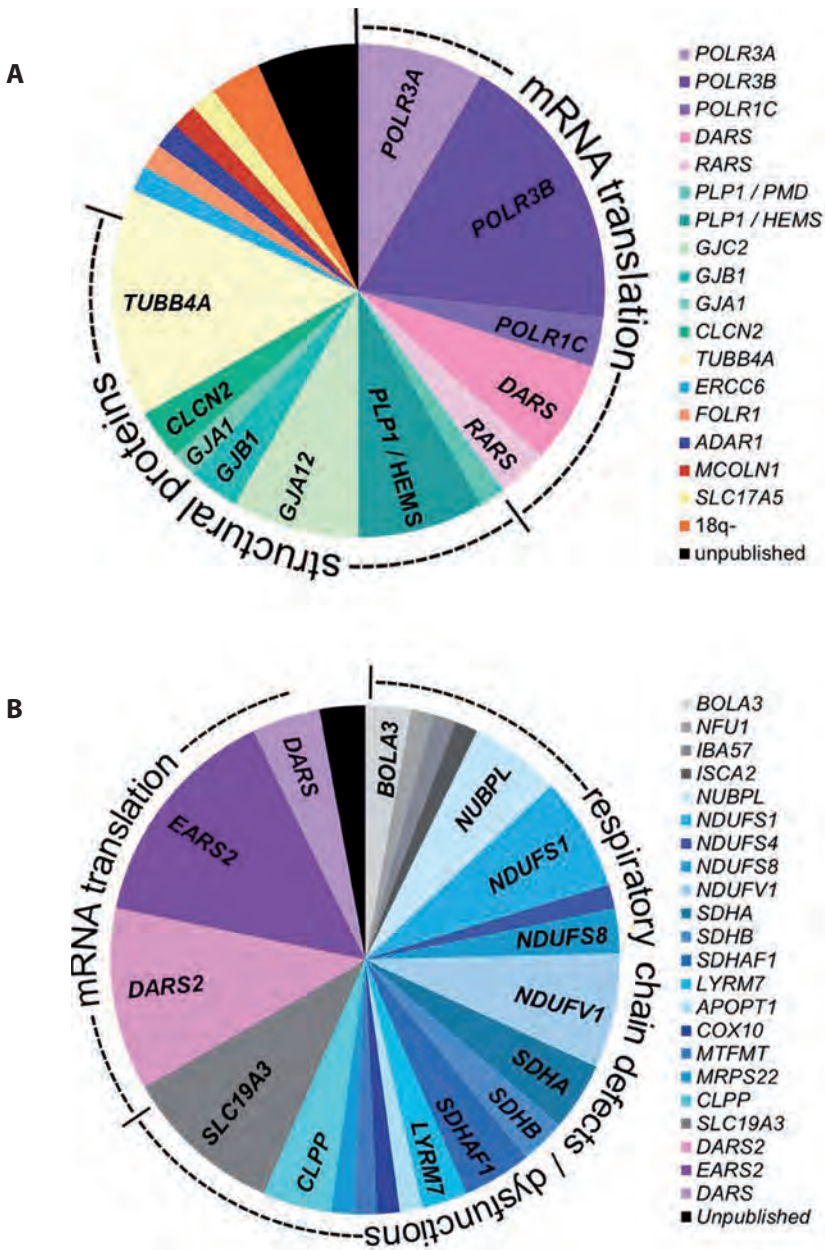


Figure 1. Overview of genes identified.

A. Genes mutated in cohort 2, hypomyelination. B. Genes mutated in cohort 3, suspected mitochondrial leukodystrophies. Each color represents a different gene. This is true for both for the hypomyelination and suspected mitochondrial leukodystrophy groups.

patients never have two mutations that would cause complete function loss, because absence of the housekeeping function would not be compatible with life. In fact, we suspect that the housekeeping function of the mutated proteins is still guaranteed and that it is not the hampered housekeeping function that causes the disease. VWM is an excellent example. Although a decreased eIF2B guanine exchange factor activity is observed in VWM patient-derived lymphoblasts and fibroblasts, no effect on protein synthesis rate is noted in these cells.^{69,70} There is no correlation between residual eIF2B activity in patient cells and severity of the VWM phenotype.⁷¹ The clinical phenotype of VWM includes no signs of overall compromised protein synthesis.⁷² Another example is the striking similarity in selectively affected brain structures in 'hypomyelination with brain stem and spinal cord involvement and leg spasticity' (HBSL) and LBSL, despite the fact that the involved aspartyl tRNA synthetases have different subcellular localization, cytoplasmic versus mitochondrial, where they are involved in unrelated mRNA translation processes.^{38,51} This observation suggests that a shared, alternative function of these enzymes is responsible for the overlapping phenotype. Most likely other, non-canonical functions of the affected proteins play a role in the pathogenesis of mRNA translation-related leukodystrophies.^{73,74}

A striking finding is that many new leukodystrophies are caused by mitochondrial defects. Formerly, defects in energy metabolism were expected to mainly affect neurons, with predominant involvement of the cerebral cortex (e.g. MELAS), basal ganglia, thalami and brain stem nuclei (e.g. Leigh syndrome).^{75,76} The identification of novel gene defects affecting proteins that are part of the respiratory chain for pure white matter disorders,^{52,53} or combined white and gray matter disorders⁴⁹ shed new light on the effect of respiratory chain dysfunction in the brain.

For some disorders accepted as leukodystrophies WES revealed defects in proteins specifically expressed in unexpected cell types. The *CSF1R* gene, mutated in HDLS, encodes a growth factor specific for microglia, macrophages and monocytes,⁷⁷ while pathology suggests a white matter axonopathy.¹³ *TUBB4A*, mutated in H-ABC, encodes a β -tubulin protein, a building block of microtubules. Microtubules are an essential component of the cytoskeleton and allow cell organelles and vesicles to move. In H-ABC, in which pathology points at primary axonal damage, the defective microtubule system may hamper axonal transport, leading to axonal dysfunction and loss and secondary myelin deficit.⁷⁸ The findings of the last five years have major implications for how we understand leukodystrophies. The original definition was focused on myelin and required a progressive disease course. With the information on newly identified defects underlying leukodystrophies, there is no justification for a myelin focused definition of

leukodystrophies. Additionally, molecular progress has made clear that there are also non-progressive or even improving leukodystrophy variants. MLC, widely accepted as a leukodystrophy,⁷⁹ was found to have an improving variant along with only transient abnormalities on MRI.^{40,80} Another example is LTBL, which is typically characterized by a single episode of deterioration early in life, followed by improvement. The timing and severity of the episode determine the outcome, which varies from no or almost no handicap to severe dysfunction or death.^{45,81} The conclusion based on these observations is that progression should not be regarded as a prerequisite for inclusion in the category of leukodystrophies.

Definitions reflect the state of knowledge at the time and should be regularly updated to reflect new insights. Recently the GLIA consortium suggested a modified leukodystrophy definition to include heritable disorders affecting the central nervous system white matter with abnormalities involving myelin or all macroglial cell types, both oligodendrocytes and astrocytes.⁷⁹ Progressive disease course was no longer a criterion. Weighing all new information, we propose to take the next step and define leukodystrophies as all genetically determined disorders primarily affecting central nervous system white matter, irrespective of the structural white matter component involved, the molecular process affected and the disease course. Leukodystrophy definitions are, although necessarily imperfect, of fundamental importance, because they determine how we understand white matter physiology and pathophysiology and how we approach treatment. Not only do remyelination and glia restoration need to be achieved, but a complex tissue that contains many more components needs to be repaired.

REFERENCES

1. Cruveilhier J. Anatomie pathologique du corps humain. vol II, fasc XXXII. Paris: JB Bailliere; 1835-1842.
2. Carswell R. Pathological anatomy. Illustrations of the elementary forms of disease. London: Longman, Orme, Brown, Green & Longman; 1838.
3. Heubner O. Über diffuse Hirnsclerose. Charité Ann 1897;22:298-310.
4. Bielschowsky M and Henneberg R. Über familiäre diffuse sklerose (Leukodystrophia cerebri progressiva hereditaria). J Psychol Neurol 1928;36:131-181.
5. Morell P and Wiesmann U. A correlative synopsis of the leukodystrophies. Neuropediatrics 1984;15 (suppl):62-65.
6. Seitelberger F. Structural manifestations of leukodystrophies. Neuropediatrics 1984;15 (suppl):53-61.
7. Barnes DM and Enzmann DR. The evolution of white matter disease as seen on computed tomography. Radiology 1981;138:379-383.
8. Young IR, Hall AS, Pallis CA, Legg NJ, Bydder GM, Steiner RE. Nuclear magnetic resonance imaging of the brain in multiple sclerosis. Lancet 1981;2:1063-1066.
9. Dietrich RB, Vining EP, Taira RK, Hall TR, Phillipart M. Myelin disorders of childhood: correlation of MR findings and severity of neurological impairment. J Comput Assist Tomogr 1990;14:693-698.
10. Demaerel P, Faubert C, Wilms G, Casaer P, Piepgras U, Baert AL. MR findings in leukodystrophy. Neuroradiology 1991;33:368-371.
11. Valle D, Beaudet AL, Vogelstein B, et al. The online metabolic and molecular bases of inherited disease. The McGraw-Hill Companies; 2016.
12. Alexander WS. Progressive fibrinoid degeneration of fibrillary astrocytes associated with mental retardation in a hydrocephalic infant. Brain 1949;72:373-81.
13. van der Knaap MS, Naidu S, Kleinschmidt-Demasters BK, Kamphorst W, Weinstein HC. Autosomal dominant diffuse leukoencephalopathy with neuroaxonal spheroids. Neurology 2000;54:463-468.
14. Valk J and van der Knaap MS. Magnetic Resonance of myelin, myelination and myelin disorders. Berlin: Springer; 1989.
15. van der Knaap MS, Valk J, de Neeling N, Nauta JJ. Pattern recognition in magnetic resonance imaging of white matter disorders in children and young adults. Neuroradiology 1991;33:478-493.
16. van der Knaap MS and Valk J. Magnetic Resonance of myelin, myelination and myelin disorders. Berlin: Springer; 1995.
17. van der Knaap MS, Breiter SN, Naidu S, Hart AA, Valk J. Defining and categorizing leukoencephalopathies of unknown origin: MR imaging approach. Radiology 1999;213:121-133.
18. van der Knaap MS, Barth PG, Stroink H, et al. Leukoencephalopathy with swelling and a discrepantly mild clinical course in eight children. Ann Neurol 1995;37:324-334.
19. Hanefeld F, Holzbach U, Kruse B, Wilichowski E, Christen HJ, Frahm J. Diffuse white matter disease in three children: an encephalopathy with unique features on magnetic resonance imaging and proton magnetic resonance spectroscopy. Neuropediatrics 1993;24:244-248.
20. Schiffmann R, Moller JR, Trapp BD, et al. Childhood ataxia with diffuse central nervous system hypomyelination. Ann Neurol 1994;35:331-340.
21. van der Knaap MS, Barth PG, Gabreels FJ, et al. A new leukoencephalopathy with vanishing white matter. Neurology 1997;48:845-855.
22. van der Knaap MS, Naidu S, Pouwels PJ, et al. New syndrome characterized by hypomyelination with atrophy of the basal ganglia and cerebellum. AJNR Am J Neuroradiol 2002;23:1466-1474.
23. van der Knaap MS, van der Voorn P, Barkhof F, et al. A new leukoencephalopathy with brainstem and spinal cord involvement and high lactate. Ann Neurol 2003;53:252-258.
24. Wolf NI, Harting I, Boltshauser E, et al. Leukoencephalopathy with ataxia, hypodontia, and hypomyelination. Neurology 2005;64:1461-1464.
25. Timmons M, Tsokos M, Asab MA, et al. Peripheral and central hypomyelination with hypogonadotropic hypogonadism and hypodontia. Neurology 2006;67:2066-2069.
26. Bernard G, Thiffault I, Tetreault M, et al. Tremor-ataxia with central hypomyelination (TACH) leukodystrophy maps to chromosome 10q22.3-10q23.31. Neurogenetics 2010;11:457-464.
27. Steenweg ME, Vanderver A, Ceulemans B, et al. Novel infantile-onset leukoencephalopathy with high lactate level and slow improvement. Arch Neurol 2012;69:718-722.

28. Steenweg ME, Wolf NI, Schieving JH, et al. Novel hypomyelinating leukoencephalopathy affecting early myelinating structures. *Arch Neurol* 2012;69:125-128.
29. Hudson LD, Puckett C, Berndt J, Chan J, Gencic S. Mutation of the proteolipid protein gene PLP in a human X chromosome-linked myelin disorder. *Proc Natl Acad Sci U S A* 1989;86:8128-8131.
30. Polten A, Fluharty AL, Fluharty CB, Kappler J, von FK, Gieselmann V. Molecular basis of different forms of metachromatic leukodystrophy. *N Engl J Med* 1991;324:18-22.
31. Kaul R, Gao GP, Balamurugan K, Matalon R. Cloning of the human aspartoacylase cDNA and a common missense mutation in Canavan disease. *Nat Genet* 1993;5:118-123.
32. Sakai N, Inui K, Fujii N, et al. Krabbe disease: isolation and characterization of a full-length cDNA for human galactocerebrosidase. *Biochem Biophys Res Commun* 1994;198:485-491.
33. Mosser J, Douar AM, Sarde CO, et al. Putative X-linked adrenoleukodystrophy gene shares unexpected homology with ABC transporters. *Nature* 1993;361:726-730.
34. Leegwater PA, Vermeulen G, Konst AA, et al. Subunits of the translation initiation factor eIF2B are mutant in leukoencephalopathy with vanishing white matter. *Nat Genet* 2001;29:383-388.
35. van der Knaap MS, Leegwater PA, Konst AA, et al. Mutations in each of the five subunits of translation initiation factor eIF2B can cause leukoencephalopathy with vanishing white matter. *Ann Neurol* 2002;51:264-270.
36. Leegwater PA, Yuan BQ, van der Steen J, et al. Mutations of MLC1 (KIAA0027), encoding a putative membrane protein, cause megalencephalic leukoencephalopathy with subcortical cysts. *Am J Hum Genet* 2001;68:831-838.
37. Zara F, Biancheri R, Bruno C, et al. Deficiency of hyccin, a newly identified membrane protein, causes hypomyelination and congenital cataract. *Nat Genet* 2006;38:1111-1113.
38. Scheper GC, van der Kloot T, van Andel RJ, et al. Mitochondrial aspartyl-tRNA synthetase deficiency causes leukoencephalopathy with brain stem and spinal cord involvement and lactate elevation. *Nat Genet* 2007;39:534-539.
39. Bernard G, Chouery E, Putorti ML, et al. Mutations of POLR3A encoding a catalytic subunit of RNA polymerase Pol III cause a recessive hypomyelinating leukodystrophy. *Am J Hum Genet* 2011;89:415-423.
40. Lopez-Hernandez T, Ridder MC, Montolio M, et al. Mutant GlialCAM causes megalencephalic leukoencephalopathy with subcortical cysts, benign familial macrocephaly, and macrocephaly with retardation and autism. *Am J Hum Genet* 2011;88:422-432.
41. Tetreault M, Choquet K, Orcesi S, et al. Recessive mutations in POLR3B, encoding the second largest subunit of Pol III, cause a rare hypomyelinating leukodystrophy. *Am J Hum Genet* 2011;89:652-655.
42. Bonkowsky JL, Nelson C, Kingston JL, Filloux FM, Mundorff MB, Srivastava R. The burden of inherited leukodystrophies in children. *Neurology* 2010;75:718-725.
43. Ng SB, Turner EH, Robertson PD, et al. Targeted capture and massively parallel sequencing of 12 human exomes. *Nature* 2009;461:272-276.
44. Rademakers R, Baker M, Nicholson AM, et al. Mutations in the colony stimulating factor 1 receptor (CSF1R) gene cause hereditary diffuse leukoencephalopathy with spheroids. *Nat Genet* 2011;44:200-205.
45. Steenweg ME, Ghezzi D, Haack T, et al. Leukoencephalopathy with thalamus and brainstem involvement and high lactate 'LTBL' caused by EARS2 mutations. *Brain* 2012;135:1387-1394.
46. Simons C, Wolf NI, McNeil N, et al. A de novo mutation in the beta-tubulin gene TUBB4A results in the leukoencephalopathy hypomyelination with atrophy of the basal ganglia and cerebellum. *Am J Hum Genet* 2013;92:767-773.
47. Boycott KM, Dymont DA, Sawyer SL, Vanstone MR, Beaulieu CL. Identification of genes for childhood heritable diseases. *Annu Rev Med* 2014;65:19-31. doi: 10.1146/annurev-med-101712-122108.:19-31.
48. Vissers LE, Gilissen C, Veltman JA. Genetic studies in intellectual disability and related disorders. *Nat Rev Genet* 2016;17:9-18.
49. Kevelam SH, Rodenburg RJ, Wolf NI, et al. NUBPL mutations in patients with complex I deficiency and a distinct MRI pattern. *Neurology* 2013;80:1577-1583.
50. Depienne C, Bugiani M, Dupuits C, et al. Brain white matter oedema due to CIC-2 chloride channel deficiency: an observational analytical study. *Lancet Neurol* 2013;12:659-668.
51. Taft RJ, Vanderver A, Leventer RJ, et al. Mutations in DARS cause hypomyelination with brain stem and spinal cord involvement and leg spasticity. *Am J Hum Genet* 2013;92:774-780.

52. Dallabona C, Diodato D, Kevelam SH, et al. Novel (ovario) leukodystrophy related to AARS2 mutations. *Neurology* 2014;82:2063-2071.
53. Melchionda L, Haack TB, Hardy S, et al. Mutations in APOPT1, encoding a mitochondrial protein, cause cavitating leukoencephalopathy with cytochrome c oxidase deficiency. *Am J Hum Genet* 2014;95:315-325.
54. Wolf NI, Salomons GS, Rodenburg RJ, et al. Mutations in RARS cause hypomyelination. *Ann Neurol* 2014;76:134-139.
55. Kevelam SH, Taube JR, van Spaendonk RM, et al. Altered PLP1 splicing causes hypomyelination of early myelinating structures. *Ann Clin Transl Neurol* 2015;2:648-661.
56. Dallabona C, Abbink TE, Carozzo R, et al. LYRM7 mutations cause a multifocal cavitating leukoencephalopathy with distinct MRI appearance. *Brain* 2016;139:782-794.
57. Vanderver A, Simons C, Helman G, et al. Whole exome sequencing in patients with white matter abnormalities. *Ann Neurol* 2016;
58. de Ligt J, Willemsen MH, van Bon BW, et al. Diagnostic exome sequencing in persons with severe intellectual disability. *N Engl J Med* 2012;367:1921-1929.
59. Srivastava S, Cohen JS, Vernon H, et al. Clinical whole exome sequencing in child neurology practice. *Ann Neurol* 2014;76:473-483.
60. Taylor RW, Pyle A, Griffin H, et al. Use of whole-exome sequencing to determine the genetic basis of multiple mitochondrial respiratory chain complex deficiencies. *JAMA* 2014;312:68-77.
61. Schiffmann R and van der Knaap MS. Invited article: an MRI-based approach to the diagnosis of white matter disorders. *Neurology* 2009;72:750-759.
62. van der Knaap MS and Valk J. *Magnetic Resonance of Myelination and Myelin Disorders*. Heidelberg: Springer; 2005.
63. Naidu S, Bibat G, Lin D, et al. Progressive cavitating leukoencephalopathy: a novel childhood disease. *Ann Neurol* 2005;58:929-938.
64. Uhlenberg B, Schuelke M, Ruschendorf F, et al. Mutations in the gene encoding gap junction protein alpha 12 (connexin 46.6) cause Pelizaeus-Merzbacher-like disease. *Am J Hum Genet* 2004;75:251-260.
65. Scheper GC, van der Knaap MS, Proud CG. Translation matters: protein synthesis defects in inherited disease. *Nat Rev Genet* 2007;8:711-723.
66. Scheper GC, Proud CG, van der Knaap MS. Defective translation initiation causes vanishing of cerebral white matter. *Trends Mol Med* 2006;12:159-166.
67. Antonellis A and Green ED. The role of aminoacyl-tRNA synthetases in genetic diseases. *Annu Rev Genomics Hum Genet* 2008;9:87-107.
68. Wolf NI, Vanderver A, van Spaendonk RM, et al. Clinical spectrum of 4H leukodystrophy caused by POLR3A and POLR3B mutations. *Neurology* 2014;83:1898-1905.
69. Kantor L, Harding HP, Ron D, et al. Heightened stress response in primary fibroblasts expressing mutant eIF2B genes from CACH/VWM leukodystrophy patients. *Hum Genet* 2005;118:99-106.
70. van Kollenburg B, Thomas AA, Vermeulen G, et al. Regulation of protein synthesis in lymphoblasts from vanishing white matter patients. *Neurobiol Dis* 2006;21:496-504.
71. Liu R, van der Lei HD, Wang X, et al. Severity of vanishing white matter disease does not correlate with deficits in eIF2B activity or the integrity of eIF2B complexes. *Hum Mutat* 2011;32:1036-1045.
72. van der Knaap MS, Pronk JC, Scheper GC. Vanishing white matter disease. *Lancet Neurol* 2006;5:413-423.
73. Kim S, You S, Hwang D. Aminoacyl-tRNA synthetases and tumorigenesis: more than housekeeping. *Nat Rev Cancer* 2011;11:708-718.
74. Yao P, Poruri K, Martinis SA, Fox PL. Non-catalytic regulation of gene expression by aminoacyl-tRNA synthetases. *Top Curr Chem* 2014;344:167-87.
75. Barkovich AJ, Good WV, Koch TK, Berg BO. Mitochondrial disorders: analysis of their clinical and imaging characteristics. *AJNR Am J Neuroradiol* 1993;14:1119-1137.
76. van der Knaap MS, Jakobs C, Valk J. Magnetic resonance imaging in lactic acidosis. *J Inherit Metab Dis* 1996;19:535-547.
77. Ginhoux F, Greter M, Leboeuf M, et al. Fate mapping analysis reveals that adult microglia derive from primitive macrophages. *Science* 2010;330:841-845.

78. Hamilton EM, Polder E, Vanderver A, et al. Hypomyelination with atrophy of the basal ganglia and cerebellum: further delineation of the phenotype and genotype-phenotype correlation. *Brain* 2014;137:1921-1930.
79. Vanderver A, Prust M, Tonduti D, et al. Case definition and classification of leukodystrophies and leukoencephalopathies. *Mol Genet Metab* 2015;114:494-500.
80. van der Knaap MS, Lai V, Kohler W, et al. Megalencephalic leukoencephalopathy with cysts without MLC1 defect. *Ann Neurol* 2010;67:834-837.
81. Kevelam SH, Klouwer FC, Fock JM, Salomons GS, Bugiani M, van der Knaap MS. Absent Thalami Caused by a Homozygous EARS2 Mutation: Expanding Disease Spectrum of LTBL. *Neuropediatrics* 2016;47:64-67.

Chapter 12

**Summary, discussion
and future perspectives**



LEUKODYSTROPHIES

Leukodystrophies are rare, inherited, neurological disorders with exclusive or predominant, primary involvement of the white matter of the central nervous system (CNS).¹ Leukodystrophies are most prevalent in children and often result in severe neurological deficits and early death.² While leukodystrophies were initially diagnosed primarily by pathology, since the introduction of MRI into medicine in the nineteen eighties the first evidence for a leukodystrophy typically comes from MRI showing extensive, prominent signal abnormalities in the CNS white matter. Pathology confirmation is usually lacking. MRI has an incredible sensitivity for white matter abnormalities, but its specificity for underlying histopathologic changes is low.^{3,4} This low sensitivity sometimes causes problems in differentiating primary from secondary white matter involvement. Cortical neuronal degeneration leads to secondary white matter abnormalities due to Wallerian degeneration with loss of axons and myelin within the white matter.⁵ Especially in infantile onset neuronal disorders, in which the neuronal degeneration disrupts the normal myelination process, MRI may show prominent cerebral white matter abnormalities. Examples are infantile onset GM1 and GM2 gangliosidoses, which present with an MRI pattern suggestive of a leukodystrophy, whereas later onset variants show the MRI picture of a neuronal degenerative disorder, dominated by cerebral atrophy and only slight white matter signal abnormalities.² The same is true for the early onset variants of *SLC19A3*- and *ITPA*-related encephalopathies, discussed in this thesis (**chapter 3 and chapter 10**). Because with the elucidation of the genetic defect it is clear that the white matter abnormalities are secondary to neuronal cell death, they may not be regarded as leukodystrophies. However, because of the prominent brain white matter abnormalities, these MRIs were part of the database of leukoencephalopathies in Amsterdam, which was the source of the MRIs for this study. Most leukodystrophy experts include such cases in their scope of interest (see GLIA consortium consensus statement).⁶

GENE DISCOVERY FOR LEUKODYSTROPHIES

A molecular diagnosis is extremely important for patients and families, because this comes with information on prognosis, options for family planning, and exploration of potential treatment options. In the past and often up to this day, patients frequently experienced and still experience a long diagnostic odyssey to reach a definitive diagnosis. The rarity of these disorders and the lack of multiple multiplex families precluded traditional gene-discovery approaches or hampered their success. In 2010 it was found that still 50% of the patients with a leukodystrophy remained without a specific diagnosis.⁷

The advent of whole-exome sequencing (WES) in 2009 has created a paradigm shift in our approach to gene discovery for rare Mendelian disorders. Numerous genes discovered with WES are genes previously associated with a known Mendelian phenotype (and assigned OMIM number), but now found in association with also other disease entities or with an expansion of the phenotypic spectrum.⁸ In a large international cohort study of 8,838 families with a Mendelian phenotype, 50% of the discovered genes were known genes associated with a known phenotype and 30% of the gene discoveries involved known genes associated with a novel phenotype or expansion of the phenotypic spectrum. 20% of the gene discoveries represented novel genes.⁸ The number of genes associated with a new or previously defined Mendelian disorder identified in the last five years using WES has been enormous. To illustrate this, from 2009 till 2011, the application of WES led to the identification of 30 novel genes associated with a Mendelian disorder and eight new clinical phenotypes linked to a known gene.⁹ In the following two years this number expanded tremendously to an additional 133 novel genes and 43 new phenotypes linked to known genes, and this number is still growing exponentially.⁹ Specifically for leukodystrophies, until now, in total 18 additional novel genes associated with a leukodystrophy were identified and four new phenotypes were added to known genes until then associated with a non-leukodystrophy phenotype.¹⁰⁻³² In addition, ten genes (eight novel, two new phenotypes) were identified for neuronal disorders with variable white matter abnormalities.^{29,33-40}

The studies for this thesis started in 2011, shortly after the introduction of WES. The aim of this thesis was to identify the molecular cause of novel, MRI-defined leukodystrophies by WES analysis. MRI pattern recognition was used to identify and define novel leukodystrophies in our large database of unclassified patients. This thesis reflects the overall success of the application of WES identifying the molecular cause of leukodystrophies and shows that the combined approach of phenotypic definition by MRI and WES is extremely powerful for gene discovery. In our studies 77% of the molecular diagnoses concerned genes associated with a known OMIM annotated diseases expanding the phenotypic spectrum (4 genes; *PLP1*, *SLC19A3*, *LAMA2* and *EARS2*) or adding a novel disease entity (3 genes; *AARS2*, *HMBS* and *CTSA*); the remaining 23% (2 genes) represented novel disorders associated with a gene not linked to a human disorder or clear phenotype (*NUBPL* and *ITPA*).

In this chapter results described in the previous chapters of this thesis are summarized and discussed in light of other published research.

Expansion of the phenotypic spectrum of a known disorder

The identification of the first gene associated with expansion of the phenotypic spectrum is described in **chapter 2**. In this chapter the search for the genetic cause of 16 patients from 10 families with the X-linked disorder ‘hypomyelination of early myelinating structures’ (HEMS) is presented. This novel disorder was previously identified and defined from our database of unclassified white matter disorders by Steenweg *et al.*⁴¹ In HEMS, brain MRI shows an intriguing pattern of abnormalities; brain structures that normally myelinate early (e.g., brainstem, hilus of the dentate nucleus, posterior limb of the internal capsule, optic tracts and tracts to the pericentral cortex) are poorly myelinated in contrast to structures that normally myelinate at a later developmental stage, which show better myelination.^{41,42} By using X-chromosome exome sequencing we found that all patients had unusual hemizygous variants of *PLP1* located in exon 3B or deep in intron 3 outside the splice consensus site. *In silico* analysis of the variants predicted an effect on *PLP1/DM20* alternative splicing, which we confirmed by a decreased *PLP1/DM20* ratio in patients fibroblasts and transfected immature immortalized oligodendrocytic cells. Our findings expand the phenotypic spectrum of *PLP1*-associated disorders and also provide new insights in the possible pathomechanisms underlying the *PLP1*-related disorders. *PLP1* mutations are known to be associated with a broad continuum of neurological phenotypes ranging from congenital Pelizaeus Merzbacher disease (PMD) with severe hypomyelination to pure spastic paraplegia type 2.⁴³⁻⁴⁵ An association is seen between the nature of the genetic alteration and the phenotype.⁴⁶ It is hypothesized that the different genetic abnormalities result in distinct cellular defects depending on their effect and location in the *PLP1* gene.⁴⁴ *PLP1* duplications may cause accumulation of the protein in the late endosome or lysosome interfering with oligodendrocyte function such as myelination.^{44,45} Missense variants result in misfolding of the protein resulting in accumulation of the protein in the endoplasmic reticulum leading to activation of the unfolded protein response and inducing oligodendrocyte apoptosis.^{44,45} *PLP1*-specific missense variants that lead only to aberrant PLP1 and not DM20 are expected to induce less oligodendrocyte apoptosis than missense variants that impact both PLP1 and DM20.⁴⁴ Null variants result in a lack of synthesis of the protein, leading to formation of compact myelin lacking PLP.⁴⁵ Our results indicate that specific variants resulting in a decreased *PLP1* to *DM20* ratio should be added to the cellular defects that may underlie *PLP1*-related disorders and in those cases specifically affect the developmental regulation of myelination.

In **chapter 3**, we identified a cohort of seven patients with an early-infantile lethal encephalopathy sharing the same novel MRI pattern characterized by incredibly fast subtotal brain degeneration, including the cerebral white matter, and elevated lactate

on magnetic resonance spectroscopy.³⁵ WES analysis performed in one patient revealed recessive variants in *SLC19A3*, encoding the second thiamine transporter, hTHTR2.⁴⁷ All other patients were also found to have recessive *SLC19A3* variants confirming the association of mutated *SLC19A3* with this phenotype.³⁵ Brain pathology findings showed similarities to what is observed in patients with Leigh-syndrome.⁴⁸ Recessive variants in *SLC19A3* were previously described in patients with three distinct different clinical phenotypes: biotin-thiamine-responsive basal ganglia disease (BTBGD) (MIM 607483), Wernicke-like encephalopathy (MIM 607483) and a more generalized encephalopathy.⁴⁹⁻⁵³ Overall these patients have a later-onset disease, milder clinical signs and symptoms, and present with more limited lesions on MRI, evidently primarily involving the gray matter.⁴⁹⁻⁵³ Although 30 additional patients have been reported since our report with different recessive (e.g. missense, nonsense, insertions and deletions, and intronic) variants in *SLC19A3*, no evident genotype-phenotype correlation could be established.⁵⁴⁻⁶² In our cohort we did, however, observe a similar phenotype within families suggesting that the genotype indeed co-determines the phenotype. Other influences like environmental, epigenetic and additional genetic factors acting on the availability of thiamine in the brain and decompensation of the oxidative phosphorylation system (OXPHOS) could account for the more severe phenotype seen in our patients.³⁵

In **chapter 4** we report on a family in which we identified with WES compound heterozygous variants in *LAMA2*, a known gene associated with congenital muscular dystrophy (now referred to as MDC1A, MIM 607855).^{63,64} Although the brain abnormalities fitted with the diagnosis of MDC1A, the neurological signs of predominantly distal weakness were atypical for the disease.⁶⁵ Specific *LAMA2* variants that result in partial laminin- α 2 chain deficiency can be associated with an adult-onset muscular dystrophy.⁶⁴ However, these patients mainly have weakness of the proximal muscles.⁶⁴ Immunohistochemical staining of muscle using an anti- α 2-chain antibody did not show (partial) deficiency of laminin- α 2 in our patients, although we cannot exclude the possibility that we would have detected partial deficiency of laminin- α 2 using a more sensitive antibody. This study is an example of phenotypic expansion of the disease spectrum as a result of WES findings.

In **chapter 5** we report a patient with a homozygous in-frame deletion in *EARS2*, encoding glutamyl-tRNA synthetase and associated with the leukodystrophy 'Leukoencephalopathy with thalamus and brainstem involvement and high lactate' (LTBL). This disorder was first described by our group in 2012.^{18,66} Patients have one episode of deterioration with a typical MRI pattern consisting of signal abnormalities

in the thalamus, brainstem, and deep cerebral white matter that improve over time in the majority of the cases. A small group of patients have an earlier, neonatal-onset, with stabilization, but no improvement.^{18,66} The patient reported in **chapter 5** had an antenatal onset of the disease with on his MRI absence of thalami with the configuration of a developmental anomaly, without evidence of a lesion. This finding has impact on the interpretation of previous MRI findings in patients with LTBL; in several reported patients the posterior part and the rostrum of the corpus callosum were absent and this was ascribed to a developmental anomaly.¹⁸ We now hypothesize that this feature is more likely the result of an early injury rather than a developmental anomaly per se. This interpretation implicates that the phenotype associated with *EARS2* variants can be associated with more than one episode of deterioration. So far no genotype-phenotype association has been established for LTBL. In fact, in the group published by Steenweg *et al*, two brothers with the same genotype had opposing phenotypes, one belonging to the group that shows improvement, and the other one to the early-onset group without improvement.¹⁸

Novel disease entity associated with a known gene

In **chapter 6** two unrelated patients with similar white matter abnormalities on MRI were independently subjected to WES. Using MRI pattern recognition an additional cohort of 11 patients was subsequently selected as potential candidates. A total of six patients (including the two probands) were found to have recessive variants in the gene *AARS2*, encoding mitochondrial alanyl tRNA synthetase (mtAlaRs) enzyme. The main clinical phenotype of these patients was a childhood to adult-onset neurological deterioration, with in all females ovarian failure, and on MRI a leukoencephalopathy with involvement of left-right connections, descending tracts, and cerebellar atrophy (described as '(ovario) leukodystrophy').²⁵ So far, variants in *AARS2* had been found only in a small number of patients with an early-onset fatal cardiomyopathy or myopathy (MIM 614096), also all identified recently with WES.⁶⁷⁻⁷⁰ To elucidate the striking differences between the two disease entities we investigated the effect of the variants present in one of our patients (p.Phe22Cys and p.Val500*) as well as variants present in cardiomyopathy patients (p.Leu55Arg) on OXPHOS functioning in a *Saccharomyces cerevisiae* yeast model.²⁵ The other cardiomyopathy-associated variant (p.Arg592Trp) could not be investigated because this residue is not conserved in yeast.²⁵ The cardinal difference observed was that the cardiomyopathy-associated missense variant behaved like a null-allele, while the (ovario)leukodystrophy-associated missense variant was only deleterious in stress conditions, suggesting a less severe effect of the (ovario)leukodystrophy variant on OXPHOS.²⁵ Beside a differential effect of the variants on OXPHOS, it was hypothesized that the variant located in the editing domain leading to mistranslation would result

in cardiomyopathy. However, recently, additional evidence for the first hypothesis was provided by Euro *et al.*, who used a full-length mtAlaRs homology model to perform a structural analysis of all published AARS2 variants to predict their effects on synthetase structure and function.⁶⁸ A differential effect of the variants on aminoacylation activity was found between the two groups. The cardiomyopathy phenotype was associated with variants that were predicted to result in a severely compromised aminoacylation activity, while the combined variants in the (ovario)leukodystrophy patients were predicted to retain partial activity.⁶⁸ The tissue-specific difference might be explained by the vulnerability of the heart for severely reduced mtAlaRS activity in early life resulting in a severe cardiomyopathy and premature death before any brain abnormalities can be observed.⁶⁸ If this hypothesis is correct, one would expect that infants who survive the infantile period would develop white matter abnormalities. However, the cardiomyopathy phenotype has thus far only been associated with a single founder variant, p.Arg592Trp, in homozygous or compound heterozygous state.⁶⁸ Another hypothesis could be that this specific variant acts on a possible noncanonical function of mtAlaRs (discussed later) that could have a differential effect on heart and brain.

In **chapter 7** and **chapter 8** two different leukodystrophies are described with a different disease entity and inheritance mode than the known disorder associated with this gene. It has now been recognized that for some genes both recessive and dominant variants may be associated with a disease, either with a rather similar clinical phenotype that is milder for the dominant variants than for the recessive variants, or with completely different disease entities. For example, recessive *GLIALCAM* variants are found in patients with classical megalencephalic leukoencephalopathy with subcortical cysts (MLC, MIM 604004) with an early-onset macrocephaly and delayed-onset neurological deterioration, while patients with dominant *GLIALCAM* variants have benign familial macrocephaly or a mild clinical phenotype with initially a leukoencephalopathy and subsequent normalization of the white matter abnormalities on MRI (MIM 613926).⁷¹ Another example is Bethlem myopathy (MIM 158810), a slowly progressive mild myopathy caused by dominant *COL6A1*, *COL6A2* or *COL6A3* variants, while recessive *COL6A1*, *COL6A2* or *COL6A3* variants are associated with Ullrich congenital muscular dystrophy (MIM 254090), a severe myopathy presenting directly after birth.⁷² Recently two large unrelated families with adult-onset dominant axonal polyneuropathy were described with a dominant variant in the gene *NAGLU*, while recessive *NAGLU* variants are associated with a severe lysosomal childhood-onset disease, mucopolysaccharidosis type IIIB (MIM 252920).⁷³

In **chapter 7** we report three siblings from one family with bi-allelic variants in the gene *HMBS* (EC 2.5.1.61), encoding the enzyme hydroxymethylbilane synthase, previously

called porphobilinogen deaminase (PBGD), the third enzyme in heme biosynthesis.⁷⁴ Autosomal dominant variants are known to cause acute intermittent porphyria (AIP, MIM 176000).⁷⁴ Our patients do not have the acute AIP-related symptoms as seen in patients with heterozygous *HMBS* variants, but present with a childhood onset very slowly progressive neurological disorder with a distinct leukoencephalopathy on MRI. *HMBS* enzyme activity and porphyrin precursors in body fluids were in the range of heterozygous *HMBS* variant carriers in our patients. In the literature five other patients with bi-allelic *HMBS* variants have been reported. These patients also had neurological symptoms, but the onset of the disease was earlier, the course more severe and the outcome less favorable.⁷⁵⁻⁷⁹ One of these cases was reported to have brain white matter abnormalities on MRI.⁷⁹ In these cases reported before, *HMBS* enzyme activity levels ranged from 1-17% of normal, with an excessive excretion of porphyrin precursors.⁷⁵⁻⁷⁹ Strikingly, also these five patients had no acute AIP-related episodes. We reason that our family and the other five patients reported previously represent a separate clinical phenotype caused by bi-allelic *HMBS* variants, in which our patients represent the more benign end of the phenotypic spectrum.

In **chapter 8** we describe two families with the same novel adult-onset autosomal dominant vascular leukoencephalopathy, referred to as CARASAL. The disease is characterized by therapy-resistant hypertension, strokes, and slow and late cognitive deterioration. The MRI pattern shows a diffuse, progressive leukoencephalopathy preceding the onset of strokes and disproportionate to the degree of clinical severity. Genetic studies, including WES, revealed one heterozygous variant; c.973C>T, p.(Arg325Cys) (NM_000308.2) in *CTSA*, encoding Cathepsin A (CathA), segregating with CARASAL in both families. An 1145 kb genomic region encompassing this gene on chromosome 20q13.12 was shared by both families suggesting that this variant originates from a common ancestor. Recessive *CTSA* variants cause the lysosomal storage disorder galactosialidosis due to deficiency of β -galactosidase and neuraminidase-1 (MIM 256540) and heterozygosity had not been associated with disease so far. We explored a potential toxic effect of the variant, but we did not find evidence of misfolding of mutant CathA in non-reducing SDS-PAGE on patients' white matter lysates. Hence, the possible functional role of the *CTSA* variant in CARASAL is as yet unexplained. Potential clues for the pathogenesis are the unusual pathologic changes of white matter small arterioles, including the vasa vasorum, and the striking increase in endothelin-1 expression in CARASAL white matter astrocytes, also compared to other vascular leukoencephalopathies, with hampered oligodendrocyte precursor cell differentiation. Galactosialidosis patients and their parents, who are obligatory carriers, have no clinical overlap with the CARASAL phenotype. However, since hypertension and hypertension-

related brain white matter lesions are common and galactosialidosis is very rare, such an association might have been overlooked easily. It could also be envisioned that only this specific *CTSA* variant is associated with the CARASAL phenotype. Until now 31 recessive *CTSA* variants associated with galactosialidosis have been described and the p.Arg325Cys CARASAL variant is not one of them (public version of the Human Gene Mutation Database (HGMD®), (<http://www.hgmd.org>)).⁸⁰ Single variants associated with a specific phenotype have been reported before. For example, one particular *de novo* variant, c.959G>A (p.Arg320His), with a dominant-negative effect was found to cause progressive myoclonus epilepsy.⁸¹ Finding additional CARASAL patients is important for the confirmation of this hypothesis. Interestingly, a recent publication of a French family with a comparable autosomal dominant vascular leukoencephalopathy with similar MRI and pathology findings showed linkage with an 11.2 Mb interval on chromosome 20q13,⁸² encompassing the 1145 kb region of the *CTSA* variant, a strong argument for the same genetic disease.

Novel disorder associated with a gene previously not linked to a human disorder or clear phenotype

In our studies two groups of patients were found to have variants in an OMIM-annotated gene not known to be associated with a well-defined phenotype or overt disease. In **chapter 9** we reported six patients with a respiratory chain complex I deficiency without molecular cause and a similar, novel MRI pattern that is characterized by predominant abnormalities of the cerebellar cortex, deep cerebral white matter and corpus callosum. On follow-up, the corpus callosum and cerebral white matter abnormalities improved, while the cerebellar abnormalities were progressive and brainstem abnormalities appeared. WES revealed recessive variants in *NUBPL*, encoding an iron-sulfur cluster assembly factor for complex I. One case with *NUBPL* mutations was previously reported but without information on phenotype or MRI findings.⁸³ In line with the supposed function of the gene we provided evidence that *NUBPL* is involved in the early assembly of the peripheral arm of complex I, detected a decreased amount of *NUBPL* protein and fully assembled complex I, and found a decreased complex I activity. It is noteworthy that all patients had a c.166G>A missense variant *in cis* with an intronic branch-site variant (c.815-27T>C) with a relatively high carrier frequency (1.2% of European haplotypes). A previous study showed that overexpression of *NUBPL* protein carrying the missense variant is able to fully complement complex I activity in a *NUBPL*-deficient cell line, while the intronic branch-site variant results in aberrant splicing of *NUBPL* mRNA,⁸⁴ which we could also confirm. Recently, more evidence for the pathogenicity of the intronic branch-site variant was provided.⁸⁵ In an *in vivo* yeast model it was shown that this intronic branch-site variant leads to a severely decreased IND1 (*NUBPL* homologue in

yeast) protein level, an 80% decreased complex I enzyme function, and the same slow cell growth as a knock-out strain of IND1.⁸⁵ These observations highlight the challenges faced with interpreting WES data, as based on initial *in silico* pathogenicity prediction models intronic variants (outside the splice consensus site) would be omitted, especially if the carrier frequency (>1%) is rather high.

In **chapter 10** we describe a group of seven patients, from four unrelated families, with a novel disorder characterized by a progressive microcephaly, seizures, variable cardiac defects and an early death. The MRI pattern showed white matter abnormalities that would be compatible with early-onset neuronal degeneration and Wallerian degeneration of the associated white matter tracts. Using WES combined with single-nucleotide polymorphism (SNP)-array we found homozygous variants in the gene *ITPA*, encoding the enzyme inosine triphosphate pyrophosphatase (ITPase). All variants were predicted to cause a loss of enzyme function, which we confirmed by severely decreased ITPase activity in patients' erythrocytes or fibroblasts. ITPase has a key function in purine metabolism by removing noncanonical triphosphate purines inosine triphosphate pyrophosphatase (ITP) and xanthosine triphosphate (XTP) and their deoxy forms (dITP/dXTP) from the cellular pool.⁸⁶⁻⁸⁸ Toxicity of accumulated noncanonical nucleotides, leading to neuronal apoptosis and interference with proteins normally using ATP and GTP can play a role in the disease pathogenesis.⁸⁹⁻⁹¹ Our report is the first associating *ITPA* variants with a human disorder. Previously, a specific homozygous missense variant (Pro32Thr) in *ITPA* associated with abolished ITPase enzyme activity in human erythrocytes has been linked to adverse reactions to specific drugs.^{89,92-96} We hypothesized that the latter variant does not abolish ITPase activity in all cell types and that the apparent discrepancy between the similar loss of ITPase activity in erythrocytes as seen in our patients and dissimilar clinical consequences may be explained by different effects of the variants on enzyme function and structure and variability of *ITPA* expression between tissues. A knock-out *itpa* mouse model shows a phenotype similar to that observed in our patients, supporting our hypothesis.⁹⁷ *ITPA*-related disease is most likely a spectrum, with the clinical problems related to the p.Pro32Thr variant at the mildest end of the spectrum and this novel disorder at the most severe end. Recognition of future *ITPA*-encephalopathy patients will be difficult, because the specific MRI pattern is only present for a few months and assessment of ITPase activity and ITP accumulation in erythrocytes does not discriminate between benign and severe variants.

STRATEGIES FOR GENE DISCOVERY

Since the first reports of WES application for gene discovery for rare Mendelian disorders in 2009/2010, an incredibly high number of new genes and new disease entities associated with known genes have been published using Next-generation-sequencing (NGS) technologies.⁹⁸ Although extremely successful, one of the biggest challenges of WES is interpretation of the data. From a massive pool of approximately 20.000-25.000 variants identified in each individual exome, a single candidate gene has to be selected.^{9,99,100} Various approaches have been explored for the identification of genes influenced by the mode of inheritance, availability of other affected or unaffected family members or unrelated patients, presumed additional value of the application of other genetic techniques and a priori knowledge of disease phenotype and possible function of the encoded protein.

Our experience is that in most situations combined approaches are helpful for successful gene finding (Figure 1). For example, in **chapter 8** and **chapter 10** we additionally used genetic techniques like homozygosity mapping and microsatellite marker analysis to identify a disease-linked region to narrow down the candidate genomic search area. For the disorder described in **chapter 9** we had strong clues for a mitochondrial etiology so we focused first on mitochondrial genes (using the MitoCarta database)¹⁰¹ to reduce the number of candidate variants. It is important to realize that every filtering step used can also discard the pathogenic variant. The rarity of leukodystrophies justifies filtering for rare variants. Our experience is that with a maximal minor allele frequency margin set at 1%, all of the variants in this study would have been detected, except the intronic branch site variant described in **chapter 9**.

However, filtering against public databases (e.g. dbSNP, 1000 Genomes and Exome Variant Server, NHLBI GO Exome Sequencing Project (ESP)) should be performed with caution, especially in the case of late-onset leukodystrophies, because such patients could be included in these databases, because at time of inclusion the disease was still subclinical. For most studies, the greatest reduction of variants was accomplished by the application of 'intra-group comparison'. By *a priori* selecting groups of patients based on their specific, distinctive MRI pattern we were able to define multiple homogeneous patient cohorts with presumably the same disorder. This approach was both extremely reliable and powerful as we so far we have had a success rate of 80-90% for gene identification by WES in small, homogeneous patients groups from the Amsterdam database of unclassified leukoencephalopathy cases, whereas several larger WES studies have reported success rate for 42% for mixed leukodystrophy

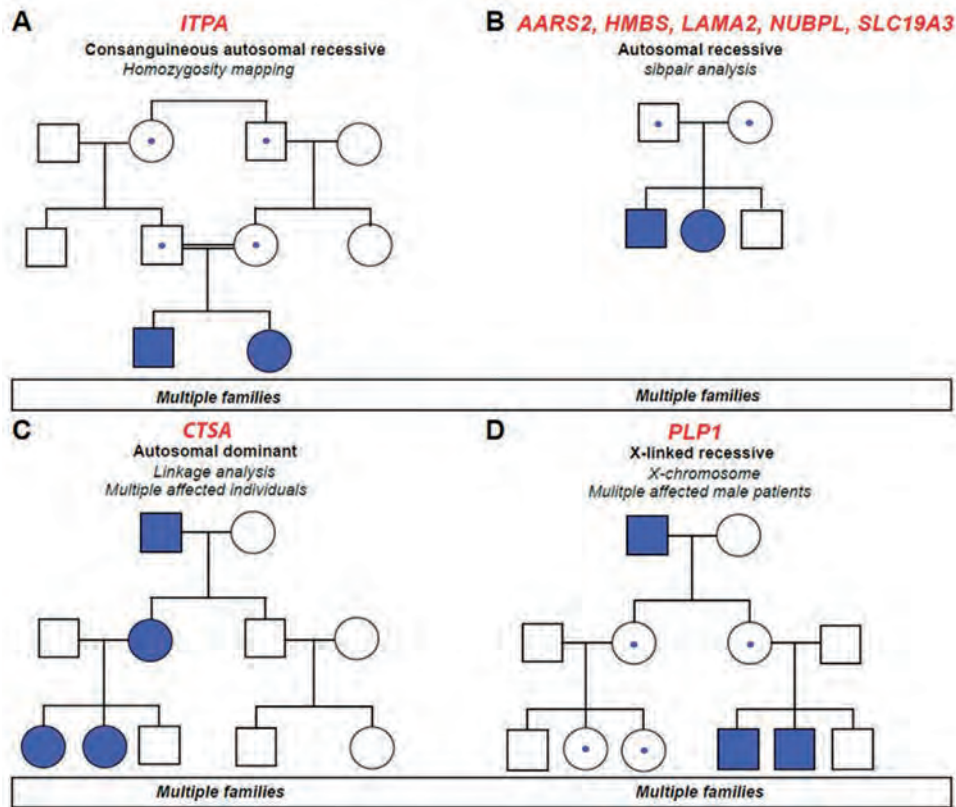


Figure 1. Overview of different inheritance patterns with different exome analysis approaches used for each gene identified.

Circles represent females; squares males. Blue solid symbols indicate affected individuals; symbols with a dot indicate unaffected carriers. (A) Several families with *ITPA* mutations were consanguineous. Therefore, the candidate region could be narrowed down by searching for overlapping homozygous regions using a SNP-array. Whole-exome sequencing (WES) was performed in multiple unrelated patients to allow intra-group comparison. (B) The families with *AARS2*, *HMBS*, *LAMA2*, *NUBPL* and *SLC19A3* mutations showed a possible autosomal recessive inheritance pattern, without reported consanguinity. For the identification of *HMBS* and *LAMA2* sibpair analysis was sufficient for detecting the gene. For the identification of *AARS2*, *NUBPL*, and *SLC19A3*, comparison of multiple unrelated patients was needed to confirm the associated phenotype. (C) The two families with *CTSA* mutations had an autosomal dominant inheritance pattern. The gene was identified using linkage analysis to narrow down the candidate region, sequencing multiple affected individuals within one family and comparison of the two families. (D) All the families with *PLP1* mutations showed a strong X-linked recessive inheritance pattern. The gene was identified by focusing on the X-chromosome, sibpair analysis and comparison of multiple unrelated patients.

cases¹⁰² and 16% to 53% in several large studies.^{69,103-108} Another advantage of using multiple unrelated patients over single cases for WES analysis is that by identification of the gene a new clinical disease entity can be described, facilitating the recognition of future patients and making the diagnostic process for these patients easier and faster. The impact of the availability of multiple unrelated patients within one group is reflected in almost every study reported in this thesis. For example, in **chapter 9** we found recessive variants in the gene *NUBPL* in six patients. In 2010 a single patient

with *NUBPL* variants had already been published but with little clinical information and no MR images.⁷⁰ The consequence was that the disease phenotype could not be recognized. Our study provides a clear description of the disease entity associated with *NUBPL* variants, which will preclude this issue and make diagnosis for future patients much easier. Furthermore, the *ITPA* variants described in **chapter 10** might not have been considered pathogenic if identified in a single case because of the known lack of clinical effect of previously described variants.^{89,96} In **chapter 2** the presence of multiple patients with HEMS contributed greatly to our success, because only after sequencing additional HEMS patients who had genomic variants in regions that were covered with WES we were able to identify the candidate gene *PLP1*.

It should be mentioned that for all studies we used multiple singleton patients instead of trios (parents and patient), but if other patients are not available sequencing trios is more successful than sequencing singleton patients.¹⁰⁵ This appears to be especially true for disorders caused by *de novo* variants, since these variants can only be promptly detected by this trio approach. Sequencing parents along with the patients is also helpful for reducing the number of potential compound heterozygous variants in cases where a recessive disorder is suspected. Still, sequencing single cases/families is rather challenging because the function of most genes in the genome is poorly understood; less than 10% of the genes are annotated with an OMIM disease association.¹⁰⁹ The main bottleneck of the filtering pipeline is our ability to interpret the effect of the variants, which is very challenging for synonymous and intronic variants, but also for missense variants. Without the presence of other patients and lack of knowledge about the function of the protein encoded by the gene, conclusions on the potential pathogenicity of a variant are based on *in silico* prediction software programs (e.g. MutationTaster,¹¹⁰ PolyPhen-2¹¹¹ and SIFT¹¹²), information on nucleotide conservation (PhyloP and GERP scores) and amino acid (GVGD) level and effect on splicing (e.g. the splice site prediction tools; Human Splice Finder,¹¹³ MaxEntScan,¹¹⁴ NetGene2,¹¹⁵ NNSplice¹¹⁶ and SpliceSiteFinder-like, and tools for prediction of splice enhancers and inhibitors (e.g. ESEfinder 3.0¹¹⁷), which are often inconclusive and make functional follow-up studies imperative. In the recently published FORGE project the disorder remained unsolved in 28 (20%) of the 174 unclassified families despite that a single candidate gene was found that could be causally related, because of a lack in knowledge of function of the protein encoded by the gene and because no additional families with the same disorder were available.¹⁰⁸ Finding another case with a presumably pathogenic variant in the same gene would provide sufficient evidence for causality.

One of the advantages of WES is the unbiased approach of gene finding; the genes

that are found in association with a disease may be completely unexpected. Prior knowledge about the gene is therefore not imperative. It is important to realize that filtering based on *a priori* knowledge (like evidence of mitochondrial dysfunction, as described in **chapter 9**) may facilitate identification of the gene mutated in the disease of interest, but this stringent filtering approach may also omit the candidate gene. The reason may be that it is not yet known that a particular protein is of importance in a specific process, but it may also be that the hypothesis concerning the disease mechanism was not correct. In **chapter 3** the patient's clinical phenotype, biochemical profile (e.g. elevated lactate), and neuropathologic features of massive neuronal cell death strongly suggested an underlying mitochondrial disorder. WES analyses revealed variants in *SLC19A3*, a thiamine transporter. Defects of this transporter indirectly impact mitochondrial function, but this gene is absent from the mitocarta database.¹⁰¹

PITFALLS AND CHALLENGES OF WES

As discussed before it has been found that the success rate for WES in providing a molecular diagnosis for unselected groups of single patients with a rare Mendelian disorder ranges from 16% to 53%.^{69,103-108} The reason that a substantial number of patients still remains without molecular diagnosis relies on several factors. The first is incomplete sequencing coverage of the exome. Typically, a minimum mean coverage of 20-30 reads per base is required for sufficient accuracy of variant detection (depending on using short or long reads). In 2011 different exome capture kits all showed an overall exome capture of around 80% (minimal coverage of 30X).¹¹⁸ However, the last four years this has significantly improved and the latest exome capture kits are able to cover up to 95% of the exome at 20X,¹¹⁹ creating a higher potential diagnostic yield. The second reason is that certain variants are elusive to the technology itself, including trinucleotide repeats (e.g. Fragile X-syndrome), inversions, a certain size range of duplications and deletions, and structural variants (chromosomal translocations and aneuploidy).¹²⁰ Ongoing improvements of the bioinformatics pipelines including the software for mapping and algorithms developed for variant calling may resolve some of these false-negatives in the future. For detection of copy number variations (CNVs) and small duplications and deletions in WES data numerous tools have been developed in the last few years, but although advances have been made, accurate detection of CNVs in WES data remains challenging.¹²¹ It is important to realize that such variants can be missed when filtering the data. This is illustrated by the gene finding process in **chapter 9**. In this case one of the pathogenic variants in *NUBPL* (c.677_688insCCTTGTGCTG (p.Glu223Alafs*4) was not detected by our bioinformatics pipeline at that time. Although we assumed

a recessive inheritance mode we fortunately filtered for genes with either one or two heterozygous variants to circumvent this possibility. Variants that by definition are refractory to WES are variants in non-coding regions (outside the splice consensus site). In **chapter 2** we encountered this problem. Initial WES analysis of two siblings with HEMS, their mother and an unrelated patient with HEMS was unrevealing. After the inclusion of four additional patients and the application of targeted X-chromosome exome sequencing we were able to identify the candidate gene, *PLP1*. In hindsight the negative WES results can be explained by the lack of coverage of the intronic variants. The second approach was successful because some of the additional sequenced patients had exonic variants. Although most disease causing variants (roughly 85%) are located in functional and coding regions of the genome, the remaining (non-coding causal) variants are still refractory to WES analysis. The non-coding variants identified in this disorder were located in a conserved regulatory intronic region affecting alternative splicing of *PLP1*.^{42,122} Splicing is a complex mechanism and regulated by the strength of the canonical splice donor and acceptor sites and branch sites, exonic or intronic enhancers and silencers and formation of RNA structures.^{123,124} It is estimated that >90% of the human protein-coding genes are subjected to alternative splicing, producing multiple mRNA isoforms.¹²⁵ Deep intronic variants leading to splicing alterations are likely to be underestimated, as they are not detected by routine DNA sequencing approaches or WES.

As discussed in the previous section of strategies for gene discovery, the main bottleneck of the filtering pipeline is our ability to interpret the effect of the variants. At present, for leukodystrophies, the best approach is WES in a group of unrelated patients with the same disease, so that conclusion for pathogenicity of the variant does not depend solely on knowledge of function of a gene or predicted effect of a variant. For leukodystrophies MRI offers an excellent tool for disease definition due to its high sensitivity and accuracy. We took advantage of this in all chapters and I would recommend it for future studies. As the unclassified leukodystrophies are becoming rarer, collaboration and pooling of data are increasingly important, as already shown by our studies that were all based on world-wide collaborations.

IMPLICATIONS FOR PATIENTS

The presence of a (molecular) diagnosis has major implications for the patients and their families. All patients described in this thesis have had an awfully long diagnostic work-up before WES was performed. Some of the families were already known to us for

over 10 years. In some families, three children had died without diagnosis and without prenatal testing ever being an option. After the application of WES the diagnosis was established rapidly for all cases. In addition to a definitive diagnosis, we were now able to inform these families about recurrence risks, options for prenatal testing and for some cases about prognosis. Occasionally a genetic diagnosis can have important therapeutic implications. For example, in a study performed by Sawyer and colleagues, six (26%) of the 105 families with a WES-identified molecular diagnosis had a dramatically change of treatment.¹⁰⁸ In **chapter 3** (*SLC19A3*-related encephalopathy) we describe a disorder, for which a fast (molecular) diagnosis can result in a specific therapy that might be life-saving in some cases. The most commonly reported phenotype associated with *SLC19A3* variants, 'BTBGD', can be successfully treated with thiamin and biotin.^{49,51,53} Haack *et al.*, reported that more severely affected patients presenting as an early-infantile Leigh-like syndrome with loss-of-function variants would also benefit from thiamin and biotin supplementation.⁵⁷ The last two years several additional reports have been published regarding successful administration of thiamine to *SLC19A3* mutated patients, although these mainly concerned the BTBGD or Leigh-like syndrome phenotype.^{54,55,57-60,62} In the case of early administration of thiamine (and biotin) the clinical and radiological abnormalities can be reversed improving neurological outcome.^{54,57,59,62} However, we are rather pessimistic about a potential positive effect of thiamine in our infantile group, because due to the very early onset and rapid disease course, the brain damage is beyond repair within one or a few days. *SLC19A3*-related disorders might be treatable, if thiamine is administrated early enough before significant damage has occurred, but even then the definitive outcome remains uncertain as many studies published so far have a short follow-up.^{54,57,59,62}

As illustrated by the study described in **chapter 7**, the unbiased approach of WES can lead to unexpected results that have direct implications for the health of siblings. In this particular case, siblings were found to be carrier of a heterozygous pathogenic *HMBS* gene variant that is associated with a life time risk of 10% for acute porphyric attacks.¹²⁶ Although this could be regarded as an incidental finding for these siblings, this knowledge has major implications for their future health because these individuals now can take preventive measures the limit the risk of potential life-threatening porphyric attacks, hypertension and liver carcinoma.^{126,127}

INSIGHT FROM GENE DISCOVERY FOR LEUKODYSTROPHIES

The original definition of leukodystrophies was highly focused on myelin. Initially it was thought that myelin and oligodendrocyte-specific proteins are involved in all leukodystrophies. In this thesis nine different genes were identified, each associated with a different leukodystrophy. Intriguingly, all identified genes, except for *PLP1*, do not encode myelin-specific proteins. Due to the unbiased approach of NGS analysis, genes were found that were totally unexpected. Strikingly, a defect in certain common pathways was found to underlie several leukodystrophies. As shown by our results in **chapter 11**, many genes associated both with hypomyelination and other leukodystrophies are involved in mRNA translation and protein synthesis. Protein synthesis is a highly complex process and numerous proteins are involved (e.g. proteins mediating the activation, initiation, elongation or termination of mRNA translation, aminoacyl tRNA synthetases (aaRSes), cofactors and modifying proteins and ribosomal proteins).^{128,129} More specifically, our results described in **chapters 5, 6** and **chapter 11** show that a large group of patients represented defects of aaRSes or RNA polymerase III. Hence, it has become evident that most genes associated with leukodystrophies do not encode intrinsic myelin proteins.

Aminoacyl tRNA synthetases

Human cells contain 17 cytoplasmic aaRSes, 18 mitochondrial aaRSes and two aaRSes present both in the cytoplasm and mitochondria.¹³⁰ AaRSes are ancient housekeeping enzymes that attach amino acids to their cognate tRNA molecules as essential step in protein synthesis.¹³⁰ Before the advent of WES in 2010 only seven disorders were known to be associated with an aaRS defect. Up to date, 26 of 37 aaRSes have been implicated in human disease, of which the vast majority (19) was found in the last four years, predominantly using WES.^{29,36-38,130-132}

Although a wide variety of disorders is each associated with a different aaRS enzyme defect, it has become clear that several of these aaRSes, both cytosolic and mitochondrial, are mutated in patients with leukodystrophies (in 2008 *DARS2*,¹³³ in 2010 *AIMP1*,¹³⁴ in 2011 *EARS2*,¹⁸ in 2012 *MARS2*,¹⁶ in 2013 *DARS*,¹⁹ in 2013 *LARS2*¹³⁵ and *AARS2*,²⁵ and in 2014 *RARS*.²⁶ Although the essential canonical function of these enzymes is the same (mRNA translation), there are striking differences between the different leukodystrophies concerning tissue and cell type specificity and clinical phenotype, like the onset, course and outcome of the disorder. For example, patients with *DARS2* variants typically have a childhood or adolescent-onset slowly progressive pyramidal, cerebellar and dorsal column dysfunction,^{133,136} whilst patients with *AARS2* variants experience a rapid

neurological deterioration in adulthood that leads to severe disabilities and sometimes death after a long period of clinical stability.²⁵ Intriguingly, for both disorders the MRI pattern shows abnormalities in very specific white matter tracts.^{25,133,136} On the other hand, it is also striking that hypomyelination with brainstem and spinal cord involvement and leg spasticity (HBSL) and LBSL have a major overlap in specifically affected white matter structures, while the involved aaRSes (encoded by *DARS* and *DARS2*), have a different subcellular localization (respectively in the cytoplasm and mitochondria).^{19,133} It is still unclear what determines the selective vulnerability of different tissues in this group of disorders, and what, within the subgroup of leukodystrophies, determines the selective vulnerability of specific structures within the nervous system, while the canonical function of the affected enzymes is the same. It is suggested that involvement of noncanonical functions of these aaRSes could determine the phenotypes and that the explanation for differences and similarities in phenotypes could be found there.^{19,133} Indeed, some of the cytosolic aaRSes are reported to have noncanonical functions in biological processes such as regulation of gene transcription and RNA splicing,¹³⁷ angiogenesis, tumorigenesis and inflammation.^{130,138} For aaRS defects, as for other defects in housekeeping genes involved in protein synthesis and associated with a leukodystrophy, like the POLR3-related disorders (described below) and VWM, no patients have been reported with two functional null-alleles, suggesting that complete abolishment of the function of the affected enzymes is not compatible with life.

RNA polymerase III

POLR3 is a DNA-directed polymerase, which is involved in the transcription of small non-coding RNAs, including tRNAs.¹³⁹ Recessive variants in *POLR3A* and *POLR3B*, encoding the largest and second largest subunit of POLR3, and *POLR1C* encoding a shared RNA polymerase I and POLR3 subunit, were found to be the cause of three overlapping leukodystrophy phenotypes: tremor-ataxia with central hypomyelination (TACH), leukodystrophy with oligodontia (MIM 607694) and 'hypomyelination, hypogonadotropic hypogonadism and hypodontia syndrome', also referred to as 4H syndrome.^{10-12,28,140,141} Since the discovery of the genes, as shown by our study in **chapter 11**, this is currently one of the most prevalent hypomyelinating disorders with a known molecular defect.¹⁴²

FUTURE PERSPECTIVES

The diagnosis and classification of leukodystrophies has changed dramatically since the 19th century.¹⁴³⁻¹⁴⁶ Although pathology and biochemical findings still play a role in the diagnostic process, they are often not mandatory for a definitive diagnosis, but rather

supportive. Although one could expect that with WES the diagnostic process would be reversed (referred to as “reversed phenotyping” (first genotyping, then phenotyping)), this has not become a common approach. Indeed, it is shown by us and many others that a priori good phenotyping is and will remain very important for successful WES analysis, at least for leukodystrophies.

The unbiased approach of WES has created huge new research opportunities to be explored. Novel genes are now discovered that would not have been studied because of the lack of correlation with the phenotype or lack of knowledge of the function of the gene. The rapidly increasing insight into genes mutated in leukodystrophies creates novel, unprecedented insight into proteins that are apparently essential for the maintenance of white matter health. It is becoming increasingly apparent that in contrast to what was thought for many years, most leukodystrophies are not caused by variants in myelin specific proteins, like PLP, but are caused by defects in diverse fundamental biological processes, such as mitochondrial respiratory function and processes of mRNA translation and protein synthesis. At present we do not understand why defects in such basic, housekeeping functions specifically affect the maintenance of brain white matter health and function. This should be the subject of future studies. It is to be expected that in the coming years 90-95% of the leukodystrophy patients will receive a molecular diagnosis. With that we will have an almost complete map of proteins that are involved one way or the other in the brain white matter.

The new insights have major implications for our understanding and definition of ‘leukodystrophies’. The original definition of a ‘leukodystrophy’ was totally myelin focused and assumed a progressive disorder. With the current knowledge of the underlying genetic defects of leukodystrophies and the variable clinical phenotype this definition should be revised. As proposed in **chapter 11**, we propose that all genetic disorders primarily and predominantly involving CNS white matter structures (and not only myelin) should be referred to as leukodystrophies, independent of the disease course. This new insight has therapy implications: not only should remyelination be achieved, but repair of all affected white matter components.

REFERENCES

1. van der Knaap MS and Valk J. Myelin and White Matter. In: *Magnetic Resonance of Myelination and Myelin Disorders*. Heidelberg: Springer; 2005. p.1-19.
2. van der Knaap MS and Valk J. *Magnetic Resonance of Myelination and Myelin Disorders*. Heidelberg: Springer; 2005.
3. Dietrich RB, Vining EP, Taira RK, Hall TR, Phillipart M. Myelin disorders of childhood: correlation of MR findings and severity of neurological impairment. *J Comput Assist Tomogr* 1990;14:693-698.
4. Demaerel P, Faubert C, Wilms G, Casaer P, Piepgras U, Baert AL. MR findings in leukodystrophy. *Neuroradiology* 1991;33:368-371.
5. van der Knaap MS and Valk J. Wallerian Degeneration and Myelin Loss Secondary to Neuronal and Axonal Degeneration. *Magnetic Resonance of Myelination and Myelin Disorders*. Heidelberg: Springer; 2005.p. 832-838.
6. Vanderver A, Prust M, Tonduti D, et al. Case definition and classification of leukodystrophies and leukoencephalopathies. *Mol Genet Metab* 2015;114:494-500.
7. Bonkowsky JL, Nelson C, Kingston JL, Filloux FM, Mundorff MB, Srivastava R. The burden of inherited leukodystrophies in children. *Neurology* 2010;75:718-725.
8. Chong JX, Buckingham KJ, Jhangiani SN, et al. The Genetic Basis of Mendelian Phenotypes: Discoveries, Challenges, and Opportunities. *Am J Hum Genet* 2015;97:199-215.
9. Boycott KM, Vanstone MR, Bulman DE, MacKenzie AE. Rare-disease genetics in the era of next-generation sequencing: discovery to translation. *Nat Rev Genet* 2013;14:681-691.
10. Bernard G, Chouery E, Putorti ML, et al. Mutations of POLR3A encoding a catalytic subunit of RNA polymerase Pol III cause a recessive hypomyelinating leukodystrophy. *Am J Hum Genet* 2011;89:415-423.
11. Tetreault M, Choquet K, Orcesi S, et al. Recessive mutations in POLR3B, encoding the second largest subunit of Pol III, cause a rare hypomyelinating leukodystrophy. *Am J Hum Genet* 2011;89:652-655.
12. Saito H, Osaka H, Sasaki M, et al. Mutations in POLR3A and POLR3B encoding RNA Polymerase III subunits cause an autosomal-recessive hypomyelinating leukoencephalopathy. *Am J Hum Genet* 2011;89:644-651.
13. Cameron JM, Janer A, Levandovskiy V, et al. Mutations in iron-sulfur cluster scaffold genes *NFU1* and *BOLA3* cause a fatal deficiency of multiple respiratory chain and 2-oxoacid dehydrogenase enzymes. *Am J Hum Genet* 2011;89:486-495.
14. Rademakers R, Baker M, Nicholson AM, et al. Mutations in the colony stimulating factor 1 receptor (*CSF1R*) gene cause hereditary diffuse leukoencephalopathy with spheroids. *Nat Genet* 2011;44:200-205.
15. Navarro-Sastre A, Tort F, Stehling O, et al. A fatal mitochondrial disease is associated with defective *NFU1* function in the maturation of a subset of mitochondrial Fe-S proteins. *Am J Hum Genet* 2011;89:656-667.
16. Bayat V, Thiffault I, Jaiswal M, et al. Mutations in the mitochondrial methionyl-tRNA synthetase cause a neurodegenerative phenotype in flies and a recessive ataxia (*ARSAL*) in humans. *PLoS Biol* 2012;10:e1001288.
17. Polvi A, Linnankivi T, Kivela T, et al. Mutations in *CTC1*, encoding the CTS telomere maintenance complex component 1, cause cerebretinal microangiopathy with calcifications and cysts. *Am J Hum Genet* 2012;90:540-549.
18. Steenweg ME, Ghezzi D, Haack T, et al. Leukoencephalopathy with thalamus and brainstem involvement and high lactate 'LTBL' caused by *EARS2* mutations. *Brain* 2012;135:1387-1394.
19. Taft RJ, Vanderver A, Leventer RJ, et al. Mutations in *DARS* cause hypomyelination with brain stem and spinal cord involvement and leg spasticity. *Am J Hum Genet* 2013;92:774-780.
20. Invernizzi F, Tigano M, Dallabona C, et al. A homozygous mutation in *LYRM7/MZM1L* associated with early onset encephalopathy, lactic acidosis, and severe reduction of mitochondrial complex III activity. *Hum Mutat* 2013;34:1619-1622.
21. Kevelam SH, Rodenburg RJ, Wolf NI, et al. *NUBPL* mutations in patients with complex I deficiency and a distinct MRI pattern. *Neurology* 2013;80:1577-1583.

22. Simons C, Wolf NI, McNeil N, et al. A de novo mutation in the beta-tubulin gene TUBB4A results in the leukoencephalopathy hypomyelination with atrophy of the basal ganglia and cerebellum. *Am J Hum Genet* 2013;92:767-773.
23. Diodato D, Melchionda L, Haack TB, et al. VARS2 and TARS2 mutations in patients with mitochondrial encephalomyopathies. *Hum Mutat* 2014;35:983-989.
24. Melchionda L, Haack TB, Hardy S, et al. Mutations in APOPT1, encoding a mitochondrial protein, cause cavitating leukoencephalopathy with cytochrome c oxidase deficiency. *Am J Hum Genet* 2014;95:315-325.
25. Dallabona C, Diodato D, Kevelam SH, et al. Novel (ovario) leukodystrophy related to AARS2 mutations. *Neurology* 2014;82:2063-2071.
26. Wolf NI, Salomons GS, Rodenburg RJ, et al. Mutations in RARS cause hypomyelination. *Ann Neurol* 2014;76:134-139.
27. Olahova M, Hardy SA, Hall J, et al. LRPPRC mutations cause early-onset multisystem mitochondrial disease outside of the French-Canadian population. *Brain* 2015;138:3503-3519.
28. Thiffault I, Wolf NI, Forget D, et al. Recessive mutations in POLR1C cause a leukodystrophy by impairing biogenesis of RNA polymerase III. *Nat Commun* 2015;6:7623.
29. Sofou K, Kollberg G, Holmstrom M, et al. Whole exome sequencing reveals mutations in NARS2 and PARS2, encoding the mitochondrial asparaginyl-tRNA synthetase and prolyl-tRNA synthetase, in patients with Alpers syndrome. *Mol Genet Genomic Med* 2015;3:59-68.
30. Al-Hassnan ZN, Al-Dosary M, Alfadhel M, et al. ISCA2 mutation causes infantile neurodegenerative mitochondrial disorder. *J Med Genet* 2015;52:186-194.
31. Hallmann K, Kudin AP, Zsurka G, et al. Loss of the smallest subunit of cytochrome c oxidase, COX8A, causes Leigh-like syndrome and epilepsy. *Brain* 2016;139:338-345.
32. Debray FG, Stumpfig C, Vanlander AV, et al. Mutation of the iron-sulfur cluster assembly gene IBA57 causes fatal infantile leukodystrophy. *J Inher Metab Dis* 2015;38:1147-1153.
33. Soreze Y, Boutron A, Habarou F, et al. Mutations in human lipoyltransferase gene LIPT1 cause a Leigh disease with secondary deficiency for pyruvate and alpha-ketoglutarate dehydrogenase. *Orphanet J Rare Dis* 2013;8:192.
34. Elo JM, Yadavalli SS, Euro L, et al. Mitochondrial phenylalanyl-tRNA synthetase mutations underlie fatal infantile Alpers encephalopathy. *Hum Mol Genet* 2012;21:4521-4529.
35. Kevelam SH, Bugiani M, Salomons GS, et al. Exome sequencing reveals mutated SLC19A3 in patients with an early-infantile, lethal encephalopathy. *Brain* 2013;136:1534-1543.
36. Hallmann K, Zsurka G, Moskau-Hartmann S, et al. A homozygous splice-site mutation in CARS2 is associated with progressive myoclonic epilepsy. *Neurology* 2014;83:2183-2187.
37. Simons C, Griffin LB, Helman G, et al. Loss-of-function alanyl-tRNA synthetase mutations cause an autosomal-recessive early-onset epileptic encephalopathy with persistent myelination defect. *Am J Hum Genet* 2015;96:675-681.
38. Schwartzentruber J, Buhas D, Majewski J, et al. Mutation in the nuclear-encoded mitochondrial isoleucyl-tRNA synthetase IARS2 in patients with cataracts, growth hormone deficiency with short stature, partial sensorineural deafness, and peripheral neuropathy or with Leigh syndrome. *Hum Mutat* 2014;35:1285-1289.
39. Arai-Ichinoi N, Uematsu M, Sato R, et al. Genetic heterogeneity in 26 infants with a hypomyelinating leukodystrophy. *Hum Genet* 2016;135:89-98.
40. Zhang X. Exome sequencing greatly expedites the progressive research of Mendelian diseases. *Front Med* 2014;8:42-57.
41. Steenweg ME, Wolf NI, Schieving JH, et al. Novel hypomyelinating leukoencephalopathy affecting early myelinating structures. *Arch Neurol* 2012;69:125-128.
42. Kevelam SH, Taube JR, van Spaendonk RM, et al. Altered PLP1 splicing causes hypomyelination of early myelinating structures. *Ann Clin Transl Neurol* 2015;2:648-661.
43. van der Knaap MS and Valk J. Pelizaeus-Merzbacher Disease and X-linked Spastic Paraplegia Type 2. In: *Magnetic Resonance Imaging of Myelination and Myelin Disorders*. Heidelberg: Springer; 2005. p. 272-280.
44. Woodward KJ. The molecular and cellular defects underlying Pelizaeus-Merzbacher disease. *Expert Rev Mol Med* 2008;10:e14.
45. Inoue K. PLP1-related inherited dysmyelinating disorders: Pelizaeus-Merzbacher disease and spastic paraplegia type 2. *Neurogenetics* 2005;6:1-16.

46. Cailloux F, Gauthier-Barichard F, Mimault C, et al. Genotype-phenotype correlation in inherited brain myelination defects due to proteolipid protein gene mutations. *Clinical European Network on Brain Demyelinating Disease. Eur J Hum Genet* 2000;8:837-845.
47. Rajgopal A, Edmondson A, Goldman ID, Zhao R. SLC19A3 encodes a second thiamine transporter ThTr2. *Biochim Biophys Acta* 2001;1537:175-178.
48. Powers J M and de Vivo D C. Peroxisomal and mitochondrial disorders. In:Graham D I and Lantos P L. *Greenfield's Neuropathology*. New York: Arnold Press; 2002.
49. Zeng WQ, Al-Yamani E, Acierno JS, Jr., et al. Biotin-responsive basal ganglia disease maps to 2q36.3 and is due to mutations in SLC19A3. *Am J Hum Genet* 2005;77:16-26.
50. Kono S, Miyajima H, Yoshida K, Togawa A, Shirakawa K, Suzuki H. Mutations in a thiamine-transporter gene and Wernicke's-like encephalopathy. *N Engl J Med* 2009;360:1792-1794.
51. Debs R, Depienne C, Rastetter A, et al. Biotin-responsive basal ganglia disease in ethnic Europeans with novel SLC19A3 mutations. *Arch Neurol* 2010;67:126-130.
52. Yamada K, Miura K, Hara K, et al. A wide spectrum of clinical and brain MRI findings in patients with SLC19A3 mutations. *BMC Med Genet* 2010;171-11.
53. Serrano M, Rebollo M, Depienne C, et al. Reversible generalized dystonia and encephalopathy from thiamine transporter 2 deficiency. *Mov Disord* 2012;27:1295-1298.
54. Perez-Duenas B, Serrano M, Rebollo M, et al. Reversible lactic acidosis in a newborn with thiamine transporter-2 deficiency. *Pediatrics* 2013;131:e1670-e1675.
55. Fassone E, Wedatilake Y, DeVile CJ, Chong WK, Carr LJ, Rahman S. Treatable Leigh-like encephalopathy presenting in adolescence. *BMJ Case Rep* 2013;200838-
56. Gerards M, Kamps R, van OJ, et al. Exome sequencing reveals a novel Moroccan founder mutation in SLC19A3 as a new cause of early-childhood fatal Leigh syndrome. *Brain* 2013;136:882-890.
57. Haack TB, Klee D, Strom TM, et al. Infantile Leigh-like syndrome caused by SLC19A3 mutations is a treatable disease. *Brain* 2014;137:e295.
58. Tabarki B, AlFadhel M, AlShahwan S, Hundallah K, AlShafi S, AlHashem A. Treatment of biotin-responsive basal ganglia disease: Open comparative study between the combination of biotin plus thiamine versus thiamine alone. *Eur J Paediatr Neurol* 2015;19:547-552.
59. Ortigoza-Escobar JD, Serrano M, Molero M, et al. Thiamine transporter-2 deficiency: outcome and treatment monitoring. *Orphanet J Rare Dis* 2014;9:92-99.
60. Distelmaier F, Huppke P, Pieperhoff P, et al. Biotin-responsive Basal Ganglia disease: a treatable differential diagnosis of leigh syndrome. *JIMD Rep* 2014;13:53-57.
61. Schanzer A, Doring B, Ondruschek M, et al. Stress-induced upregulation of SLC19A3 is impaired in biotin-thiamine-responsive basal ganglia disease. *Brain Pathol* 2014;24:270-279.
62. Ortigoza-Escobar JD, Molero-Luis M, Arias A, et al. Free-thiamine is a potential biomarker of thiamine transporter-2 deficiency: a treatable cause of Leigh syndrome. *Brain* 2015;342.
63. Gavassini BF, Carboni N, Nielsen JE, et al. Clinical and molecular characterization of limb-girdle muscular dystrophy due to LAMA2 mutations. *Muscle Nerve* 2011;44:703-709.
64. Geranmayeh F, Clement E, Feng LH, et al. Genotype-phenotype correlation in a large population of muscular dystrophy patients with LAMA2 mutations. *Neuromuscul Disord* 2010;20:241-250.
65. Kevelam SH, van Engelen BG, van Berkel CG, Kusters B, van der Knaap MS. LAMA2 mutations in adult-onset muscular dystrophy with leukoencephalopathy. *Muscle Nerve* 2014;49:616-617.
66. Steenweg ME, Vanderver A, Ceulemans B, et al. Novel infantile-onset leukoencephalopathy with high lactate level and slow improvement. *Arch Neurol* 2012;69:718-722.
67. Gotz A, Tynnismaa H, Euro L, et al. Exome sequencing identifies mitochondrial alanyl-tRNA synthetase mutations in infantile mitochondrial cardiomyopathy. *Am J Hum Genet* 2011;88:635-642.
68. Euro L, Konovalova S, Asin-Cayuela J, et al. Structural modeling of tissue-specific mitochondrial alanyl-tRNA synthetase (AARS2) defects predicts differential effects on aminoacylation. *Front Genet* 2015;6:21.
69. Taylor RW, Pyle A, Griffin H, et al. Use of whole-exome sequencing to determine the genetic basis of multiple mitochondrial respiratory chain complex deficiencies. *JAMA* 2014;312:68-77.
70. Calvo SE, Compton AG, Hershman SG, et al. Molecular diagnosis of infantile mitochondrial disease with targeted next-generation sequencing. *Sci Transl Med* 2012;4:118ra10.

71. van der Knaap MS, Boor I, Estevez R. Megalencephalic leukoencephalopathy with subcortical cysts: chronic white matter oedema due to a defect in brain ion and water homeostasis. *Lancet Neurol* 2012;11:973-985.
72. Bushby KM, Collins J, Hicks D. Collagen type VI myopathies. *Adv Exp Med Biol* 2014;802:185-199.
73. Tetreault M, Gonzalez M, Dicaire MJ, et al. Adult-onset painful axonal polyneuropathy caused by a dominant NAGLU mutation. *Brain* 2015;138:1477-1483.
74. Grandchamp B, Picat C, Mignotte V, et al. Tissue-specific splicing mutation in acute intermittent porphyria. *Proc Natl Acad Sci U S A* 1989;86:661-664.
75. Villeneuve de V, Wadman S K, Heuvel van de JM. Een kind met een bijzondere vorm van porfyrie. *Maandschrift voor de kindergeneeskunde* 1964;731-742.
76. Picat C, Delfau MH, de Rooij FW, et al. Identification of the mutations in the parents of a patient with a putative compound heterozygosity for acute intermittent porphyria. *J Inherit Metab Dis* 1990;13:684-686.
77. Beukeveld GJ, Wolthers BG, Nordmann Y, Deybach JC, Grandchamp B, Wadman SK. A retrospective study of a patient with homozygous form of acute intermittent porphyria. *J Inherit Metab Dis* 1990;13:673-683.
78. Llewellyn DH, Smyth SJ, Elder GH, Hutchesson AC, Rattenbury JM, Smith MF. Homozygous acute intermittent porphyria: compound heterozygosity for adjacent base transitions in the same codon of the porphobilinogen deaminase gene. *Hum Genet* 1992;89:97-98.
79. Solis C, Martinez-Bermejo A, Naidich TP, et al. Acute intermittent porphyria: studies of the severe homozygous dominant disease provides insights into the neurologic attacks in acute porphyrias. *Arch Neurol* 2004;61:1764-1770.
80. Stenson PD, Mort M, Ball EV, Shaw K, Phillips A, Cooper DN. The Human Gene Mutation Database: building a comprehensive mutation repository for clinical and molecular genetics, diagnostic testing and personalized genomic medicine. *Hum Genet* 2014;133:1-9.
81. Muona M, Berkovic SF, Dibbens LM, et al. A recurrent de novo mutation in KCNC1 causes progressive myoclonus epilepsy. *Nat Genet* 2015;47:39-46.
82. Herve D, Chabriat H, Rigal M, et al. A novel hereditary extensive vascular leukoencephalopathy mapping to chromosome 20q13. *Neurology* 2012;79:2283-2287.
83. Calvo SE, Tucker EJ, Compton AG, et al. High-throughput, pooled sequencing identifies mutations in NUBPL and FOXRED1 in human complex I deficiency. *Nat Genet* 2010;42:851-858.
84. Tucker EJ, Compton AG, Thorburn DR. Recent advances in the genetics of mitochondrial encephalopathies. *Curr Neurol Neurosci Rep* 2010;10:277-285.
85. Wydro MM and Balk J. Insights into the pathogenic character of a common NUBPL branch-site mutation associated with mitochondrial disease and complex I deficiency using a yeast model. *Dis Model Mech* 2013;6:1279-1284.
86. Vanderheiden BS. Purification and properties of human erythrocyte inosine triphosphate pyrophosphohydrolase. *J Cell Physiol* 1979;98:41-47.
87. Holmes SL, Turner BM, Hirschhorn K. Human inosine triphosphatase: catalytic properties and population studies. *Clin Chim Acta* 1979;97:143-153.
88. Lin S, McLennan AG, Ying K, et al. Cloning, expression, and characterization of a human inosine triphosphate pyrophosphatase encoded by the itpa gene. *J Biol Chem* 2001;276:18695-18701.
89. Simone PD, Pavlov YI, Borgstahl GE. ITPA (inosine triphosphate pyrophosphatase): from surveillance of nucleotide pools to human disease and pharmacogenetics. *Mutat Res* 2013;753:131-146.
90. Pang B, McFaline JL, Burgis NE, et al. Defects in purine nucleotide metabolism lead to substantial incorporation of xanthine and hypoxanthine into DNA and RNA. *Proc Natl Acad Sci U S A* 2012;109:2319-2324.
91. Dong JH, Chen X, Cui M, Yu X, Pang Q, Sun JP. beta2-adrenergic receptor and astrocyte glucose metabolism. *J Mol Neurosci* 2012;48:456-463.
92. Sumi S, Marinaki AM, Arenas M, et al. Genetic basis of inosine triphosphate pyrophosphohydrolase deficiency. *Hum Genet* 2002;111:360-367.
93. Maeda T, Sumi S, Ueta A, et al. Genetic basis of inosine triphosphate pyrophosphohydrolase deficiency in the Japanese population. *Mol Genet Metab* 2005;85:271-279.
94. Shipkova M, Lorenz K, Oellerich M, Wieland E, von Ahsen N. Measurement of erythrocyte inosine triphosphate pyrophosphohydrolase (ITPA) activity by HPLC and correlation of ITPA genotype-phenotype in a Caucasian population. *Clin Chem* 2006;52:240-247.

95. Bakker JA, Lindhout M, Habets DD, van den Wijngaard A, Paulussen AD, Bierau J. The effect of ITPA polymorphisms on the enzyme kinetic properties of human erythrocyte inosine triphosphatase toward its substrates ITP and 6-Thio-ITP. *Nucleosides Nucleotides Nucleic Acids* 2011;30:839-849.
96. Zelinkova Z, Derijks LJ, Stokkers PC, et al. Inosine triphosphate pyrophosphatase and thiopurine s-methyltransferase genotypes relationship to azathioprine-induced myelosuppression. *Clin Gastroenterol Hepatol* 2006;4:44-49.
97. Behmanesh M, Sakumi K, Abolhassani N, et al. ITPase-deficient mice show growth retardation and die before weaning. *Cell Death Differ* 2009;16:1315-1322.
98. Boycott KM, Dymant DA, Sawyer SL, Vanstone MR, Beaulieu CL. Identification of genes for childhood heritable diseases. *Annu Rev Med* 2014;65:19-31.
99. Ng SB, Turner EH, Robertson PD, et al. Targeted capture and massively parallel sequencing of 12 human exomes. *Nature* 2009;461:272-276.
100. Gilissen C, Hoischen A, Brunner HG, Veltman JA. Disease gene identification strategies for exome sequencing. *Eur J Hum Genet* 2012;20:490-497.
101. Pagliarini DJ, Calvo SE, Chang B, et al. A mitochondrial protein compendium elucidates complex I disease biology. *Cell* 2008;134:112-123.
102. Vanderver A, Simons C, Helman G, et al. Whole exome sequencing in patients with white matter abnormalities. *Ann Neurol* 2016;submitted.
103. Farwell KD, Shahmirzadi L, El-Khechen D, et al. Enhanced utility of family-centered diagnostic exome sequencing with inheritance model-based analysis: results from 500 unselected families with undiagnosed genetic conditions. *Genet Med* 2015;17:578-586.
104. Yang Y, Muzny DM, Xia F, et al. Molecular findings among patients referred for clinical whole-exome sequencing. *JAMA* 2014;312:1870-1879.
105. Lee H, Deignan JL, Dorrani N, et al. Clinical exome sequencing for genetic identification of rare Mendelian disorders. *JAMA* 2014;312:1880-1887.
106. Yang Y, Muzny DM, Reid JG, et al. Clinical whole-exome sequencing for the diagnosis of mendelian disorders. *N Engl J Med* 2013;369:1502-1511.
107. de Ligt J, Willemsen MH, van Bon BW, et al. Diagnostic exome sequencing in persons with severe intellectual disability. *N Engl J Med* 2012;367:1921-1929.
108. Sawyer SL, Hartley T, Dymant DA, et al. Utility of whole-exome sequencing for those near the end of the diagnostic odyssey: time to address gaps in care. *Clin Genet* 2015;10.
109. Ng PC, Levy S, Huang J, et al. Genetic variation in an individual human exome. *PLoS Genet* 2008;4:e1000160.
110. Schwarz JM, Cooper DN, Schuelke M, Seelow D. MutationTaster2: mutation prediction for the deep-sequencing age. *Nat Methods* 2014;11:361-362.
111. Adzhubei I, Jordan DM, Sunyaev SR. Predicting functional effect of human missense mutations using PolyPhen-2. *Curr Protoc Hum Genet* 2013;Chapter 7:Unit7.20.
112. Ng PC and Henikoff S. Predicting deleterious amino acid substitutions. *Genome Res* 2001;11:863-874.
113. Desmet FO, Hamroun D, Lalande M, Collod-Beroud G, Claustres M, Beroud C. Human Splicing Finder: an online bioinformatics tool to predict splicing signals. *Nucleic Acids Res* 2009;37:e67.
114. Yeo G and Burge CB. Maximum entropy modeling of short sequence motifs with applications to RNA splicing signals. *J Comput Biol* 2004;11:377-394.
115. Hebsgaard SM, Korning PG, Tolstrup N, Engelbrecht J, Rouze P, Brunak S. Splice site prediction in *Arabidopsis thaliana* pre-mRNA by combining local and global sequence information. *Nucleic Acids Res* 1996;24:3439-3452.
116. Reese MG, Eeckman FH, Kulp D, Haussler D. Improved splice site detection in Genie. *J Comput Biol* 1997;4:311-323.
117. Cartegni L, Wang J, Zhu Z, Zhang MQ, Krainer AR. ESEfinder: A web resource to identify exonic splicing enhancers. *Nucleic Acids Res* 2003;31:3568-3571.
118. Parla JS, Iossifov I, Grabill I, Spector MS, Kramer M, McCombie WR. A comparative analysis of exome capture. *Genome Biol* 2011;12:R97-12.
119. Lelieveld SH, Spielmann M, Mundlos S, Veltman JA, Gilissen C. Comparison of Exome and Genome Sequencing Technologies for the Complete Capture of Protein-Coding Regions. *Hum Mutat* 2015;36:815-822.

120. Biesecker LG and Green RC. Diagnostic clinical genome and exome sequencing. *N Engl J Med* 2014;19:2418-2425.
121. Tan R, Wang Y, Kleinstejn SE, et al. An evaluation of copy number variation detection tools from whole-exome sequencing data. *Hum Mutat* 2014;35:899-907.
122. Taube JR, Sperle K, Banser L, et al. PMD patient mutations reveal a long-distance intronic interaction that regulates PLP1/DM20 alternative splicing. *Hum Mol Genet* 2014;23:5464-5478.
123. Scotti MM and Swanson MS. RNA mis-splicing in disease. *Nat Rev Genet* 2015;10.
124. Warf MB and Berglund JA. Role of RNA structure in regulating pre-mRNA splicing. *Trends Biochem Sci* 2010;35:169-178.
125. Pan Q, Shai O, Lee LJ, Frey BJ, Blencowe BJ. Deep surveying of alternative splicing complexity in the human transcriptome by high-throughput sequencing. *Nat Genet* 2008;40:1413-1415.
126. Puy H, Gouya L, Deybach JC. Porphyrrias. *Lancet* 2010;375:924-937.
127. Stewart MF. Review of hepatocellular cancer, hypertension and renal impairment as late complications of acute porphyria and recommendations for patient follow-up. *J Clin Pathol* 2012;65:976-980.
128. Scheper GC, van der Knaap MS, Proud CG. Translation matters: protein synthesis defects in inherited disease. *Nat Rev Genet* 2007;8:711-723.
129. Boczonadi V and Horvath R. Mitochondria: impaired mitochondrial translation in human disease. *Int J Biochem Cell Biol* 2014;48:77-84.
130. Antonellis A and Green ED. The role of aminoacyl-tRNA synthetases in genetic diseases. *Annu Rev Genomics Hum Genet* 2008;9:87-107.
131. Yao P and Fox PL. Aminoacyl-tRNA synthetases in medicine and disease. *EMBO Mol Med* 2013;5:332-343.
132. Coughlin CR, Scharer GH, Friederich MW, et al. Mutations in the mitochondrial cysteinyl-tRNA synthase gene, CARS2, lead to a severe epileptic encephalopathy and complex movement disorder. *J Med Genet* 2015;52:532-540.
133. Scheper GC, van der Kloot T, van Andel RJ, et al. Mitochondrial aspartyl-tRNA synthetase deficiency causes leukoencephalopathy with brain stem and spinal cord involvement and lactate elevation. *Nat Genet* 2007;39:534-539.
134. Feinstein M, Markus B, Noyman I, et al. Pelizaeus-Merzbacher-like disease caused by AIMP1/p43 homozygous mutation. *Am J Hum Genet* 2010;87:820-828.
135. Pierce SB, Gersak K, Michaelson-Cohen R, et al. Mutations in LARS2, encoding mitochondrial leucyl-tRNA synthetase, lead to premature ovarian failure and hearing loss in Perrault syndrome. *Am J Hum Genet* 2013;92:614-620.
136. van der Knaap MS, van der Voorn P, Barkhof F, et al. A new leukoencephalopathy with brainstem and spinal cord involvement and high lactate. *Ann Neurol* 2003;53:252-258.
137. Yao P, Poruri K, Martinis SA, Fox PL. Non-catalytic regulation of gene expression by aminoacyl-tRNA synthetases. *Top Curr Chem* 2014;344:167-187.
138. Kim S, You S, Hwang D. Aminoacyl-tRNA synthetases and tumorigenesis: more than housekeeping. *Nat Rev Cancer* 2011;11:708-718.
139. Dieci G, Fiorino G, Castelnuovo M, Teichmann M, Pagano A. The expanding RNA polymerase III transcriptome. *Trends Genet* 2007;23:614-622.
140. Wolf NI, Harting I, Boltshauser E, et al. Leukoencephalopathy with ataxia, hypodontia, and hypomyelination. *Neurology* 2005;64:1461-1464.
141. Wolf NI, Harting I, Innes AM, et al. Ataxia, delayed dentition and hypomyelination: a novel leukoencephalopathy. *Neuropediatrics* 2007;38:64-70.
142. Wolf NI, Vanderver A, van Spaendonk RM, et al. Clinical spectrum of 4H leukodystrophy caused by POLR3A and POLR3B mutations. *Neurology* 2014;83:1898-1905.
143. Bielschowsky M and Henneberg R. Über familiäre diffuse sklerose (Leukodystrophia cerebri progressiva hereditaria). *J Psychol Neurol* 1928;36:131-181.
144. Menkes J H. The leukodystrophies. *N Engl J Med* 1990;332:54-55.
145. Morell P and Wiesmann U. A correlative synopsis of the leukodystrophies. *Neuropediatrics* 1984;15 (suppl):62-65.
146. Seitelberger F. Structural manifestations of leukodystrophies. *Neuropediatrics* 1984;15 (suppl):53-61.

Chapter 13

Nederlandse samenvatting

Dankwoord

List of publications

Curriculum Vitae



NEDERLANDSE SAMENVATTING

Leukodystrofieën zijn zeldzame, erfelijke neurologisch aandoeningen die gekenmerkt worden door uitsluitend of voornamelijk afwijkingen die primair de witte stof van het centrale zenuwstelsel aantasten, al dan niet samen met een aandoening van de perifere zenuwen. Het zijn de genetische “witte stofziekten”. Deze aandoeningen openbaren zich meestal op de kinderleeftijd en gaan gepaard met ernstige neurologische afwijkingen en overlijden op jonge leeftijd. Een genetische diagnose is belangrijk voor patiënten en hun families omdat deze kennis mogelijkheden biedt ten aanzien van bijvoorbeeld prenataal onderzoek en het ontwikkelen van nieuwe behandelingen, en ook informatie kan opleveren over de prognose van de aandoening. Helaas duurt het traject voordat een diagnose gevonden wordt dikwijls erg lang, vaak jaren, en zelfs dan kon er in 2010, een jaar voordat mijn onderzoek begon, in de helft van de gevallen geen specifieke diagnose gesteld worden. De reden hiervoor is dat witte stofziekten erg zeldzaam zijn en heterogeen van origine, waardoor conventionele genetische technieken ontoereikend zijn. Ook is het vaak niet duidelijk welk gen getest moet worden, met als gevolg dat er vele genen na elkaar worden geanalyseerd, wat erg lang duurt en duur is.

Recent is er een nieuwe genetische laboratorium techniek ontwikkeld waarbij in één experiment alle coderende delen van het erfelijk materiaal (het exoom) geanalyseerd kunnen worden. Dit wordt 'exoom sequencing' genoemd. Uit verschillende onderzoeken is gebleken dat deze nieuwe techniek heel goed gebruikt kan worden voor het vinden van de genetische oorzaak bij patiënten met een (zeer) zeldzame erfelijke aandoening. Deze techniek zou dus ook zeer geschikt zijn om de genetische oorzaak te vinden van witte stofziekten.

Het doel van het onderzoek, dat in dit proefschrift wordt beschreven, was om de genetische oorzaak te vinden van onbekende witte stofziekten door gebruik te maken van de nieuwe genetische techniek exoom sequencing. Om patiënten met een identieke aandoening te selecteren uit de grote groep van patiënten met onbekende witte stofziekten hebben we gebruik gemaakt van specifieke kenmerken op de MRI scan van de hersenen, ook wel 'MRI patroonherkenning' genoemd. Individuele witte stofziekten tonen een gelijksoortig patroon van afwijkingen en verschillende witte stofziekten hebben verschillende patronen. De focus van dit onderzoek ligt bij witte stofziekten met een mogelijke mitochondriële oorzaak of hypomyelinisatie (refereert aan een permanent, substantieel tekort aan myeline in de hersenen). Een deel van de genen die we gevonden hebben met ons onderzoek was reeds geassocieerd met een bekend fenotype, maar blijkt nu ook geassocieerd met een ander

fenotype (fenotypische expansie) of een andere aandoening (nieuwe ziekte entiteit). Een ander deel van de genen was voorheen nog helemaal niet geassocieerd met een aandoening. De hoofdstukken zijn ingedeeld in deze drie groepen: expansie van het fenotypisch spectrum van een bekend gen, een nieuwe ziekte entiteit geassocieerd met een bekend gen, en een nieuwe aandoening die geassocieerd is met een gen dat nog niet eerder gevonden is bij een aandoening.

Expansie van het fenotypisch spectrum van een bekend gen

In **hoofdstuk 2** beschrijven we de zoektocht naar de genetische oorzaak van 16 patiënten (10 families) met de X-gebonden aandoening 'Hypomyelinisatie van vroeg myeliniserende structuren', ofwel 'HEMS'. Het MRI patroon van deze patiënten toont dat hersenstructuren die normaliter vroeg tijdens de ontwikkeling myeliniseren, nu slecht gemyeliniseerd zijn, terwijl structuren die normaliter laat myeliniseren, relatief goed gemyeliniseerd zijn. Exoom sequencing van het X-chromosoom toonde bij alle patiënten varianten in het gen *PLP1*, dat codeert voor twee eiwitten: PLP1 en DM20. Deze twee eiwitten zijn belangrijke componenten van myeline in het centrale zenuwstelsel. De varianten waren gelokaliseerd in één specifiek deel van het gen: exon 3B of in intron 3 (een niet-coderende deel van het gen). *In silico* analyse van het effect van de varianten, onderzoek in fibroblasten en in een transfectie model toonden aan dat de varianten een effect hebben op de splicing van *PLP1/DM20*, waardoor de ratio van *DM20/PLP1* verandert. Andere aandoeningen geassocieerd met *PLP1* varianten worden gekarakteriseerd door een ander patroon van hypomyelinisatie. Onze bevindingen verbreden het fenotypisch spectrum geassocieerd met *PLP1* varianten en leveren nieuwe inzichten op betreffende de mogelijke onderliggende werkingsmechanismes van *PLP1* varianten.

In **hoofdstuk 3** hebben we een groep van zeven patiënten geïdentificeerd met een ernstige, letale wittestofziekte, mogelijk van mitochondriële origine. Exoom sequencing in één patiënt toonde autosomaal recessieve varianten aan in het *SLC19A3* gen. Analyse van dit gen in de andere patiënten toonde bij allen varianten in dit gen aan. Het *SLC19A3* gen codeert voor één van de twee thiamine transporters. Deze transporteren thiamine de cel in. Thiamine speelt een belangrijke rol in de afbraak van koolhydraten in de citroenzuurcyclus. Hersenweefsel van twee patiënten werd onderzocht en toonde kenmerken van een mitochondriële aandoening. *SLC19A3* varianten zijn voorheen beschreven bij patiënten met andere MRI afwijkingen en een milder klinisch beloop. De identificatie van dit nieuwe, ernstigere fenotype, dat gekarakteriseerd wordt door een vroeg optredende, snelle subtotaal hersendegeneratie, verbreedt het klinisch spectrum geassocieerd met *SLC19A3* varianten. Herkenning van het MRI-patroon is belangrijk

omdat dit leidt tot een snelle diagnose. Er is nog geen duidelijke relatie tussen de soort varianten en de ernst van het fenotype. In **hoofdstuk 3** bespreken we de behandeling van deze aandoening. Thiaminesuppletie kan levensreddend zijn voor een deel van de patiënten met *SLC19A3* varianten. Of dit ook geldt voor patiënten met een zeer jonge manifestatie, zoals hier beschreven, is niet bekend, maar onwaarschijnlijk, omdat de hersenen van deze kinderen al ernstig beschadigd zijn bij presentatie. Er zijn een aantal onderzoeken gepubliceerd waarbij er bij minder ernstig aangedane patiënten met *SLC19A3* varianten gekeken is naar het effect van thiaminesuppletie. Zowel de MRI afwijkingen als de symptomen verbeterden in een deel van deze patiënten. Echter, de follow-up tijd was erg kort, dus wat de uitkomst is op lange termijn blijft onzeker.

In **hoofdstuk 4** beschrijven we een familie met drie aangedane familieleden die een combinatie van wittestofafwijkingen en een in de puberteit ontstane spierdystrofie hebben. Deze familie was eerder gepubliceerd in 1992 door B.G.M. van Engelen et al. Exoom sequencing toonde varianten in *LAMA2*, dat codeert voor het eiwit laminine α -2. Varianten in *LAMA2* zijn geassocieerd met de aandoening 'congenitale spierdystrofie'. Deze patiënten hebben meestal een op kinderleeftijd ontstane proximale spierzwakte en MRI afwijkingen. Er bestaat een totale of gedeeltelijke deficiëntie van laminine α -2 in spierweefsel. De MRI afwijkingen van onze patiënten komen overeen met deze diagnose. Een verschil is echter dat onze patiënten vooral een distale spierzwakte hebben, de ziekte op latere leeftijd ontstaat en dat de laminine α -2 kleuring in spier normaal is. Het laatste zou echter ook verklaard kunnen worden doordat ons antilichaam niet gevoelig genoeg was om deficiëntie van laminine α -2 te detecteren. Onze bevindingen verbreden het fenotypisch spectrum geassocieerd met *LAMA2* varianten.

In **hoofdstuk 5** beschrijven we een patiënt met autosomaal recessieve varianten in het *EARS2* gen, dat codeert voor het enzym glutamyl tRNA synthetase en betrokken is bij de eiwitsynthese in de mitochondriën. Patiënten met *EARS2* varianten presenteren zich met een specifiek MRI patroon en klinische symptomen. Deze patiënt heeft echter opvallende, niet eerder beschreven afwijkingen op de MRI. Beide thalami (hersenkernen) zijn afwezig, lijkend op een stoornis in de ontwikkeling van de hersenen, zonder duidelijke afwijkingen die wijzen op een laesie. Wij denken dat deze bijzondere configuratie tot stand is gekomen door een zeer vroege (antenatale) beschadiging van de thalami, wat nadien in de normale ontwikkeling van het hersenweefsel is opgenomen, waardoor het resultaat lijkt op een ontwikkelingsstoornis. Deze observatie is van belang voor de interpretatie van de MRI bevindingen van eerder gepubliceerde patiënten met *EARS2* varianten. Sommige patiënten hadden een niet volledig gevormd corpus callosum, wat toegeschreven werd aan een ontwikkelingsstoornis. Echter, ook

hier zou er sprake kunnen zijn van een zeer vroege laesie. Onze bevindingen verruimen het fenotype geassocieerd met *EARS2* varianten.

Nieuwe ziekte entiteit geassocieerd met een bekend gen

In **hoofdstuk 6** werden twee onafhankelijke exoom sequencing studies verricht in twee niet-verwante patiënten met een nog onbekende wittestofaandoening. Deze twee patiënten deelden hetzelfde, nog niet eerder beschreven, MRI patroon. De specifieke MRI bevindingen werden vergeleken met MRI's van een groep patiënten met een nog niet geclassificeerde wittestofziekte. Hieruit werden 11 patiënten geselecteerd. Exoom sequencing van de twee niet-verwante patiënten toonde autosomaal recessieve varianten aan in het gen *AARS2* dat codeert voor het mitochondriële alanyl-tRNA synthetase enzym. Dit enzym speelt een belangrijke rol in de eiwitsynthese in de mitochondriën. Analyse van dit gen in de overige 11 patiënten toonde varianten aan in vier andere patiënten. De klinische verschijnselen van de zes patiënten met *AARS2* varianten ontstonden op kinderleeftijd of adolescentie en bestonden uit neurologische symptomen, zoals ataxie, spasticiteit en cognitieve achteruitgang met kenmerken van frontaalkwabdysfunctie. De MRI toonde diffuse wittestofafwijkingen met opvallende afwijkingen in het corpus callosum, de lange descenderende wittestofbanen, en cerebellaire atrofie. Prematuur ovarieel falen was aanwezig bij alle vrouwelijke patiënten. Varianten in *AARS2* zijn eerder beschreven in twee families met een ernstige vorm van infantiele cardiomyopathie en myopathie. In een gistmodel hebben we onderzocht wat het verschil is tussen het effect van de varianten geassocieerd met de cardiomyopathie en het door ons gevonden fenotype. We vonden dat de cardiomyopathie-geassocieerde variant een ernstiger effect had op de functie van het enzym dan onze variant. Mogelijk speelt dit een rol in het verschil van fenotype tussen de patiënten. Onze bevindingen laten zien dat het fenotypisch spectrum van patiënten met *AARS2* varianten aanzienlijk breder is dan voorheen beschreven.

In **hoofdstuk 7** beschrijven we drie patiënten uit één familie met een langzaam progressieve neurologische aandoening die ontstaan is rond de kinderleeftijd. De afwijkingen op de MRI zijn voor alle drie de patiënten hetzelfde met wittestofafwijkingen in de cerebrale hemisferen en ook thalamusafwijkingen. Met exoom sequencing vonden we varianten in het *HMBS* gen, dat codeert voor het enzym hydroxymethylbilaan synthase dat een belangrijke rol speelt in de synthese van heem. Bijzonder is dat heterozygote, autosomaal dominante varianten in dit gen geassocieerd zijn met de stofwisselingsziekte acute intermitterende porfyrie (AIP). De hier beschreven patiënten hebben echter bi-allelische, autosomaal recessieve varianten, en geen klachten die geassocieerd zijn met AIP, zoals aanvallen van buikpijn, diarree, hoge bloeddruk en spierzwakte. In de literatuur

zijn vijf andere patiënten beschreven met bi-allelische varianten in dit gen. Ook deze patiënten hebben geen AIP klachten maar wel neurologische symptomen. Bij één patiënt werden wittestofafwijkingen gedocumenteerd, maar bij de andere patiënten werden geen MRIs verricht. In vergelijking met onze patiënten hebben deze patiënten veel ernstiger klachten en toont het biochemische onderzoek meer afwijkingen. Bi-allelische *HMBS* varianten veroorzaken dus een nieuw wittestof-fenotype. De resultaten van dit onderzoek zijn ook van belang voor de gezonde familieleden die drager zijn van één *HMBS* variant. Zij lopen het risico van 10% om in hun leven acute porfyrie aanvallen te krijgen en hebben een verhoogde kans op hypertensie en leverkanker. Preventieve maatregelen kunnen deze risico's verlagen.

In **hoofdstuk 8** beschrijven we twee families met dezelfde autosomaal dominante wittestofziekte. Deze aandoening wordt gekenmerkt door een rond het 30^e-40^e levensjaar ontstane therapie-resistente hypertensie, beroertes en langzame cognitieve achteruitgang. De MRI toont diffuse wittestofafwijkingen die al bestaan voordat de vasculaire problemen (bloedingen en infarcten) debuten. Met exoom sequencing vonden we in beide families dezelfde heterozygote (autosomaal dominante) variant in het *CTSA* gen, dat codeert voor het eiwit cathepsine-A. Met aanvullend genetisch onderzoek vonden we aanwijzingen dat beide families waarschijnlijk ver weg verwant aan elkaar zijn. Recessieve varianten in *CTSA* zijn geassocieerd met de lysosomale stapelingsziekte 'Galactosialidose'. Het is niet bekend dat galactosialidose patiënten en hun ouders, die obligate dragers zijn, wittestofafwijkingen of hypertensie hebben. Echter, gezien de zeldzaamheid van galactosialidose kan deze associatie gemist zijn. Op dit moment hebben we nog niet kunnen verklaren waarom de door ons gevonden variant resulteert in een wittestofziekte. Meer families met deze wittestofziekte en varianten in dit gen zijn nodig om dit verder uit te zoeken.

Nieuwe ziektes geassocieerd met een gen dat voorheen niet bij de mens is beschreven, of zonder duidelijk fenotype

In **hoofdstuk 9** beschrijven we een groep van zes patiënten met een wittestofziekte en een deficiëntie van één van de ademhalingsketen enzymen, complex 1. De MRI van deze patiënten wordt gekarakteriseerd door een combinatie van cerebrale wittestofafwijkingen, cerebellaire cortex afwijkingen en afwijkingen in het corpus callosum. Tijdens follow-up van deze patiënten verbeterden de afwijkingen in de cerebrale witte stof en het corpus callosum, maar verergerden de afwijkingen in het cerebellum en ontstonden er ook afwijkingen in de hersenstam. Alle patiënten presenteerden zich in de eerste twee levensjaren met verlies van motorische mijlpalen of een vertraagde motorische ontwikkeling en symptomen passend bij cerebellaire

dysfunctie. Exoom sequencing toonde autosomaal recessieve varianten in *NUBPL*, een gen dat codeert voor een ijzer-sulfaat cluster assemblage factor voor complex I. Alle zes patiënten bleken varianten te hebben in dit gen. De biochemische consequenties van de *NUBPL* varianten werd onderzocht in fibroblasten van twee patiënten. Er was sprake van een sterk verminderde hoeveelheid van zowel het *NUBPL* eiwit alsook van volledig geassembleerd complex I. Analyse van het effect van gemuteerd *NUBPL* op de assemblage van de perifere arm van complex I liet zien dat *NUBPL* betrokken is bij de assemblage van de ijzer-sulfaat clusters vroeg in de complex I assemblage. Concluderend tonen deze data dat *NUBPL* varianten geassocieerd zijn met een uniek, herkenbaar en consistent MRI patroon. Herkenning van het MRI patroon leidt tot een snelle diagnose en maakt ingrijpende en vaak lastige onderzoeken zoals biochemische onderzoek in een spierbiopt of fibroblasten (huidcellen) overbodig.

In **hoofdstuk 10** hebben we een groep van zeven jonge patiënten (vier niet-verwante families) geïdentificeerd die, op basis van het MRI-patroon, dezelfde onbekende genetische wittestofaandoening leken te hebben. Het klinisch beeld was desastreuus: een neonataal of vroeg-infantiel presenterende encefalopathie met een progressieve microcefalie, variabele hartafwijkingen, refractaire epilepsie, en uiteindelijk overlijden van tot nu toe zes van de zeven patiënten vóór de leeftijd van 2,5 jaar. Het MRI patroon van de patiënten was suggestief voor vroege neuronale degeneratie met Wallerse degeneratie van de geassocieerde wittestofbanen. Exoom sequencing gecombineerd met de genetische techniek 'SNP-array' toonde varianten aan in het gen *ITPA*, dat codeert voor het enzym inosine trifosfaat pyrofosfatase (ITPase), in alle patiënten. Onderzoek in fibroblasten en erythrocyten van de patiënten toonde een verminderde ITPase functie. ITPase speelt een belangrijke rol in het nucleotide metabolisme waarbij het niet-essentiële nucleotiden uit de cel verwijderd. Een defect van dit enzym kan leiden tot stapeling van niet-essentiële nucleotiden en kan leiden tot neuronale celdood en interferentie met enzymen die normaal ATP en GTP gebruiken. Tot op heden waren varianten in *ITPA* alleen geassocieerd met een verhoogde gevoeligheid voor bepaalde medicamenten, maar nog niet met een specifieke aandoening in de mens. Herkenning van toekomstige *ITPA* deficiënte patiënten zal lastig zijn omdat het beschreven specifieke MRI patroon slechts gedurende enkele maanden aanwezig is en screenend metabool onderzoek normaal is.

Sinds de start van ons onderzoek in 2011 zijn er met WES 18 nieuwe genen geïdentificeerd die betrokken zijn bij een wittestofziekte. Wij verwachten dat door de toepassing van deze nieuwe techniek veel patiënten die aanvankelijk geen diagnose hadden nu wel een genetische diagnose zullen hebben. In **hoofdstuk 11** hebben we in drie verschillende cohorten patiënten met in 2011 nog een onbekende wittestofziekte onderzocht of ze op

dit moment wél een genetische diagnose hebben. Een diagnose kan nu worden gesteld bij 80% van de patiënten, en waarschijnlijk is dit nog een aanzienlijke onderschatting gezien de retrospectieve aard van de studie. In dit hoofdstuk wordt de revolutie van de genetica binnen de wittestofziekten besproken en nieuw opgedane inzichten uiteen gezet.

DANKWOORD

Dit proefschrift is mede tot stand gekomen dankzij het werk en steun van velen. Ik wil iedereen hiervoor van harte bedanken, maar een aantal mensen wil ik in het bijzonder noemen.

Als eerste gaat mijn dank uit naar alle patiënten, families en dokters die hebben bijgedragen aan het onderzoek. Zonder deze medewerking was dit onderzoek nooit tot stand gekomen.

Grote dank gaat ook uit naar mijn promotor, Prof. dr. M.S. van der Knaap en mijn copromotoren, dr. N.I. Wolf en dr. Q. Waisfisz. Beste Marjo, jouw toewijding en enthousiasme voor het onderzoek en de patiëntenzorg waren en zijn voor mij een grote inspiratie bron. Vanaf het begin, tot het einde heb je je ingezet om mij te begeleiden en het onderzoek in goede banen te leiden. Veel dank hiervoor! Ik heb veel van je geleerd en hoop dat we in de toekomst nog veel zullen samenwerken. Beste Nicole, samen hebben we intensief samengewerkt aan de ziekte "HEMS". Het vinden van de oorzaak van deze aandoening was een hoogtepunt in het onderzoek, wat fantastisch was met jou te kunnen delen. Ik heb veel bewondering voor al het werk dat je doet. Beste Quinten, vrijwel altijd had je een antwoord op mijn vragen, en dat waren er best veel. Als ik het een keer niet wist, had jij altijd nog een verfrissend nieuw idee om uit te proberen.

Leden van de leescommissie, Prof. dr. M.A.A.P. Willemsen, Prof. dr. R. van Coster, dr. T. Kleefstra en dr. E. Siermans hartelijk dank dat u de tijd nam het manuscript te lezen en te beoordelen.

Beste collega's van de onderzoeksgroep wittestofziekten; Vivi, Liane, Mohit, Gerbren, Prisca, Eelke, Stephanie D, Stephanie H, Aish, Lianne, Dwayne, Timo, Ferdy, Rogier, Laura, Lisa en Anna. Bedankt voor jullie input tijdens de vele labmeetings en voor de gezellige etentjes. Marianna, jouw hulp was onmisbaar! Met veel plezier heb ik met je samengewerkt. Nienke, Emiel, en Carola, bedankt voor al het werk dat jullie hebben verricht en dat jullie ondanks al mijn ongeduldige telefoontjes en mailtjes altijd behulpzaam zijn gebleven. Super! Truus, gelukkig was jij er altijd en zorgde je dat alles gestroomlijnd verliep in het lab. Bedankt voor al je hulp, tijd en energie.

Lieve Eline en Diane, mijn paranimmen. Eline, tevens mijn 'roomie', vanaf het begin van het onderzoek. Lief en leed hebben we gedeeld. Menig gezwijmel over

onderzoekresultaten, maar ook over mijn kinderen heb je moeten aan horen. Bedankt voor je altijd beschikbare luisterend oor en voor je kritische blik en input. Diane, bedankt voor je hulp op de momenten dat het iets minder ging. Dat waardeer ik zeer!

Hannemieke en Marjan, mijn 'voorgangers'. Jullie hulp bij aanvang van mijn promotietraject was heel fijn. Marjan, zonder jouw werk hadden we niet zoveel kunnen bereiken.

Lieve collega's van PK4X (Jonneke, Bibian, Stefanie, Lindsay, Raphaële, Dana, Marita, Mirjam, Charlotte, Gerrit, Suzanne, Marieke, Jolice, Marc, Hester, Katja, Annelies, Willemijn, Miret, Femke, Ineke, Anne, Fatma, Marloes, Sophie, Annemieke, Stijn, en Sandra). Wat waren de lunches toch fijn! Bedankt voor de "gastvrijheid" en alle gezelligheid.

Ook wil ik Prof. dr. P. Heutink en iedereen van de onderzoeksgroep bedanken voor hun hulp bij de aanvang van het onderzoek.

Sinds 1 maart ben ik begonnen als AIOS Klinische Genetica in het Radboud UMC in Nijmegen. Ik wil mijn nieuwe collega's, en in het bijzonder; Thatjana, Anneke en Janneke bedanken voor hun hulp en steun tijdens de eindsprint van mijn promotie traject.

Behalve promoveren, was er op z'n tijd ook ontspanning nodig. Mijn lieve vriendinnen, Femke en Janneke; wat fijn dat jullie er zijn! Onze avondjes uit en uitstapjes met de kids waren een welkome afwisseling. Fijne momenten om te koesteren. Lieve Aniek, samen hebben we in Groningen gestudeerd. We wisten toen allebei al wat we wilden, en het is ons gelukt! Bedankt voor de vele gezellige avonden en urenlange telefoongesprekken. Jeske en Merel, jullie hebben mij gesteund vanaf het begin en mij vertrouwen gegeven in de toekomst, zowel als vriendinnen als (nu) collega's.

Ook wil ik graag mijn familie bedanken. Mijn broertjes; Wouter, Marten, Folkert en Steven en mijn zusje Jette. Pap, bedankt dat je altijd in mij hebt geloofd! Mam, jou wil ik nog in het bijzonder bedanken. Je hebt mij de mogelijkheid geboden om het onderzoek tot een goed einde te brengen. Na de geboorte van Aimée en Thijmen heb je dagen, weken, maar ook nachten opgepast. Bij ziekte, ongevallen, of gewoon zomaar, ik kon je altijd bellen. Ook nu ben je nog steeds onze rots in de branding. Beste Eibert en Neelien, wat fijn dat jullie mijn schoonouders zijn. Bedankt voor alle goede zorgen.

Lieve Jurr, de afgelopen jaren waren mooi, doch enigszins stressvol. Het vergde geduld en begrip. Bedankt voor al je hulp en steun op de momenten dat ik het hardst nodig had. En Aimée en Thijmen, ik ben ontzettend blij dat jullie er zijn. Thuis komen is altijd een feest.

LIST OF PUBLICATIONS

This thesis

Kevelam SH*, Klouwer FCC*, Fock JM, Salomons GS, Bugiani M, van der Knaap MS. Absent thalami caused by a homozygous *EARS2* mutation: expanding disease spectrum of LTBL. *Neuropediatrics*. 2016 Jan;47 (1):64-67.

Kevelam SH, Bierau J, Salvarinova R, Agrawal S, Honzik T, Visser D, Weiss MM, Salomons GS, Abbink TE, Waisfisz Q, van der Knaap MS. Recessive *ITPA* mutations cause an early-infantile encephalopathy. *Ann Neurol*. 2015 Oct;78(4):649-658.

Kevelam SH, Taube JR, van Spaendonk RM, Bertini E, Sperle K, Tarnopolsky M, Tonduti D, Valente EM, Travaglini L, Sisternans EA, Bernard G, Catsman-Berrevoets CE, van Karnebeek CD, Østergaard JR, Friederich RL, Fawzi Elsaid M, Schieving JH, Tarailo-Graovac M, Orcesi S, Steenweg ME, van Berkel CG, Waisfisz Q, Abbink TE, van der Knaap MS, Hobson GM, Wolf NI. Altered *PLP1* splicing causes hypomyelination of early myelinating structures. *Ann Clin Transl Neurol*. 2015 Jun;2(6):648-661.

Van der Knaap MS and **Kevelam SH**. Reply: Infantile Leigh-like syndrome caused by *SLC19A3* mutations is a treatable disease. *Brain* 2014;137:e297.

Kevelam SH*, Dallabona C,* Diodato D,* Haack TB, Wong LJ, Salomons GS, Baruffini E, Melchionda L, Mariotti C, Strom TM, Meitinger T, Prokisch H, Chapman K, Colley A, Rocha H, Ounap K, Schiffmann R, Salsano E, Savoirdo M, Hamilton EM, Abbink TE, Wolf NI, Ferrero I, Lamperti C, Zeviani M, Vanderver A,** Ghezzi D** and van der Knaap MS**. Novel (ovario) leukodystrophy related to *AARS2* mutations. *Neurology* 2014;82:2063-2071.

Kevelam SH, van Engelen BG, van Berkel CG, Küsters B and van der Knaap MS. *LAMA2* mutations in adult-onset muscular dystrophy with leukoencephalopathy. *Muscle Nerve* 2014;49:616-617.

Kevelam SH, Rodenburg RJ, Wolf NI, Ferreira P, Luning RJ, Nijtmans LG, Mitchell A, Arroyo HA, Rating D, Vanderver A, van Berkel CG, Abbink TE, Heutink P and van der Knaap MS. *NUBPL* mutations in patients with complex I deficiency and a distinct MRI pattern. *Neurology* 2013;80:1577-1583.

Kevelam SH, Bugiani M, Salamons GS, Feigenbaum A, Blaser S, Prasad C, Häberle J, Baric I, Bakker IM, Postma NL, Kanhai WA, Wolf NI, Abbink TE, Waisfisz Q, Heutink P and van der Knaap MS. Exome sequencing reveals mutated *SLC19A3* in patients with an early-infantile, lethal encephalopathy. *Brain* 2013;136:1534-1543.

Other scientific publications

van de Pol LA, Wolf NI, van Weissenbruch MM, Stam CJ, Weiss MM, Waisfisz Q, **Kevelam SH**, Bugiani M, van de Kamp JM, van der Knaap MS. Early onset severe encephalopathy with epilepsy: the *BRAT1* gene should be added to the list of causes. *Neuropediatrics*. 2015. Dec;46(6):392-400.

Nicolaou N,* Margadant C,* **Kevelam SH**, Lilien MR, Oosterveld MJ, Kreft M, van Eerde AM, Pfundt R, Terhal PA, van der Zwaag B, Nikkels PG, Sachs N, Goldschmeding R, Knoers NV, Renkema KY** and Sonnenberg A**. Gain of glycosylation in integrin $\alpha 3$ causes lung disease and nephrotic syndrome. *J. Clin. Investigation* 2012; 122:4375-3287.

Kevelam SH, van Harsseel JJ, van der Zwaag B, Smeets HJ, Paulussen AD and Lichtenbelt KD. A patient with a mild holoprosencephaly spectrum phenotype and heterotaxy and a 1.3 Mb deletion encompassing *GLI2*. *Am. J. Med. Genet. A* 2012;158A:1519.

Kevelam SH, Jansen FE, van Binsbergen E, Braun KP, Verbeek NE, Lindhout D, Poot M and Brilstra EH. Copy number variations in patients with Electrical status Epilepticus in sleep. *J. Child. Neurol.* 2012;27:178-182.

* These authors share first authorship

** These authors share senior authorship

CURRICULUM VITAE

Sietske Hanneke Geertje Kevelam was born on the 30th of July 1985 in Nijmegen, the Netherlands. After completing her pre-university education at the 'Atrium' in Amersfoort in 2003, Sietske started to study Medicine at the University Medical Center Groningen. Her final research internship concerned the search for the genetic etiology of electrical status epilepticus in sleep, which she performed at the department of Child Neurology and the department of Clinical Genetics at the University Medical Center Utrecht. In 2009, Sietske graduated medical school with honors/cum laude. For the following two years she worked as a medical doctor at the department of Neurology at the St. Antonius Hospital in Nieuwegein and at the department of Clinical Genetics at the Wilhelmina Children's Hospital in Utrecht. In 2011, she started her Ph.D. studies at the Center for Childhood White Matter Disorders with as subject the definition of novel brain white matter disorders by MRI pattern analysis and identification of related gene defects by Next-Generation Sequencing, under supervision of Prof. dr. M.S. van der Knaap, dr. N.I. Wolf and dr. Q. Waisfisz. Her work resulted in several oral presentations at international genetic congresses. In 2015 she received the second prize at the annual genetics retreat at Rolduc for an oral presentation about the work described in chapter 2. Sietske is currently working as a resident at the Clinical Genetics department at the Radboud University Medical Center in Nijmegen.

